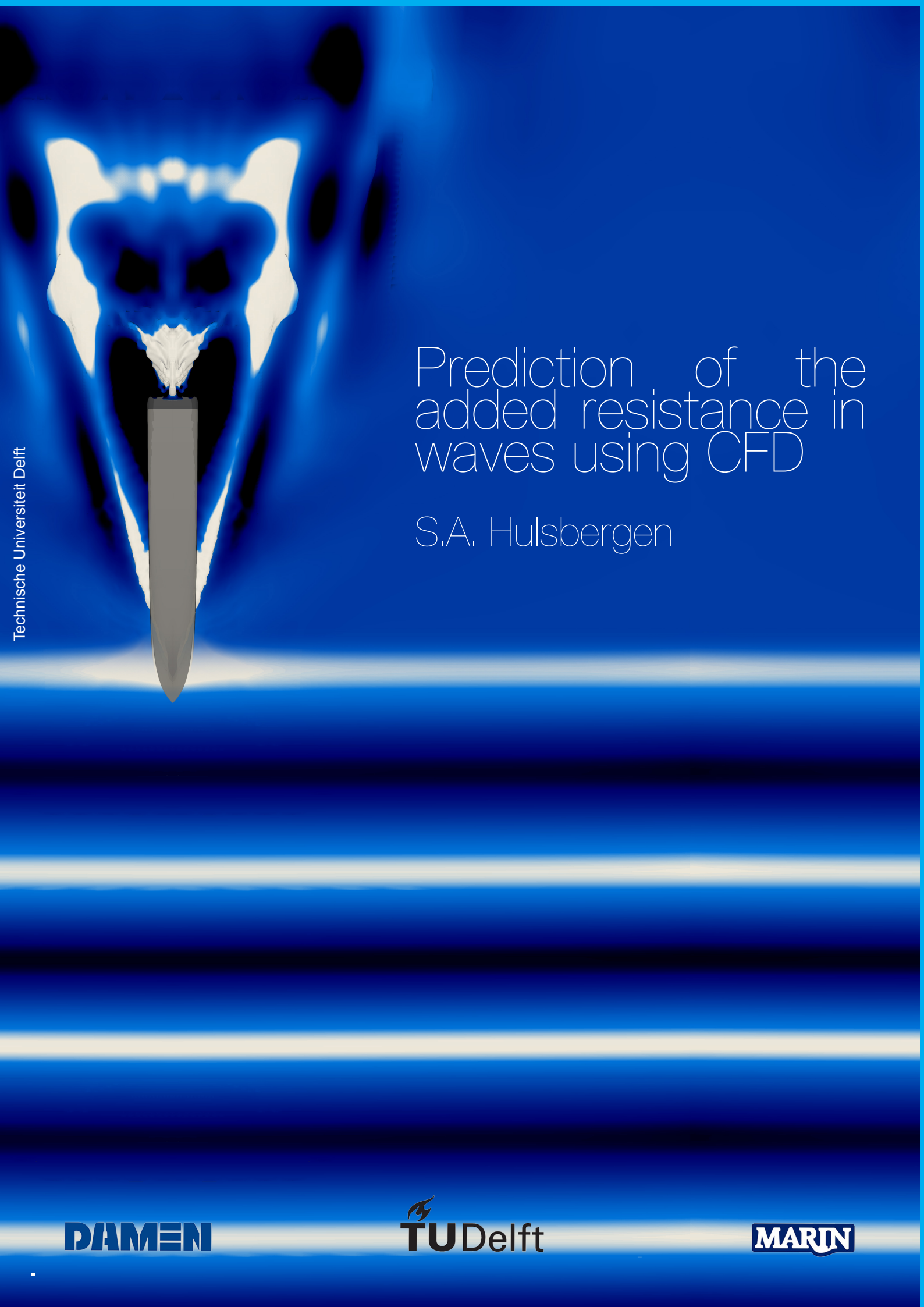

Prediction of the added resistance in waves using CFD

S.A. Hulsbergen

Technische Universiteit Delft

DAMEN

TU Delft

MARIN

Prediction of the added resistance in waves using CFD

by

S.A. Hulsbergen

to obtain the degree of Master of Science

at the Delft University of Technology,

to be defended publicly on Friday February 15th, 2019 at 15:15 PM.

Student number:	4017692	
Project duration:	April 1, 2018 – January 30, 2019	
Thesis committee:	Dr. ir. P.R. Wellens	TU Delft
	Dr. ir. I. Akkerman	TU Delft
	Dr. A.A. Kana	TU Delft
	Dr. S.J. Hulshof	TU Delft
	Ir. A. Mikelic	DAMEN
	Ir. P. Crepier	MARIN

Colophon

Title	Prediction of the added resistance in waves using CFD
Author	
Name	Sebastiaan Antonie Hulsbergen
E-mail	s.a.hulsbergen@student.tudelft.nl
Study program	
Master program	MSc Offshore Engineering
Faculty	Mechanical, Maritime and Materials Engineering (3mE)
University	Delft University of Technology
Graduation committee	
Chair	Dr. ir. P.R. Wellens
Supervisor	Dr. ir. I. Akkerman
External supervisor	ir. A. Mikelic
	ir. P. Crepier
Committee member	Dr. A.A. Kana
	Dr. S.J. Hulshof
Institution	Delft University of Technology Mekelweg 5 2628 CD Delft www.tudelft.nl
Graduation company	DAMEN Schelde Naval Shipbuilding (DSNS) De Willem Ruysstraat 99 4381 NK Vlissingen www.damennaval.com

Preface

This thesis forms the final proof of competence for obtaining the Master of Science (MSc) degree in Offshore Engineering. This master is taught at Delft University of Technology, The Netherlands. The research was supervised by Delft University and executed partially at DAMEN Schelde Naval Shipyards (DSNS) and partially at the Maritime Research Institute Netherlands (MARIN).

My journey in Delft began in 2009 when I started studying Mechanical Engineering in Delft. The choice for Mechanical Engineering was an easy one for me. For as long as I can remember I was trying to figure out how mechanical things were working and at my seventh birthday I got my first set of tools so I would stop borrowing my father's. After finishing my bachelor's I was eager to get some hands-on experience at a company. The choice for an internship in the offshore sector came to me as a logical one. As a teenager I have had the opportunity to visit my father on board of several vessels that he was working on as an engineer. The sheer size of these vessels and the use of innovative solutions fascinated me. During the internship I got a small preview of what a career in the offshore industry would look like and I felt right at home. There, I decided that I wanted to expand my knowledge regarding hydrodynamics, seakeeping and computer simulations and so I signed up for the master Offshore Engineering, with this thesis as a direct result.

I want to thank my supervisor Andrea Mikelic at DSNS, thanks to your clear explanations of hard concepts I gained a lot of new insights. I'd also like to thank Ido Akkerman for always keeping me and the research focused and Pierre Crepier for welcoming me at MARIN and all the invaluable help setting up the simulations. Finally I would like to thank all my colleagues at DSNS and MARIN who aided in this research.

As for my family I would like to thank my mother for all the years of continuous support. Your help and unconditional love proved invaluable throughout my study. My father for his wisdom, you always motivated me to think for myself. Our long talks helped me to focus on what is important in life. Thanks to the both of you I have been able to grow into the person that I am to day and I will always be thankful for that. Furthermore I would like to thank my girlfriend Anne-Claire. Thank you for being there and supporting me in this sometimes stressful period.

S.A. Hulsbergen
Delft, January 2019

Abstract

Shipyards these days see an increase in customers that specify combined speed and seakeeping ability design requirements. This requires the shipyard to make a prediction of the additional installed power required to maintain a certain speed when waves are encountered. The additional required installed power is directly related to the average extra resistance that the vessel is subjected to when it's sailing in waves. This extra resistance is known as the time-averaged added resistance in waves.

In the maritime industry Computational Fluid Dynamics (CFD) is increasingly used for resistance predictions as it promises cheaper and faster predictions than model testing. The result does come without the comforting 'truth' of the towing tank. In this study, the applicability of CFD for the estimation of the time-averaged added resistance in regular head waves is researched by assessing the error and uncertainty of the solution. For fast sailing vessels, no standard procedure for the estimation of the time-averaged added resistance in waves using CFD has yet been developed. Therefore the secondary research objective is to establish such a procedure.

For this research the resistance predictions are done for the Fast Displacement Ship (FDS) hull form. Extensive research was conducted on this hull form by the Cooperative Research Ships (CRS) organisation. Their model tests results are used for the validation of the solution. The discretisation error is determined through a procedure developed by L.Eça and M.Hoekstra [25] which is based on a grid refinement study.

The time-averaged added resistance is estimated by simulating the vessel both in calm water and waves. The time-averaged calm water and total resistance in waves are determined from these simulations. The time-averaged added resistance estimate is then calculated by subtracting the calm water resistance from the total resistance.

First a grid topology is optimised to simulate the incoming waves as well as the vessels response to them accurately and efficiently. Grid sensitivity studies of the simulation of incoming waves as well as simulations of the static vessel in waves and the vessel subjected to forced motion are used to determine an efficient topology. To determine if the vessel's response is accurate, it is compared to the solution from potential flow code solver PRECAL. The comparison proved that accurately propagating waves and accurate vessel response to the waves and motions are achieved on grids with less than 3 M cells in total.

Verification estimated an uncertainty that varies between 0.5 % and 1.3 % for the time-averaged total resistance in waves and between 15.1 and 36.2% for the time-averaged calm water resistance on grids with a total number of cells ranging between 1.3 and 6.6 M.

Comparison with the results from the model test revealed that an error of 1.4 % was present in the time-averaged added resistance estimate. This error is smaller than the uncertainty margin of the model test result.

Using the proposed method, the time-averaged calm water resistance estimate didn't converge well, resulting in a large discretisation uncertainty. As the added resistance prediction is dependent on the calm water resistance prediction, it is also affected by this uncertainty. Therefore it's concluded that the proposed method for the estimation of the time-averaged wave added resistance using CFD is not yet applicable in its proposed form.

However, by using the proposed method, it is possible to estimate the time-averaged total resistance in waves accurately and efficiently. Therefore it's concluded that further research is required to improve the uncertainty present in the time-averaged added resistance due to the uncertainty seen in the calm water resistance for the used grids.

Keywords: CFD, ReFRESCO, added resistance, regular waves, 2D waves, radiated waves, diffracted waves, FDS, discretisation uncertainties, verification and validation

Contents

List of Figures

List of Tables

Nomenclature

Symbol	Description	Unit
B	Beam	m
C_{λ_d}	Cells per diffracted wavelength	–
C_{λ}	Cells per wavelength	–
C_{ζ_a}	Cells per waveamplitude	–
C	Courant number	–
E_k	Kinetic energy	J
L_2	Average residual norm	–
L_∞	Largest residual norm	–
L	Cell dimension	m
N	Total number of cells	–
R_c	Calm water resistance	N
R_t	Total resistance in waves	N
R_{ad}	Added resistance due to diffracting waves	N
R_{aw}	Added resistance in waves	N
R_{td}	Total resistance in diffracting waves	N
R_{td}	Total resistance in radiating waves	N
S	Viscous layer cell size at hull	m
T_e	Encountered wave period	s
T	Wave period	s
λ_d	Diffracted wave length	m
λ	Wave length	m
ω_e	Encounter frequency	$\frac{rad}{s}$
ω	Wave frequency	$\frac{rad}{s}$
ρ	Density	$\frac{kg}{m^3}$
θ_{wmax}	Maximum angle of the wave's tangent	m
ζ_a	Wave amplitude	m
d	Grid refinement diffusion	–
f	Force	N
g	Gravitational acceleration	$\frac{m}{s^2}$
h	Waterdepth	m
k	Wavenumber	$\frac{rad}{m}$
n_f	Elliptical from factor	–
n	Grid refinement level	n
r_e	Elliptical radius	m
r_v	Viscous layer growth ratio	–
r	Residual	–
t	Time	s
u	Velocity vector	$\frac{m}{s}$
v	Velocity vector	$\frac{m}{s}$
w	Velocity vector	$\frac{m}{s}$
x	Spatial vector	m
y	Spatial vector	m
z	Spatial vector	m

Acronyms

(U)RANS	(Unsteady) Reynolds Averaged Navier-Stokes
App	Aft perpendicular
BC	Boundary Condition
CAD	Computer Aided Design
CFD	Computational Fluid Dynamics
CFL	Courant-Friedrisch-Lewy
CoG	Centre of Gravity
CRS	Cooperative Research Ships
DNS	Direct Numerical Simulation
DoF	Degree of Freedom
DSNS	DAMEN Schelde Naval Shipbuilding
EoM	Equations of Motion
FDS	Fast Displacement Ship
LES	Large Eddy Simulation
LPP	Length between Perpendiculars
Lpp	Length between perpendiculars
MARIN	MAritime Research Institute Netherlands
N-S	Navier-Stokes
NUA	Numerical Uncertainty Analysis
PDE	Partial Differential Equations
QTF	Quadratic Transfer Function
QUICK	Quadratic Upwind Interpolation for Convective Kinetics
RaNS	Reynolds averaged Navier-Stokes
ReFRESCO	Reliable & Fast Rans Equations (solver for) Ships, Cavitation (and) Offshore
RHIBs	Ridgid Hull Inflatable Boats
RHINO	Rhinoceros 3D
TF	Transfer Function
TU Delft	Delft University of Technology
TVD	Total Variation Diminishing

1

Introduction

When a vessel is sailing in waves it is subjected to an additional resistance compared to when it would be sailing in calm water. This extra resistance is known as the added resistance in waves. In a paper on the added resistance in waves by J.Strom-Tejsen et. al. [30] it is mentioned that the traditional way to account for this added resistance was to increase the engine power between 15 and 30 percent of the calm water resistance . With the availability of increased computational power in the recent years however, more accurate computational techniques for the estimation of the added resistance have come into focus.

In the maritime industry Computational Fluid Dynamics (CFD) is increasingly used for the prediction of a vessel's resistance in calm water. The application for the extra resistance that a vessel experiences in waves however, is still under focus. CFD promises cheaper and faster predictions than model testing but this result comes without the comforting "truth" of the towing tank. A need for a structured procedure as well as an assessment of the accuracy of this resistance prediction emerges.

DAMEN shipyards is an active participant in research regarding the use of CFD for hydrodynamic optimisation through cooperative research projects. This Master's thesis in an example of such research and was conducted through a cooperation of Delft University of Technology (TU Delft), DAMEN Schelde Naval Shipbuilding (DSNS) and MAritime Research Institute Netherlands (MARIN).

1.1. Wave added resistance - A shipyard's perspective

In 2015 the Dutch coastguard (Rijkswaterstaat) spent one million euros on two Rigid Hull Inflatable Boats (RHIBs) which would be used for the inspection of the Dutch fishing fleet on the North Sea. In order to increase the surprise effect of the inspection, a high top speed was specified in the design requirements. As these vessels would be sailing on the North Sea, the requirements also included operability in sea conditions common to the North Sea. During the seatrails concerns were raised about the seakeeping ability of the vessel at speed. These concerns were later confirmed by tests performed at MARIN). The vessels were deemed unsafe, resulting in the waste of a million euros in taxes.

Although top speed and operating conditions were specified in the design requirements, their combined case was not. As the vessel was performing according to the specifications it was not possible to hold the manufacturer responsible. A lesson that can be learned from this, is that the customer should specify not only single parameters such as speed or seakeeping ability but also their combined case.

These days shipyards such as DSNS see an increase in customers specifying such combined cases. The shipyard will need to make a prediction of the installed power required to maintain the specified speed in waves. Traditionally only the resistance the vessel feels when sailing in calm water would be estimated. In this case however, the vessel experiences additional resistance due to the vessel-wave interaction, which is known as wave added resistance. This requires the yard to make an estimate of this extra resistance.

Current methods available unfortunately have significant downsides such as inaccuracy and costs. Potential flow solvers for example tend to overestimate the wave added resistance, which would result in over dimensioning of the engines. Model tests on the other hand do provide reliable results, but they are very costly and are thus used sparsely, usually only once, at a late stage in the design process. Therefore a more economic and reliable alternative is of interest.

These days the use of CFD has become more and more significant in the maritime industry. CFD has the potential to provide results with lower turnaround times and possibly lower costs compared to model tests. Also, iterations in the design can be implemented without the necessity to perform costly adaptations to the scale model. Furthermore CFD can provide detailed information regarding the flow surrounding the vessel which is very useful for hull optimisation during the design phase.

Currently DSNS is developing a naval oriented range of vessels whose operational seaways can include challenging sea states. The success of such a ship's design depends on the ability of the ship to sustain its speed in a seaway. Therefore it is of interest to predict the maximum speed in a specified seastate for such vessels. This maximum speed is dependent on the resistance subjected to the vessel when it is sailing in these waves . The purpose of this research is to evaluate the capability of CFD to predict the added resistance in waves and to develop a procedure that will help to improve current predictions. If this research proves CFD is a viable alternative to wave added resistance model tests, shipyards can save significant time and costs and naval architects will gain access to a powerful design tool.

Finally, in order to make the lessons learned from this research fit for use at a shipyard, they are bundled into a set of guidelines. These guidelines will enable other engineers to set up their own wave added resistance CFD simulations for similar shaped hulls.

1.2. Previous work

For this research the FDS naval hull form, designed by MARIN is used. DSNS requested to use this specific hull form for two main reasons. First, it shares many characteristics with typical naval vessels as built by DSNS which would make the results applicable to them. Second, this specific hull form was used in an extensive research that was conducted by the CRS organisation. Availability of this data enables the validation of the results from this research.

The CRS is an organisation which started in 1969 and consists of 25 members including DAMEN shipyards and MARIN. According to their website [5], their purpose is to obtain general data about the hydrodynamics and related problems of large and high-powered ships . Both in 1986 and 2014 the CRS conducted research on the added resistance in waves. The focus of the 2012 study was the nature and magnitude of added resistance in waves with a focus on contemporary hull forms. This research was stimulated by new promising techniques such as CFD and numerical solvers based on linear potential flow theory such as PRECAL. One of the purposes of this research was to obtain accurate validation data for such methods.

In this research a comparison was made between the results from the model tests and the linear potential flow solver PRECAL. For experiments performed with a containership model the tests showed a good correlation which concludes that linear theory covers the added resistance in waves of this kind of hull fairly well.

However, this same solver yielded a poor prediction for the FDS hull form sailing at high speed. In the test report [11] it is stated that this is most likely related to non-linear wave breaking at the bow of the vessel . Images of the model test indeed show large breaking waves at the bow as can be seen in figure 1.1. In paragraph 2.1 the theory behind this phenomenon is discussed further.

By simulating the vessel in waves using CFD it is possible to simulate the breaking waves at the bow. The hypothesis is therefore that this method is able to predict the wave added resistance well.

On a more fundamental level Rapuc et al. [28] studied consistent wave propagation in CFD simulations. Consistent wave propagation is key when simulating wave added resistance as inaccuracies in the wave propagation will influence the resistance prediction. The authors propose a grid topology based on the kinetic energy in the waves in combination with wave absorption at the edges of the domain. Results from this study show that a very low error on the wave dispersion, dissipation and reflection

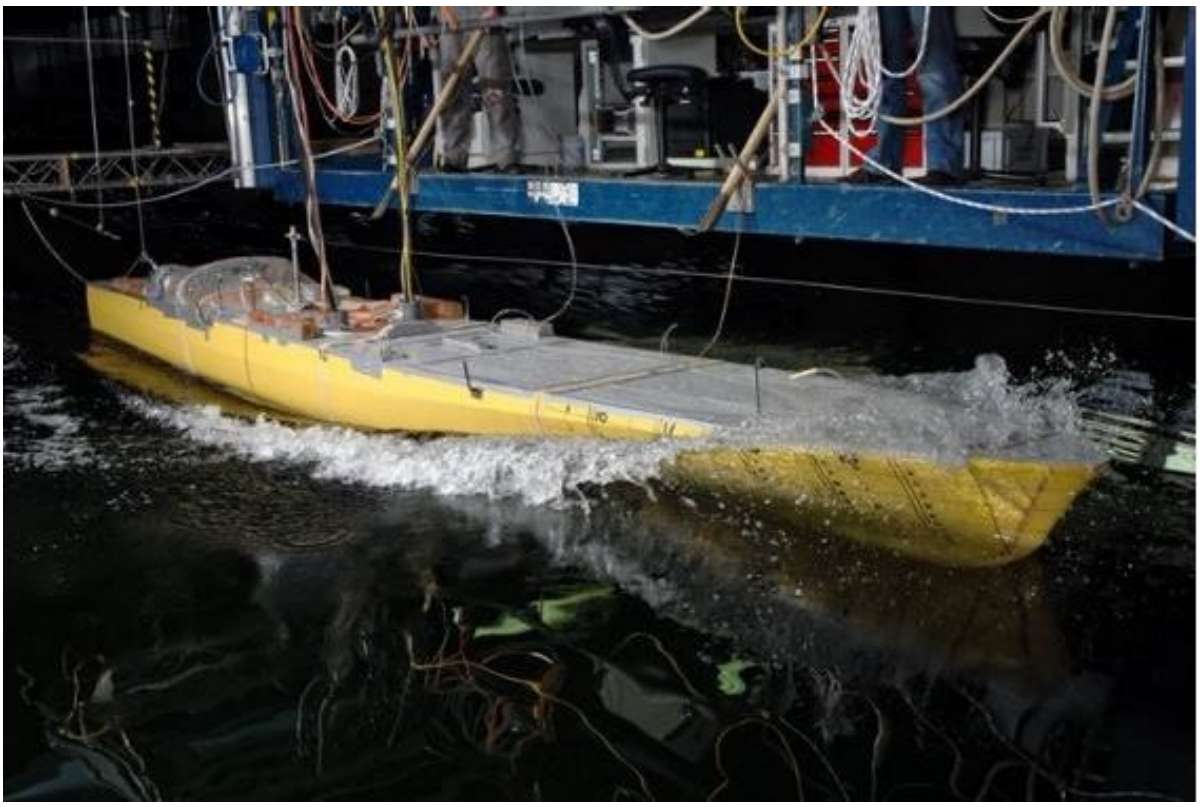

Figure 1.1: Wavebreaking during the FDS model test

can be achieved using a reasonable number of cells. Details regarding this research can be found in chapter 4. The findings from this study are implemented in this research and tested for their effect on the wave propagation.

1.3. Problem definition and scope

The primary research objective is to determine the applicability of CFD to predict the added resistance in waves. In order to do so, the error and uncertainty of the solution must be determined in a process which is known as verification and validation. The uncertainty is determined using a grid refinement study as described in paragraph 2.4.2. The error is determined by comparing the result from the simulation to the result from the model test. The primary research objective is formulated as:

Conclude on the applicability of CFD for wave added resistance predictions by assessing the error and uncertainty of the solution

For fast sailing vessels, no standard procedure for the estimation of the added resistance in waves using CFD has yet been developed. It is therefore that the secondary research objective states:

Establish a procedure for the prediction of the added resistance in waves for a fast sailing hull form using CFD

The scope of this research will now be explained in the rest of this paragraph.

At DSNS the wave added resistance estimation will be used to determine the speed that a vessel can maintain in a seaway as well as to improve the design of the ship. For these purposes only the time-averaged wave added resistance is of interest. Therefore this single value, and not the wave added resistance time trace is requested from this research.

It is convenient to be able to extrapolate the added resistance to other encountered wave heights using a Transfer Function (TF). The added resistance in waves is proportional to the square of the amplitude of the wave ζ^2 [30]. Due to this quadratic relation a QTF is required for this purpose. Therefore the

time-averaged wave added resistance is converted to a QTF by dividing it by ζ^2.

Furthermore, it is the wish of DSNS to determine the QTFs over a range of wave frequencies so as to capture the wave added resistance for multiple wave heights and frequencies. Therefore the procedure for the estimation of the added resistance in waves should not just work for one wave frequency, but work for a range of frequencies.

This research restricts itself to regular waves from ahead. This is done for multiple reasons. First of all because the largest added resistance is experienced in head waves. Second because the simulations will be validated with the data from CRS model tests which were also performed in regular head waves. Third, simulating the added resistance in waves in regular waves is much more economical than irregular waves as the latter requires very long simulation times represent the irregular wave spectrum in a statistical sense [2].

In this research the numerical solver ReFRESCO is used. This solver is under continuous development an MARIN. In chapter 3.2 this theory behind this solver and its use is discussed. The scope of this research limits itself to the use of this CFD solver only.

Furthermore, this research focuses on the added resistance due to waves. Therefore, all other resistance components except for the vessel's resistance in calm water are considered to be outside of the scope of this research.

More details regarding the scope of this research are described in the remainder of this chapter as well as in chapter 2 where the theoretical background is discussed.

1.4. Research approach

In this paragraph the research approach will be explained. This is divided into three main parts. First the complexity of the problem is reduced. Second, the approach used to determine the time averaged wave added resistance is explained. This second step requires relatively complex simulations. To give structure to the approach of such complex simulations a stepwise procedure is used which is explained in the third part.

Part 1: Reduce complexity The purpose of this research is to predict the added resistance in waves for a fast sailing hull form using CFD. Different approaches can be used to reduce the complexity of these expensive unsteady (time dependent) computations. The simplifications were selected in such a way as to have minimal effect on the resistance prediction. A first advantage of this approach is that it will reduce the cost of the simulations and the time that they will take to run. Second, it is much easier to evaluate a simplified problem compared to a more complex one. Three main simplifications are applied to the problem:

1. In this research only half of the vessel will be simulated, See figure 1.2. Theoretically this halves the computational power required. The idea behind this is as follows. The vessel is only simulated in head waves. Therefore the flow around the hull and the resulting the forces and moments on the hull are all symmetrical. This means that the forces and moments on the vessel are either zero (transverse force, roll and yaw moment) or are double the value of the force/moment that acts on the half vessel. By simulating half of the vessel it is possible therefore possible to determine all the forces and moments acting on the complete hull.
2. A second reduction in the complexity of the problem is that frictional resistance is neglected. The complete details regarding this decision are given in paragraph 2.1 where the theory behind wave added resistance is described. The short explanation is that it has been proven that the frictional resistance component of the wave added resistance is at least an order of magnitude smaller than the potential resistance component. Capturing this small component of the friction would require a significant increase in the complexity of the simulation resulting in increased computational time and cost.
3. The third reduction in complexity of the problem is that the vessel is simulated with 2 DoF, namely heave and pitch, instead of the full 6. The idea behind this is that heave and pitch are the motions that influence the wave added resistance the most. This is explained further in paragraph 2.1. Furthermore, a vessel is sailing in head waves theoretically should not experience any sway, roll

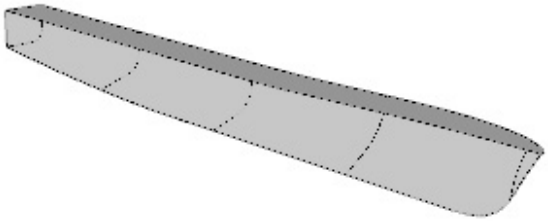

Figure 1.2: Geometry of half of the vessel

or yaw motions. If the vessel were free to move in surge direction it would not be possible to determine the total resistance in waves at a constant specified speed since its speed would be influenced by the encountered waves. This surge motion would thus influence estimation of the added resistance. Therefore, the vessel's surge motion has to equate to zero.

In part 2 the procedure that will be used to estimate the added resistance in waves using CFD is explained.

Part 2: Estimation of the added resistance in waves

A general procedure for the estimation of the added resistance in waves using CFD is described in the International Towing Tank Conference (ITTC) recommended procedures and guidelines 7.5-02-07-02.8 [1]. This procedure is followed in this research. In the rest of this paragraph this procedure and the implementation in this research is explained. In figure 1.3 a flowchart of the approach is shown.

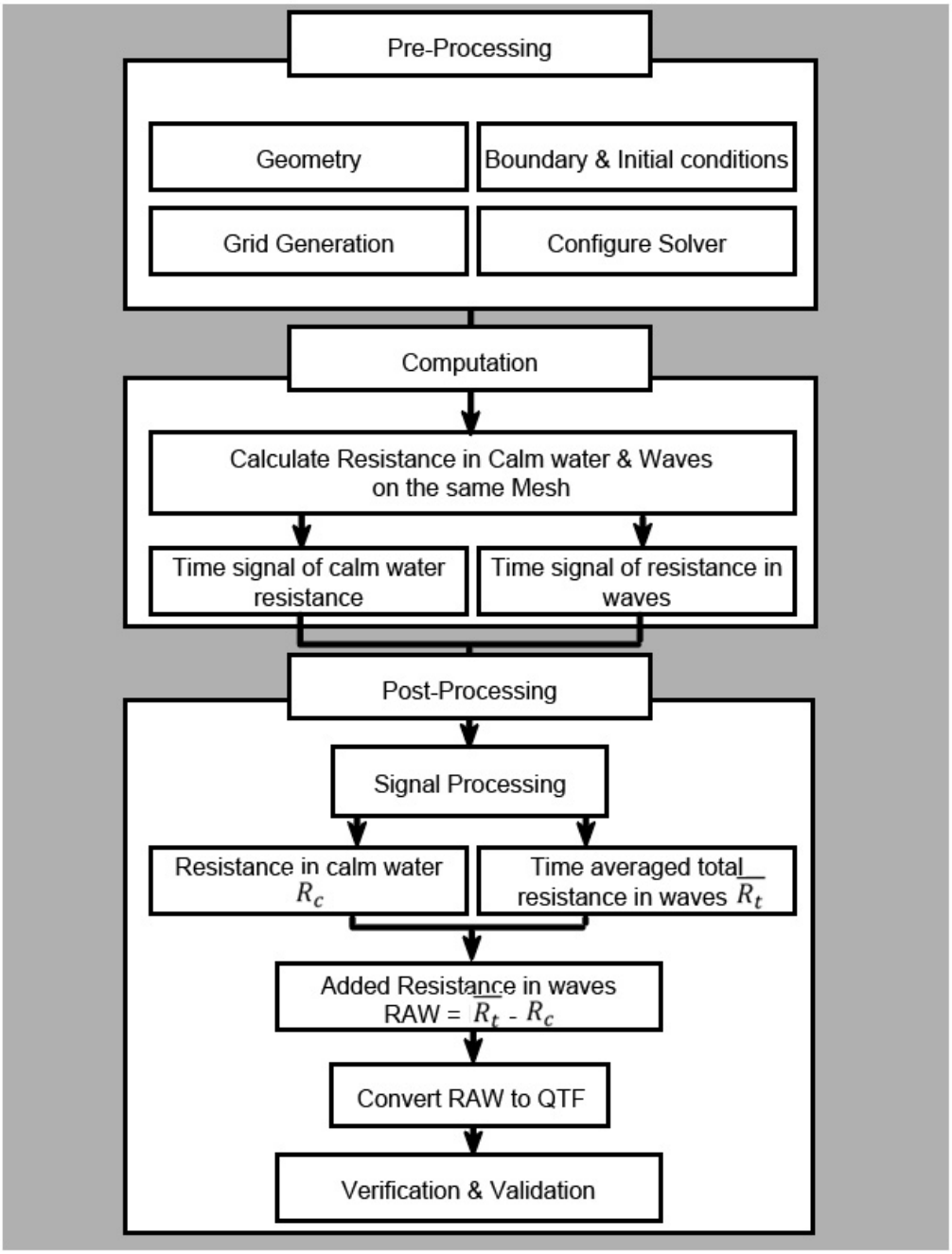

Figure 1.3: Flowchart for the estimation of the added resistance in waves with CFD

The procedure consists of three main steps, pre-processing, computation and post-processing. These are described in the rest of this part:

Pre-processing The pre-processing is composed of defining the geometry of the vessel and domain, setting boundary and initial conditions, the configuration of the solver and grid generation. In this research ReFRESCO is used as a numerical solver and the grid is generated using HEXPRESS by Numeca. More information on the geometry, boundary/initial conditions, ReFRESCO and HEXPRESS can be found in chapter 3.

Computation To obtain the added resistance in waves two different simulations are required. One with the vessel sailing in calm water and the other with the vessel sailing in waves. According to the ITTC[1] the grid should be maintained as identical as possible in both simulations to keep numerical errors induced by the grid the same. For both simulations time traces of the resistance felt by the vessel are generated. These are known as the calm water resistance and the total resistance in waves. The idea is to subtract the calm water resistance from the time averaged total resistance in waves. This way the time averaged added resistance in waves is obtained. Here the five steps A through E that are performed in this procedure are explained in more detail. Step A and B are part of the computation step while step C through E are part of the post processing step.

- A: Determine calm water resistance time trace.

  In this step the vessel is simulated sailing in calm water at a constant speed. This speed corresponds to the speed at which the wave added resistance is to be determined. The vessel keeps sailing until the measured resistance converges. This is the resistance that the vessel feels when it is sailing at the specified speed in calm water and is known as the calm water resistance. See figure 1.4 for a time trace of the stabilising calm water resistance. The second plot, shown in red, features a zoomed in section of the first plot. From this plot the convergence of the signal can be seen clearly.

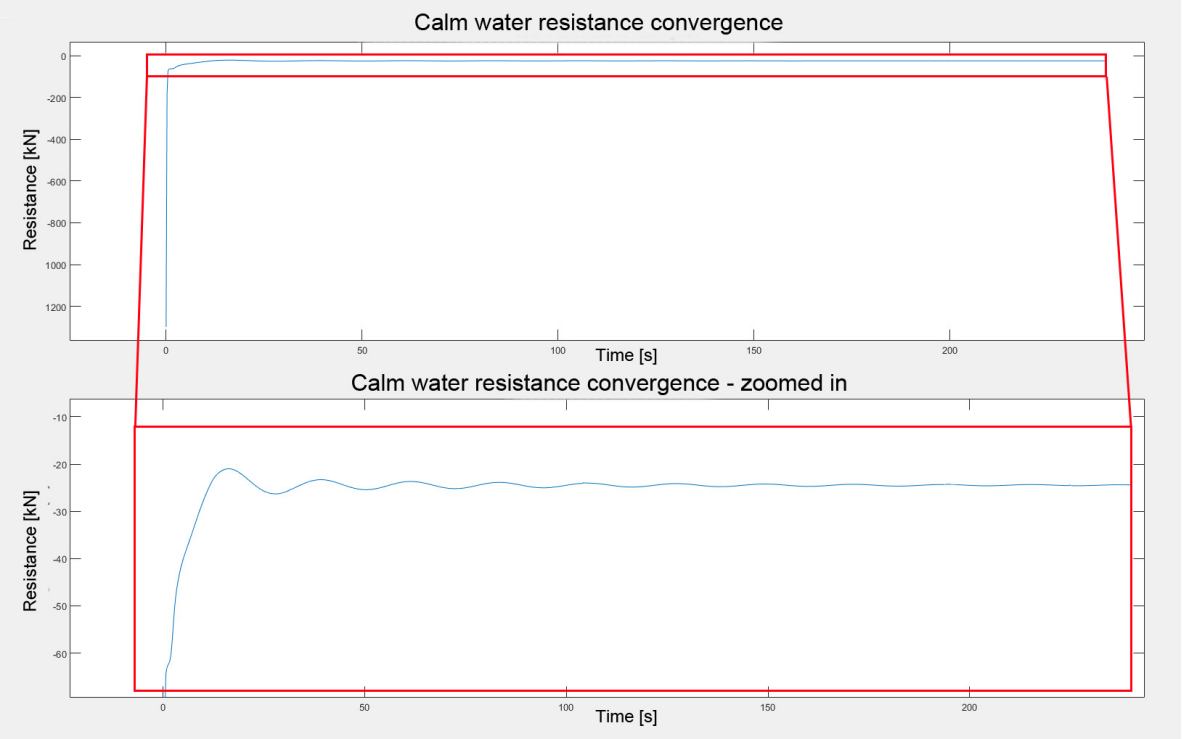

Figure 1.4: Typical calm water resistance time trace

- B: Determine total resistance in waves time trace.

  Next the same vessel sails at the same speed in regular head waves with the amplitude and frequency of interest. The resistance felt by the vessel sailing forward is known as the total resistance in waves. This resistance is influenced by the wave and is therefore time dependent. Only the time average of this signal is of interest. In order to determine this average with suffi-

cient accuracy two rules are followed. First, the resistance is monitored to determine when has converged. Converged in this case refers to a constant repeating pattern without a change in the mean over time. After that, according to a recommendation by the ITTC [1], the simulation will run for ten more wave encounters. In figure 1.5 a plot is shown of a typical total resistance in waves measurement. Indicated are the time when the signal has converged and the 10 encountered waves.

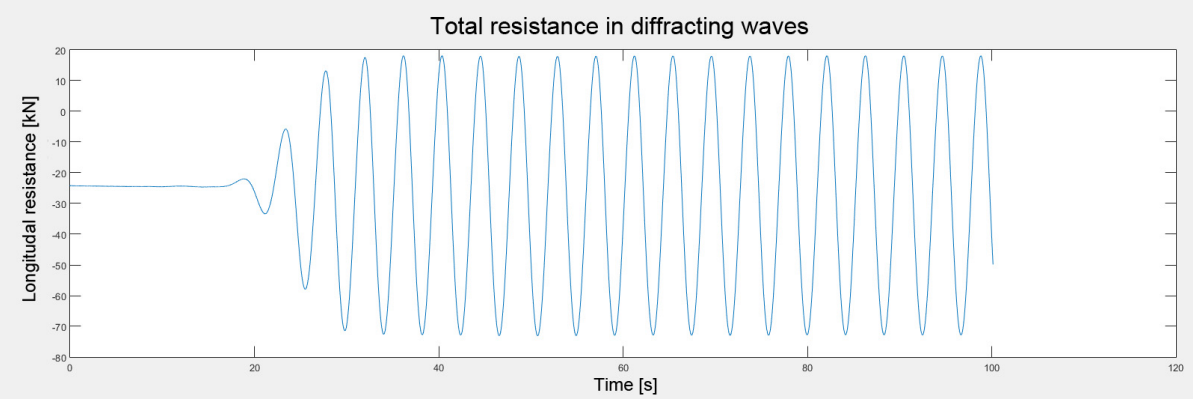

Figure 1.5: Typical total resistance in waves time trace

Post-processing

In the post-processing phase, first, the calm water resistance and time averaged total resistance in waves are determined.

- C: Determine calm water resistance R_c

  The calm water resistance R_c equates to the converged value of the calm water time trace.

- D: Determine time averaged total resistance in waves $\overline{R_t}$

  The time-averaged total resistance in waves $\overline{R_t}$ is determined by taking the time average of the resistance signal over these last ten wave periods.

From these two values the time averaged added resistance in waves $\overline{R_w}$ can be determined.

- C: Determine time averaged added resistance in waves, The time averaged wave added resistance is then obtained by subtracting the calm water resistance from the time averaged total resistance in waves.

$$\overline{R_w} = \overline{R_t} - R_c \tag{1.1}$$

The obtained wave added resistance is then converted to a QTF by dividing it by the square of the wave amplitude so the resistance can be extrapolated to other wave amplitudes.

The main research objective of obtaining the time averaged added resistance in waves is now completed. The next step is to verify and validate the result.

The verification consists of the estimation of the numerical uncertainty of the solution. The is done through a procedure developed by L.Eça and M.Hoekstra [25], based on a grid refinement study. This method is described in detail in paragraph 2.4.2. Finally the validation is performed by comparing the results to the results from the CRS ship model tests.

In a general sense the research approach is now clear. However, simulating a vessel in calm water and waves is quite a complex task. Therefore, this complex simulation task it is divided up into several small steps which build up to the complex simulations.

Part 3: Stepwise simulation approach Several steps are taken to build up to the simulations of the vessel sailing at speed with 2 DoFs in calm water and waves. The advantage of this approach is that it is possible to evaluate the influence of each small step taken instead of having to oversee the large and complex problem at once.

- The first step is to simulate the generation and absorption of waves in an empty domain. According to the ITTC [1] it is of importance to accurately generate and propagate the incident waves in order to make an accurate estimation of the added resistance in waves. This is because inaccuracies in the wave height and length will result in inaccuracies in the resistance prediction . The purpose of this simulation is to set up a configuration that can be solved efficiently and that will generate waves propagating with a constant height and length within the domain. Research performed by Rapuc et al [28] is used as a basis for this step. This step is discussed in chapter 4

The second and third step ensure that the vessel's responses to both waves and motions are correct. D.L.Chow and K.A.McTaggart [13] have validated that the potential flow code based solvers such as PRECAL are capable of accurately estimating these responses. To determine if the vessels responses, as determined with CFD, are correct, they will be compared to the responses calculated using PRECAL.

- The second step is to ensure that the excitation force due to the incoming wave is correct. Here, the static vessel is simulated in regular head waves as the waves diffract off of the hull. The phasing and amplitude of the induced force in heave direction and moment in pitch direction are then compared to PRECAL. In chapter 5 this step is further explained.
- The third step is to ensure that the reaction force on the vessel as it moves in heave and pitch in the water is correct. Here, the vessel is simulated, sailing in calm water as it is forced to periodically oscillate in heave and pitch whilst radiating waves away from it. From this simulation, the phase and amplitude of the reaction force in heave direction and reaction moment in pitch direction are determined. These are then converted to the vessel's added mass and added damping so they can be compared to PRECAL. In chapter 6 this step is further explained.
- Finally, all the learnings from the previous three steps are combined. This final setup is now capable of accurately simulating incoming waves as well as simulating the vessel that has the correct response to both the waves as well as it's motions. The combined setup is used to simulate the vessel as its sailing with 2 DoFs in regular head waves. These simulations are discussed in chapter 7.

1.5. Automation

The proposed procedure for the prediction of the added resistance in waves using CFD is automated using a python script. These script is set up in terms of general parameters such as the vessel's dimensions and speed at which it sails. This way the procedure is applicable to other vessels and test cases.

1.6. Thesis outline

This thesis is structured as follows. In this first chapter the introduction and research approach are described. A literature study regarding wave added resistance, CFD and verification and validation is found in chapter 2. This is followed by chapter 3, which describes the numerical setup of the simulations. Details regarding the software used for the grid generation (HEXPRESS) and numerical solving of the problem (ReFRESCO) are found here. In this same chapter the domains used for all the different simulations are also presented. In chapter 4, 5 and 6 the simulations of consistently propagating waves, diffracting waves and radiating waves are covered. In each of these chapters the used approach is verified through a grid refinement study. The vessel's responses, determined in the diffracted and radiated wave simulations are compared to PRECAL to ensure that they are correct. From these studies guidelines for efficient and accurate simulations are derived. In chapter 7 the knowledge gained from the past 3 chapters is bundled and used to simulate a vessel with 2 DoFs both in calm water and waves. Finally this thesis is concluded with chapter 8 and 9 which cover the conclusions and recommendations.

2

Literature study and background

The aim of this chapter is to inform the reader on the theoretical background of this research. This chapter covers theory regarding wave added resistance, CFD and the errors and uncertainty in CFD.

2.1. Wave added resistance

The extra resistance that a vessel experiences when it is sailing in waves compared to when it is sailing in calm water is known as the added resistance in waves. Basic principles regarding the added resistance in waves are explained in 2.1.1.

Added resistance in waves is of interest of naval architects and shipyards as it can increase the resistance that a vessel experiences significantly. As waves are a phenomenon that a ship encounters on a regular basis this is a resistance that has to be accounted for. According to J.J.Blok [7] the added resistance can be responsible for up to 50 percent of the total resistance depending on the type of vessel and it's speed.

J.Strom-Tejsen et. al. [30] stated that in the past this added resistance was estimated either by adding between 15 and 30 percent to the calm water resistance, or by performing model tests. More information on the estimation of the added resistance in waves through model tests is given in paragraph 2.1.2. Later in the 1950's, when seakeeping analysis based on potential flow theory came into existence, analytical methods for the estimation of the added resistance were developed. In paragraph 2.1.3 more can be found on these analytical methods. This paragraph does not constitute an exhaustive survey of all known analytical methods but rather is a summary of several important methods.

In recent years, an increase in available computational power has made it possible to estimate the added resistance in waves numerically using CFD. The fundamental idea behind CFD is to use a numerical method to approximate a solution to the (simplified) Navier-Stokes (N-S) equations which define fluid flows. Information on the theory behind CFD and its application in relation to the estimation of the added resistance in waves can be found in 2.2.

2.1.1. Basic principles of added resistance in waves

A ship at speed experiences a resistant force due to the two fluids, water and air through which it moves. J.J. Blok [7] stated that even though the density of air is about a thousand times smaller than that of water, the resulting forces can be of equal order of magnitude due to the higher air flow velocity. As this research focuses on the added resistance due to waves, resistance due to wind and the effect of the superstructure are not accounted for.

As stated in the TU Delft reader Offshore Hydrodynamics [21], engineer, hydrodynamicist and naval architect W.Froude was the first to recognize that the total resistance that a vessel experiences when sailing through water can be broken up into two different parts. A frictional resistance, due to the viscosity of the fluid, and a residual resistance which is caused mainly pressure on the hull due to the wave system set up at the surface of the water.

In practice the resistance in water is decomposed in the resistance in calm, undisturbed water plus a variety of additional effects known as added resistances. Examples of such added resistances are for example the added resistance due to roughness of the surface of the body, due to a change in attitude (trim, heel, drift angle) and due to bottom effects (shallow water effects).

The added resistance in waves is the extra resistance that a vessel experiences when it encounters waves. G. Vossers [32] stated the wave added resistance in head waves consists mainly of these components.

- ”Radiation force” Resulting from the waves generated by the vessel, mainly due to its heave and pitch motions.
- ”Diffraction force” Resulting from the incident waves reflecting off of the vessel.

These components are related to changes in pressure on the hull of the vessel and are thus of potential origin. Only a very small part of the added resistance in waves occurs due to viscous friction. It can therefore be said that the added resistance due to waves is considered a non-viscous phenomenon. J.J.Blok [7] has proven in his 1993 dissertation that the increase of this frictional resistance is at least an order of magnitude smaller than the potential resistance. .

Capturing this relatively small frictional component with CFD would significantly increase the simulation time and cost as it would require the simulation of the boundary layer at the hull. Taking the small contribution of this effect and the significant extra costs it would take to capture it into consideration, the decision was made to not simulate this frictional resistance. The assumption is that frictional effects will have a marginal contribution to the added resistance in waves. This same conclusion was drawn by J.Strom-Tejsen et. al. [30] in his paper on the added resistance in waves as well as by J.J. Blok [7] . Validation with the model test results will point out if this assumption is justified.

Moreover, the conclusion can be drawn that a CFD simulation that is capable of capturing the resistance due to radiating waves and due to diffracting waves separately would also be capable of capturing the resistance of a vessel sailing free in waves.

Let us further specify the pressure based wave added resistance. When a ship is sailing in regular waves the ship experiences oscillating pressures on the hull. These oscillating pressures are partly caused by the motion of the free surface and partly due to the oscilatory motions of the ship itself. The integration of these oscillating pressures on the hull yields an oscillating force with a non-zero, time-averaged mean value. The longitudal component of this time-averaged force is what is known as the time-averaged wave added resistance.

J. Strom-Tejsen et al. [30] also researched the wave added resistance from an analytical point of view and, based on their research they were able to draw several general conclusions regarding this resistance.

1. The added resistance in waves is proportional to the square of the wave amplitude
2. The added resitance in waves is independent of the calm-water resistance
3. The added resistance in head waves depends mainly on the heave and pitch motion of the vessel
4. The added resistance in waves depends on the motions and their phase relation to the wave field
5. The maximum added resistance in waves will occur in the region of heave and pitch resonance

The first conclusion forms the basis for use of a QTF to extrapolate the found added resistance in waves to other wave amplitudes. This QTF is calculated by dividing the added resistance in waves by the square of the wave amplitude. The second conclusion states that it is impossible to compute the added resistance in waves from the calm water resistance. From the third, fourth and fifth conclusion it becomes clear that accurate simulation of the phase and motion of the vessel’s heave and pitch in relation to the waves is of importance.

Now that the basic principles of the added resistance in waves are known, it is time to focus on various techniques and methods that are/were used to determine this added resistance.

2.1.2. Experimental techniques

Determination of a vessel's added resistance in waves is possible through the use of experimental procedures. In this sub-paragraph the most commonly used towing tank test method is explained. The purpose of this paragraph is not to elaborate on the details of towing tank tests in general, but rather to focus on the specifics that distinguish of this type of towing tank test. For a detailed explanation regarding this test method and others the reader is referred to the paper by J.Strom-Tejsen et. al. [30].

The most commonly used towing tank test method used to estimate the added resistance in waves is known as the 'constant velocity method'. In this method a scale model of a ship is attached directly to a sensor measuring the longitudal resistance felt by the vessel. This sensor is then bolted straight to the towing tank carriage which pulls the ship forward at a constant velocity. This way there is no velocity difference possible between the carriage and the model. In this setup the model can move free in heave and pitch direction and is constrained in surge, yaw, roll, and sway. In figure 2.1 a typical towing tank setup is shown. The carriage can easily be distinguished as it is painted in orange.

Figure 2.1: Typical towing tank setup - Seoul national university [6]

To determine the added resistance, the model is towed at the speed under consideration in both calm water and regular head waves. In these tests the longitudal resistance, ship speed, wave frequency and wave amplitude are measured. Next the time-averages of the measured resistances for both calm water and waves are calculated and subtracted to determine the time-averaged added resistance in waves.

A problem in this method is that the added resistance is obtained as a rather small difference between the resistance measured in calm water and waves. Therefore even small inacuaracies in the individual measurements can result in sizable errors in the added resistance. G.K. Kapsenberg [18] has shown that even a small error of 2% in both measurements can result in an error ranging between 5 and 22.5 % in the calculated added resistance. The size of this error is dependent on the size of the added resistance in relation to the total resistance in waves.

An interesting fact is that the scale of the model is not as important in this study as it may be in other resistance tests performed in a towing tank. From practice it is known that even small models are very suitable for accurate measurements of added resistance in waves. This is explained by a conclusion in paragraph 2.1.1, namely that the added resistance in waves is primarily a nonviscous effect.

2.1.3. Analytical methods

With the development of seakeeping as a branch of science in the 1950's the opportunity opened up to make predictions of wave added resistance in a theoretical fashion. According to J.J.Blok [7] these theories can be categorised into five main categories. . This paragraph will give an overview of these categories as well as a summary of some of the most important theories within them. The five main categories are:

1. theories based on energy conservation
2. theories based on momentum considerations
3. theories based on pressure integration over the wetted surface
4. theories based on the 'ray' theory of reflection
5. computational models based on regression of model experiment data

It must be noted that some existing theories are combinations of the mentioned approaches. The first four theories are all based on potential theory.

Theories in the first category are based on potential damping. The moving ship creates waves which radiate away from the vessel which. This process draws energy from the ship and transfers it in the form of waves to the surrounding water. This energy equates to the work that is done by the ship on the water. This work can only be withdrawn from the propulsive power. The radiated waves can be determined using strip theory based methods.

Theories from the second category are based on the momentum equation applied to a volume of fluid. This volume has an inner boundary, which equates to the hull of the ship, and an outer boundary, which can be imagined to be located at a sufficiently large distance away from the ship. The change in momentum of the flow of the fluid through those two boundaries is then related to the force that the fluid exerts on the ship. Green's theorem is used here to transfer the integration over the hull to the outer boundary. This makes it possible to perform the whole integration just over the outer boundary far away from the ship.

Theories that fall under the third category are based on the Bernoulli equation to determine the pressure on the hull based on the flow velocity of the fluid near the hull surface. The force on the hull is then found by integrating the pressure over the surface of the hull.

Theories in the fourth category are also based on potential theory. The idea behind these theories is that very short, high frequency waves reflect completely of the vessel which results in an added resistance. "Ray" theory based solutions are therefore only usable for very short waves.

In general it can be said that theories for the estimation of the added resistance in waves based on potential flow can work very well in some cases. For container ships for example potential flow based solutions approximate model testing based solutions very well. They do have their shortcomings though. Viscous effects are not taken into consideration and non-linear effects such as wave breaking are not captured. For fast sailing vessels with a breaking bow wave, such as the FDS for example, this results in an over estimation of the added resistance in waves.

Finally, the fifth category contains methods that are based on the regression of the results from a large number of model tests. These methods analyse the results from many tests based on parameters such as the length, draft, beam and block coefficient of the vessel but also the speed and seastate. They try to derrive relations for a certain type of hull form with coefficients that fit within a certain bandwidth. For ship designs that fall within the specifications, the results from these regression based models can be very accurate and useful.

2.1.4. Concluding remarks

Determining the added resistance in waves is a challenging task. Model testing has shown to be capable of predicting the added resistance in waves for all model ships, ranging from large container vessels to high-speed hull forms. This does come at a price though, as model testing is both expensive and time consuming. Furthermore the error on the estimation can be sizable as the wave added resistance is a relatively small quantity that is determined by subtracting two large numbers that are each subjected to a small error. Analytical methods based on potential flow theory have shown their value for certain hull forms, showing results similar to those from model testing. Between the different methods though the results do vary significantly. Also, as viscous effects and non-linearities such as wave breaking are not captured these methods are not suitable for every hull form and case. This is where methods based on CFD could have the potential to improve the accuracy of the estimate.

2.2. Computational Fluid Dynamics

This sections gives an introduction into CFD and the theory behind it. This includes the governing equations that describe the fluid flow, as well as the boundary conditions that define the interaction between the fluids and surfaces. A further look is given into different CFD simulation and grid types as well as the numerical procedure that is used in this simulation.

2.2.1. Governing equations

The equations that govern the flow of a fluid are also known as the N-S equations. These represent the conservation of mass, momentum and energy. For this thesis the conservation of energy is of less importance and is therefore not treated in this section. A formulation of these equations including a description of the terms within them is given in this subsection. For a more detailed description the reader is referred to the book on the theory behind CFD by F.Moukalled et. al. [26]

Conservation of mass:

The continuity equation represents the conservation of mass in fluid dynamics. It states that the rate at which mass enters the system must be equal to the rate at which the mass leaves the system, assuming that no mass is generated within the system. The differential form of this equation is shown in equation 2.1. Here u_i represents the velocity vector and x_i represents the spatial vector.

$$\frac{\partial u_i}{\partial x_i} = 0 \tag{2.1}$$

Conservation of momentum:

The Navier-Stokes momentum equation describes the conservation of momentum in a flow. It can be seen as Newton's second law of motion for fluids. For an incompressible flow it is represented by equation 2.2.

$$\frac{\partial u_i}{\partial t} + u_j \frac{\partial u_i}{\partial x_j} = -\frac{1}{\rho}\frac{\partial p}{\partial x_1} + \nu \frac{\partial^2 u_i}{\partial x_j \partial x_j} + f_e xt \tag{2.2}$$

In this equation the two terms on the left side represent the local acceleration and transportation and correspond to the inertial forces that are applied to the fluid. On the right side the terms from left to right represent the local pressure gradients, viscous forces and all the external forces that are applied to the fluid. There are a total of seven known variables and four unknown variables in the two equations described in this subsection. The known variables consist of the three spatial coordinates **x**, **y**, and **z**, here represented with x_i , the density of the fluid ρ, kinematic viscosity ν, external forces $\mathbf{f_e xt}$ and time **t**. The external force in this research consists of the gravitational force. These variables are specified by the fluid used in the simulation, the domain and the surroundings. The unknown variables are the three components of the velocity **u**, **v**, and **w**, here represented with u_i , and the pressure **p**. Since there are four equations (conservation of mass and the three Navier-Stokes momentum equations) and four unknowns, this system can be solved.

2.2.2. Boundary conditions

In CFD simulations boundaries are used to direct the flow. For instance, they are used to define how the flow enters and exits the domain and how the flow interacts with a solid placed in it such as the hull of a ship. In ReFRESCO a variety of different Boundary Conditions (BCs) are available. The ones used in this research are covered here in general, for a more detailed description the reader is referred to the ReFRESCO theory Manual [3]

At the inlet of the domain the flow is simulated by specifying the inlet velocity. The pressure at the boundary is extrapolated from the interior. At the outflow boundaries the flux is evaluated using zeroth order extrapolation, implying that the cell center values substitute the face value. Another way to simulate outflow boundaries is to use a pressure boundary condition. In this boundary condition the pressure is specified on the whole boundary. The velocities are then extrapolated.

To simulate the interaction between the fluid and a solid surface such as the hull, a wall boundary condition is used. Two options here are to use either a slip or a non-slip wall BC. Both specify that the normal velocity of the fluid relative to the wall must be zero. This condition ensures that the wall will not leak. The difference between the two wall conditions is the non-slip condition. This condition specifies if the effect of shear stress is modelled or not. When using the non-slip wall, the tangential velocity of the fluid at the surface equals that of the solid. This way it mimics the actual behaviour of a flow near a surface. In the case of the non-slip wall however, the tangential velocity of the fluid at the surface of the solid is not influenced by it. This simplifies the problem and can be useful in certain cases. For example when the user is not interested in the frictional effects between the fluid and the surface.

Finally the last BC used is the symmetry BC. This BC in ReFRESCO is identical to the slipwall BC. It has zero normal velocity and zero normal gradient on all terms. It is used when the physical geometry of interest and the expected flow pattern have mirror symmetry at the plane where this BC is used.

2.2.3. Simulation types

Fluid flows are governed by Partial Differential Equations (PDE) which represent conservation laws for mass, momentum and energy. These are also known as the N-S equations. It is believed that any flow can be resolved with this set of equations.

As stated by Prof. D. Kuzmin [24] of the Dortmund University of Technology in his introductory course to CFD, *'CFD is the art of replacing such PDE systems by a set of algebraic equations which can be solved using computers'*.

There are several ways to numerically solve flows available. When it comes to computational effort, the most demanding type of simulation is Direct Numerical Simulation (DNS). DNS solves the system directly which requires that the whole range of spatial scales of turbulence must be resolved in the domain. A consequence of this is that the computational cost of simulations with large Reynolds numbers i.e. high turbulence become very high. For Reynolds numbers encountered in industrial applications the computational requirements are deemed too high for practical purposes. That is where alternatives, such as Large Eddy Simulation (LES) and Reynolds averaged Navier-Stokes (RaNS) are used. The principle idea behind LES is to reduce these costs by only looking at the longer length scales when solving the N-S. LES solvers demand less computational power than DNS but can still be expensive. For industrial applications RaNS solvers are often used. These solvers use time-averaged versions of the N-S and models to approximate turbulence which result in the average flow as an output. The use of this method significantly reduces the computational requirements.

As wave added resistance is considered an non-viscous phenomenon only the forces due to pressure are of interest in this research. Therefore it is not necessary simulate the boundary layer at the hull in order to determine the viscous forces. As the viscous effects are not simulated, it becomes possible to use use DNS to solve the problem. Rather than using a very fine grid to resolve the whole range of spatial scales of turbulence within the boundary layer, a relatively coarse grid is used in combination with a slip wall BC on the hull. This way no boundary layer will develop, nor will the solver attempt to solve it.

2.2.4. Grid

Numerical methods are based on a discrete representation of the solution. This therefore requires the computational domain to be spatially discretized. This is done by a procedure called meshing Meshing means discretely representing the geometry that is to be solved. Basically, the domain is divided up into elements, also known as cells, over which the equations can be approximated. The resulting discretisation of the domain is called the grid. In general there are two main grid types that can be distinguished, namely structured and unstructured grids. Examples of both types can be seen in figures 2.2 and 2.3.

Structured grids

Structured grids comprise of internal cells that are topologically similar and all have the same number and type of connections to neighbouring cells. The term ”structured” refers to the structure provided to the organisation of the cells in an array. In a structured grid it is possible to know which cells are adjacent to one cell implicitly. In other words, a point in the grid numbered (i,j,k) has neighbours (i+1,j,k), (i-1, j,

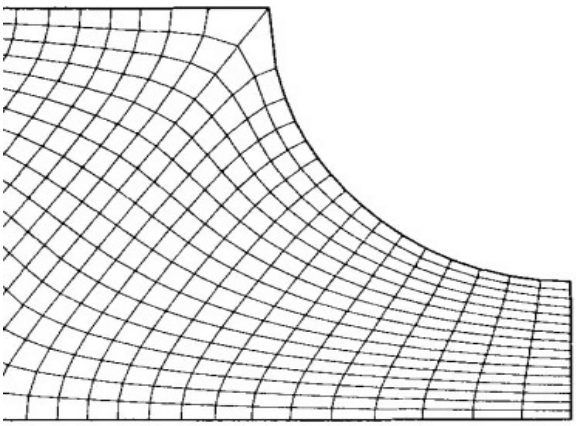

Figure 2.2: Structured grid

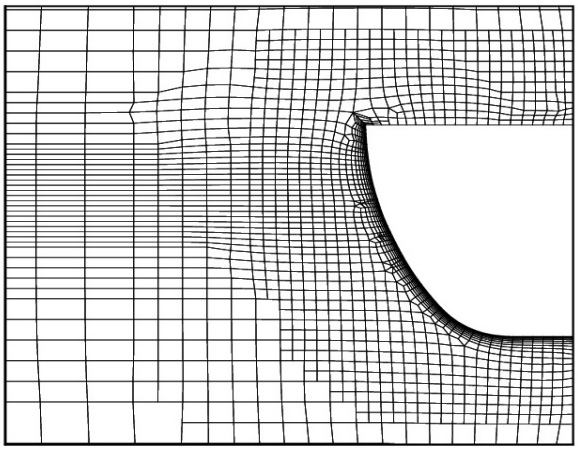

Figure 2.3: Unstructured grid

k), etc. [9]. See figure 2.4. The advantages of such a grid are that they have a simple data structure and in general can be solved more efficient. The downside however is that for complex geometries it can become very difficult to construct a structured grid.

Unstructured grids

Unstructured grids have can have elements with an arbitrary topology and there is no general rule to describe a cells connectivity with its neighbours. Due to this arbitrary topology and lack of general rule for connectivity it is not possible to structure the location of cells in the way that was done for a structured grid. In order to keep track of the position and connections of each cell a connectivity matrix must be used which complicates the data structure. See figure 2.5. The advantage of a structured grid is that it can handle complex geometries, such as the hull of a ship very well. For this very reason unstructured grids were used in this research.

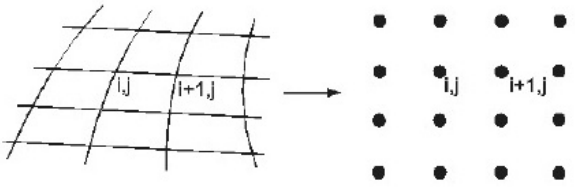

Figure 2.4: Simple structured cell data structure

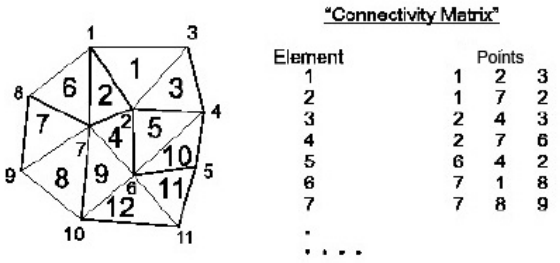

Figure 2.5: Complex unstructured cell data structure

2.3. Minimising reflections

In real life, when a wave propagates at sea, it propagates in an almost infinite domain. With CFD simulations however, due to computational restrictions, waves propagate within a finite domain. To simulate a wave properly, it should just disappear once it reaches the boundary of the domain. A problem occurring in CFD simulations with propagating waves is the inability of the domain boundary to absorb the propagating waves and reflecting them back into the domain. In ReFRESCO two possible solutions for this problem are available.

One solution is to use a Sommerfeld BC. This BC aims to be transparent to the waves in order to avoid reflections. As concluded by V.Denisart in his 2018 paper [12] "this boundary condition is very effective to absorb a single wave, propagating perpendicular to the boundary at a known frequency. However, it does not allow to absorb an irregular wavefield or the radiated spectrum coming from a marine structure". Although this is exactly the case that is simulated here, later on, reflections will be diffracted and radiated by the vessel in all directions and over a range of frequencies. Therefore, a second method which is able to absorb waves over a range of frequencies and propagating in multiple directions is used.

This second solution uses so called "Relaxation Zones". A relaxation zone progressively replaces the CFD solution towards the edge of the domain by the original propagating wave as created at the inlet boundary. This way no reflection problem occurs at the boundary of the domain, as the original wave is known and can easily be let through.

2.3.1. relaxation zone

The relaxation zone is dimensioned by setting up an inner and an outer three dimensional ellipse. The area within these two ellipses is what is known as the relaxation zone. This zone is configured by specifying the origin, the radii of the inner and outer ellipses and a squareness coefficient. This coeficient determines how round or square the ellipses will be. See equation 2.3.

$$\left(\frac{x-x_0}{r_x}\right)_f^n + \left(\frac{y-y_0}{r_y}\right)_f^n + \left(\frac{z-z_0}{r_z}\right)_f^n = 1 \tag{2.3}$$

Here, (x_0, y_0, z_0) are the coordinates of the origin of the ellipse. (r_x, r_y, r_z) are the radii in x, y and z-direction of the ellipse and n_f is a form factor for the ellipse. This must always be an even number in order to maintain an elliptical shape. A low coefficient, such as for example two results in a rounded ellipse, where as a high number, for example 50 will result in a relaxation zone that is close to rectangular .

In the area within the inner ellipse, the full CFD solution is used. Outside of the outer ellipse, the solution consists only of the original wave as created at the inlet boundary. In the area within the two ellipses the solution consists of a mixture of both solutions. The so called "relaxation factor indicates the ratio between those two solutions. When the relaxation factor equals zero the solution comprises only of the solution calculated with CFD, which is the case within the inner ellipse. Outside of the outer ellipse, the relaxation factor equals one which means that the solution here consists only of the original wave. Within the two ellipses, the relaxation factor is calculated using either a cosine or an exponential function. The exact definition of the used functions is quite extensive and will not be covered here. For a detailed description the reader is referred to equations 3.2.2.4, 5, 6.B and 7.B documented in V.Denisart's report on wave absorption [12].

In CFD simulations, sharp transitions can potentially cause unwanted reflections. In order to prevent such reflections as much as possible the exponential equation for the relaxation factor is selected as this replaces the CFD solution the most gradual at the inner ellipse.

See 2.6 for a visualisation of the inner and outer ellipse as well as the relaxation within an arbitrary sized domain.

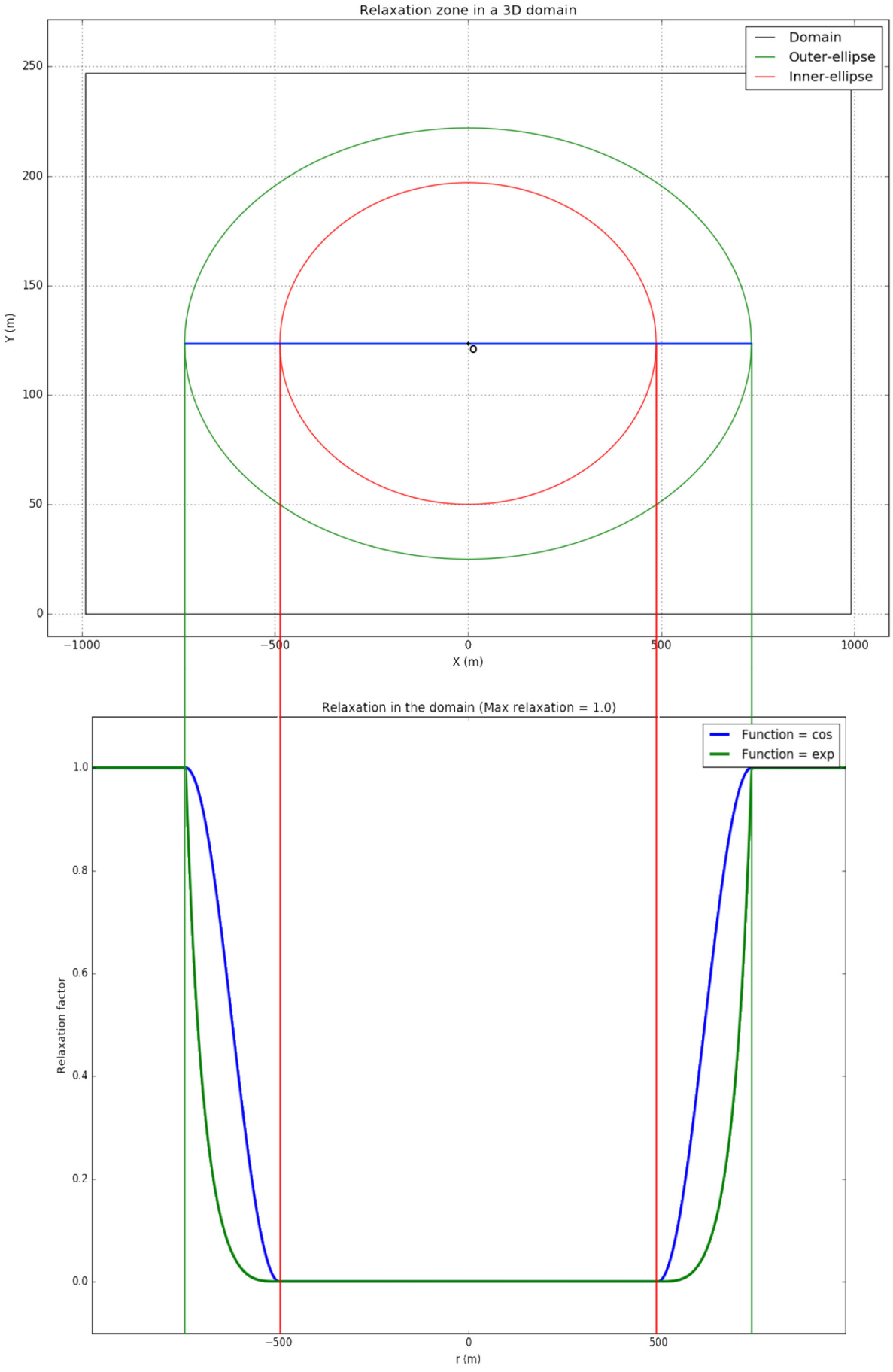

Figure 2.6: Relaxation zone and factor [12]

2.4. Errors and uncertainty in CFD

When CFD is used approximate an problem that occurs in the real world, it is of interest to determine the accuracy and validity of the solution for the users of the results. In order to say something about the accuracy and validity of a result solved with CFD the errors present in the solution must be quantified. According to Ferziger and Perić [20] the errors present in CFD can be divided up in two groups.

- Numerical errors are errors in the solution of the set of equations that describe the problem.
- Modelling errors are errors due to the fact that the used model doesn't represent the real world case

The quantification of the numerical error is known as verification. The numerical error and it's quantification are discussed in paragraph 2.4.1 and 2.4.2. Validation is used to determine how close the mathematical model represents physical reality. Modelling errors are discussed in paragraph 2.4.3.

2.4.1. Numerical errors

The numerical error is the difference between the exact solution to a mathematical problem and the numerical solution. This is shown in equation 2.4. Quantifying the numerical error requires knowledge of the exact solution.

$$e(\phi) = \phi_{num} - \phi_{exact} \tag{2.4}$$

with $e(\phi)$ the numerical error, ϕ_{num} the approximate numerical solution and ϕ_{exact} the exact solution.

According to Ferziger and Perić [20] the numerical error comprises of three error sources, namely the round-off error, convergence or iterative error and the discretisation error.

- Round-off errors are caused by the finite precision of the computer. This error is inevitable as there exists no such thing as a computer with infinite precision. However, according to L.Eça [15], this error will be negligeble compared to other sources of error when a system with double-precision, as was the case in this research, is used. In such a case the simulations are performed with 14 digits of accuracy.
- The convergence error, also known as the iterative error is the result of the CFD software iteratively trying to solve the implemented system of equations within a finite number of steps. This iterative process is required to solve the non-linearities in the system of equations. The idea is that after each time step the differences between the left and right hand side of the equations implemented in the solver become smaller. These differences are what is known as a residual.

  In theory it should be possible to let the order of the iterative error converge to the order of the round-off error. In practice however, this is considered too expensive and therefore this iterative process is stopped before that point is reached. The difference remaining after the last iteration is what is known as the convergence or iterative error. According to L.Eça and M.Hoekstra [25], it is considered acceptable to full ascribe the numerical uncertainty to the discretization error if the iterative error is at least two orders of magnitude smaller than the discretisation error.

  In CFD common methods used to monitor residuals are the L_2 and L_∞ norms. These monitor the average and largest residual in the domain after each iteration.

$$L_2(r) = \sqrt{\frac{\sum_{i=1}^{N} r_i^2}{N}} \tag{2.5}$$

$$L_\infty(r) = max(r_i) \quad 1 \leq i \leq N_p \tag{2.6}$$

  With N the total numer of cells in the grid and r the residual of a specific flow quantity.

- Discretisation errors are a consequence of the discretisations applied to the system of partial differential equations. By representing a continuous function by a finite number of evaluations, one is bound to introduce an error. The discretisation error decreases with grid refinement as a finer grid would represent the continuous flow field better than a coarse grid.

  Under the assumption that double-precision was used and that the residuals are at least two orders of magnitude smaller than the discretisation error, the complete numerical error can be ascribed to the discretisation error. Solution verification is used to estimate this discretisation error.

2.4.2. Verification of the numerical error

Verification is about estimating the numerical error of a solution. As stated in the previous paragraph, under the assumption that the round-off and convergence error can be neglected, the numerical error equates to the discretisation error. Equation 2.4 shows that the exact solution to the problem must be known to be able to determine the numerical error. Unfortunately the exact solution to the mathematical problem is not known and therefore it is not possible to determine the discretisation error. As a consequence, verification focuses on the estimation of the discretisation error of a numerical solution ϕ, which is converted in a numerical uncertainty $U(\phi)$ that is supposed to bound the exact solution ϕ_{exact} within a 95% confidence interval [15], i.e.,

$$\phi - U(\phi) \leq \phi_{exact} \leq \phi + U(\phi) \tag{2.7}$$

L.Eça and M.Hoekstra [25] propose a method for the estimation of the discretisation error based on grid refinement studies. This method uses the results from a series of geometrically similar grids with increased refinement. A power function is then fitted to the results. This fit will enable the estimation of the exact solution to the problem assuming infinite grid refinement. Based on this exact solution an estimation of the discretisation can be made for each grid. At MARIN the Numerical Uncertainty Analysis (NUA) tool was developed to perform the estimation of the discretisation uncertainty based on this method. The NUA tool was used in this research.

Geometrically similar grids

The method by Eça and Hoekstra is designed for use with geometrically similar grids. L. Eça [15] states that if the used grids are not geometrically similar, the trend of the results tends to not converge monotonic, resulting in a very large uncertainty estimation . The use of structured grids is preferred as these grids remain geometrically similar when their grid refinement is changed. In practice however, unstructured grids are much more popular because they are easy to generate even for complex geometries. For that same reason they were also used in this research. The challenge that occurs is that it is more difficult to generate multiple geometrically similar grids with increased grid refinement using unstructured grids.

P.Crepier [27] researched this topic and developed a method for the generation of geometrically similar grids using HEXPRESS . The two main ideas in this method regard maintaining the location of hanging nodes and the size of the viscous layer. Although no actual viscous layer is used in this research, a very coarse viscous layer is present in the grid to define some refinement near the hull of the vessel. The main principles behind Crepier's method are explained now.

Hanging nodes - Refinement diffusion

Hanging nodes occur when a cell on one side of a face boundary is split in half, but its neighbour is not split. See figure 2.7 for an example.

To obtain grids that are as geometrically similar as possible, hanging nodes are kept at the same location for increasingly refined grids. This is done by adapting the refinement diffusion. The refinement diffusion controls the number of cells that are placed between two levels of refinement. An example of this refinement diffusion is given in figure 2.8

Equation 2.8 is used to determine the required refinement diffusion for a certain grid refinement level n.

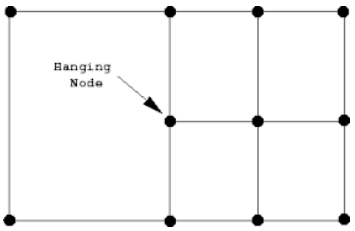

Figure 2.7: Hanging node

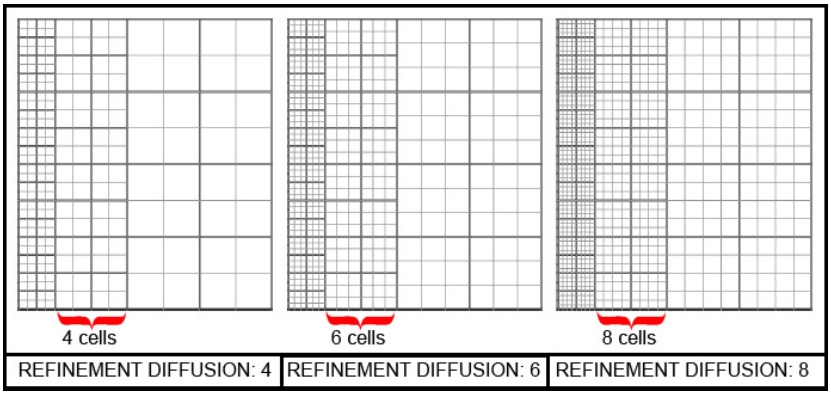

Figure 2.8: Refinement diffusion visualised

$$d_n = 2nd_1 - 1 \tag{2.8}$$

Where d_1 is the refinement level of the initial grid and d_n the refinement level.

To further clarify this principle an example is given here with five geometrically similar grids. The grid that is used as a basis is square, has a diffusion of 1 and its initial grid was 4 cells wide and high. The original cell size of this grid is decreased by 2, 3, 4 and 5 in each direction by using 2,3,4, or 5 times more cells in each direction. By adapting the initial cell size of the grid, the refinement of the grid n is increased. The grid refinement level n is defined by the increase in the number of cells in one direction The corresponding refinement diffusion is then calculated according to equation 2.8. In table 2.1 the number of cells in x and y direction N_x and N_y as well as the refinement level n and diffusion d_n are shown for all five grids.

Grid	1	2	3	4	5
N_x	4	8	12	16	20
N_y	4	8	12	16	20
n	1	2	3	4	5
d_n	1	3	5	7	9

Table 2.1: Parameters for 5 geometrically similar grids

Viscous layer - Initial cell size and growth

The viscous layer near the hull is generated according to a geometric series of a first term S_0, which corresponds to the dimension of the smallest cell at the hull, and ratio r_v. The size of the k^{th} cell is then defined by equation 2.9

$$S_k = S_0 r_v^k \tag{2.9}$$

With this definition, if the size of initial cell is reduced to generate a more refined grid, the result will not be geometrically similar. Figure 2.9 shows what happens when the initial grid is refined two times. In the initial grid (red line) 10 cells cover a distance of 0.025 units. The refined grid should have 20 cells covering the same distance. When half the original cell size is used in combination with the same ratio r however, about 13 to 14 cells are used to cover this distance instead of 20. For the new grid to be geometrically similar to the original grid, both the size of the size of the first cell as well as the ratio will have to be adjusted according to equations 2.10 and 2.11.

$$S_n = S_1 \frac{s - r_1^{\frac{1}{n}}}{1 - r_1} \tag{2.10}$$

$$r_n = r_1^{\frac{1}{n}} \tag{2.11}$$

Where S_1 and r_1 are respectively the first cell size and growth ratio from the original grid, and S_n and r_n are the first cell size and growth ratio for the grid refinement level n. In figure 2.10 examples of the geometrically similar viscous layer for a grid refinement level of 2 and 3 are shown together with the original viscous layer.

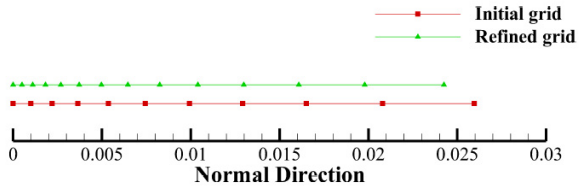

Figure 2.9: Viscous layer refinement resulting in geometrically non-similar grid [27]

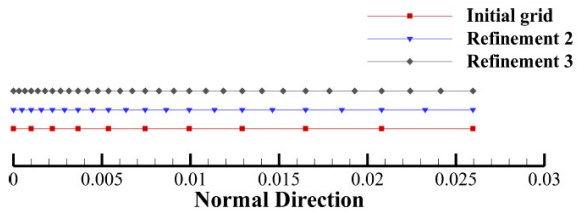

Figure 2.10: Adapted viscous layer [27]

2.4.3. Modelling error and validation of the solution

Modelling errors are errors due to the fact that the used model doesn't represent the real world. Validation is about estimating this modelling error. To validate the CFD solution, it is validated by comparing it with data from the CRS model tests.

3

Additional information and numerical setup

The purpose of this chapter is to give the reader an impression of the set-up of the simulations. This regards both the set-up of the domain as well as the numerical solver. The chapter starts off with two paragraphs on the software used in this research after which a description of the domain is given.

The idea here is not to be complete on the explanation of the used software, but rather to focus on the specific settings and details that are relevant for this research. These explanations will aid the reader in the understanding of the choices made in the rest of the research.

Specifics regarding the working principles of the used grid meshing software are explained first. The understanding of these working principles will become of importance in the following chapters where choices regarding the spatial discretisation of the domain are based on it. Second relevant specifics and limitations regarding the numerical solver ReFRESCO are explained. Finally the chapter is concluded with the descriptions of the domains used in this research, this includes used dimensions, boundary conditions and implemented measures to prevent reflections.

3.1. Hexpress - Grid generation

For the generation of the grid, HEXPRESS by NUMECA international is used. This programme is capable of generating hexahedral unstructured grids. An explanation on certain working principles of HEXPRESS is given here to aid the reader in the understanding of the choices made.

HEXPRESS uses the geometry of the vessel as an input and meshes a grid which is then given as an output. In practice the geometry of the vessel in a 3D Computer Aided Design (CAD) programme such as for example Rhinoceros 3D (RHINO). For this research the geometry was provided by MARIN.

HEXPRESS will then take several steps in which it generates a mesh, see figure 3.1. These are discussed here:

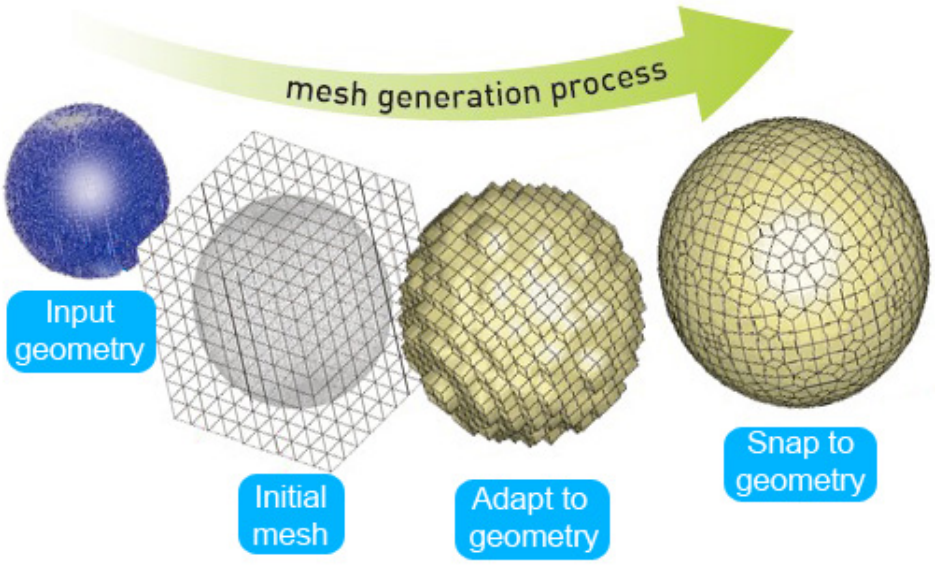

Figure 3.1: Grid generation in HEXPRESS

1: Input geometry Initially hexpress is provided with an input geometry. In case of the example seen in figure 3.1, this is a sphere.

2: Initial grid Next the dimensions of the domain are specified by the user and an initial coarse grid is generated over the entire domain. This will be the coarsest part of the whole domain.

3:Adapt to geometry In this step the coarse grid is refined in order to provide the required detail in certain areas of the domain. One can for example specify the required refinement within an area or on a surface of the geometry. More on grid refinement is explained in subsection 3.1.

Specifying which level of refinement is required as well as where is one of the challenges that an engineer faces when he is working with CFD. Proper meshing is very important as it has a large influence on the accuracy and cost of the simulation.

4:Snap to geometry Finally the refined grid is snapped to the geometry of the hull. Here, several optimization steps are performed that align the faces of the cells with the geometry of the hull.

3.1.1. Grid refinement

In order to understand how the initial coarse grid is refined one must understand how grid refinement is implemented in HEXPRESS. HEXPRESS starts of with an initial grid, comprised of large cells of the same size. From there it is possible to refine the grid by splitting cells along either the x, y or z-axis. A cell can thus be subdivided into 2, 4 or 8 cells. See fig. 3.2.

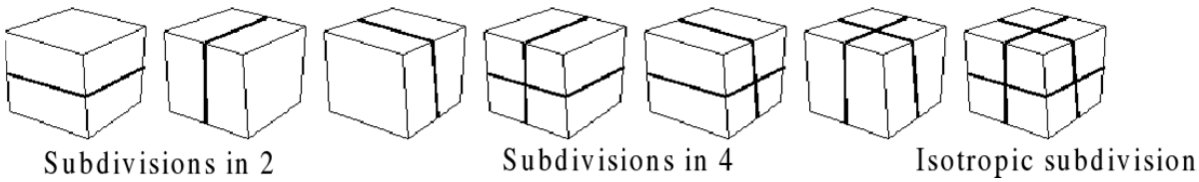

Figure 3.2: Cell refinement in HEXPRESS

The number of times a cell is split up into sub cells is known as the refinement level n. This poses a limitation on the cell sizes that can be generated this way. The available cell sizes are a function of the initial cell dimension and the refinement level. See eq. 3.1

$$L_{avail}(n) = L_{init} \cdot 0.5^n \tag{3.1}$$

With L_{avail} and L_{init} the available and initial cell dimensions and n the refinement level. In HEXPRESS the required cell size in an area or on a surface can be specified by specifying the required refinement level. An example is given here:

In this example, the initial grid consists of 6*4 square cells each with a vertice length of 1 [m]. See figure 3.3. The user wants to specify a cell vertice length of 0.5 [m], 0,25[m] and 0,125[m] in the top right, bottom right and bottom left quarter respectively. See figure 3.4.

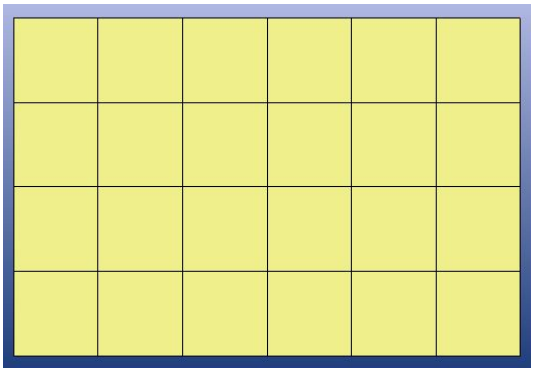

Figure 3.3: Initial 6x4 grid

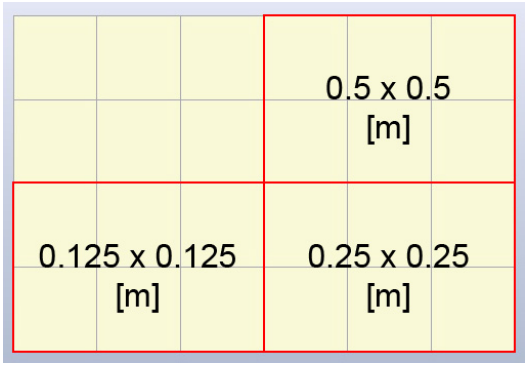

Figure 3.4: Desired cell dimensions

Due to the discrete nature of the refinement used in HEXPRESS, the available sizes of the cells can be calculated from the initial cell dimensions according to equation 3.1 and are shown in table 3.5. From this table it is clear that the specified cell sizes correspond to a refinement level of 1, 2, and 3 respectively. Next, the three refinement areas are implemented. This is done by using HEXPRESS's refinement boxes. These boxes define the area in which a specified refinement level is to be generated. See figure 3.6.

Refinement level 'n' []	cell dimension [m]
0	1
1	0,5
2	0,25
3	0,125
4	0,0625
5	0,03125
6	0,015625
7	0,0078125
8	0,00390625
9	0,001953125
10	0,000976563

Figure 3.5: Available cell dimensions

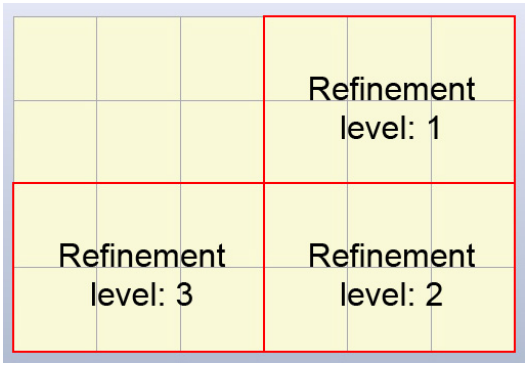

Figure 3.6: Refinement boxes

Finally, HEXPRESS refines the grid and the result is shown in figure 3.7

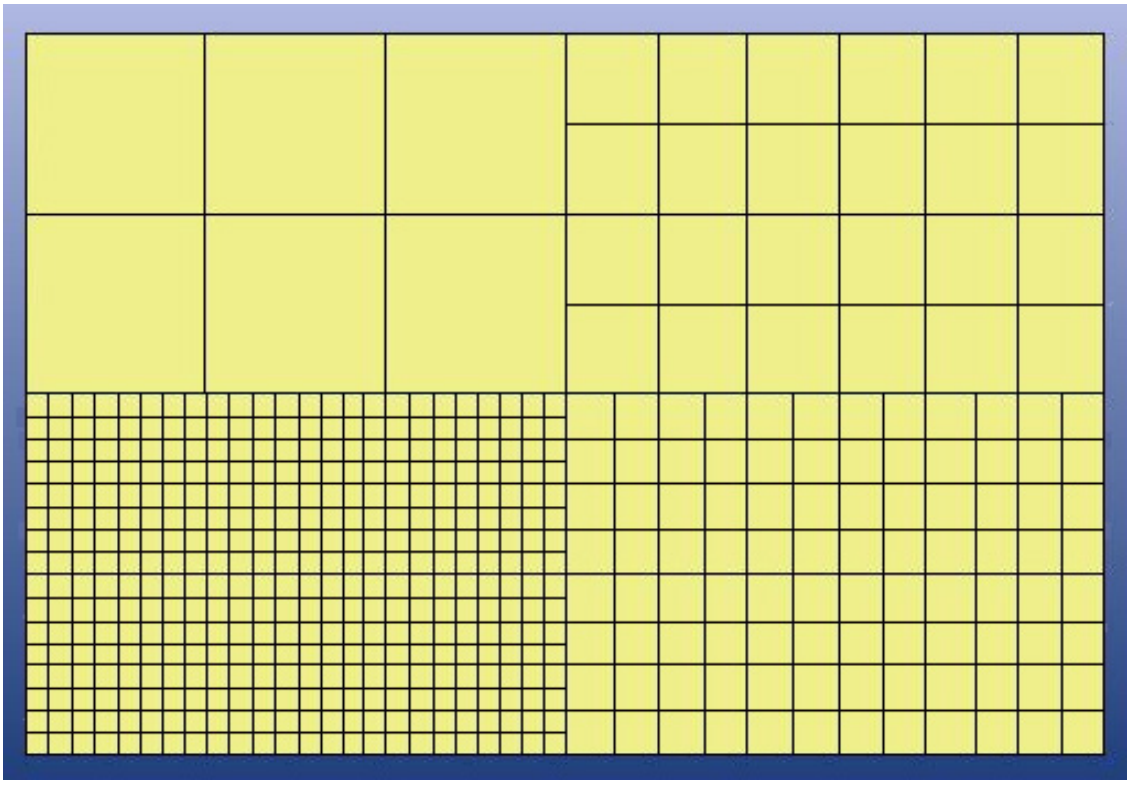

Figure 3.7: Refined grid

3.2. ReFRESCO - Numerical solver

ReFRESCO stands for Reliable&Fast Rans Equations (solver for) Ships, Cavitation (and) Offshore and is developed by MARIN in collaboration with several institutes and universities including Delft University of Technology. The code solves multiphase unsteady flows with the incompressible RaNS equations complemented with turbulence and cavitation models. The code is also capable of solving the N-S directly and thus function as a DNS solver, which is what is used in this research. The software runs on Linux workstations and is optimized to run in parallel on HPC clusters. For this research the release version 2.4.0 as well as a beta version of 2.5.0 were used. The beta version was only used for the last set of simulations with the vessel sailing with 2 DoFs in waves as this version was able to solve the rigid-body Equations of Motion (EoM) of the vessel with increased robustness.

3.2.1. Spatial discretization scheme

For the spatial discretization a cell-centred finite volume method is used. This means that the integral form of the equations are integrated for each cell, after which the resulting values are assumed to be defined in the centre of the cell. In order to determine the value on a surface of a cell the Quadratic Upwind Interpolation for Convective Kinetics (QUICK) scheme is used. This scheme uses a quadratic function passing through two upwind and one downwind nodes. QUICK takes into account the second derivative and is therefore third order accurate [31] . See figure 3.8.

The advantage of this scheme is that it is very accurate compared to other available schemes. The downside is that it can have stability problems in areas with strong gradients. To prevent such problems, ReFRESCO has build in limiters that monitor if this happens. When this is the case, the solver switches to a first order scheme for that iteration.

A note must also be made that instability problems in the QUICK scheme are affecting this type of simulation to a lesser extent due to the fact that the boundary layer at the hull is not simulated. This is an area where potentially problematic strong gradients would occur.

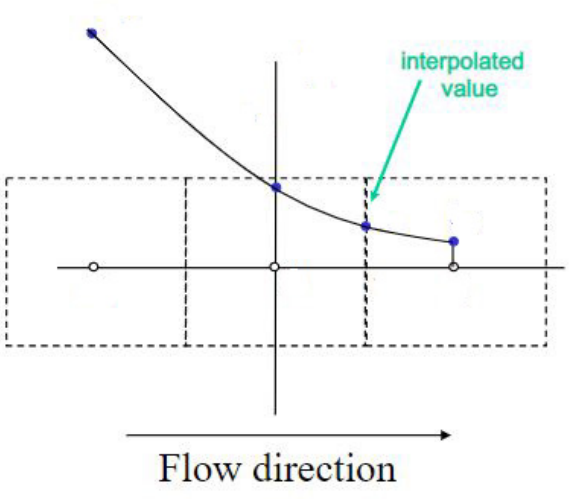

Figure 3.8: QUICK interpolation scheme

3.2.2. Time discretization scheme

In ReFRESCO there are two available time discretization schemes, namely 'Backward Euler', which is a first order scheme and 'Backward difference formula - order 2', which is a second order scheme. The advantage of the higher order scheme is increased accuracy, but this comes at the cost of requiring smaller time-steps in the simulation which is more costly. From experience at MARIN it is known that the first order scheme can cause instabilities in the type of simulations performed in this research. Therefore the second order scheme, with its higer accuracy is selected for this research. For more information on these schemes the interested reader is referred to the ReFRESCO theory manual [4].

3.2.3. Maximum time-step and the CFL condition

Richard Courant, Kurt Friedrichs and Hans Lewy [10] stated a condition for convergence while solving partial differential equations numerically in their 1928 paper. The condition takes the speed at which information is traveling in the mesh into account and poses a limit on the corresponding time-step. When applied to CFD this condition states that a wave may not travel more than one cell in one time-step in the simulation in order to ensure correct results. This condition is known as the Courant-Friedrisch-Lewy (CFL) condition. On a basic level this condition states that small grid cells require small time-steps. This condition is met when the Courant number is smaller than or equal to 1. See equation 3.2 for the three dimensional formulation of this condition. A Courant number of 1 indicates that the wave is traveling exactly one cell in one time-step. This condition is used as a guideline for the maximum allowable time-step Δt in the CFD solution.

$$C = \frac{u\Delta t}{\Delta x} + \frac{v\Delta t}{\Delta y} + \frac{w\Delta t}{\Delta z} \leq C_{max} \tag{3.2}$$

where:

- $u, v, w[m/s]$ is the local velocity of the wave
- $\Delta t[s]$ is the time step
- $\Delta x, y, z[m]$ is the cell size
- $C_{max}[]$ is the maximum Courant number, in this case 1

ReFRESCO CFL constraint

Due to the way ReFRESCO is set up, a more restrictive CFL constraint of $C_{max} = \frac{1}{6}$ is advised. The full explanation goes beyond the topic of this research but a general explanation is given in this subsection. For a more detailed explanation the reader is referred to [23], where a full explanation is given.

In CFD non-physical oscillations can occur when an area with a steep gradient is resolved using a relatively coarse grid in combination with certain discretisation schemes [17]. To prevent such oscillations, the discretisation scheme is required to be Total Variation Diminishing (TVD). For variable u, a scheme is said to be TVD if it doesn't increase the total variation of the solution over one time-step t. i.e.

$$TV(u^{t+1}) \leq TV(u^t) \tag{3.3}$$

Where n indicates the iteration step and the is defined as:

$$TV(u^n) = \sum_i \left| u_i^t - u_{i-1}^t \right| \tag{3.4}$$

where i indicates the iteration step.

By using a TVD scheme sharper gradient predictions are possible on coarse grids and non-physical oscillations are prevented.

In ReFRESCO, a second order scheme is used to integrate time. This scheme is only TVD for CFL numbers below $\frac{1}{6}$ [14]. To ensure that no non-physical oscillations occur, the grid refinement and time-step combination should be selected in such a way that the CFL number remains below $\frac{1}{6}$.

3.3. Domain

In this section the physical dimensions, axis conventions, boundary conditions and wave absorption zones used to set up the CFD domain are described.

3.3.1. Dimensions and axis conventions

In order to make the method of simulating wave added resistance applicable to other vessels, the decision was made to base the domain dimensions on the Length between Perpendiculars (LPP) of the vessel. This way, the domain will scale along with the length of the vessel. As stated in the research approach, only half of the vessel is simulated. The waves travel in negative x-direction, with the z-direction pointing upward. The origin of the axis is located on the free surface at the Aft perpendicular (App).

The 3D domain has a length of 6 LPP, a width of 2 LPP and a height of 4 LPP with the free surface located at 2 LPP in height. The vessel is positioned with 2 LPP of water ahead and 3 LPP behind it. These dimensions are selected based on guidelines from MARIN which are based on the experience of MARIN CFD users. It is their experience that the used dimensions lead to accurate and efficient simulations of a vessel in waves.

In order to test wave propagation only a 2D domain is required. The 2D domain used in these simulations has the same specifications as the 3D domain with the one exception that it only measures 1 [m] wide in y-direction and that it doesn't have a relaxation zone on the side of the domain. The 2D domain is meshed in such a way that it is only one cell wide in order to generate a quasi-2D domain.

See figure 3.9 and 3.10 for a visual representation of the domain with its dimensions and axis conventions.

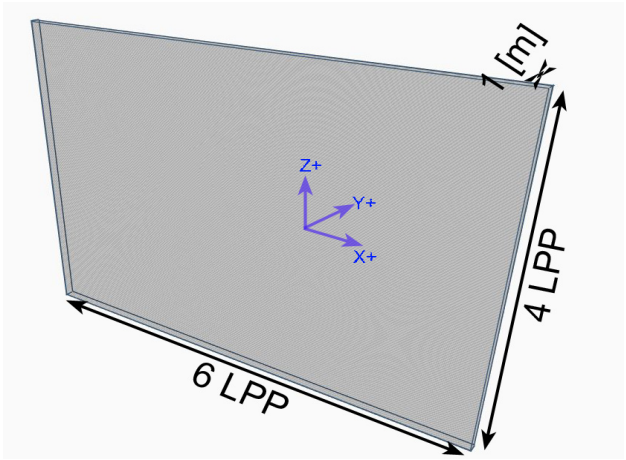

Figure 3.9: 2D domain dimensions

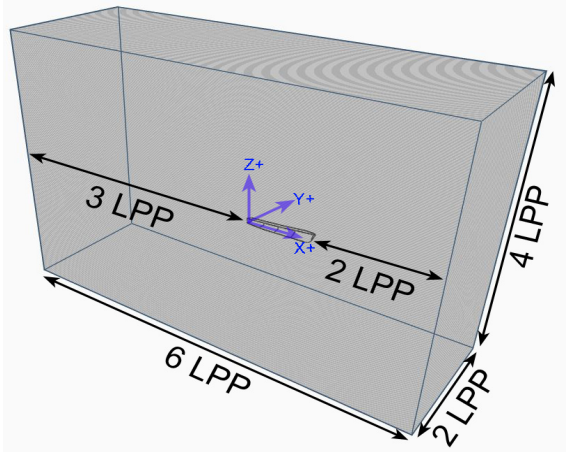

Figure 3.10: 3D domain dimensions

3.3.2. Boundary conditions

The BCs described in subsection 2.2.2 are applied to the 2D and 3D domain from the previous section. The 2D domain comprises of a wave BC on the inlet and outlet of the domain. At this boundary the elevation of the free surface and the inflow velocity of the fluid are specified. The 3D domain is set-up similarly but also features this BC on the left boundary.

Both domains also feature a slip wall at the bottom of the domain which simulates the sea floor. The reasoning behind this is as follows. According to equation 3.5 all the waves in this research, including the longest, which measure 2 LPP, occur in deep water.

In the TU Delft reader Offshore hydromechanics [21] it is explained that when waves are propagating in deep water, they do not 'feel' the seafloor. If this is the case it is not necessary to simulate the effects of the seafloor on the waves such as shear. This justifies the use of a slip wall as a boundary condition.

$$\begin{aligned} Deepwater: h &> \frac{1}{2}\lambda \\ h &= 200[m] \\ \lambda_{max} &= 200[m] \end{aligned} \tag{3.5}$$

With h = water depth and λ_{max} = maximum wave length.

As concluded in paragraph 2.1.1, the added resistance in waves is considered a non-viscous phenomenon. Therefore the decision was made to not model the frictional resistance that the fluid imposes on the hull. Therefore, the interaction between the hull and the fluids is simulated using a slip wall.

For the 2D case the expected flow pattern is expected to have mirror symmetry at the side planes, these are defined using symmetry BCs. For the 3D domain this is the case for the boundary on the right side. Schematizations of the domain for both the 2D and 3D cases with the boundary conditions in place are shown in figure 3.11 and 3.12

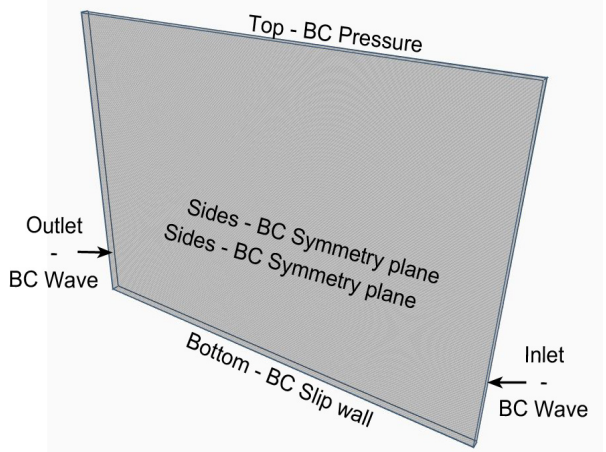

Figure 3.11: 2D domain boundary conditions

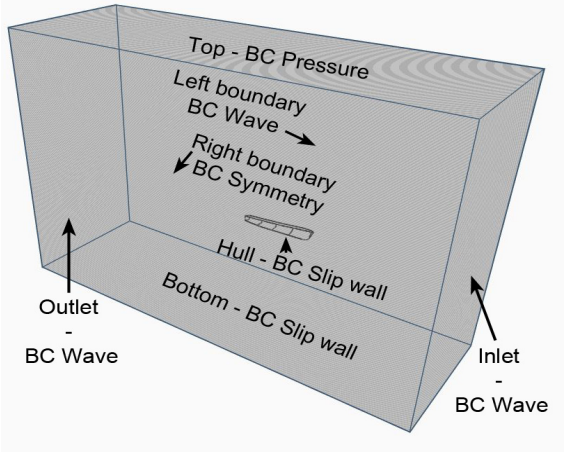

Figure 3.12: 3D domain boundary conditions

3.3.3. Wave absorption zones

In order to prevent waves reflecting back at the sides of the domain, wave absorption zones are implemented. The theoretical background of these zones is described in paragraph 2.3. In this subsection the implementations for both the 2D and 3D domain are described.

2D domain wave absorption

For the 2D domain two wave relaxation zones are placed at the inlet and outlet of the domain. The relaxation zones measure 1 LPP in width.

The decision to dimension the relaxation zones based on the size of the vessel may seem unusual as it would seem more logical to dimension them based on the length of the wave. However, as the wave lengths themselves are a function of Lpp, ranging from 0.5 Lpp up to 2 Lpp in length, the relaxation zones actually are dimensioned based on the wave length.

3D domain wave absorption

The 3D domain has relaxation zones all around the perimeter of the domain, measuring 1 LPP in width. This way, all waves, including diffracting and radiating waves will be absorbed towards the boundaries of the domain.

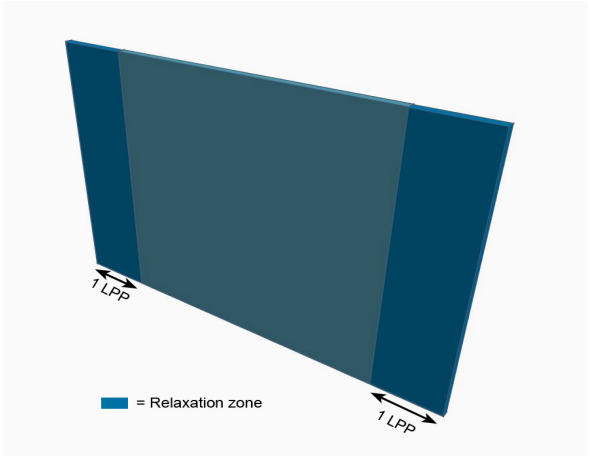

Figure 3.13: 2D domain - relaxation zones

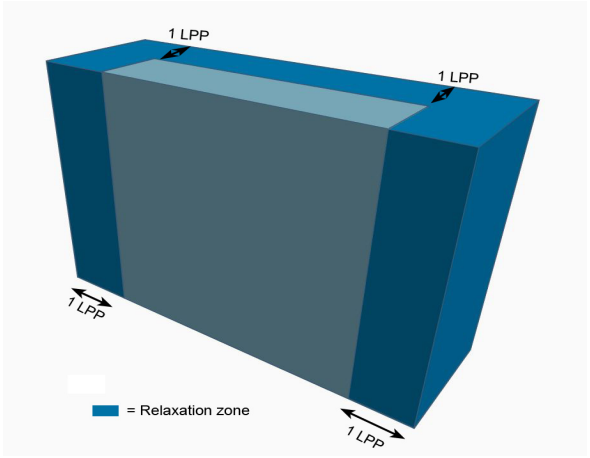

Figure 3.14: 3D domain - relaxation zones

4

Simulating 2D regular waves

A regular wave is a wave that is defined by a function such as a sine, cosine, or an n^{th} order stokes wave for example. Such a wave is specified by its amplitude ζ , wave length λ and wave period T. In wave added resistance simulations it is of importance that the parameters of the regular waves present in the simulation are correct and constant over the domain. This is because accurate predictions of the wave added resistance are dependent on consistent wave propagation. An inconsistency in the simulated waves would result in inconsistent vessel motions, which would in turn result in inconsistent derived quantities such as the wave added resistance. Wave consistency can be achieved by setting the numerical settings of the simulation such that the wave dispersion is remained constant whilst wave dissipation and wave reflection are minimised.

In the TU Delft reader Offshore Hydrodynamics [21] an explanation of wave dispersion is given. Wave dispersion relates the length of a wave to its frequency. For waves traveling in deep water, the wave length is a function of the wave frequency ω and the gravitational acceleration g . See equation 4.1 for this relation. If wave dispersion is simulated well, the propagating waves should have the correct and constant wave length over the entire domain.

$$\lambda = \frac{2\pi g}{\omega^2} \tag{4.1}$$

Wave dissipation is a process where the wave loses energy whilst propagating and results in a reduction of the wave amplitude over the domain. This causes an unwanted inconsistency in the wave elevation over the domain. Wave reflections are known to occur in CFD simulations at the domain boundaries and result in waves bouncing back into the domain. These reflected waves influence the height and length of the waves within the domain and are therefore undesirable. Therefore it is required prevent the occurence of such reflections. A compromise between the required simulation time and accuracy must be found as simulation time is costly. To find this best compromise, a grid refinement study is performed. In this study both the temporal as well as the spatial discretisation are varied to determine the optimum combination.

4.1. Spatial discretisation: Minimising dissipation and dispersion

In order to minimise the dissipation and dispersion, it is important to know where these errors come from. When waves are simulated with CFD, the domain is discretised in by meshing it and in time by using a time-step in the solver. According to J.W.Slater [22] these discretisations introduce errors in both the wave length and height as a finite number of cells and time-steps are not able to describe a continuous form such as a propagating wave. These errors in the wave length and wave height over the domain are known as dispersion and dissipation. In order to minimise these errors, both the cell size as well as the time-step Δt must be set small enough to ensure low wave dissipation and dispersion.

4.1.1. Standard grid refinement

According to H.Brandinga et. al. as well as M.Hoekstra et. al. ([19], [16]), when meshing waves, it is customary to assign a region at the free surface where the cell density is increased in order to capture the air-water interface. Here, a number of cells per wave length and height are assigned . Using such settings in an automated wave meshing programme will yield a mesh that depends to a great extent on the way the software increases the cell density towards this region. In order to capture the kinetic energy present in the waves better a wave meshing topology based on this kinetic energy in the wave is used.

4.1.2. Kinetic energy based grid refinement

The grid topology that is used to mesh the 2D waves is based on a method designed to efficiently and accurately propagate waves in the CFD domain, developed by S.Rupac et. al. [28]. This method assigns three refinement areas which are used to capture the air-water interface, 90% and 99.9% of the kinetic energy in the wave according to linear wave theory. The idea is to capture the motions in the fluid accurately. Kinetic wave energy is used as a measure of this motion. Linear wave theory describes wave orbital motions in the velocity field as follows:

$$\left.\begin{matrix} u = \zeta_a \omega e^{kz} cos(kz - \omega t) \\ v = \zeta_a \omega e^{kz} sin(kz - \omega t) \end{matrix}\right\} v = \sqrt{u^2 + v^2} = \zeta_a \omega e^{kz} \tag{4.2}$$

With u the horizontal and v the vertical velocity component, ζ_a, ω and k respectively the wave amplitude, wave frequency and wave number and z the depth below the free surface. The equation shows that the orbital velocity decreases with depth as a function of e^{kz}. From the orbital velocity, the local cumulative kinetic energy as a function of the water depth in the wave is calculated according to equation 4.3.

$$E_k(z) = \frac{1}{2}\rho \int_z^0 v^2 = \frac{1}{4}\rho \frac{\zeta_a^2 \omega^2}{k}[1 - e^2 kz] = \frac{1}{4}\rho g \zeta_a^2 [1 - e^2 kz] \tag{4.3}$$

This function is plotted in Figure 4.1 as a function of the normalised water depth and shows that 90% and 99.9% of the wave energy is contained in 20% and 60% of the wave length below the free surface.

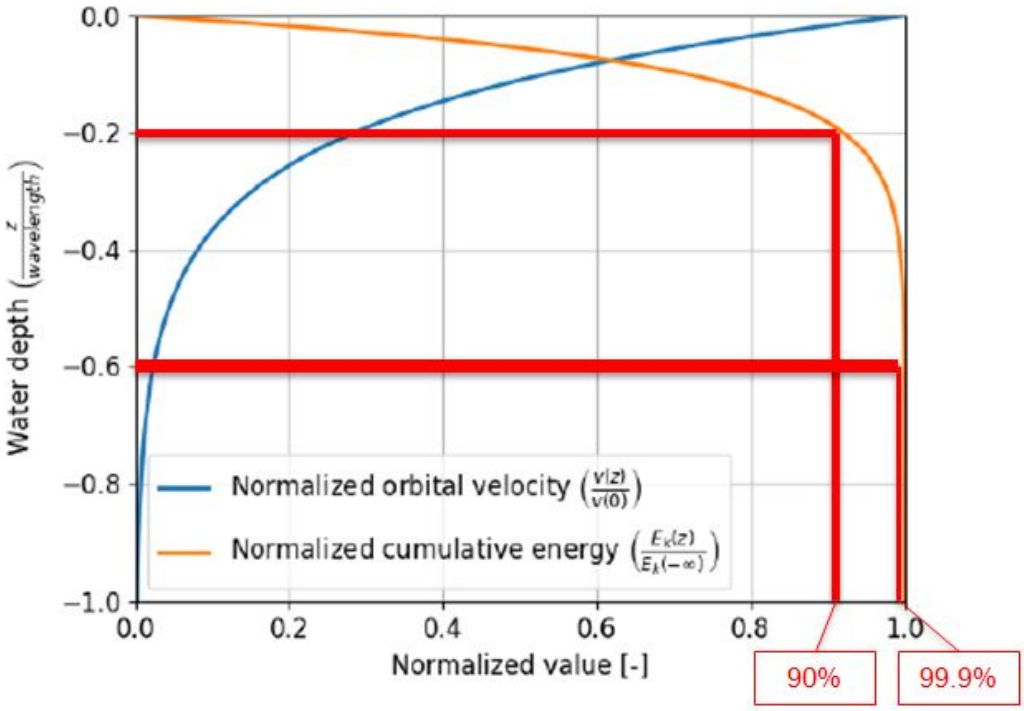

Figure 4.1: Cumulative energy and normalized orbital velocity plotted as a function of the water depth

The kinetic energy in the wave is used as a basis for a grid topology using the three refinement zones. These refinement zones are assigned in order to capture the motions in the fluid accurately and efficiently. In Figure 4.2, these refinement zones are shown. The zones are defined as follows:

Free surface refinement box
: This zone is refined according to a number of cells per wave amplitude in order to capture the free surface and stretches from +1.1 ζ_a to -1.1 ζ_a in order to capture the air water interface from the wave crest down to the trough.

Upper refinement box
: This zone is refined according to a number of cells per wave length in order to accurately capture 90% of the kinetic energy in the wave. The zone stretches from the wave crest to 20% of a wave length below the free surface

Lower refinement box
: This zone is refined according to half the number of cells per wave length of the upper refinement box in order to reasonably capture the remaining 9.9% of the kinetic energy in the wave. The zone stretches from 20% to 60% of a wave length below the free surface.

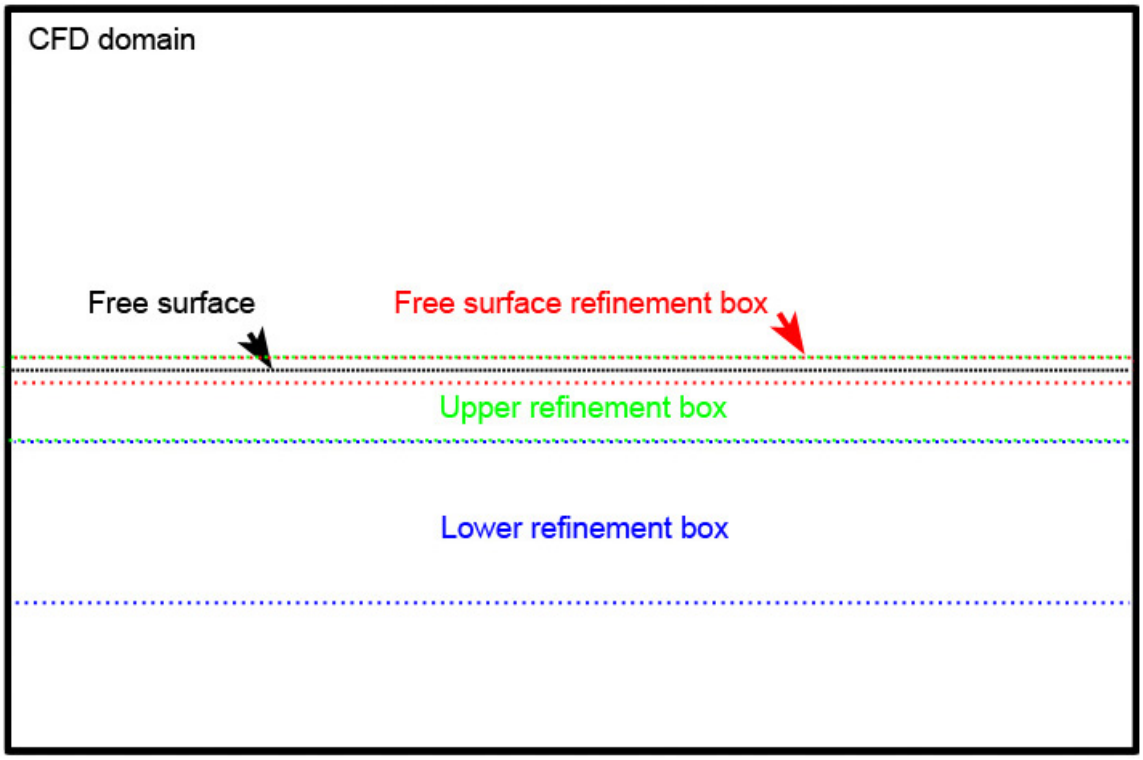

Figure 4.2: Computational domain with the three refinement boxes

4.1.3. Implementation in HEXPRESS

Now that the grid topology is known it will be used to mesh a grid using the hexahedral unstructured grid meshing software HEXPRESS. The first step is to determine what the desired cell dimensions L_{req} are fore each refinement box. This dimension is calculated as a function of the wave length and height and he required number of cells per wave length and amplitude. See equation 4.4.

$$\begin{gathered} L_{req} = \frac{C_\lambda}{\lambda} \qquad or \qquad L_{req} = \frac{C_{\zeta_a}}{\zeta_a} \\ with: \quad \lambda = \frac{2\pi g}{\omega^2} \quad (Deep\ water\ wave\ length) \end{gathered} \tag{4.4}$$

With L_{req} the required cell dimension and C_λ and C_{ζ_a} the specified number of cells per wave length and amplitude. By inserting the initial cell size l_init in equation 4.5 it is possible to calculate the resulting cell dimension L_{res} for each refinement level. See equation 4.5

$$L_{init} * 0.5^n = L_{res} \tag{4.5}$$

By combining equation 4.4 and 4.5, the minimum required refinement level can be calculated for each refinement box. See equation 4.6.

$$\begin{gathered} L_{res} \leq L_{req} \\ L_{init} 0.5^n \leq \frac{C_\lambda}{\lambda} \qquad or \qquad L_{init} 0.5^n \leq \frac{C_{\zeta_a}}{\zeta_a} \\ n = \left\lceil \frac{log(\frac{\lambda}{C_\lambda * L_{init}})}{log(0.5)} \right\rceil \qquad or \qquad n = \left\lceil \frac{log(\frac{\zeta_a}{C_{\zeta_a} * L_{init}})}{log(0.5)} \right\rceil \end{gathered} \tag{4.6}$$

The dimensions of the refinement boxes are calculated according to their specifications as given in section 4.1.2. Once both the required refinement and the dimensions of the refinement box are known,

they are inserted into HEXPRESS. In Figure 4.3 the setup of refinement boxes in HEXPRESS is shown, note the refinement level input field in yellow. The refinement boxes and the resulting grid are shown in Figure 4.4 and 4.5.

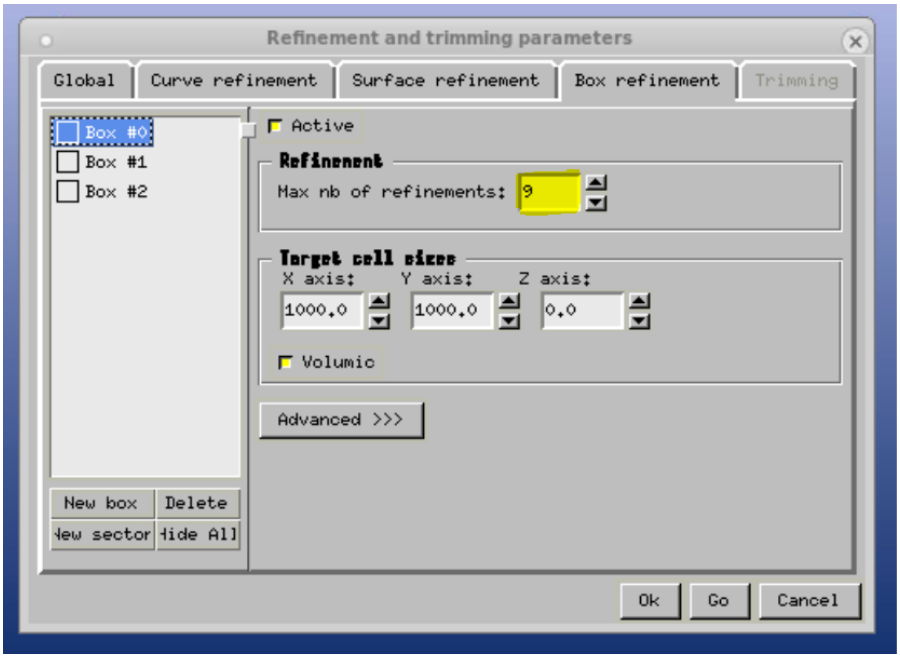

Figure 4.3: Setup of a refinement box in HEXPRESS

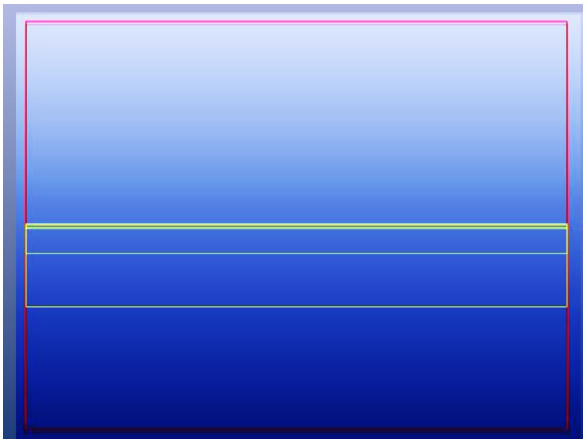

Figure 4.4: The free surface, upper and lower refinement boxes

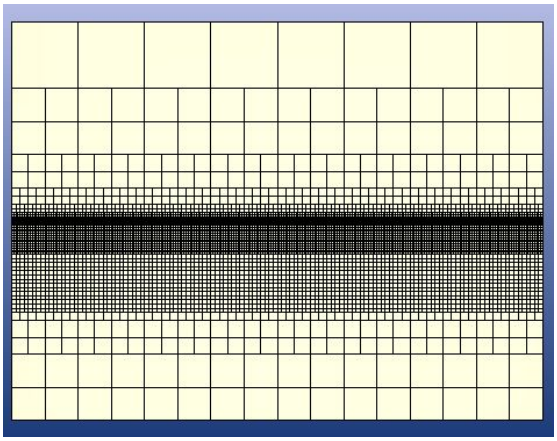

Figure 4.5: The resulting grid

4.1.4. Comparison of the meshing methods

In figure 4.6 both a standard mesh and a kinetic wave energy based mesh are shown. Both the meshes have the same number of cells at the free surface, but the energy based approach shows more refinement below the free surface which should yield a more accurate description of the motions in the fluid. A comparison of the dissipation and dispersion using both grids was made in order to assess the advantage of using a kinetic energy based grid. The details regarding these tests are described in chapter 4.3. The results show that the kinetic energy based mesh uses approximately 2 times more cells to minimise the dispersion by 66% and the dissipation by a 89%.

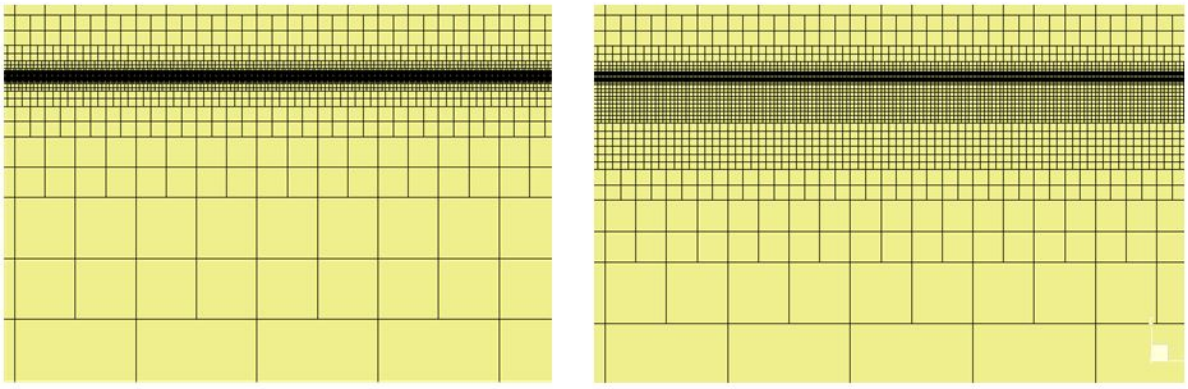

Figure 4.6: Comparison of a traditional grid (left) and a kinetic energy based grid (right)

4.2. Single grid for multiple wave frequencies

The grid described in the previous section is designed for a single wave length. In practice wave added resistance simulations will be run for multiple wave lengths. It would be desirable to use a single grid for all these simulations for two main reasons. First, comparing added resistance forces that were determined on the same grid is more consistent as we assume that the errors induced by the spatial discretisation stay constant. Second, the added resistance simulation for multiple wave lengths will require only one calm water simulation as all simulations in waves use the same grid.

This single grid is composed out of all the individual grids by using their common refinement. According to J.Xiangmin [33] the common refinement of two meshes is a mesh composed of elements that combine both grids by intersecting the elements of the input meshes. In figure 4.7 the common refinement of two grids is shown.

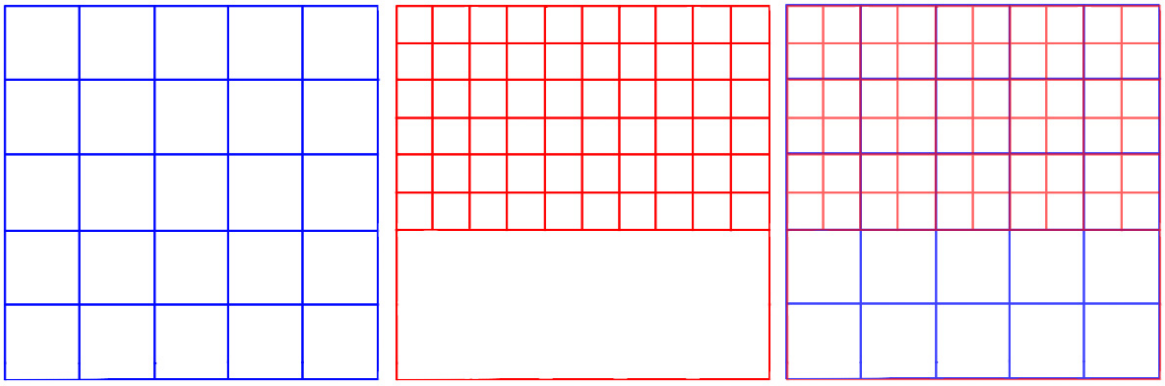

Figure 4.7: Left: Coarse grid (blue), Middle: fine grid (red) and their common refinement (blue + red) on the right)

In HEXPRESS this common refinement grid is build up out of refinement boxes with a similar procedure as used for the single frequency grid. The approach using three refinement zones is applied as before, however, as a range of frequencies will now have to be simulated, the refinement zones will have to be adapted. This works as follows:

- The free surface refinement box has dimensions and refinement based on the wave amplitude. As the wave amplitude is held constant over the range wave frequencies, a single box can still be used.
- Both the upper and lower refinement boxes have dimensions and refinement levels based on the wave length. As this length is changing over the range of wave frequencies, the upper and lower refinement boxes will have to be adapted. The method used to adapt these boxes is explained below.

4.2.1. Upper and lower refinement boxes

The upper and lower refinement boxes have to be adapted to be used over a range of wave lengths. These boxes are defined by their refinement level and their dimensions in x, y and z direction. As all boxes span the width and length of the domain, three parameters remain to be adjusted, namely the refinement level and the vertical coordinates of the top and bottom of the box.

First the refinement level is discussed. Due to the discrete nature of the refinement levels used in HEXPRESS, it is not possible to match the number of cells per wave length exactly for each wave length. For example, imagine an initial cell size of 100 [m]. By using grid refinements in HEXPRESS it is possible to reduce the cell size to 50, 25, 12,5 and 6.125 [m] using 1, 2, 3 and 4 refinement levels respectively. If a user would prefer a different cell size however, this is not possible.

In case of the grid refinement boxes specified in paragraph 4.1.2 the required number of cells per wave length is specified. If this required cell size is not available the solution would be to select the nearest smaller cell size available. This way the specified number of cells per wave length / height is always maintained as a minimum requirement. This does mean that in some cases a higher number of cells per wave length / height will be used, resulting in a finer than strictly required grid.

In practice this means that a single grid refinement level used in one of the refinement boxes can be used for a range of wave lengths rather than just one wave length. Equation 4.7 shows the range of wave lengths that can be covered with a singe grid refinement level n.

$$L_i * 0.5^n * C_\lambda \leq \lambda_{range}(n) < L_i * 0.5^{n-1} * C_\lambda \tag{4.7}$$

Where L_i is the size of the initial cells in the grid, C_{min} the minimum number of cells per wave length or height and $\lambda_{range}(n)$ the range of wave lengths that is covered by a refinement level n.

Next the corresponding refinement box height has to be defined. This size also has to be adapted to cover a range of wave frequencies. For the top refinement box, its dimensions will stretch from the top of the wave crest down to 0.2λ. In this case λ will be the longest wave length that can still be covered by the refinement level. This way, the shorter wave lengths will be covered by the box as well. The same approach is used for the lower refinement box, with the exception that it will stretch down to 0.6λ.

The choice has been made to let all refinement boxes start at the top of the wave crest. This approach reduces the number of calculations for the dimensions of the refinement boxes by half as it is not necessary to calculate the upper coordinate of each box anymore. This does imply that all the boxes will overlap each other. When using HEXPRESS as a mesher, this does not pose an issue as HEXPRESS will use the highest refinement level in an area where multiple refinement levels are specified.

4.2.2. Setup of refinement boxes

We now have a method is available to determine the required refinement level and dimensions of the refinement box. As the range of wave lengths over which the waves will be simulated is also known, it is possible to calculate all the refinement boxes that are required. The approach used works as follows:

1. Calculate the required refinement level for both the longest and shortest wave length using eq. 4.6
2. Calculate the refinement box with the lowest refinement level
   (a) For the lowest refinement level (i.e. the longest wave length) , the shortest wave length that can still be covered by the refinement level is calculated using equation 4.7

(b) For the longest wave length covered by this box, the dimensions of the corresponding refinement box are calculated according to the dimensions as stated in section 4.1.2

The resulting refinement box will cover wave lengths from the longest wave length up to the shortest wave length that can still be covered by their corresponding refinement level.

3. Calculate the other refinement boxes

   (a) The previous refinement level is now increased by 1.

   (b) The new upper and lower limit of the wave lengths that will be covered by the new refinement level are calculated using eq. 4.7.

   (c) For the longest of those two wave lengths, the dimensions of the refinement box are calculated as stated in section 4.1.2

   The resulting refinement box will cover wave lengths from the longest wave length up to the shortest wave length that can be covered by the corresponding refinement level.

4. If the resulting refinement level used in the last 4 steps was equal to the refinement level of the shortest wave length, the approach is finished. If this is not the case, Step 3 is repeated until this does happen.

For further understanding of this method a calculation example is given in the next paragraph.

4.2.3. Calculation example

To illustrate the use of the method described in the previous section, an example will now be given. A mesh generated that is capable of simulating wave frequencies ranging from 0.55 up to 1.1 [rad/s] for a wave with an amplitude of 1 [m]. Deep water is assumed, which allows the calculation of the wave lengths from these wave frequencies according to equation 4.4. The range of wave lengths that will be simulated stretches from the shortest wave length, measuring 50.9 [m] up to the longest wave length measuring 203.8 [m] The specifications for the three refinement boxes are that a minimum of 5 cells per ζ_a are required in the free surface refinement box and respectively 48 cells and 24 cells per λ in the upper an lower refinement box. The initial grid consists of cells that have a vertice length of 1 Lpp, which is in this case 100 [m]. Here a description of the calculation of the free surface, upper and lower refinement boxes are given.

Free surface refinement box As all the waves will have the same amplitude, only one free surface refinement box is needed. According to equation 4.5 a grid refinement level of 9 is required to achieve a minimum of 5 cells per ζ_a. The dimensions of this box are calculated according to the dimensions stated in section 2b. The box ranges form + to - 1.1 ζ_a which equates to +1.1 [m] down to -1.1 [m].

Upper refinement boxes The upper refinement boxes will be calculated according to the approach stated in the previous section.

1. The required refinement levels for the longest and shortest wave are calculated according to equation 4.6. This results in a required refinement level of 5 $\left(\left\lceil \frac{log(\frac{203.8}{48*100})}{log(0.5)} \right\rceil\right)$ and 7 $\left(\left\lceil \frac{log(\frac{50.94}{48*100})}{log(0.5)} \right\rceil\right)$ for the longest wave and the shortest wave.

2. The refinement box with the lowest refinement level, which is 5, is now calculated.

   (a) The shortest wave length that can still be covered with a refinement of 5 is calculated according to equation 4.7. This is 150.0 [m] $\left(100[m]^{cell} * 0.5^5 * 48\right)$.

   (b) The dimensions of the refinement box will range from +1.1 [m] $(1.10 * 1.0[m])$ down to -40.8 [m] $(0.2 * 203.8[m])$

   The resulting refinement box has a refinement level of 5, stretches from the crest of the wave down to -40.8 [m].

3. The refinement box with a refinement level of 6 is now calculated.
   (a) The range of wave lengths that will be covered with a refinement level of 6 reaches from 75 [m] $\left(100[m]^{cell} * 0.5^6 * 48\right)$ up to 150 [m] $\left(100[m] * 0.5^5 * 48\right)$
   (b) The dimensions of the refinement box will range from +1.10 [m] $(1.1 * 1.0[m])$ down to -30.0[m] $(0.2 * 150.0[m])$

   The resulting refinement box has a refinement level of 6, stretches from the crest of the wave down to -30.0 [m].

4. The final refinement box, which has a refinement level of 7 is now calculated
   (a) The range of wave lengths that will be covered with the refinement level in this refinement box reaches from 37.5 [m] $\left(100[m]^{cell} * 0.5^7 * 48\right)$. up to 75.0 [m] $\left(100[m] * 0.5^6 * 48\right)$, which covers the shortest wave length of 50.9 [m].
   (b) The dimensions of the refinement box will range from +1.10 [m] $(1.1 * 1.0[m])$ down to -15.0[m] $(0.2 * 75.0[m])$ The resulting refinement box has a refinement level of 7, stretches from the crest of the wave down to -15.0 [m].

Lower refinement boxes The approach for the lower refinement boxes follows the approach for the upper refinement boxes with the exception that a minimum of 24 cells per wave length are required instead of 48 and that the refinement box stretches up to 0.6 λ instead of 0.2 λ. The three resulting lower refinement boxes are:

1. A refinement box with the lowest refinement level, which is 4, that stretches from +1.1 [m] $(1.10 * 1.0[m])$ down to -122.3 [m] $(0.6 * 203.8[m])$
2. A refinement box with a refinement level of 5 that stretches from +1.1 [m] $(1.10 * 1.0[m])$ down to -90 [m] $\left(0.6 * 100[m] * 0.5^4 * 24\right)$
3. The last refinement box with a refinement level of 6 that stretches from +1.1 [m] $(1.10 * 1.0[m])$ down to -45 [m] $\left(0.6 * 100[m] * 0.5^5 * 24\right)$

4.2.4. Resulting grid

The grid described in the previous section is now meshed in HEXPRESS. It is meshed using a total of 7 refinement boxes. One refinement box is used for the free surface, and two sets of three boxes are used for the upper and lower refinement zones. A description of these 7 boxes is given in table 4.1

Refinement boxes	Refinement level []	Upper limit [m]	Lower limit [m]
Free surface box	9	+1.100	-1.100
Upper refinement boxes	5 6 7	+1.100 +1.100 +1.100	-40.80 -30.00 -15.00
Lower refinement boxes	4 5 6	+1.100 +1.100 +1.100	-122.3 -90.00 -45.00

Table 4.1: Grid refinement boxes

See figure 4.8 for the resulting grid. The red square zooms in extra on the grid refinement near the free surface.

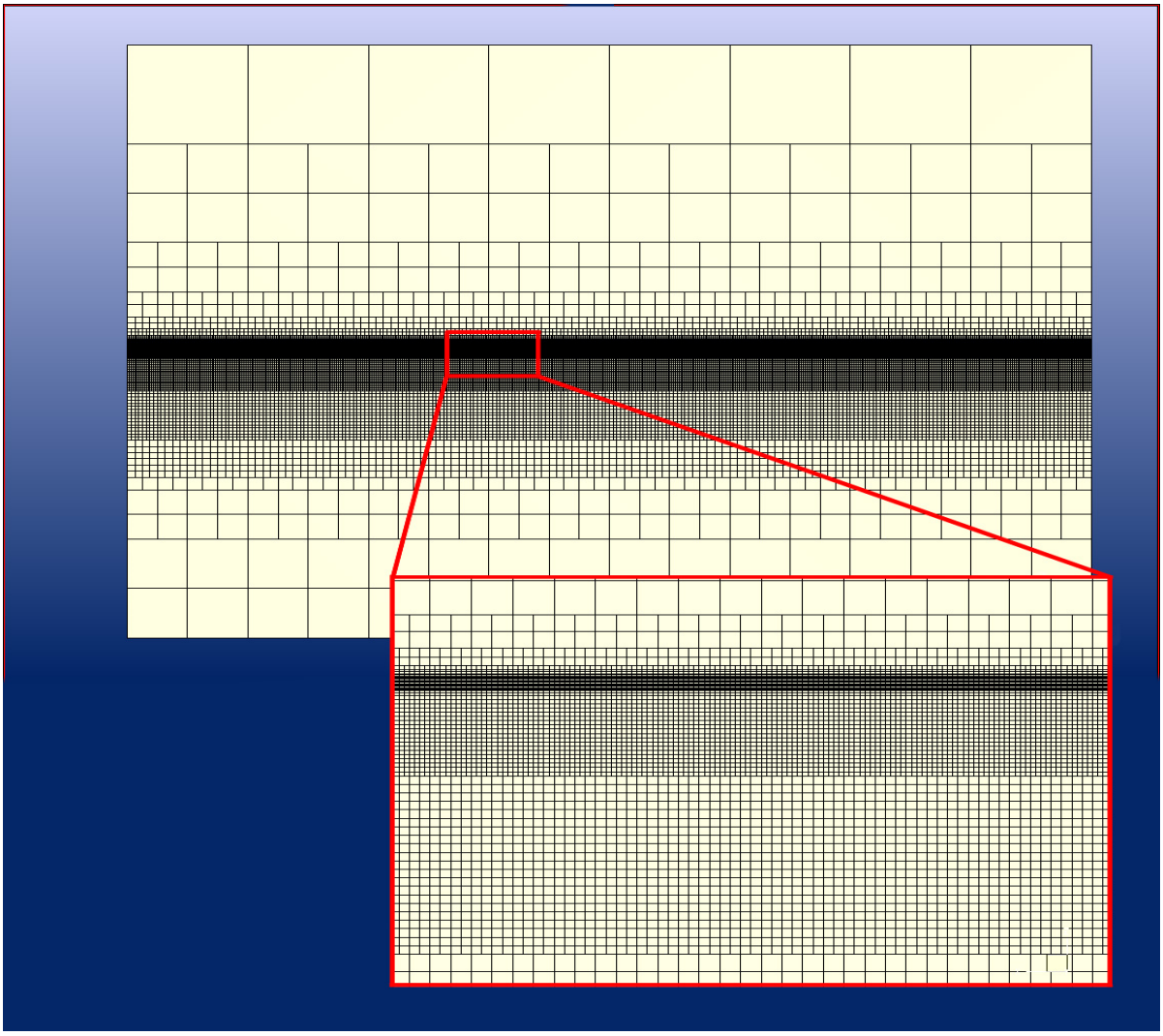

Figure 4.8: Final 2D wave grid

4.3. Grid refinement study

A grid refinement study is used to determine the effects of the discretisations both in time and space on the dissipation and dispersion. The refinement study will show which grid and time-step combination will result in the most efficient set-up that can accurately describe the waves. A total of five systematically refined grids are tested with four different time steps.

All these tests are performed for both the longest and shortest wave length that were tested in the CRS model test experiments. This way it is possible to test the effects of the discretisations over the range of wave lengths. In the CRS model tests, tests were performed in waves ranging from 50.9 up to 204 [m]. These lengths correspond to roughly 0.5x and 2.0x the length of the vessel, which measures 100 [m] between the perpendiculars.

A special note must be made regarding the CFL condition, the full extent of this note can be read in paragraph 3.2.3. Summarising, it can be said that in order for ReFRESCO to run stable under all circumstances it is recommended to keep the Courant number below $\frac{1}{6}$. This poses a limitation on allowed combinations of grid refinement and time-stepping.

4.3.1. Overview of the simulations

In table 4.2 the five grid refinements that are tested are shown at the top including their specified number of cells per wave height and per wave length in the upper refinement box.

Grid number	**1**	**2**	**3**	**4**	**5**
N_{cells} / ζ_a	2	3	5	6	9
N_{cells} / λ *in upper refinement box*	24	36	48	64	96

Table 4.2: Overview of the five grid refinements

In table 4.3 all combinations of the five grid refinements and the four different time-steps that are tested can be seen. The time-step is defined as a fraction of the waveperiod T in order to match the time-step with the waveperiod of the simulated wave. Combining five grid refinement levels and four time-steps results in a total of twenty different combinations that are to be. Furthermore, they will all be tested for both the shortest and the longest wave, thus resulting in a total of forty simulations.

For each grid refinement and time-step combination, the Courant number was calculated for the smallest cell size, which occurs at the free surface. As stated in paragraph 3.2.3 to prevent instabilities when running simulations in ReFRESCO it is recommended to keep the Courant number below the theoretical limit of $\frac{1}{6}$. Despite that recommendation, tests with courant numbers exceeding $\frac{1}{6}$ were tested in this study. These tests showed that it was impossible to run simulations on cases with Courant numbers exceeding 0.25 as these simulations would not converge over time. This result endorses the theory regarding the theoretical limit.

To ensure that simulations will run stable, no combinations with courant numbers exceeding $\frac{1}{6}$ are considered for the most efficient combination. With this Courant restriction a total of 10 combinations remain, which are shown in green. The simulations that are not considered an option are shown in red.

Grid number		**1**	**2**	**3**	**4**	**5**
		Courant number				
time-step Δt	T/100	0.126	0.188	0.314	0.377	0.565
	T/150	0.084	0.126	0.209	0.251	0.377
	T/200	0.063	0.094	0.157	0.188	0.283
	T/300	0.042	0.063	0.105	0.126	0.188

Table 4.3: Courant number of the grid refinement and time-step combinations

Finally table 4.4 shows the total number of cells used in each of the five grids.

Grid number	1	2	3	4	5
Total number of cells	1.88E4	5.11E4	5.87E4	8.35E4	2.05E5

Table 4.4: Total number of cells in the grids

4.3.2. Results

In figure 4.9 a plot of the propagating wave with a frequency of 1.10 [rad/s] is shown. In this case 48 cells were used per wave length in combination with a time-step of $T/200$. In yellow a zoomed in section of the free surface is shown.

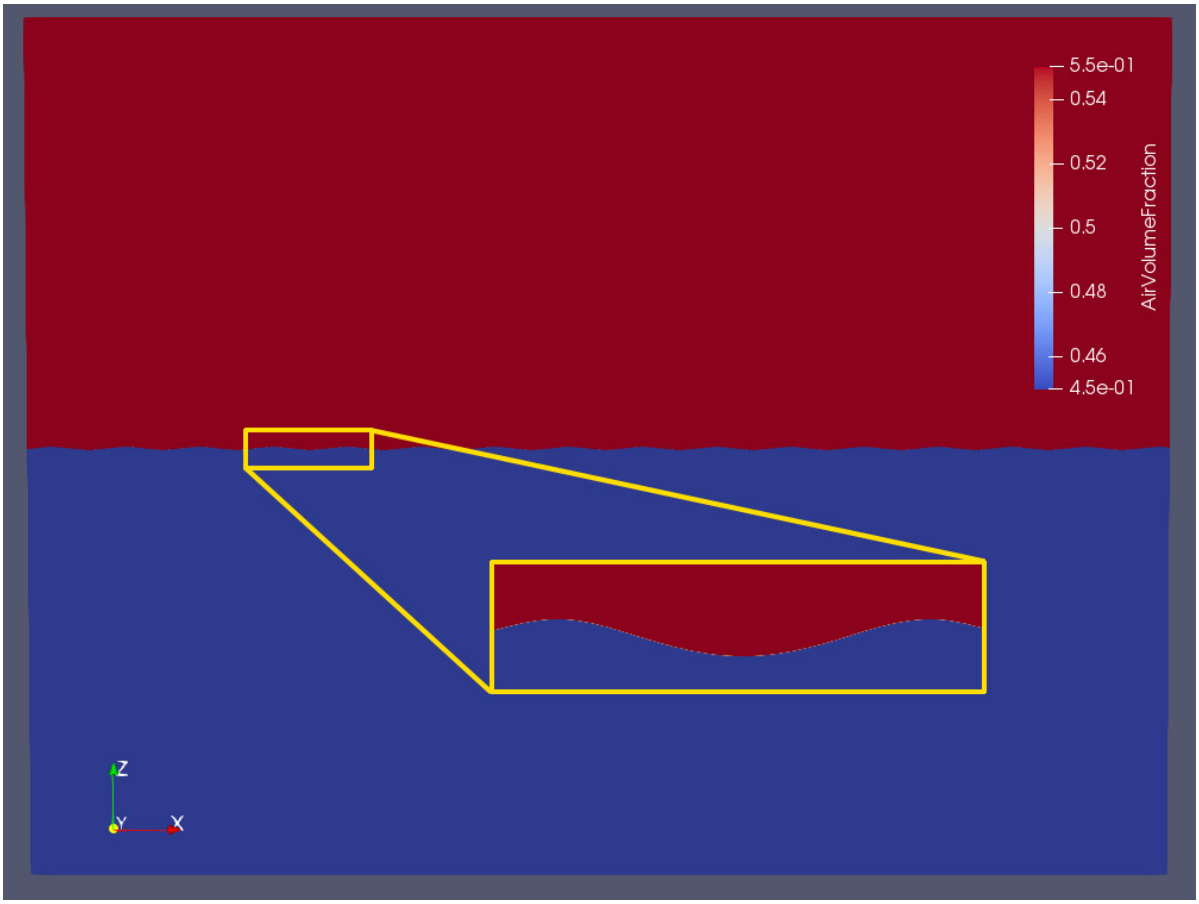

Figure 4.9: 2D waves simulated with ReFRESCO

The analysis of the results will now be discussed. In this analysis the wave dissipation, dispersion and reflection were checked.

Wave dispersion and dissipation First wave dissipation and dispersion were checked for all cases. Dissipation is defined as the reduction in waveheight of the wave over one wave length. The dispersion is defined largest error in wave length measured within the domain compared to the theoretical wave length as calculated according to equation 4.4. For this check a tool developed at MARIN was used. This tool determines the wave height and length of each wave that was simulated within the domain and then determines the largest error.

The results from the grid refinement study for both wave dissipation and dispersion are shown below in figure 4.10 and 4.11. Dissipation and dispersion are shown on the vertical axis. On the horizontal axis all grid refinement and time-step combinations are shown.

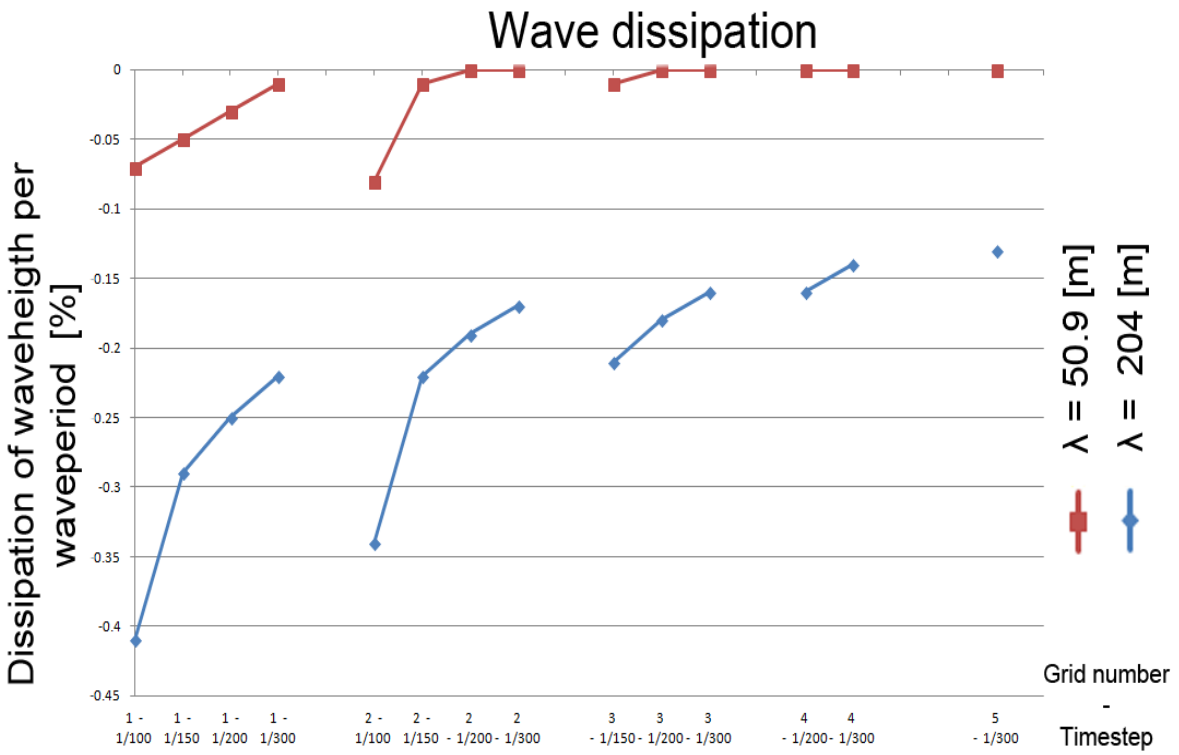

Figure 4.10: Wave dissipation plotted for each case

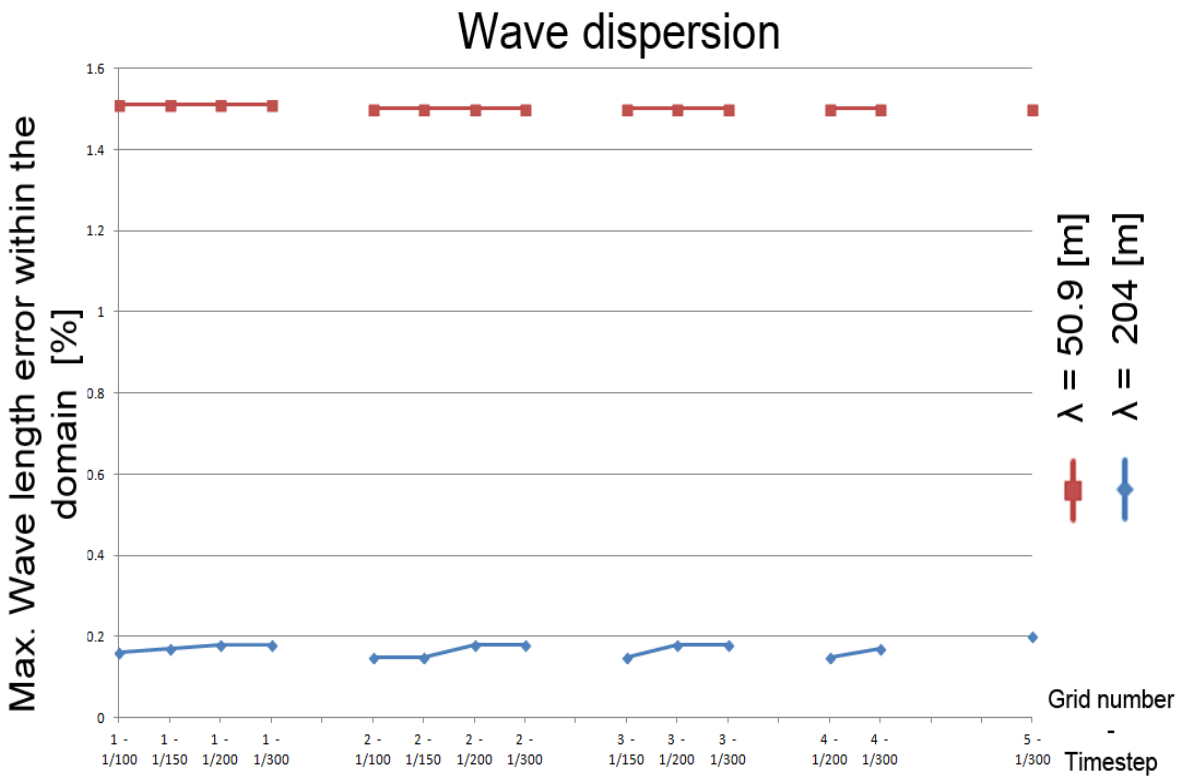

Figure 4.11: Wave dispersion plotted for each case

Wave reflection Wave reflections back into the domain at the boundaries are unwanted as they can disturb the shape of the propagating waves within the domain. To prevent such reflections, relaxation zones are implemented in the domain. Information regarding these zones can be found in paragraphs 2.3 and 3.3.3. The effectiveness of these relaxation zones was tested to ensure that wave reflections were kept to an acceptable level. The wave reflection C_r is defined as the relative amplitude of the wave that is coming back into the domain ζ_{in} in relation to the outgoing wave amplitude ζ_{out}. See equation 4.8. The same MARIN tool used to determine the dissipation and dispersion of the waves was used to determine the reflection of the wave at the boundary.

$$C_r = \frac{\zeta_{in}}{\zeta_{out}} \tag{4.8}$$

The reflection was checked for all the tested grid and time-step combinations with a Courant number below $\frac{1}{6}$. The results are shown in table 4.5. Red indicates that the Courant number limitation was exceeded.

Grid number		**1**	**2**	**3**	**4**	**5**
wave length λ [m]	time-step [s]	Wave reflection [%]				
50.9	T/100	0.36	-	-	-	-
	T/150	0.34	0.60	-	-	-
	T/200	0.32	0.63	0.61	-	-
	T/300	0.32	0.62	0.62	0.48	-
204	T/100	1.54	-	-	-	-
	T/150	1.26	0.97	-	-	-
	T/200	1.20	0.85	0.83	-	-
	T/300	1.16	0.78	0.75	0.62	-

Table 4.5: Wave reflection results

4.4. Discussion of the results

Now that the results are known it is now possible to determine the optimum grid. This decision is based on the following aspects.

- The wave dispersion must be small enough such that the wave length is constant over the domain and agrees with the length calculated from the dispersion relation.
- The wave dissipation must small enough such that the wave height is constant over the domain
- The wave absorbing zones are effective enough to limit the amount of wave reflections to few percent

Furthermore, an acceptable compromise must be found between simulation cost and acceptable wave dispersion and dissipation levels. Simulation costs depend on many factors, but in general it can be said that they scale roughly linear with the number of cells in the grid and with the decrease in step size.

Taking these aspects into account, the following can be noticed from the results. For the wave absorption:

- The wave absorption limit the reflections to values between 0.3 and 1.5 % for all simulations.

For the wave dispersion:

- Wave dispersion appears to be insensitive to the grid refinements. All grid refinements and time-step combinations result in similar values for the maximum dispersion error, being 0.18 % for the longest wave and 1.5 % for the shortest wave. This means that the largest error of the wavelength

compared to the theoretical value within the entire domain is 0.4 m for the 204 m long wave and 0.7 m for the 50.9m long shortest wave.

- The wave dispersion appears to not converge to zero for increased grid refinement. This could be explained by a modeling error. The wave introduced into the domain is a stokes-5 wave rather than a natural waveshape. As the wave is propagating over the domain, it takes on this natural waveshape, which could explain the 0th order error. Another explanation could be that the water is not infinitely deep, which could have an influence on the wavelenght. A third explanation could be that the method used to determine the dispersion is the cause of the 0th order error. The method uses zero crossing analysis to determine the length of the wave. Due to the spatial discretisation of the domain, it can be the case that the method is not able to exactly pinpoint the location of the zero crossing point, but rather take the closes point available, which would explain the error in the wavelength estimation.
- The maximum wavelength error of 0.4 m up to 0.7m for the 204 m and 50.9 m long wave respectively are considered small enough to ensure a constant wave length over the domain for all grid refinement and time-step combinations.

For the wave dissipation:

- The wave dissipation appears to converge to zero for increased refinement in the grid and time-step.
- For the time-step $T/100$, the wave height would decrease by 0.07 % and 0.41 % per waveperiod for the short 50.9 m wave and the long 204 m wave respectively. For the short wave it takes about 6 waveperiods from the moment that it is generated at the inlet until it reaches the vessel as it has to travel about 300m. For the long wave this equates to 1.5 periods. Over this distance the dissipation of the waveheight would equate to 0.0080 m and 0.0120 m for the short 50.9 m and long 204 m wave respectively.
- The decrease in dissipation from timestep $T/100$ compared to $T/150$ equates to about 25 %. This results in a dissipation of the waveheight from the inlet to the vessel of 0.0060m and 0.0090 m for the short 50.9 m and long 204 m wave respectively
- The decrease in dissipation from timestep $T/100$ compared to $T/200$ equates to about 40 %. This results in a dissipation of the waveheight from the inlet to the vessel of 0.0048m and 0.0072 m for the short 50.9 m and long 204 m wave respectively
- The decrease in dissipation from timestep $T/100$ compared to $T/300$ equates to about 45 %. This results in a dissipation of the waveheight from the inlet to the vessel of 0.0044m and 0.0066 m for the short 50.9 m and long 204 m wave respectively
- The maximum dissipation of the waveheight between 0.0048 and 0.0072 m achieved using a timestep of $T/200$ is deemed small enough to be accepted.
- A decrease of the timestep from $T/200$ to $T/300$ would roughly result in an increase of the computation cost of about 50 % as the number of timesteps required in the simulation would increase by that amount.
- When the 50 % increase in cost from the timestep $T/200$ to $T/300$ is compared to the decrease in wave dissipation of about 0.0004 m and 0.0006 m for the short 50.9 m and long 204 m wave respectively, the increase in accuracy is deemed insignificant to the increase in cost. Therefore the timestep of $T/200$ is deemed to be the optimum
- Using this timestep of $T/200$ it can be seen from a comparison of grid 1 to grid 2 that the dissipation decreaseses by 87 and 25 % for the short 50.9 m and 204 m long wave respectively. This results in a decrease of the dissipation of 0.04 and 0.25 % to 0.005 and 0.19 % for the short 50.9 m and long 204 m wave respectively.
- Using this timestep of $T/200$ it can be seen from a comparison of grid 1 to grid 3 that the dissipation decreaseses by 93 and 32% for the short 50.9 m and 204 m long wave respectively. This results in a decrease of the dissipation of 0.04 and 0.25 % to 0.003 and 0.17 % for the short 50.9 m and long 204 m wave respectively.

- Using this timestep of $T/200$ it can be seen from a comparison of grid 1 to grid 4 that the dissipation decreaseses by 93 and 32% for the short 50.9 m and 204 m long wave respectively. This results in a decrease of the dissipation of 0.04 and 0.25 % to 0.003 and 0.17 % for the short 50.9 m and long 204 m wave respectively.
- The increase in grid refinement from grid 2 to grid 3 would increase the cost of the simulation by about 14 % as the number of cells in the grid increase by that amount.
- When the 14 % increase in cost from grid 3 compared to grid 2 is compared to the decrease in the wave dissipation, going from 0.005 and 0.19 % down to 0.003 and 0.17 % respectively for the short 50.9 m and long 204 m wave respectively, the increase in accuracy is deemed significant enough to justify the increase in cost.
- When comparing grid 4 to grid 3, the same values for the dissipation, being 0.003 and 0.17 % for the short 50.9 m and long 204 m wave respectively are seen.
- As the increase in accuracy from grid 3 compared to grid 2 is deemed in line with the increase in computational cost and the comparison between grid 4 to grid 3 has shown no decrease in dissipation, grid 3 is deemed the optimal.

4.5. Conclusion

- Grid number 3, using 48 cells per wave length in the upper refinement box, in combination with a time-step of $T/200$ is found to be the most efficient combination that satisfies all the requirements. Waves simulated using this combination of settings have a very low wave dissipation ranging between 0 and 0.18 % for wave with a length of 50.9 m up to 204 m. This translates to a dispersion of the waveheight of 0 m and 0.005 m for the short 50.9 m and long 204 m waves respectively.
- The dispersion ranges between 0.19 and 1.5 %, which translates to a maximum wavelength error of 0.4 m up to 0.7m for the long 204 m and short 50.9 m wave respectively.
- The relaxation zone is capable of keeping reflections at the domain boundaries below 1% for this grid refinement and time-step combination.

Considering the relatively low dissipation, dispersion and reflections, the accuraly of the incoming waves is deemed sufficient for this research.

5

Simulating diffracting waves

Now that we are able to simulate consistently propagating 2D regular waves, it is time to move on to the simulation of the vessel in a 3D domain.

The purpose of this chapter is to determine the optimal grid refinement for the correct simulation of the vessel's response to incoming regular head waves. As unsteady CFD simulations such as these are costly, a compromise must be made between accuracy and cost. Therefore the most optimal grid refinement refers in this case to the best compromise between the cost of the simulation and the accuracy of vessels response.

In this chapter a grid topology is presented that is designed to capture both the incoming as well as the diffracting waves accurately. The optimum grid refinement will be determined using a grid refinement study. D.L.Chow and K.A.McTaggart [13] have proven in their validation of PRECAL that it's capable of providing an accurate estimate of the vessel's response to incoming waves. To ensure that the response determined using CFD is correct, it is compared to PRECAL.

5.1. Test procedure

The process used to estimate the vessels response to incoming waves is referred to as a "static vessel in regular waves" test. The short explanation of this test is given here first.

In this test the vessel sails at a constant forward speed. It has zero DoFs, hence the name "static" in the name of the test. This means that the vessel can't move, with the exception of having a constant forward speed. The vessel is simulated in calm water to estimate its calm water resistance first.

Then it is subjected to regular incoming head waves. The incoming waves diffract off of the hull, inducing an oscillating force in heave direction and moment in pitch direction. The amplitude of these responses, as well as their phase in relation to the incoming wave are then determined and compared to PRECAL.

The more detailed explanation follows now. The implementation of the "static vessel in regular waves" simulation that is used in this research consists of three parts. These are referred to as the 'start up', 'calm water' and 'static vessel in regular waves' simulations.

5.1.1. Start up simulation

For the first two parts, the vessel will sail at a constant speed in calm water. The purpose of the start up simulation is to instantly get the vessel up to its desired speed. The advantage of this approach is that this approach will take less computation time compared to slowly accelerating the vessel to the desired speed. The challenge in this simulation part however, is that for the first few iterations of the simulation, the solver is likely to encounter problems converging the solution. This is due to the fact that large gradients can occur in the flow surrounding the hull as it's accelerated instantaneous in the first time-step.

At MARIN a method is developed that will enable this instant start up of the simulation. The details of this method stretch beyond the topic of this research but a short explanation is given here. For the first few time steps the simulation runs using different settings compared to the rest of the calm water simulation. These settings will aid the convergence of the solution. One example of such an aid is a damping zone surrounding the vessel which dampens out the initial large gradients. After a few iterations, when the solution has converged the settings of the simulation are returned to normal and the second part of the calm water simulation is started.

5.1.2. Calm water simulation

In the second part of the process, the vessel will continue to sail in calm water. At the beginning of the second part, the flow surrounding the vessel has not completely stabilised from the harsh instantaneous start up yet.

Therefore, the simulation of the vessel in calm water will continue to run until the flow, as well as the forces that are induced by it on the vessel have stabilised to an acceptable level. In this research the acceptable level of convergence was specified as a maximum variation of the force in heave direction felt by the vessel compared to the running mean over the last two seconds of 0.1%. Once the criterion has been passed the simulation will stop.

Note that in this research, the simulations ran longer than strictly required by this criterion, resulting in an even more stabilised flow. Figure 5.1 shows al time traces of the calm water resistance. From the zoomed in section of the plot, shown in red, the convergence of the signal can be observed clearly. In this case the maximum variation compared to the running mean was 0.04% and the calm water resistance was estimated at 24.12 [kN].

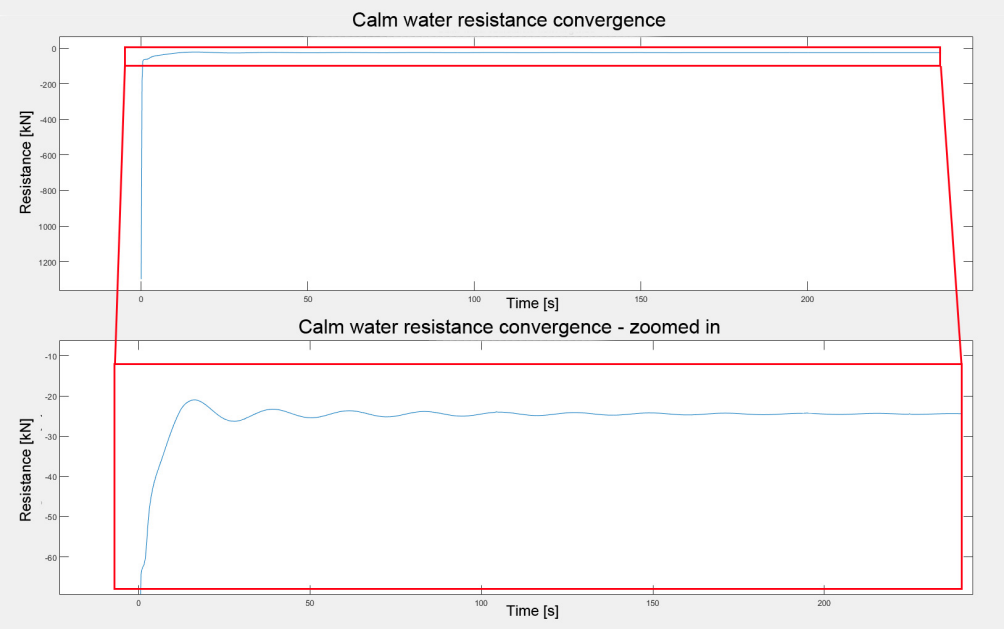

Figure 5.1: Calm water resistance time trace

In figure 5.2 the wave system of a vessel in calm water is visualised.

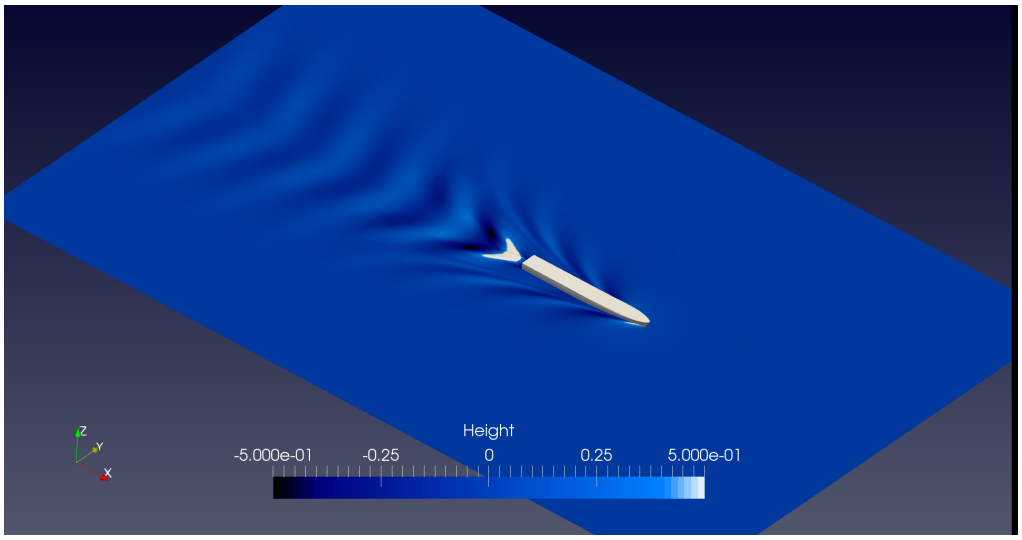

Figure 5.2: Calm water simulation

5.1.3. Static vessel in regular waves simulation

In the final part of the process, the static vessel with forward speed is simulated in regular head waves. The purpose of this part is to estimate the amplitude and phase of the force in heave direction and moment in pitch direction induced by the incoming waves as they are diffracting off of the hull. The simulation starts up from the last time step of the calm water simulation.

At the start of this simulation, regular waves are generated at the inlet of the domain. The simulation then runs until the first wave has propagated to the other side of the domain, after which it continues to run for ten more wave encounters. The amplitude of the force and moment are then estimated by taking the time average of the resistance signal over the last ten encountered wave periods. Theire phase is determined by comparing the signal to the signal of the wave elevation at the Centre of Gravity (CoG) over the last 10 waves and taking the average. This approach is designed to ensure sufficient statistical certainty as is recommended by the ITTC [1].

By waiting until the regular waves have filled the domain, the induced forces on the vessel have time to stabilise. Stabilise in this case refers to the forming of a repetitive pattern with no significant change in the mean value over time. This way an accurate estimate of the vessel's response is ensured.

In figure 5.3 the wave system of a static vessel in regular waves is visualised.

5.2. Simulation parameters

The parameters used for the diffraction simulations are now explained in this paragraph.

5.2.1. Domain, boundary conditions and wave absorption

In chapter 3.3 the domain, boundary conditions and wave absorption zone used in these simulations are described. In short, a three dimensional, stretched version of the grid used for the 2D wave propagation simulations is used with similar boundary conditions. A wave absorption zone is located at the perimeter of the domain to prevent waves from reflecting back into the domain.

5.2.2. Vessel speed and wave frequency

Due to the limited time that is available for this research, the simulations will be restricted to a single speed for the vessel and a single frequency for the incoming regular waves. The idea behind this decision is that it is better to focus on quality and just simulate one case very well, rather than researching multiple cases in less detail and to just go for quantity. By selecting the case carefully it is still possible to conclude on the ability of CFD to estimate the added resistance in regular waves.

The selected speed and wave frequency match the values at which the CRS model tests of the FDS

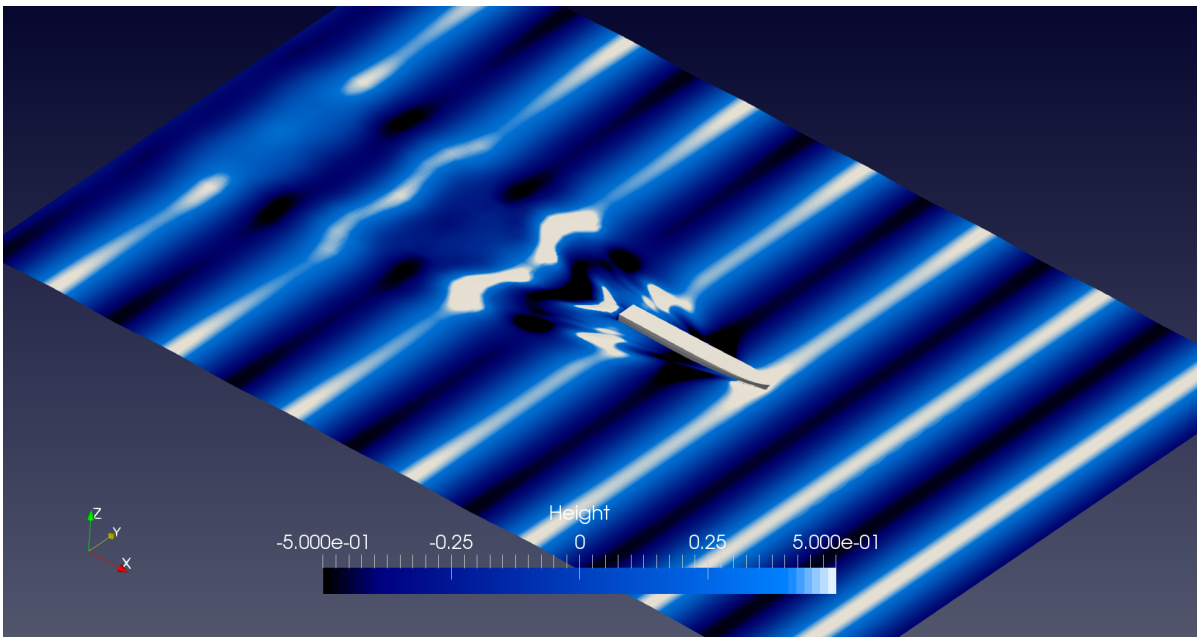

Figure 5.3: Static vessel in regular waves

were performed. This way a better comparison of the results can be made during the validation part of the research. The speed of the vessel is selected to match the 17.31 [Kts] speed used in the model tests. For the incoming wave frequency a value was selected that would result in the largest wave added resistance. The reasoning behind this decision is that shipyards are most interested in the maximum added resistance in regular waves.

In the CRS study model tests were performed for multiple incoming wave frequencies. Their results are used to determine at which of their simulated wave frequencies the largest added resistance would occur. In figure 5.4 a plot is shown of the QTF of the added resistance in regular waves in relation to the frequency of the incoming waves. The measured values are shown as green dots. The blue line indicates the expected value of the QTF in between those points.

The model test performed with an incoming wave frequency of 0.85 [rad/s], indicated with the red line, resulted in the largest measured added resistance in regular waves. This is also the wave frequency that will be used in this research.

5.2.3. Wave amplitude

The wave amplitude used in the simulations of the vessel with 2DoFs in regular waves, will be the same 1[m] amplitude as was used in the CRS model tests. For the diffraction simulations however, more moderate 0.5[m] was selected. The reasoning is as follows.

From video footage of the CRS model tests, it can be seen that the bow of the vessel is pitching violently in and out of the water during the test. At the maximum pitch angle the bow even clears the water completely. See figure 5.5. This could cause issues in the simulation which would make it hard to determine whether the implemented grid refinements are actually working as intended or not. Therefore a more moderate wave amplitude of 0.5[m] was used first.

5.2.4. Time step

For the time step of the calm water simulation a MARIN guideline was used that is based on the experience of MARIN CFD users. The use of this time step ensures the efficient and accurate simulation of the calm water resistance. The guideline uses the vessels speed and length as an input to determine an appropriate time step.

The guideline states that the time step for a calm water simulation Δt_c should be selected such that it takes about 40 to 50 time steps for the flow to move from the bow to the stern of the vessel. See

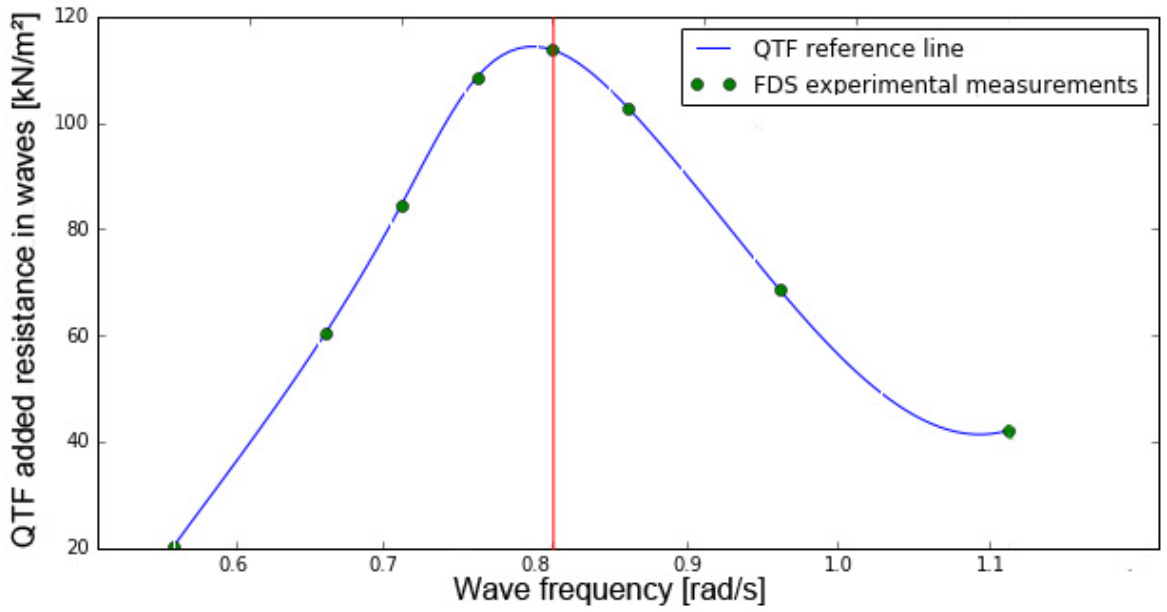

Figure 5.4: CRS model test QTF plot of the added resistance in regular waves

equation 5.1.

$$\Delta t \frac{40+50}{2} \approx \frac{Lpp}{v} \tag{5.1}$$

Where Lpp is the length between the vessel's perpendiculars and v is the vessels speed.

By inserting the 100 [m] Length between perpendiculars (Lpp) of the FDS and the 17.3 [Kts] speed into equation 5.1 and solving for Δt, a time-step of 0.24[s] is found to be optimal for the calm water simulation.

For the start up simulation, running for just a few iterations, another MARIN guideline states that $1/10^{th}$ of this value should be used to aid in the convergence of the simulation. See equation 5.2. Thus a time step of 0.024[s] will be used for the start up.

$$\Delta t_{start} = \frac{1}{10} \Delta t_c \tag{5.2}$$

With Δt_{start} the time step of the start up simulation.

Finally, for the static vessel in regular waves simulation a time step must be used that will ensure accurate propagation of the waves. In the simulation of accurately propagating 2D waves a time step was already determined that will do this whilst also ensuring an efficient simulation in terms of cost. Therefore, this same optimal time step of $T/200$ is used.

In these simulations however, the reference frame, being the vessel, is moving. This changes the period of the wave from the point of view of the vessel. The selected time step must be adapted to account for this effect.

When a wave is seen from a moving reference frame, such as a moving vessel, the velocity of the vessel has an influence on the wave period observed from the vessel. This observed, or encountered wave period, known as T_e does not equate to the actual period of the wave T. The following practical example will clarify this principle:

- The encountered wave period can be imagined as the time that it takes for the wave to pass as observed from the vessel. If the vessel has zero forward speed during the wave encounter, this encountered wave period T_e will be equal to the actual wave period T of the wave.

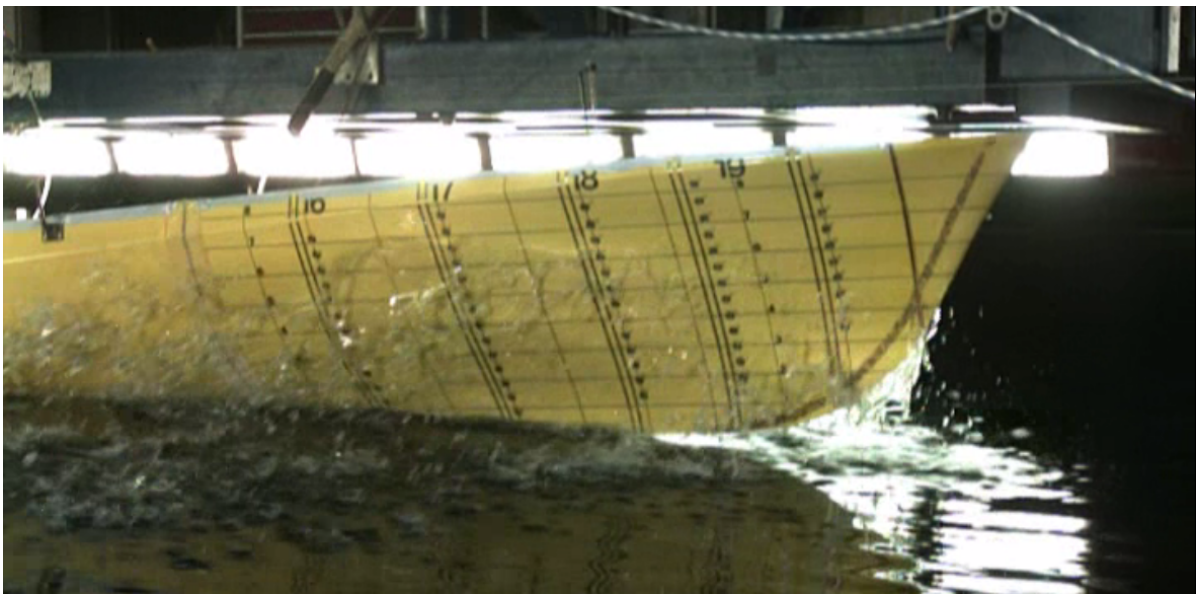

Figure 5.5: CRS model test footage [11] - bow lifting out of the water

- Now imagine the vessel sailing with forward speed, trying to outrun a wave coming from behind. Assuming that the wave is moving faster than the vessel it will now take longer for the wave to pass the vessel. In this case, the encountered wave period T_e is thus longer than the actual period of the wave T.
- The opposite occurs when a vessel sails into a head wave, which is the case in this simulation. The time it takes for the wave to pass the vessel will be shorter than the actual wave period of the vessel.

To accommodate for the shorter encountered wave period, the time step has to be adapted. This is done by substituting the encountered wave period T_e with wave period T in the optimum time step $T/200$.

The encountered wave period can be calculated from the wave frequency ω, speed of the vessel v and the approach angle relative to the wave θ_e according to equation 5.6. (Assuming head waves and deep water). Equation 5.6 is derived as follows:

The frequency of the encountered wave ω_e can be calculated with equation 5.3 which relates it to the wave frequency ω, approach angle relative to the wave θ_e, speed of the vessel v and wavenumber K.

$$\omega_e = \omega - cos(\theta_e)Kv \tag{5.3}$$

Where a head on approach angle corresponds to $\theta = 180°$

Under the condition that the waves are propagating in deep water, which is the case, the wave number K can be rewritten according to deep water dispersion theory as is described in equation 4.4.

$$K = \frac{\omega^2}{g}v \qquad (assuming\ deep\ water) \tag{5.4}$$

Substituting equation 5.4 into equation 5.3 and assuming head waves ($\theta = 180°$) this becomes:

$$\omega_e = \omega + \frac{\omega^2}{g}v \tag{5.5}$$

Finally, the encountered wave frequency ω_e is rewritten to the encountered wave period T_e by dividing 2π by ω_e

$$T_e = \frac{2\pi}{\omega_e} = \frac{2\pi}{\omega + \frac{\omega^2}{g}v} \tag{5.6}$$

In the case simulated here, with a vessel sailing at 17.31 [Kts] in regular head waves with a wave frequency of 0.85 [rad/s], the encountered wave period T_e will equate to 4.17 [s]. This is significantly shorter than the actual wave period T of 7.4[s]

The time step for the simulation in regular waves is then calculated by dividing this 4.17 [s] by 200. This results in a time step for the simulation in regular waves Δt_w of 0.021 [s].

5.2.5. Simulation time static vessel in regular waves

The static vessel in regular waves simulation will run for the time that it takes to fill the domain with waves plus an additional 10 wave encounters. The length of the domain is 600[m]. Assuming deep water, the length of the waves can be calculated from its frequency according to the deep water dispersion relation as is described in equation 4.4.

For the regular waves in this simulation, with a wave frequency of 0.85 [rad/s], this results in a wavelength of 85.3[m]. It would therefore require $(600/85.4 \approx)$ 7 encountered wave periods for a wave to propagate to the other side of the domain.

However, we are not dealing with a single wave here, but rather a group of waves. In the TU Delft reader Offshore hydromechanics [21], it is stated that the propagation speed of a group of waves equals to half the propagation speed of a single wave. Therefore, it would actually take about 14 encountered wave periods to fill the domain with waves. A further 10 wave encounters must be simulated in order to determine the time averaged resistance in diffracting waves with sufficient statistical certainty.

Thus a total of 24 encountered waves are to be simulated. As the encountered wave period is known to be 4.17 [s], this results in a total simulation time of about 100 [s]

5.3. Spatial discretisation

In this paragraph the spatial discretisation of the grid is discussed. The goal of these spatial discretisations is to simulate the waves within the domain accurately. This way, the resulting forces felt by the vessel should also be captured accurately. The spatial discretisations used for the diffracting wave simulations can be divided up into three main groups based on their purpose.

5.3.1. Incoming regular waves

The first group consist of discretisations that are designed to ensure that the incoming regular waves will propagate consistently through the domain. Optimal settings for these discretisations were derived in the previous chapter on 2D wave propagation and are now adapted for use in 3D. The same free surface, upper and lower grid refinement boxes are used, although their width has now increased to the width of the 3D domain. The same optimised number of cells per wave length and height that were found from the 2D wave propagation study are used in their respective boxes. In figure 5.6 these grid refinement boxes with their optimal grid refinements are shown.

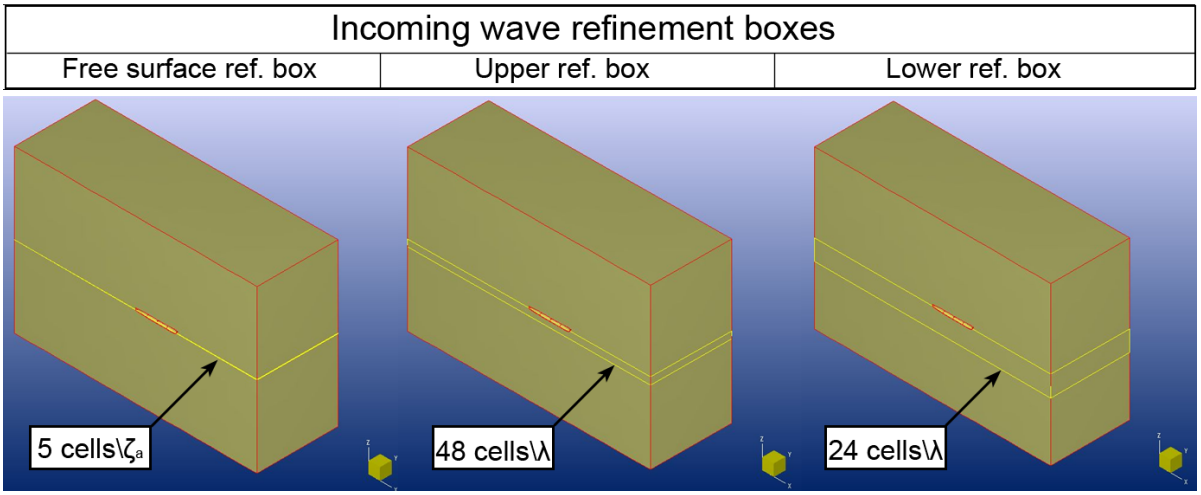

Figure 5.6: Refinement boxes for the incoming regular waves

Table 5.1 summarises the dimensions and refinement levels of these boxes used in this simulation. The dimensions of the boxes are given by their maximum and minimum x, y and z coordinates. As a reminder, the origin is located on the free surface, at App on the mirror boundary.

Refinement box	Refinement	Coordinates [m]					
		x+	x-	y+	y-	z+	z-
Free surface	$5\ cells/\zeta_a$	+300	-300	+200	0	+1.1 ζ_a	-1.1 ζ_a
Upper	$48\ cells/\lambda$	+300	-300	+200	0	+1.1 ζ_a	-0.2 λ
Lower	$24\ cell/\lambda$	+300	-300	+200	0	+1.1 ζ_a	-0.6 λ

Table 5.1: Refinement boxes for the incoming regular waves

5.3.2. Hull - fluid interaction (MARIN recommended)

The second group consists of spatial discretisations that were recommended by experienced MARIN CFD users. These discretisations are designed to ensure that the interaction between the hull and the fluid as well as the flow near the vessel is captured accurately. These grid refinements are based on a MARIN guideline that ensure sufficient refinement is placed at the surface of the vessel and in the area near the vessel.

The guideline relates the size of the cells on the hull at the midship and in the area surrounding the vessel to the beam dimension B of the vessel. These cells should have a dimension between $\frac{B}{30}$ and $\frac{B}{40}$.

A higher grid refinement is required in areas with steeper gradients in the solution. Therefore, at the bow, stern and transom refinements twice and four times as high are used. Furthermore the area surrounding the vessel is defined as a box that extends 0.1 Lpp ahead and behind the vessel. Furthermore, it extends 0.25 B to the side of the vessel and 1.1 ζ_a above and below the free surface.

See figure 5.7 for a visualisation of the MARIN recommended surface and area refinements.

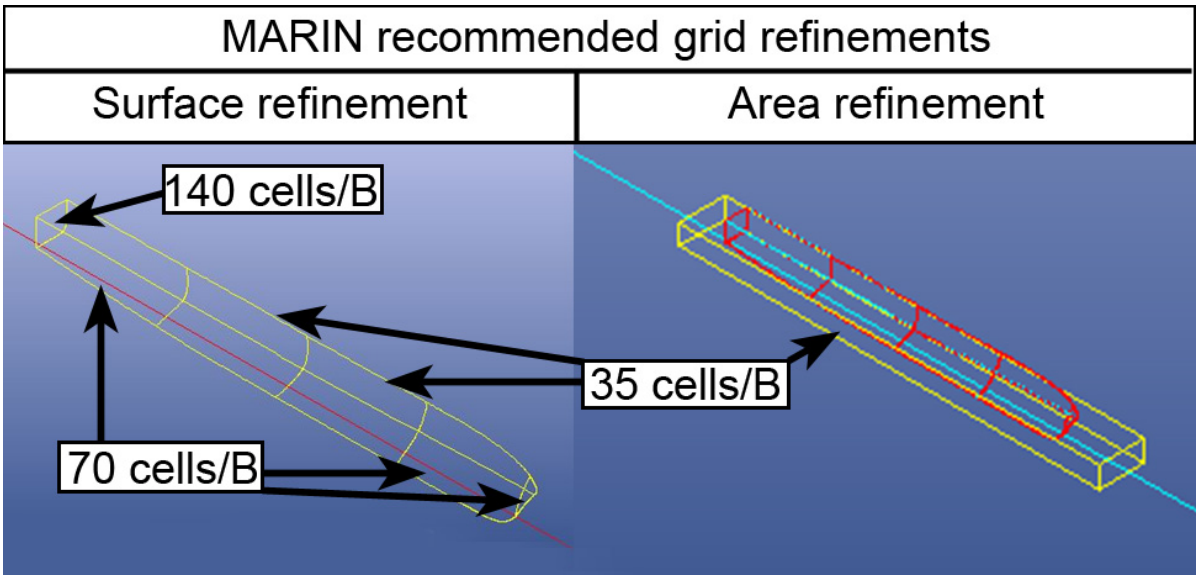

Figure 5.7: MARIN recommended grid refinements

In table 5.2 the specifications of the MARIN recommended surface and area refinements are presented in a similar fashion as was done for the incoming regular wave boxes.

Refinement box / surface	Refinement	Coordinates [m]					
		x+	x-	y+	y-	z+	z-
Area near vessel	35 cells / B	Lpp + 0.1 Lpp	-0.1 Lpp	B/2 + 0.25 B	0	+1.1 ζ_a	-1.1 ζ_a
Surface midship	35 cells / B	-	-	-	-	-	-
Surface bow & stern	70 cells / B	-	-	-	-	-	-
Surface transom	140 cells / B	-	-	-	-	-	-

Table 5.2: MARIN recommended grid refinements

5.3.3. Diffracted waves

Finally the third group consists of discretisations that are specifically designed to capture the propagating diffracting waves accurately. The discretisations used here are based on the diffracted wavelength λ_d.

As stated before, the moving vessel encounters waves with a higher wave frequency ω_e than the actual wave frequency ω. As a consequence, it will diffract the waves off of its hull with a frequency equal to this encountered wave frequency. Using the deep water dispersion relation as seen in equation 4.4 the length of these diffracted waves can be calculated from the encountered wave frequency ω_e. This wavelength is known as the diffracted wavelength λ_d. See equation 5.7

$$\lambda_d = \frac{2\pi g}{\omega_e^2} \tag{5.7}$$

In the case studied here, with a vessel sailing at 17.31 [Kts] in regular head waves with a wave frequency of 0.85 [rad/s], the encounter frequency will be 1.51 [rad/s] and the corresponding diffracted wave length λ_d will be 27 [m].

It is clear that this wavelength is significantly shorter than the incoming wavelength of 85.3[m]. Therefore it is likely that the grid refinements which were designed for the incoming regular waves are too coarse to capture the diffracting waves accurately. To mitigate this issue, areas of higher refinement are added near the vessel.

These refinement areas are based on the same principles as the refinements used for the incoming waves. An upper and a lower refinement box are used to capture the kinetic energy in the diffracted waves accurately. In these boxes the same optimised number of cells per wave length C_λ are used. The only difference is that the refinement level is now based on the shorter length of the diffracted waves λ_d, rather than the incoming wavelength λ. This results in a higher grid refinement within these areas compared to the rest of the grid.

The implementation of a free surface diffraction refinement box is not required as this refinement is already covered by the free surface refinement box implemented to capture the incoming regular waves.

The dimensions of the upper and lower diffraction refinement boxes are based on the dimensions of the diffracted wavelength. The idea is to capture the propagating diffracted waves near the vessel accurately. An optimum must be found between the cost of adding extra cells in a larger area surrounding the vessel and the accuracy of the resistance prediction. To find this optimum, three different sized sets of diffraction refinement boxes are tested. These are labelled the small, medium and large set.

The medium sized set of diffraction boxes will stretch $0.5\lambda_d$ to the side and behind the vessel. Due to its high forward speed, the vessel will overtake the waves diffracted ahead of it. As a consequence, it is unnecessary to expand the diffraction refinement box far ahead of the bow. Therefore the decision was made to stretch the box $0.1\lambda_d$ ahead of the vessel.

The height of the boxes is based on the kinetic energy in the diffracted wave using a similar approach as was used for the incoming regular waves. The boxes will stretch from $+1.1\zeta_a$ above the free surface down to -0.2 and $-0.6\lambda_d$ respectively. See Figure 5.8 for a visualisation of the medium sized set of diffraction refinement boxes.

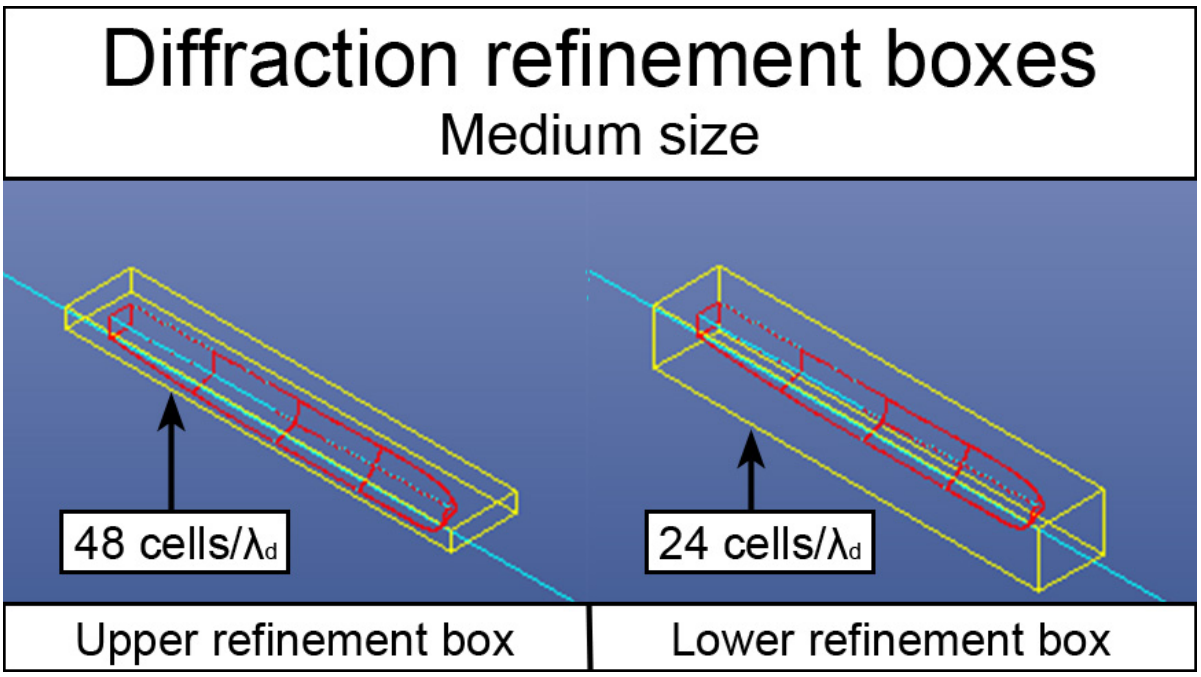

Figure 5.8: Diffraction refinement boxes - medium sized

The small and large sized sets of diffraction boxes will measure 0.5 and 1.5x the dimensions of the medium set in width and length. Their height will match that of the medium set as the kinetic energy in the waves remains the same. In table 5.3 the refinement and dimensions of the three sets of diffraction refinement boxes are presented in a similar fashion as was done for the MARIN recommended and incoming wave refinements.

Ref. box set	Ref. box	Refinement	Coordinates [m] x+	x-	y+	y-	z+	z-
Small	Upper	$48\ cells/\lambda_d$	Lpp + 0.05 λ_d	-0.25 λ_d	B/2 + 0.25 λ_d	0	+1.1 ζ_a	-0.2 λ_d
-	Lower	$24\ cells/\lambda_d$	Lpp + 0.05 λ_d	-0.25 λ_d	B/2 + 0.25 λ_d	0	+1.1 ζ_a	-0.6 λ_d
Medium	Upper	$48\ cells/\lambda_d$	Lpp + 0.10 λ_d	-0.50 λ_d	B/2 + 0.50 λ_d	0	+1.1 ζ_a	-0.2 λ_d
-	Lower	$24\ cells/\lambda_d$	Lpp + 0.10 λ_d	-0.50 λ_d	B/2 + 0.50 λ_d	0	+1.1 ζ_a	-0.6 λ_d
Large	Upper	$48\ cells/\lambda_d$	Lpp + 0.15 λ_d	-0.75 λ_d	B/2 + 0.75 λ_d	0	+1.1 ζ_a	-0.2 λ_d
-	Lower	$24\ cells/\lambda_d$	Lpp + 0.15 λ_d	-0.75 λ_d	B/2 + 0.75 λ_d	0	+1.1 ζ_a	-0.6 λ_d

Table 5.3: Diffraction grid refinement boxes

5.3.4. Combined spatial discretisation

The three groups of spatial discretisations are combined into one set. This set is thus designed to capture the interaction between the hull and the flow as well as the incoming and diffracted waves accurately.

5.4. Optimising the dimensions of the diffraction boxes

In order to determine an optimum dimension for the diffraction refinement boxes three tests were performed. Optimum in this case refers to the best compromise between simulation cost and accuracy of the vessel's response.

First, three grids were generated in which the MARIN recommended refinements and the refinements for the incoming regular waves were kept the same. The size of the implemented diffraction boxes however, was varied from small to medium to large. In figure 5.9 the three resulting grids are shown. The purpose of the red lines is to make the comparison between the grids easier.

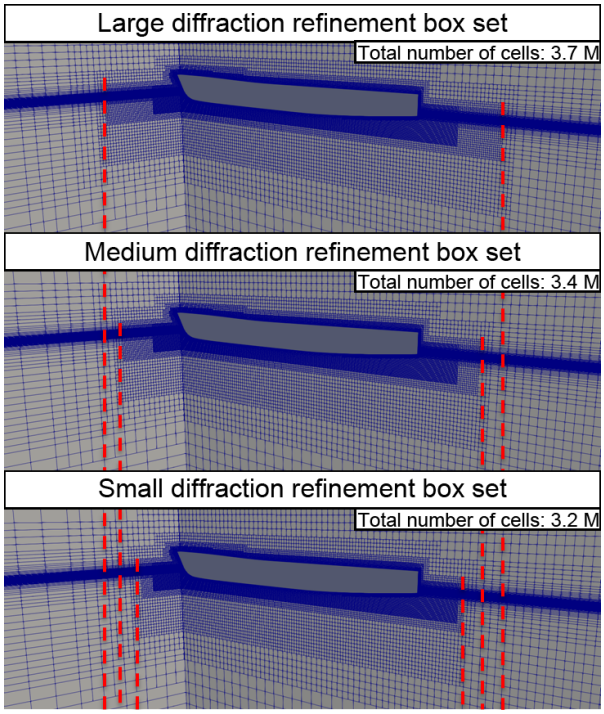

Figure 5.9: Three grids with varying dimensions of the diffraction box set

Next, the vessel's response due to the diffracting waves was determined by performing the static vessel in regular waves simulation procedure as described in chapter 5.1 for each of the three grids. The results are presented in figures 5.10 and 5.11.

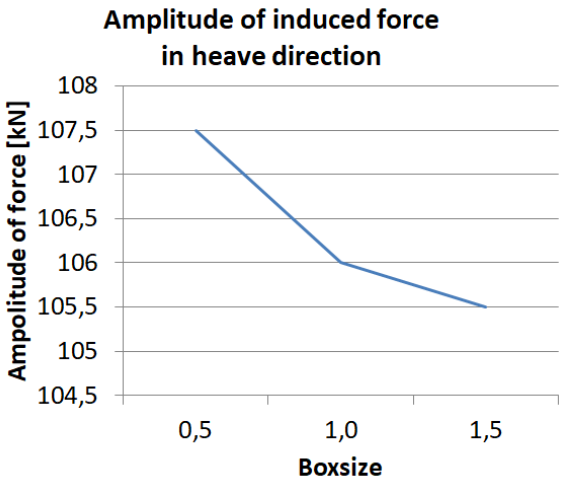

Figure 5.10: Amplitude of the induced force in heave direction for all three refinement boxsizes

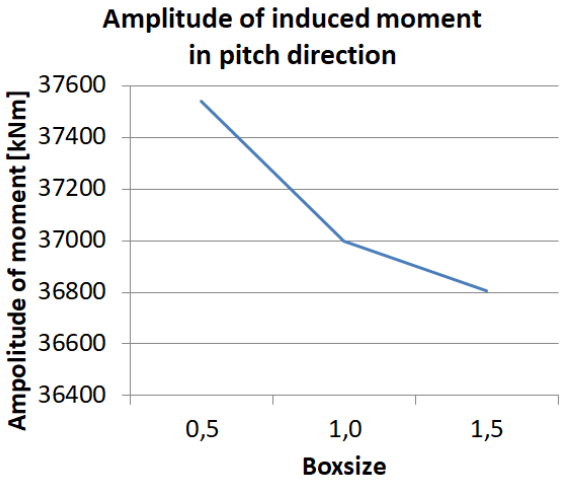

Figure 5.11: Amplitude of the induced pitch moment for all three refinement boxsizes

The following conclusions can be drawn from these test results:

- It appears that the induced force in heave and moment in pitch direction converge well for increased box sizes.
- The absolute difference between the maximum and minimum values for heave and pitch are 2 kN and 734 kNm respectively
- The added resistance estimate decreases by 1.40% and 1.45% for the force in heave direction and the moment in pitch direction respectively, when the results of medium set are compared to the small set.
- When the results from the large set are compared to the medium set, the responses decrease by 0.47% and 0.52% respectively.
- The increase in computation cost from the medium to the large set is about 9% as the total number of cells in the grid is increased by this amount.

Based on the small change in resistance from the medium to the large sized set of refinement boxes, the resistance determined using the medium dimensioned set is considered sufficiently converged. The use of the large set will result in a marginal improvement of the solution at the cost of a significant increase in computation time. Therefore the medium sized refinement box set is selected as the optimum.

5.5. Grid refinement study

To determine an optimum grid refinement level for the simulation of the correct vessel response in diffracting waves, a grid refinement study is performed. Optimum in this case refers to the best compromise between simulation costs and the accuracy of the vessel's reponse.

The grid refinements that are implemented to capture the incoming regular waves, as well as the MARIN recommended refinements are considered optimised already. Both in terms of their dimensions as well as their refinement level. For the diffraction refinement boxes the optimum dimensions were determined in the previous paragraph. The remaining task is to determine an optimum grid refinement level for these boxes.

In this study the number of cells per diffracted wavelength C_{λ_d} are varied in the diffraction refinement boxes whilst all other grid refinements are kept constant. This method ensures that it is possible to evaluate the effect that just these refinements have on the vessel's response.

For this study a total of five systematically increased grid refinements were tested, ranging from 12 up to 192 cells per diffracted wavelength C_{λ_d}. In table 5.4 an overview of the refinements used in the diffraction boxes for the five grids are shown.

Grid name	Refinement level Upper diffusion refinement box [Cells/ λ_d]	Refinement level Lower diffusion refinement box [Cells/ λ_d]	Total number of cells [-]
Very coarse	12	6	2.8M
Coarse	24	12	3.2M
Medium	48	24	3.5M
Fine	96	48	5.0M
Very fine	192	96	14M

Table 5.4: Overview of diffraction refinement box refinement levels

Furthermore, table 5.5 presents the refinement levels of the refinements that were kept the same over all the grids. The dimensions of all grid refinement boxes are kept consistent with the specifications as given in paragraph 5.3.

Refinement group	Refinement box / surface	Refinement
Incoming regular waves	Free surface box	5 cells / ζ_a
	Upper refinement box	48 cells / λ
	Lower refinement box	24 cells / λ
MARIN recommended	Near vessel box	$\sim$35 cells / B
	Surface midship	$\sim$35 cells / B
	Surface bow & stern	$\sim$70 cells / B
	Surface transom	$\sim$140 cells / B

Table 5.5: Overview of refinements used in all grids

In figure 5.12 cross sections of the grid at the vessel's CoG position are shown for these five grid refinements. From these figures the effect of the refinement level can be seen on the grid.

For each of these grids the added diffracted wave resistance is determined by performing the static vessel in regular waves simulation procedure as described in chapter 5.1. This results in a total of 10 simulations as both a calm water and a static vessel in regular waves simulation are performed for each of the grids.

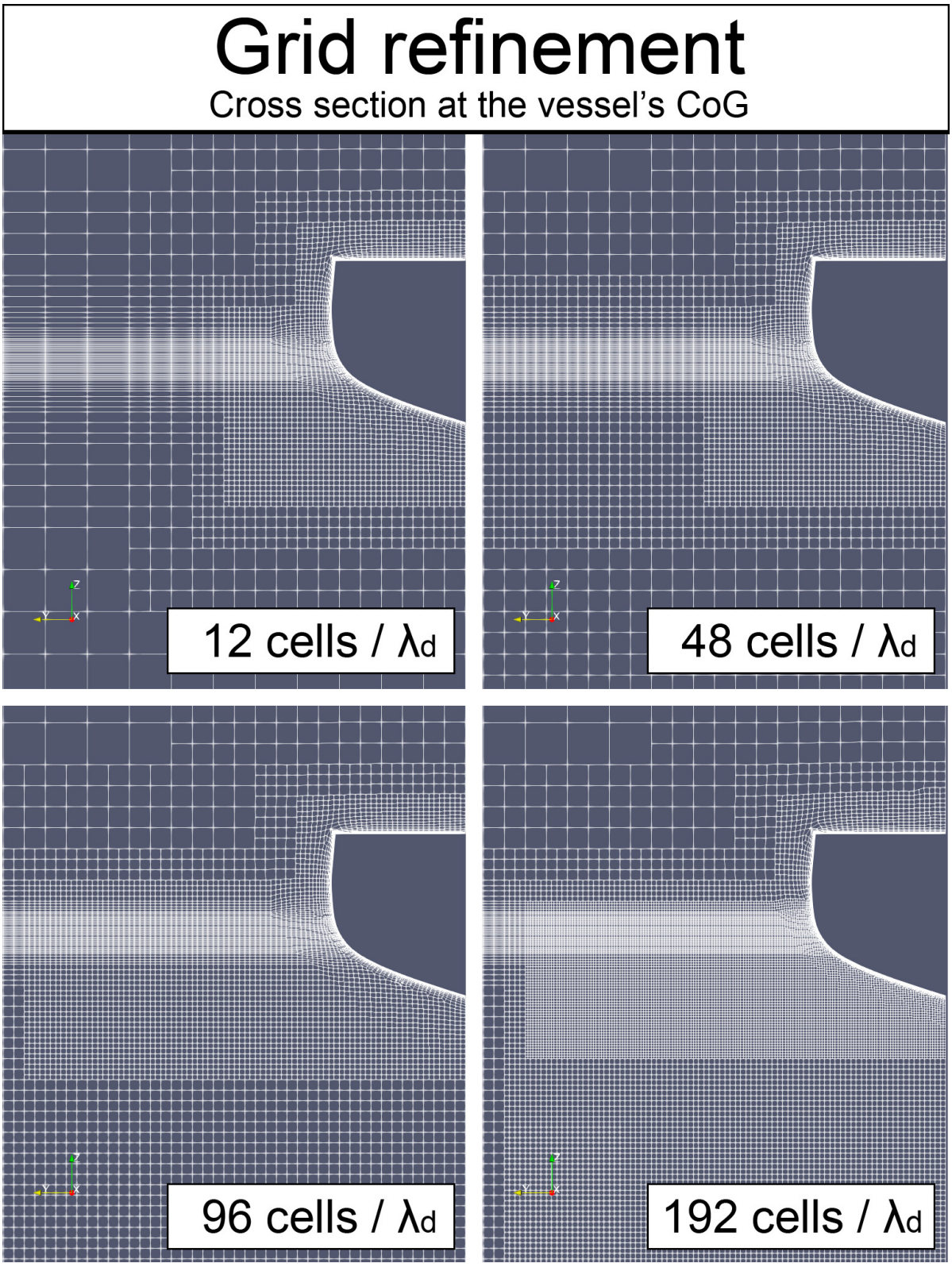

Figure 5.12: Cross sections of the grid for the various refinement levels

5.6. Results of the grid refinement study

In this paragraph the results from the grid refinement study will be discussed. First a visual impression of the test will be presented. Next the residuals in the simulations will be analysed. After that, the effect of the grid refinement on the wave elevation near the vessel and on the wave pattern is checked. Finally the convergence of the vessel's response for increased grid refinement is checked.

5.6.1. Visual impression

In this section images of the diffracting wave simulations are presented. The idea is to give the reader a visual impression of what happens in the simulation. This is done through a series of photos that will present the different steps through which the simulation runs. See figure 5.13

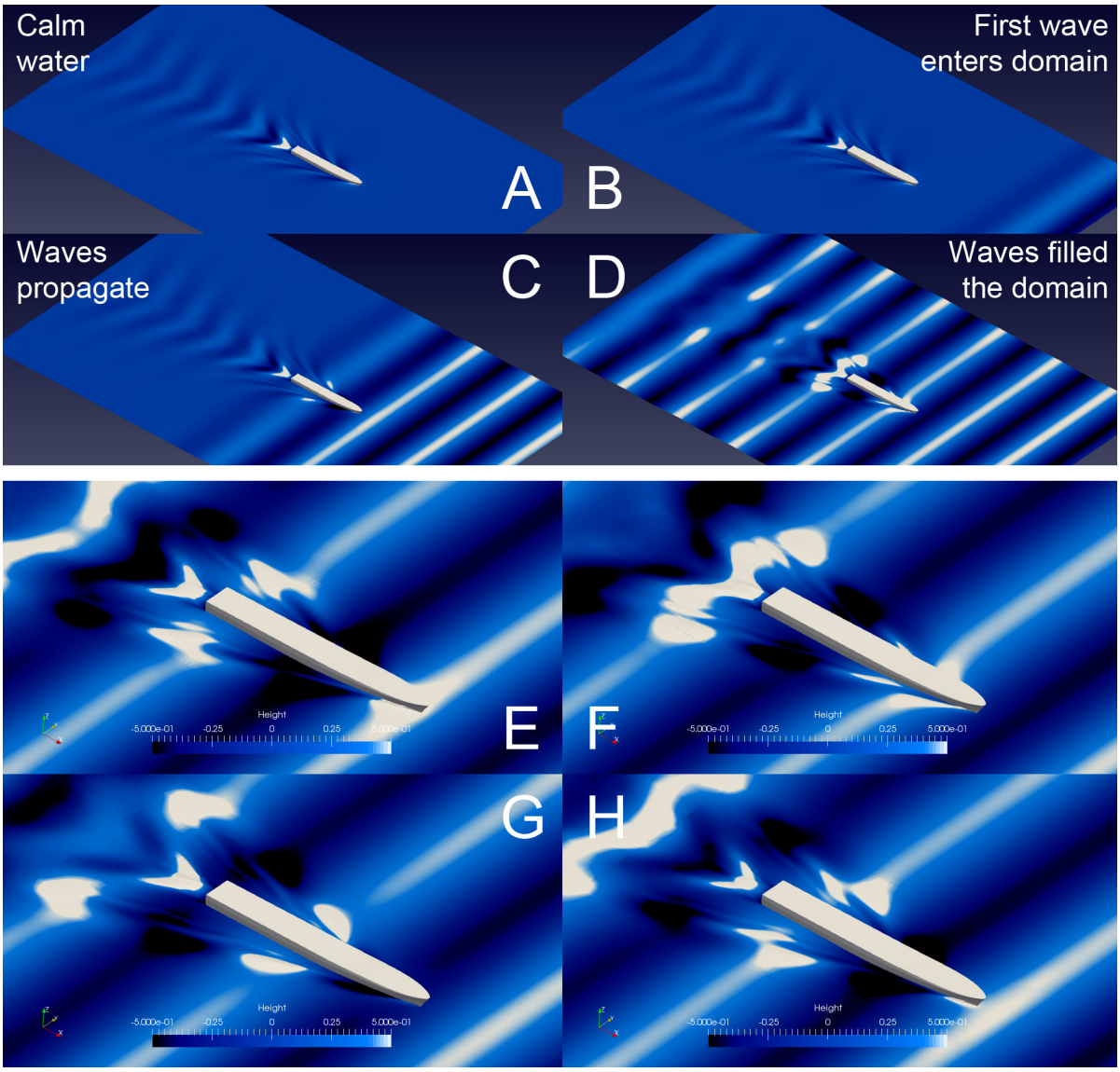

Figure 5.13: Visual impression of the simulation, A- D = steps of the simulation, E - H = one wave encounter

The simulation starts off in calm water, where the vessel is instantaneously accelerated to full speed. After that initial start it continues to sail in calm water until forces on the vessel have stabilised up to an acceptable level. Then this simulation is stopped. Step A shows the vessel sailing in calm water. Next, the wave simulation is started from the last time step of the calm water simulation. Then, the regular waves are introduced and will propagate through the domain. This can be seen in Steps B through D.

Once the first waves have reached the other side of the domain a further 10 more wave encounters will

be simulated. In step E through H one complete wave encounter is shown step by step. From these 10 last wave encounters the vessels responses due to the diffraction of the waves are calculated.

5.6.2. Residuals

In order to determine if the convergence error is considered small enough to be neglected, the residuals r were analysed. For details regarding the convergence error and residuals the user is referred to chapter 2.4.1.

ReFRESCO was set up to output time traces of the L_2 and L_∞ norm for all the simulations. From these time traces it was clear that the velocity parameter was subjected to the largest residuals. Even for the very coarse grid, the $L2$ norm converged to a value of about 1E-6. This is considered converged enough as the order of magnitude is at least two orders of magnitude lower than the discretisation error.

The L_∞ norm however didn't converge as well. It had only converged to a value of about 1E-2. However, it must be considered that this norm evaluates the largest residuals present within the domain. To assess whether these large residuals are actually present throughout the entire domain, or if there are some local convergence issues, they were inspected visually. For the visualisation of the residuals a threshold was set. Only the residuals larger than this value are shown.

In figure 5.14 the residuals for the velocity parameter are visualised for the very coarse grid using three different thresholds.

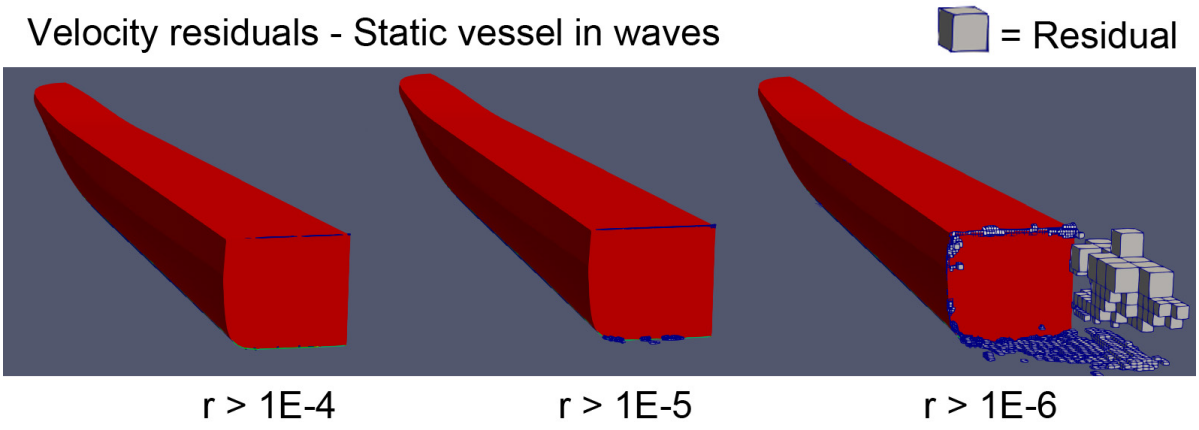

Figure 5.14: Visualisation of the residuals of the velocity parameter

It is clear that the larger residuals only occur in small numbers at the transom of the vessel. This can be explained by the fact that the transom barely sits below the free surface. When the transom moves in and out of the water, large gradients occur in the solution which are hard for ReFRESCO to resolve. Since residuals larger than larger than 1E-5 only occur in small quantities and only very local they are considered acceptable.

5.6.3. Wave elevation and pattern

Next the wave elevation and pattern are checked to analyse the effect of the grid refinement on them. First, a wave cut is made close to the vessel. Two interesting moments in time are selected for this plot. These are the moments when the vessel has pitched to its maximum upward and downward positions. In figures 5.15 and 5.16 plots of these wave cuts can be seen for all tested grid refinements.

The first thing to notice is that no real distinct differences are seen in these plots. The wave cuts for all grid refinements, ranging from the coarse 12 cells all the way up to the 192 cells per diffracted wavelength C_{λ_d} show almost the same pattern. It is only at the peaks of the waves that some minute differences can be spotted.

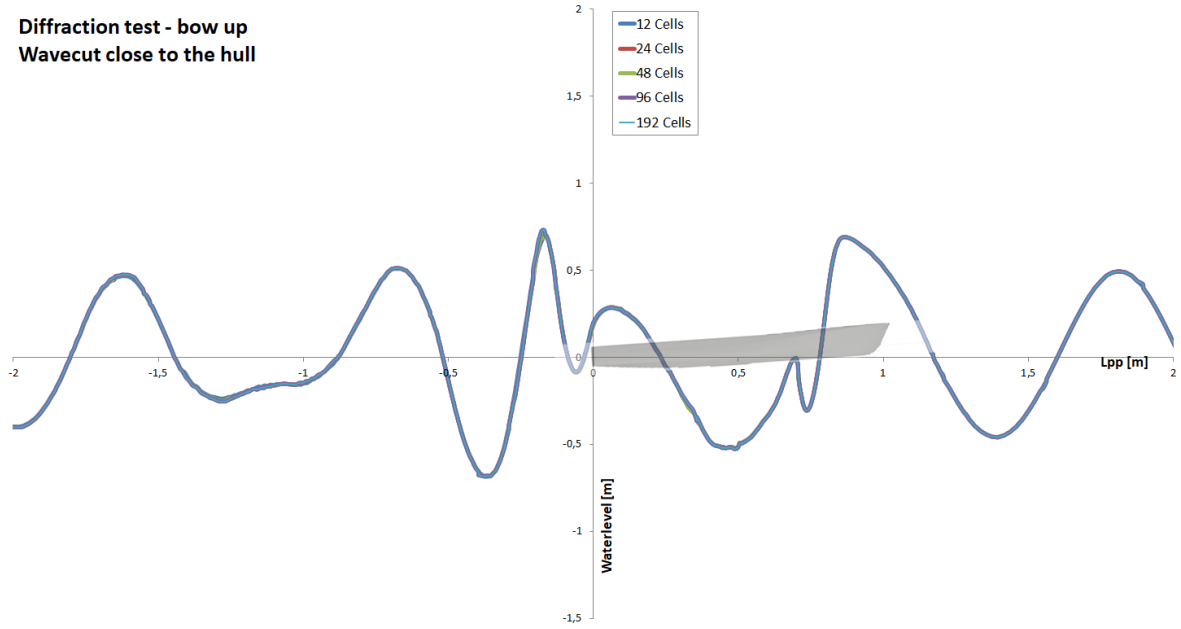

Figure 5.15: Wave cut near vessel, bow up

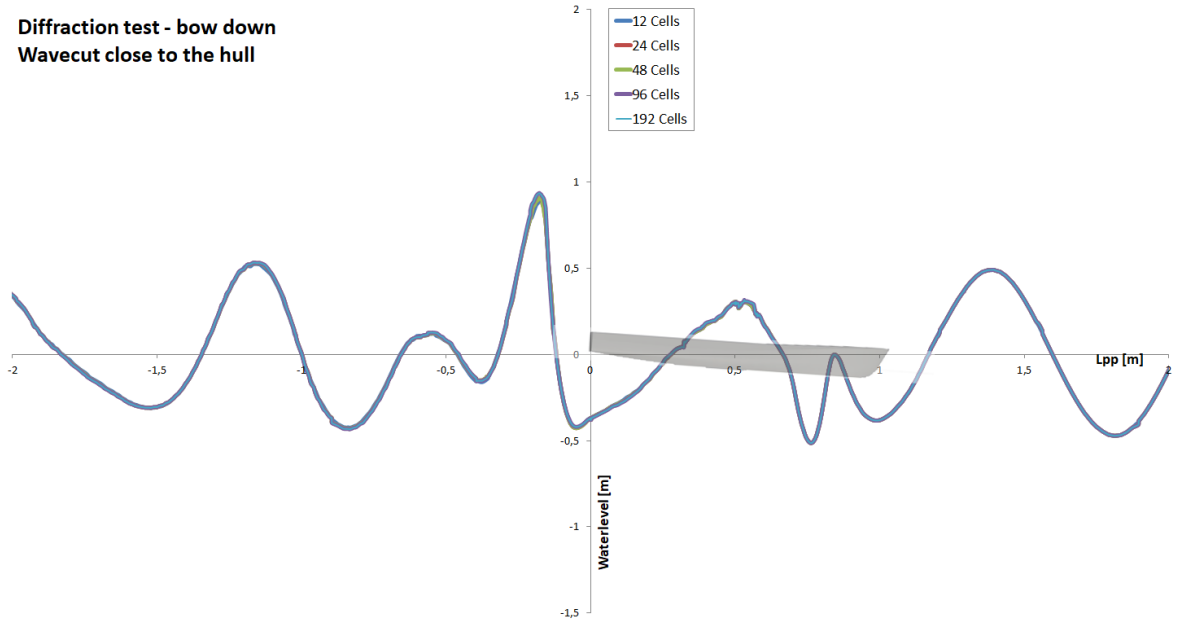

Figure 5.16: Wave cut near vessel, bow down

When comparing top down views of the free surface elevation a similar effect is noticed. Some minute differences between the lowest and highest grid refinement are visible, but in general the wave patterns all appear to be very similar.

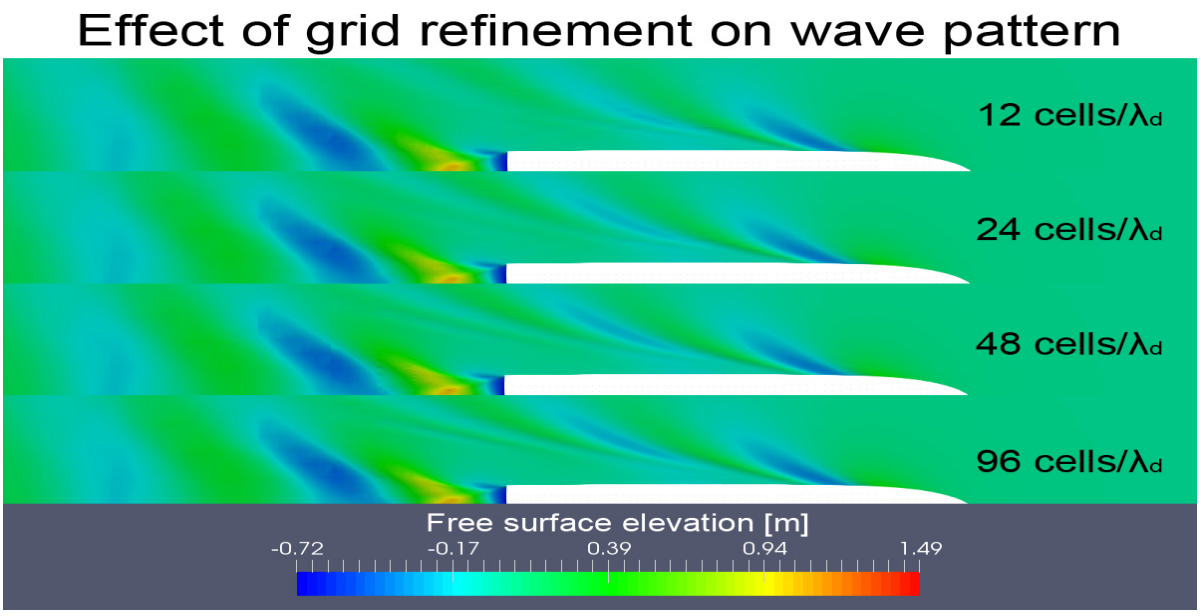

Figure 5.17: Wave pattern change for the studied grid refinement levels from coarse (top) to fine (bottom)

From the wave elevation and pattern analysis it can be concluded that the grid refinements appear to have almost no influence on the wave pattern, although it is possible to notice subtle differences.

5.6.4. Response convergence

The determined amplitudes of the vessels responses in heave and pitch direction are presented in figure 5.18. Here, a chart is shown that plots the amplitude of the force in heave direction and moment in pitch direction for the grid refinements ranging from 12 up to 96 cells per diffracted wave length. The highest grid refinement of 192 cells per λ_d is not included in the results as this simulation would have taken more than two weeks to finish. This was not feasible at the time and therefore the simulation was canceled before it finished. The plot shows that the grid refinement has an almost negligible effect on the simulated resistances. The amplitude of the force in heave direction varies no more than 0.4 kN between the lowest and highest measured value, which is less than 0.4% of the force amplitude. The amplitude of the pitch moment varies no more than 70 kNm over all the grid refinements, which is less than 0.2% of the moment amplitude.

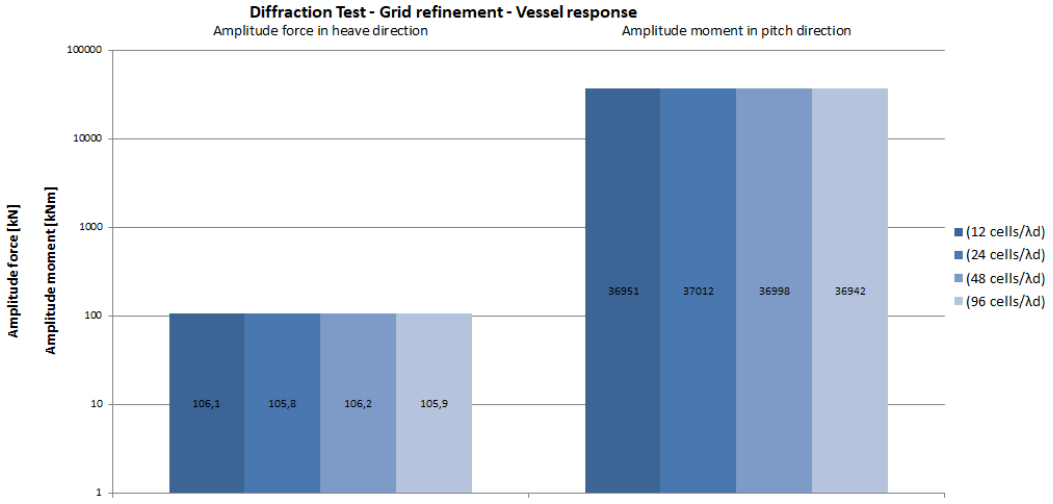

Figure 5.18: Amplitudes of the vessel's responses in heave and pitch direction due to the diffracting waves for the tested grid refinements

5.7. Comparison with potential flow code

To confirm that the order of magnitude and the phasing of the responses calculated with ReFRESCO is correct, it is now compared to potential flow code PRECAL. In figure 5.19 time traces of the vertical force and pitch moment are plotted for both the ReFRESCO simulation with the lowest grid refinement (12 cells/ λ_d) and PRECAL.

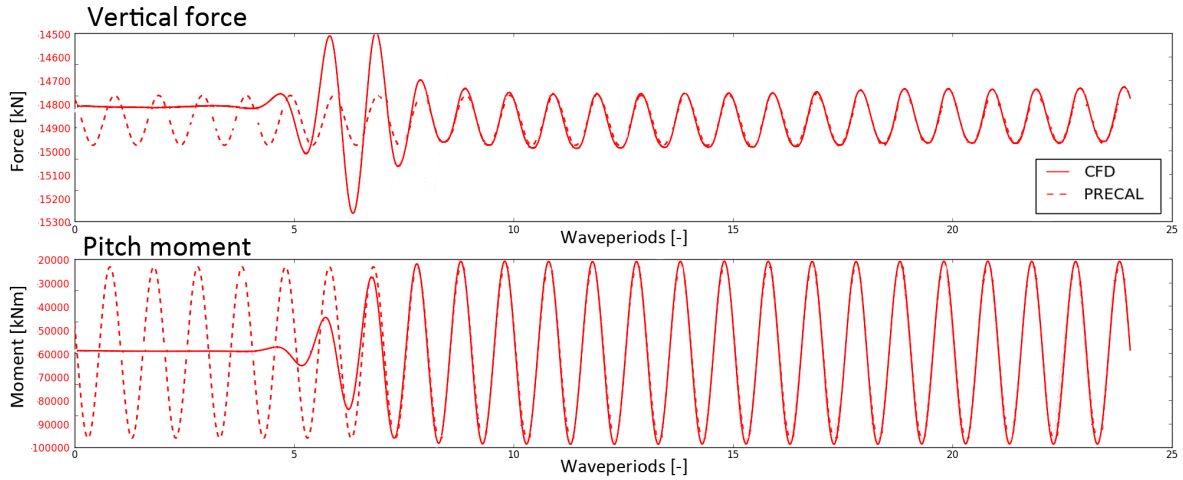

Figure 5.19: Comparison of vessel responses between the ReFRESCO and PRECAL time traces

From this plot it can be seen that the time-traces from the ReFRESCO simulation resemble the PRECAL time trace. The phases of both signals appear to be similar and the amplitude of the CFD resistance has the right order of magnitude.

The amplitudes and phases of the vessel's response for all the ReFRESCO simulations as well as the PRECAL, are shown shown in table 5.6 .

	Vertical force		Pitch moment	
	Amplitude [kN]	Phase [deg]	Amplitude [kNm]	Phase [deg]
PRECAL	105	-118	36991	-79
ReFRESCO 12 $cells/\lambda_d$	106.1	-117	36951	-78
ReFRESCO 24 $cells/\lambda_d$	105.8	-119	37012	-80
ReFRESCO 48 $cells/\lambda_d$	106.2	-118	36998	-77
ReFRESCO 96 $cells/\lambda_d$	105.9	-117	36942	-78

Table 5.6: Amplitude and phase relative to the wave at the vessel's CoG of the vessel's response for al the ReFRESCO simulations as well as PRECAL

5.8. Discussion and conclusion

On this diffracting waves study the following conclusions can be drawn:

- The amplitude of vessel's responses to the incoming waves vary less than 0.4 kN and 70 kNm for the vertical force and pitch moment respectively over all four grid refinements. This is less than 0.4 and 0.2 % of the total amplitude respectively.
- The phase shift of the vessel's responses in relation to the phase of the incoming wave varied no more than 3 degrees over all the grid refinements for both the vertical force as well as the pitch moment.
- From the relatively similar results for both the response amplitude as well as the phase of the vessels responses over the four grid refinements that were tested, it is seen that the vessel's responses appear insensitive to the grid refinement implemented to capture the diffracting waves.
- A comparison with potential flow solver PRECAL indicates that both the amplitude and phase of the vessel's responses, as determined using CFD, have the right order of magnitude.
- The grid refinements implemented to capture the propagating diffracted waves appear to have a negligible effect on the accuracy of the vessel's responses. Therefore the lowest grid refinement of 12 cells per diffracted wavelength C_{λ_d} is selected as the optimum for the set of diffracting wave refinement boxes.
- Compared to the most refined grid this simulation costs about 5 times less and delivers a similar resistance estimate. This estimation is based on the number of cells in each respective grid.

6

Simulating radiating waves

Now that we are able to accurately simulate the vessels response to incoming waves, it is time to focus on the vessel's response to motions in heave and pitch direction. The purpose of this chapter is to find optimum mesh settings for the accurate simulation of the vessel's response to those motions. As was the case in the previous chapter, optimum refers in this case to the best compromise between the cost of the simulation and the accuracy of the vessel's response to the motions.

The grid topology presented in this chapter is designed to accurately capture the radiating waves that are generated by the vessel as it moves. The optimum grid refinement will be determined using a grid refinement study.

From a validation study by D.L.Chow and K.A.McTaggart [13], it is known that PRECAL is able to provide accurate estimates of the vessels added mass and damping coefficients. These values are used to check whether the vessels responses to the heave and pitch motion are correct. First, the amplitude and phase of the reaction force and moment are determined from forced heave and pitch simulations. Here the vessel is periodically oscillating in heave or pitch direction whilst moving forward at a constant speed in calm water. Second, these values are converted to the vessels added mass and damping. Finally, the results are compared to the values from PRECAL, which are known to be accurate.

6.1. Test procedure

The process used to estimate the vessels response to motion is referred to as a 'forced motion' test. The short explanation of this process is given first after which a more detailed explanation follows.

When a vessel is moving, it generates waves that radiate away from the hull. This process draws energy away from the ship and transfers it to the surrounding water resulting in forces and moments felt by the vessel.

As was mentioned in chapter 2.1.1, J. Strom-Tejsen et. al. [30] concluded that the added resistance in regular waves is mainly dependent on the vessel's heave and pitch motion. It is therefore that this test focuses on these motions.

In the test, the vessel is forced to either heave or pitch with a constant frequency and amplitude whilst moving forward at a constant speed. Like in the 'static vessel in regular head waves' test, a calm water simulation is performed first in order to start the 'forced motion' simulation with a stabilised flow surrounding the vessel. Then the 'forced heave' or 'forced pitch' tests are restarted from the calm water simulation. The amplitude and phase of the vessel's responses to the heave and pitch motion are determined from these last tests.

6.1.1. Calm water simulation

The calm water simulation follows almost the same procedure as was used in the diffracted wave simulations. For information on this procedure, the reader is referred to chapter 5.1.1 and 5.1.2.

6.1.2. Forced heave and pitch simulation

The second part of the test procedure consists of the simulation of the vessel with forward speed whilst it is forced to heave or pitch. The simulation starts up from the last time step of the calm water simulation. This way the flow surrounding the vessel, and thus their resulting forces upon the vessel have had the time to stabilise, which which improves the accuracy of the estimate of the total resistance. In the forced motion simulations, the vessel will have one DoF, being either heave or pitch depending on the simulation. The heave or pitch motion is imposed on the vessel by the solver and has a constant frequency and amplitude.

At the beginning of the simulation the vessel has no periodic heave or pitch motion but is just sailing forward in calm water with its adjusted trim and sinkage. The amplitude of the motion is then slowly increased over the course of two motion periods in order to prevent instabilities in the simulation. A further three periods are required for the resistance to stabilise to a consistent periodic pattern. After the vessel is moving with the right amplitude and the resistance has stabilised, the simulation is continued for ten more periods of the motion.

The amplitude and phase of the vessel's response to the forced motion are then calculated by taking the average of these values over the last ten motion periods. The approach of averaging the force over ten periods is similar to the approach used in the wave diffraction simulations. In figure 6.2, the wave system of a vessel that is forced to heave whilst moving forward is visualised.

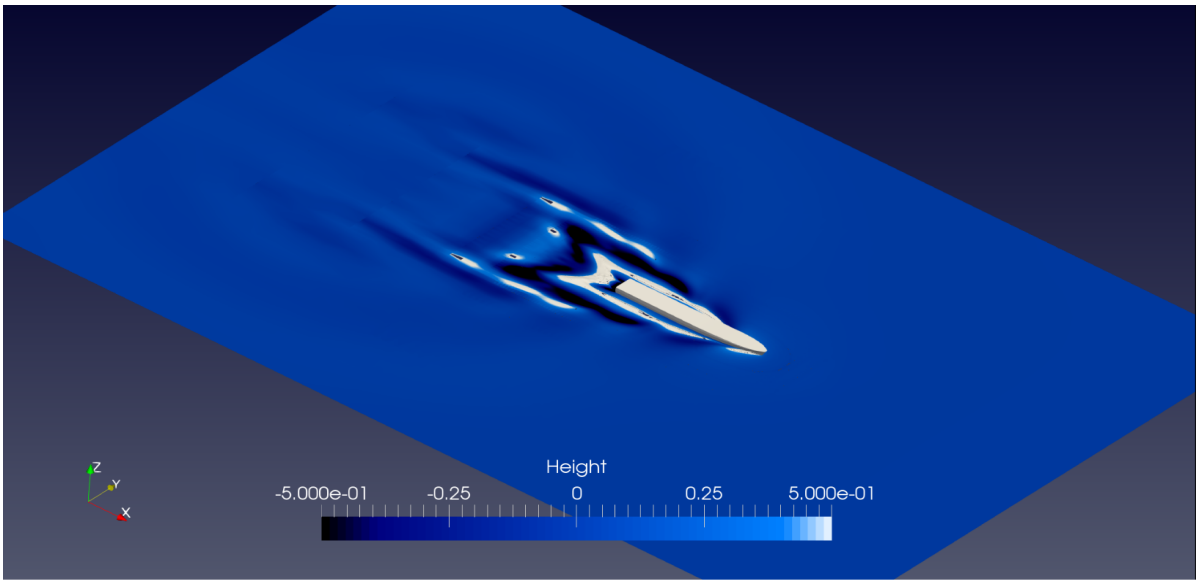

Figure 6.1: Vessel with forced heave motion

These values are then converted to the vessel's added mass and damping and compared to values determined using PRECAL, which are known to be accurate.

6.2. Simulation parameters

The parameters used for the radiation simulations are now explained in this paragraph

6.2.1. Domain, boundary conditions, and speed of the vessel

The domain, boundary conditions and the speed of the vess used in these simulations are described in chapter 3.3. A summary of these parameters is given in table 6.1.

6.2.2. Forced motion amplitude and frequency

The motions in these simulations are designed to resemble the motions that the vessel could experience if it would sail in the regular waves that were used in the previous 'static vessel in regular waves' simulations. These regular waves have an amplitude of 0.50 [m] and a frequency of 0.85 [rad/s].

Domain specifications			
Length [m]	Width [m]	Height [m]	Wave absorption [m]
6 Lpp	2 Lpp	4 Lpp	1 Lpp perimeter

Boundary	Boundary Condtion
Inlet	BC wave
Outlet	BC wave
Left	BC wave
Right	BC symmetry
Upper	BC pressure
Lower	BC slipwall
Vessel	BC slipwall

Vessel speed	17.31 [Kts]

Table 6.1: Summary of the domain, boundary condition and speed specifications used in the radiation simulations

The amplitudes of the heave and pitch motion are based on the maximum motion that the vessel theoretically could experience in those regular waves. In the unrealistic case that the vessel would just perfectly follow the wave, its maximum heave and pitch would match the wave's height and maximum angle of its tangent.

In practice the motions will always be smaller due to the vessel's inertia. However, in order to test if the simulation, and in particular the grid, can handle the largest motions of the vessel, these values are used. The forced heave amplitude is thus selected to be 0.50 [m].

In order to determine the pitch amplitude, the maximum angle of the regular wave's tangent Θ_{wmax} has to be determined. This can be calculated using equation 6.1

$$\Theta_{wmax} = \zeta_a K \tag{6.1}$$

Under the assumption that the regular waves are propagating in deep water, which is the case, the deep water dispersion relation from equation 5.4 can be used to rewrite K. By substituting equation 5.4 for K in equation 6.1 this becomes:

$$\Theta_{wmax} = \zeta_a \frac{\omega^2}{g} \tag{6.2}$$

For the regular wave under consideration in this case, with a wave amplitude of 0.50 [m] and a frequency of 0.85 [rad/s], this results in a maximum angle of 0.037 [rad] or 2.1 [deg]. Therefore the pitch amplitude is selected to match this 0.037 [rad] angle.

Regarding the frequency, this is selected such that the motions will resemble the motions that the vessel could experience in the regular waves from the previous simulations. Therefore the frequency is selected to match that of the encountered wave frequency.

Thus, the frequency of both the forced heave and pitch motion will be 1.51 [rad/s].

6.2.3. Time step

If the vessel is heaving or pitching with a frequency of 1.51 [rad/s], it will generate radiating waves with that same frequency. In order to capture those propagating waves accurately an optimum time step has to be selected. As always, optimum refers in this case to the best compromise between simulation cost and accuracy of the resistance prediction.

From the tests performed in the '2D wave simulations' as well as the 'diffracted wave simulations' it is known that this optimum time step is equal to $T/200$. In this case, the radiating waves will have

a frequency of 1.51 [rad/s] which corresponds to a wave period T of 4.17 [s]. The time step used to capture the radiating waves accurately is thus calculated by dividing 4.17 [s] by 200.

This results in a time-step Δt of 0.021 [s] for the forced heave and pitch simulations.

6.2.4. Simulation time

The simulation will run for an initial 2 motion periods to slowly build up the amplitude of the motion. After that it will run for another 3 periods to let the vessel's response form a consistent recurring pattern. After that the simulation will continue for another 10 periods. This results in a total simulation time of 15 periods of the motion. As one period takes 4.17 [s] this results in a total simulation time of 62.5 [s].

6.3. Spatial discretisation

In this paragraph the spatial discretisation of the grid used in the radiation simulations is explained. The goal of these discretisations is to capture the interaction between the hull and the fluid as well as the radiating waves accurately. This way the resulting forces and motions felt by the vessel will also be captured accurately. Furthermore, extra refinements were implemented that were required for the simulation of the vessel's motions.

The spatial discretisations used in these simulations can be divided up into four main groups based on their purpose.

6.3.1. Hull - fluid interaction (MARIN recommended)

This first group comprises of discretisations that are designed to ensure that the interaction between the hull and the fluid as well as the flow near the vessel is captured accurately. These discretisations are recommended by experienced MARIN CFD users and were also used in the diffracted wave simulations. For more information on them, the reader is referred to chapter 5.3.2 where they are described in detail.

6.3.2. Radiating waves

The second group consists of discretisations that are specifically designed to capture the propagating radiated waves accurately. The discretisations used here are based on the radiated wavelength λ_r.

In paragraph 6.2.3, it was already mentioned that a vessel, heaving or pitching at a frequency equal to the encounter frequency ω_e of 1.51 [rad/s] will radiate waves that have that same frequency. Therefore the following can be stated:

$$\omega_r = \omega_e \tag{6.3}$$

Where ω_r is the frequency of the radiated wave.

By using the deep water dispersion relation from equation 4.4 it is now possible to relate the frequency of the radiated wave ω_r to its length λ_r. This calculation of the required radiated wavelength λ_r seems to be quite straight forward.

The difficulty lies in the fact that the radiated waves are observed from a moving reference frame, namely the forward moving vessel. Due to its forward speed the vessel will overtake the waves that are radiated in front of it and sail away from the waves that it radiates behind it. This will cause the wavelength of the radiated waves λ_r to appear shorter in front of the vessel and longer behind it. This observed wavelength, as seen from the vessel, is known as the apparent wavelength.

The effect shows similarities to the Doppler effect which describes the change in apparent frequency from the point of view of an observer who is moving relative to the wave source.

By modelling the forward moving vessel that is radiating waves as a forward moving, pulsating source it is possible to analytically describe the wave pattern. This is exactly what J.Bougis [8] did in his study.

J.Bougis managed to relate the apparent wave length λ_{ra} to the propagation angle θ, speed of the source v and the oscillation frequency ω_r. See equation 6.4.

$$\lambda_{ra}(\theta) = \frac{\pi g}{\omega_r^2}[1 + \sqrt{1 - 4\tau cos(\theta)}] \qquad with: \quad \tau = \frac{v\omega_r}{g} \tag{6.4}$$

In which $\theta = 0°$ refers to a wave propagating in the same direction as the source.

By substituting the encounter frequency ω_e t for the oscillation frequency ω_r as was described in equation 6.3, equation 6.4 can be used to describe the apparent radiated wave length for our vessel, as shown in equation 6.5.

$$\lambda_{ra}(\theta) = \frac{\pi g}{\omega_e^2}[1 + \sqrt{1 - 4\tau cos(\theta)}] \qquad with: \quad \tau = \frac{v\omega_e}{g} \qquad and: \quad \omega_e = \omega + \frac{\omega^2}{g}v \tag{6.5}$$

In figure 6.2 a polar plot is shown of this apparent wave length in relation to the propagation angle for several speeds of the vessel at a constant wave frequency ω. The apparent wave length λ_{ra} is plotted on the radial axis in [m]. Note that the wave frequency ω refers to the actual wave frequency and not to the encountered wave frequency ω_e.

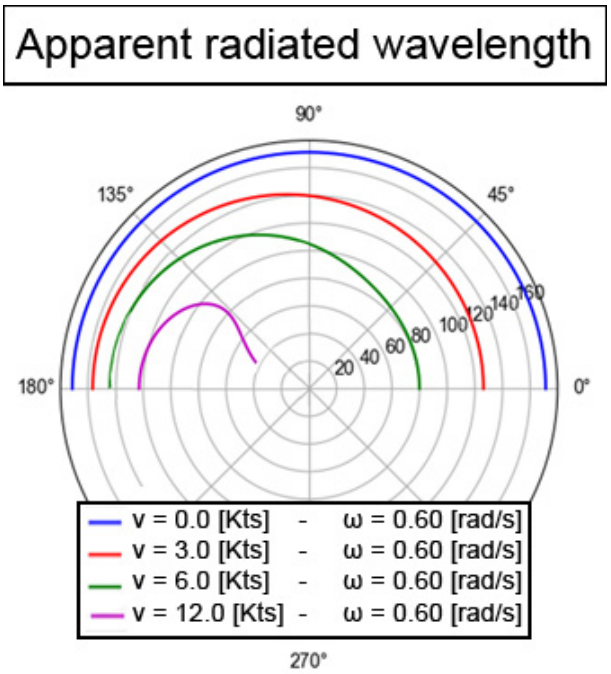

Figure 6.2: Apparent wave length for several speeds

From this figure it can be seen that the waves in front of the vessel will become significantly shorter as the vessel sails faster. At a certain speed, as is illustrated by the 12.0 [Kts] case in the figure, the vessel will overtake the waves propagating in front of it. This happens once $\tau > 0.25$. Figure 6.3 gives a good illustration of the wave pattern created by the oscillating vessel at cases with zero speed, τ smaller than 0.25 and τ larger than 0.25.

For the case under consideration here, with the vessel sailing at 17.31 [Kts] in head waves with a wave frequency of 0.85 [rad/s] and an encountered wave frequency of 1.51 [rad/s], the corresponding τ value is 1.37. This means that the vessel is definitely overtaking its own own waves.

This can also be seen from the polar plot for this case. See figure 6.4.

From this polar plot a few things can be noted:

- For the case in this simulation the waves will only be radiating away from the vessel with a propagation angle between 135 and 180 [deg]

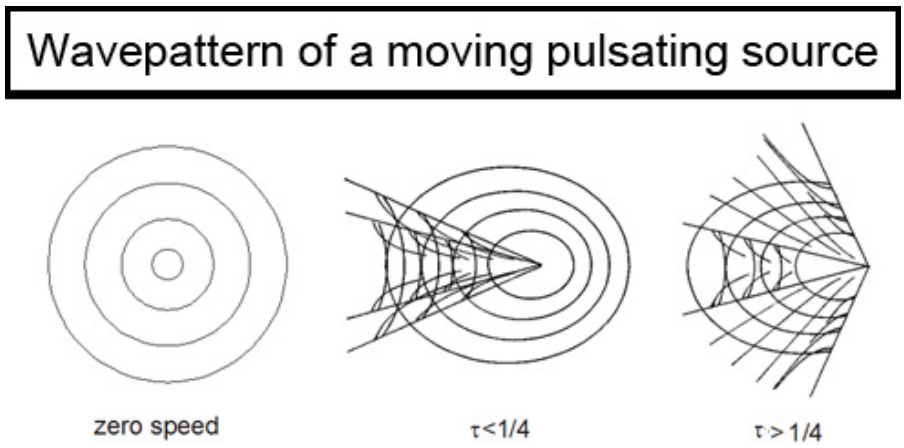

Figure 6.3: Wave patterns of steady moving pulsating source - MARIN memo on grid refinement by S.Rapuc [29]

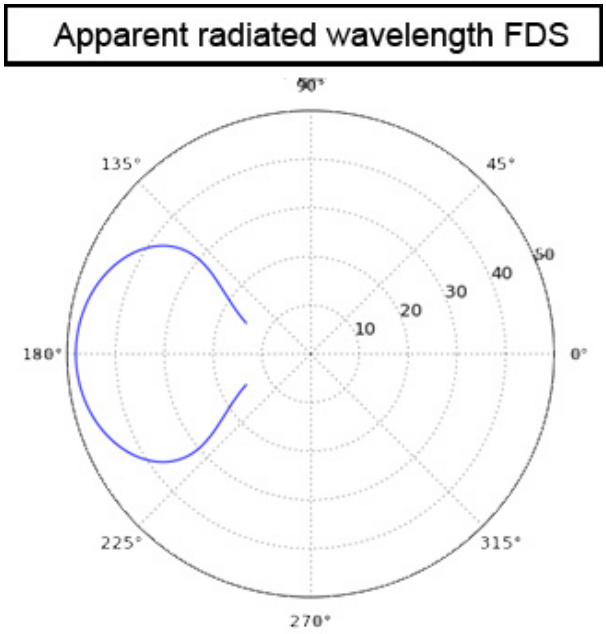

Figure 6.4: Apparent radiated wave length FDS

- The shortest radiated wave length λ_{rmin} has a length of 15 [m] and propagates at an angle of about 135 [deg]
- The longest radiated wave length λ_{rmax} will always propagate away at an angle of 180 [deg]. In the case under consideration here it has a length of 48 [m].

Based on these findings a grid topology is designed that aims to capture the radiating waves accurately. The grid topology proposed here has been developed by combining a grid topology for near ship refinement by S.Rapuc [29] with the grid topology designed to capture the kinetic energy in the wave as was used in the simulation of 2D waves in chapter 4. This grid topology is only designed for fast sailing vessels with $\tau > 0.25$ as no refinement is implemented for forward propagating waves.

The grid topology limits the number of required refinement boxes by focusing on the longest and shortest radiated wave. For both wavelengths, an upper and lower grid refinement box are implemented. The purpose of these boxes is to capture the kinetic energy in the radiating waves. This results in a total of four refinement boxes.

The width and length of these boxes are based on the topology by S.Rapuc while their height is based

on the kinetic energy grid topology. The dimensions of the boxes are given by their maximum and minimum x, y and z coordinates in a similar fashion as was used in the previous chapter.

The width and length of the refinement boxes are defined as follows:

- For the shortest wave length λ_{rmin}, the dimensions for both the upper and lower refinement box are:
  - x+ = $Lpp + 0.1Lpp$
  - x- = $\lambda_{rmin} cos(\theta_{min})$
  - y+ = $\frac{B}{2} + \lambda_{rmin} sin(\theta_{min})$
  - y- = 0
- For the longest wave length λ_{rmax}, the dimensions for both the upper and lower refinement box are:
  - x+ = $Lpp + 0.1Lpp$
  - X- = $-\lambda_{rmax}$
  - y+ = $\frac{B}{2} + \lambda_{rmax}$
  - y- = 0

With θ_{min} the propagation angle associated with λ_{min}.

For the case studied here, this resulting refinement boxes can be seen in figure 6.5.

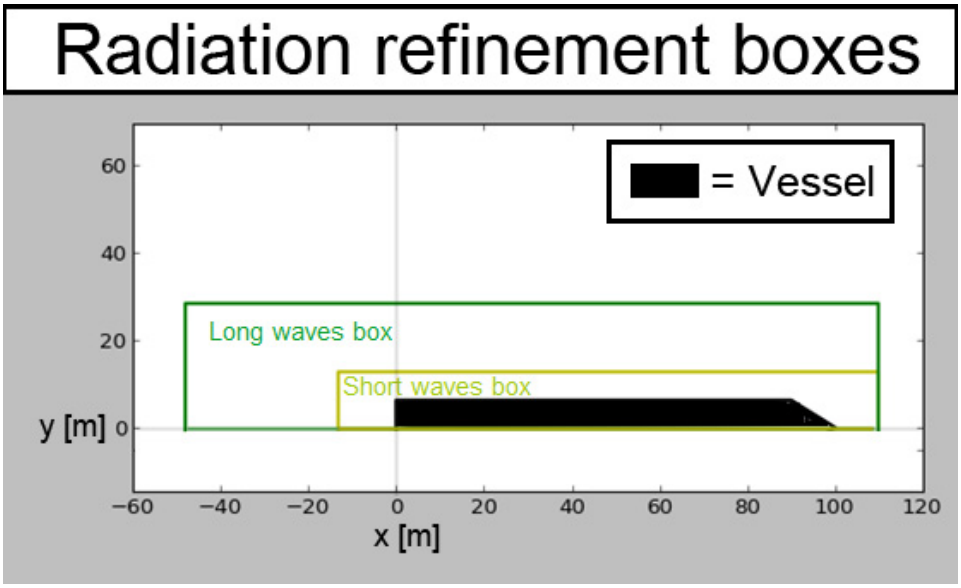

Figure 6.5: Radiation refinement boxes

Regarding the vertical dimensions of the refinement boxes, all boxes stretch from $1.1\zeta_a$ above the free surface down to 0.2 and 0.6 of their wave length below it for the upper and lower refinement box respectively. In table 6.2 these vertical dimensions of the four refinement boxes are summarised.

In order to determine the optimum dimensions for these radiation refinement boxes, a study is performed in which their dimensions are varied. Three sets will be tested, measuring 0.5, 1.0 and 1.5x the dimensions mentioned above in width and length. Their height will remain constant as the kinetic energy in the waves will remain the same. These sets are referred to as the small, medium and large sized sets.

In table 6.3 the dimensions of these three sets of refinement boxes are specified.

Refinement box	Coordinates [m]	
	z+	z-
λ_{rmin} upper	+ 1.1 ζ_a	-0.2 λ_{rmin}
λ_{rmin} lower	+ 1.1 ζ_a	-0.6 λ_{rmin}
$\lambda_{rmax}upper$	+ 1.1 ζ_a	-0.2 λ_{rmax}
$\lambda_{rmax}lower$	+1.1 ζ_a	-0.6 λ_{rmax}

Table 6.2: Vertical dimensions radiation refinement boxes

Ref. box set	Ref. box	Ref.	Coordinates [m]			
			x+	x-	y+	y-
Small	λ_{rmin} upper	$C_{\lambda_{rmin}} = 48$	1.05 Lpp	0.5 $\lambda_{rmin}cos(\theta_{min})$	B/2 + 0.5 $\lambda_{rmin}sin(\theta_{min})$	0
	λ_{rmin} lower	$C_{\lambda_{rmin}} = 24$	”	”	”	0
	λ_{rmax} upper	$C_{\lambda_{rmax}} = 48$	”	-0.5 λ_{rmax}	B/2 + 0.5 λ_{rmax}	0
	λ_{rmax} lower	$C_{\lambda_{rmax}} = 48$	”	”	”	0
Medium	λ_{rmin} upper	$C_{\lambda_{rmin}} = 48$	1.1 Lpp	$\lambda_{rmin}cos(\theta_{min})$	B/2 + $\lambda_{rmin}sin(\theta_{min})$	0
	λ_{rmin} lower	$C_{\lambda_{rmin}} = 24$	”	”	”	0
	λ_{rmax} upper	$C_{\lambda_{rmax}} = 48$	”	- λ_{rmax}	B/2 + λ_{rmax}	0
	λ_{rmax} lower	$C_{\lambda_{rmax}} = 24$	”	”	”	0
Large	λ_{rmin} upper	$C_{\lambda_{rmin}} = 48$	1.15 Lpp	1.5 $\lambda_{rmin}cos(\theta_{min})$	B/2 + 1.5 $\lambda_{rmin}sin(\theta_{min})$	0
	λ_{rmin} lower	$C_{\lambda_{rmin}} = 24$	”	”	”	0
	λ_{rmax} upper	$C_{\lambda_{rmax}} = 48$	”	-1.5 λ_{rmax}	B/2 + 1.5 λ_{rmax}	0
	λ_{rmax} lower	$C_{\lambda_{rmax}} = 24$	”	”	”	0

Table 6.3: Radiation grid refinement boxes

For the refinement level of these boxes the same approach is taken as was used in the grid topology based on the kinetic energy in the waves. In that approach a ratio of the wave length was selected as the refinement level for the upper refinement box. The corresponding lower refinement box is then specified with half of that refinement level.

For the refinement boxes based on the shortest waves the refinement will be a ratio of this short wavelength. Similarly, for the refinement boxes based on the longest waves, the refinement level will be a ratio of the longest wave length. A grid refinement study is performed to determine the optimum refinement level of the radiation boxes.

6.3.3. Grid deformation

The third group consists of an extra grid refinement that is implemented to ensure that ReFRESCO can solve the vessel's motions using grid deformations whilst maintaining the accuracy of the solution. Some background information regarding grid deformations in ReFRESCO is explained here as it is required to understand why these extra refinements are needed.

Grid deformations are used in ReFRESCO to make simulations of a moving vessel possible. In CFD the shape of the vessel is defined by the boundary of the domain that represent the hull. In our case this boundary is a slip wall in the shape of half of the vessel.

In order to simulate the vessel's motions, the boundary representing the hull must be moved accordingly. As a result, the cells of the grid that touch this boundary have to move with it. This adaptation of the grid is what is known as a grid deformation.

The deformation takes place over all the cells within a specified area surrounding the hull. The advantage of deforming the grid over this large area is that the grid will remain fairly similar to its original form. The user can specify the dimension of this area by defining a radius which surrounds the vessel. This parameter is called the 'support radius'. In this research a 'support radius' of $0.5Lpp$ was used.

In figure 6.6 three section cuts of the grid are shown that visualise the grid deformation performed by ReFRESCO to simulate heave and pitch.

In areas with a low refinement level, ReFRESCO has a low number of cells over which it can deform the grid. Here, grid deformations can result in sharp transitions in the grid which will compromise the

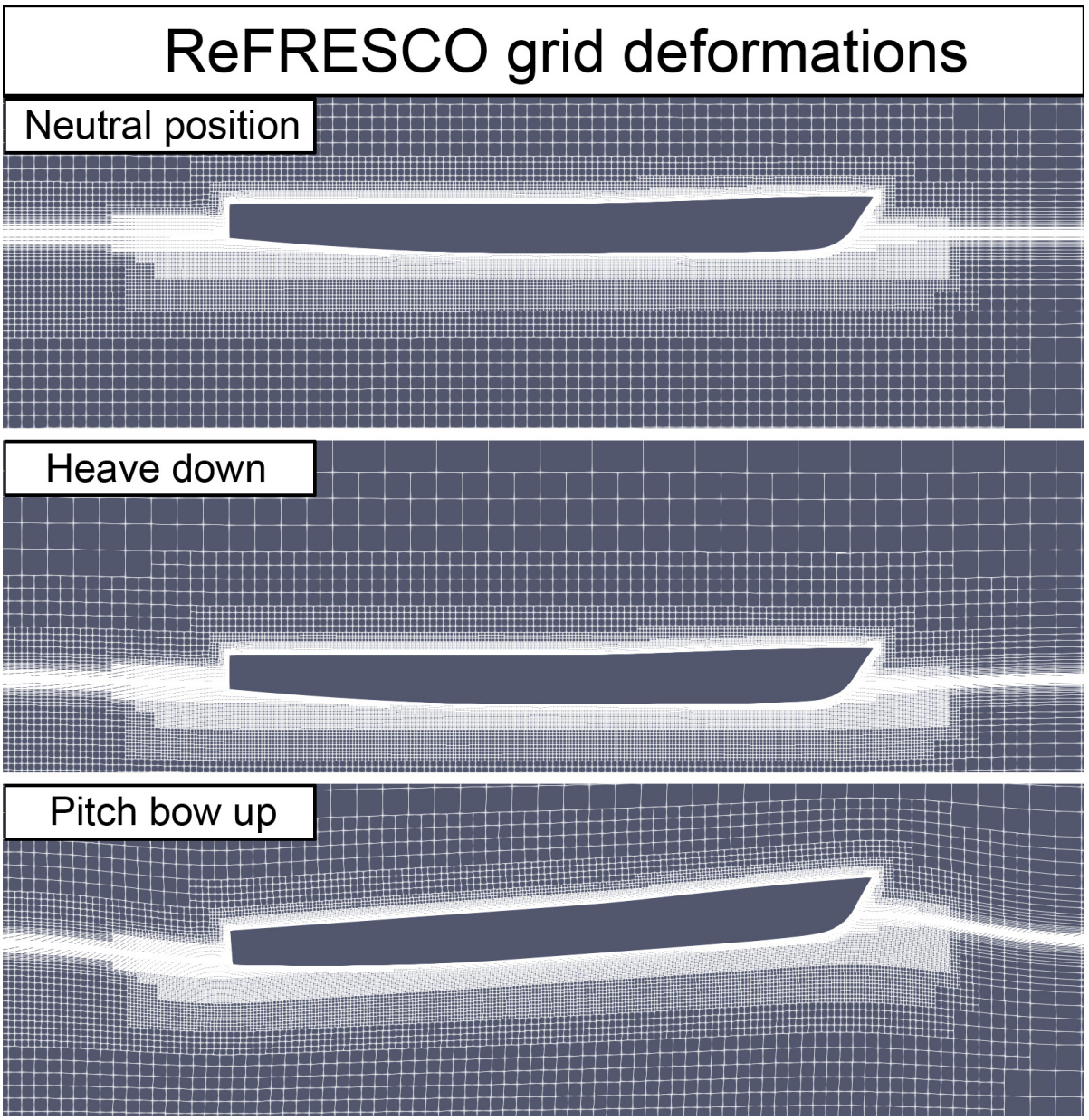

Figure 6.6: ReFRESCO grid deformations

accuracy of the simulation.

Imagine that the ship is moving upwards as a result of a pitch or heave motion. ReFRESCO will then deform the grid, moving the free surface near the vessel upwards in the process. The grid refinement above the free surface, where the air is located, is very low. This low refinement will prevent ReFRESCO from generating a smooth grid deformation above the free surface in the area near the vessel. This will lead to a non-accurate capturing of the wave.

In order to mitigate this problem, the grid refinement box at the free surface must be must be expanded to the area surrounding the vessel where the grid is deformed the most. Guidelines from experienced MARIN CFD users are used here to specify this additional refinement.

The guideline states that for the refinement level within this box, the same refinement level of the free surface refinement box must be used. This way it will extend the same free surface refinement to a larger area.

The dimensions of this expanded refinement area are based on the length of the longest radiated wave λ_{rmax} as well as the amplitude of the height over which the free surface is deformed ζ_{fmax}. The refinement box measures $\frac{1}{3}$ of λ_{rmax} ahead, behind and to the side of the vessel.

The height of the refinement area is based on the maximum deformation of the free surface. The maximum deformation of the free surface will occur when the vessel would reach its maximum heave and pitch at the same time. In real life this extreme case would never occur. However, it is used here to ensure that there is always sufficient refinement available.

The maximum deformation of the free surface can be calculated according to equation 6.6.

$$\zeta_{fmax} = \zeta_a + \Theta_{wmax}\frac{Lpp}{2} \tag{6.6}$$

Where Θ_{wmax} is the maximum angle of the tangent of the wave as was described in equation 6.1.

In this equation the maximum heave amplitude ζ_a is added to the vertical elevation of the vessel's as the vessel reaches its maximum pitch angle. Its assumed here that the App and are positioned at about an equal distance of $Lpp/2$ from the vessel's CoG.

See figure 6.7 for a visualisation of the maximum elevation of the free surface.

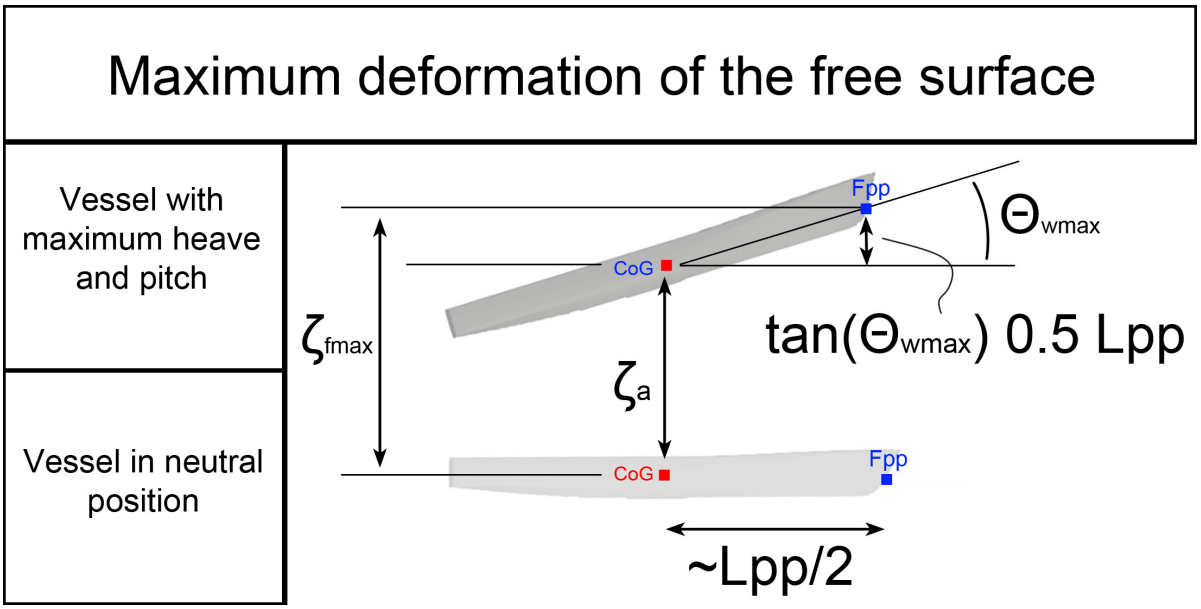

Figure 6.7: Maximum deformation of the free surface

In table 6.4 an overview is given of the dimensions and refinement level implemented in the grid deformation refinement box

Refinement box	Refinement	Coordinates [m]					
		x+	x-	y+	y-	z+	z-
Grid deformation	$\frac{5\ cells}{\zeta_a}$	Lpp + $\frac{\lambda_{rmax}}{3}$	- $\frac{\lambda_{rmax}}{3}$	B/2 + $\frac{\lambda_{rmax}}{3}$	0	$\zeta_{fmax} + \zeta_a$	$-\zeta_{fmax} - \zeta_a$

Table 6.4: Grid deformation refinement box

6.3.4. Free surface refinement

Finally the fourth group consists of a free surface refinement over the entire domain. In this simulation no incoming regular waves are simulated. Therefore the 'incoming regular wave' refinements used in the 'diffracting waves' simulations are not required. However, as the interface still needs to be captured, a 'free surface refinement box' was implemented.

This might not be strictly necessary, but it ensures that small waves will continue to propagate when they leave the refinement areas defined by the other refinement boxes For details regarding the specifications of the free surface refinement box the reader is referred to chapter 5.3.1.

6.3.5. Combined spatial discretisation

The four groups of spatial discretisations are combined into one set. This set is thus designed to capture the interaction between the hull and the flow as well as the radiating waves. Furthermore combined set is designed to handle grid deformations and has some extra refinement at the free surface implemented.

6.4. Optimising the dimensions of the radiation boxes

A study on the size of the radiation refinement boxes was performed in order to find an optimum. As always, optimum refers to the best compromise between the simulation cost and the accuracy of the response predictions.

First, three grids were generated in which the spatial discretisations for the 'hull - fluid interaction', 'grid deformation' and 'free surface refinement' as mentioned in chapter 6.3 are implemented and kept the same. The size of the implemented radiation boxes however was varied from small to medium to large. In figure 6.8 the three resulting grids are shown. The purpose of the red lines is to make the comparison between the grids easier.

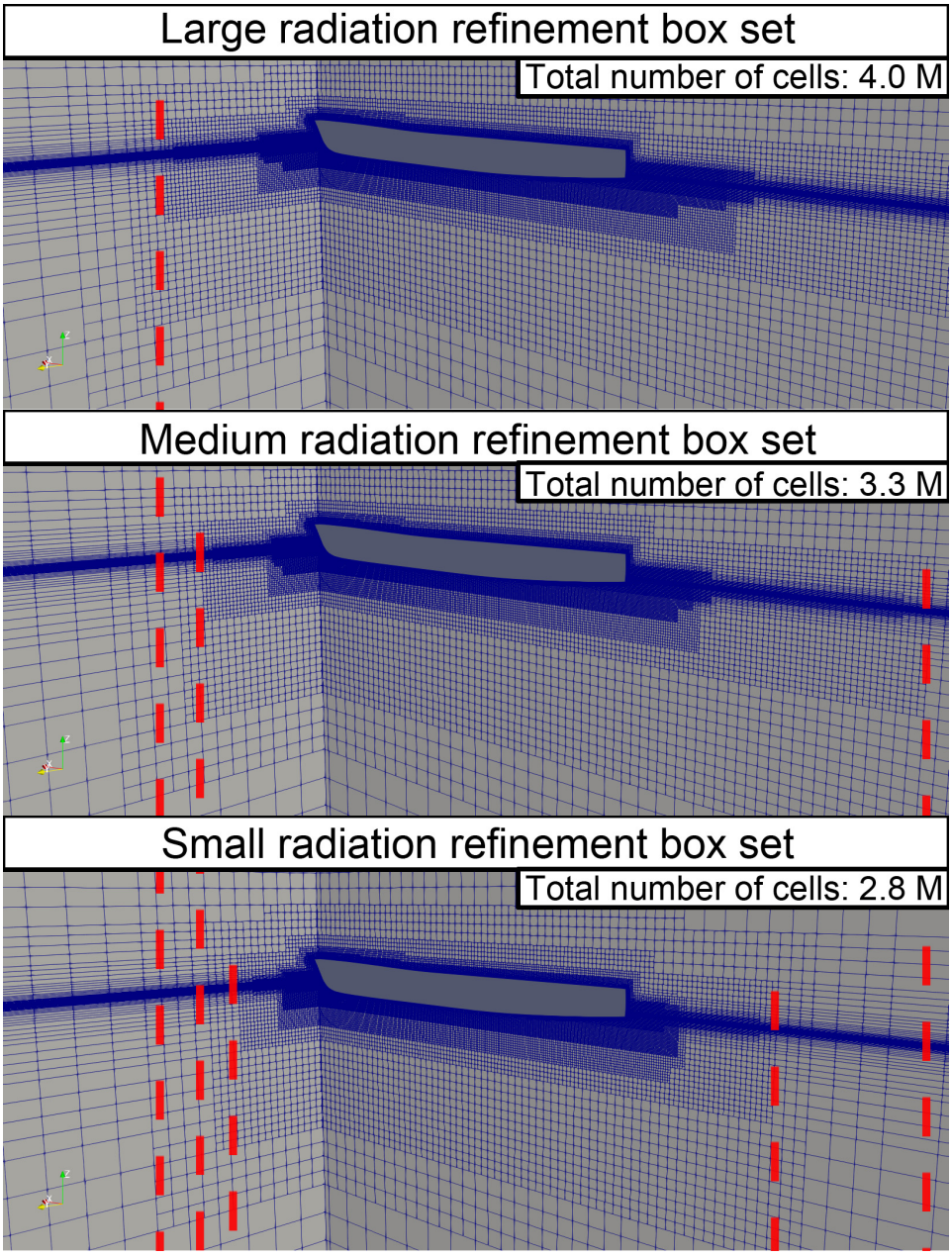

Figure 6.8: Three grids with varying dimensions of the radiation box set

Next, the vessel's responses due to the forced heave and pitch motion were determined by performing the 'forced motion' simulation procedure as described in chapter 6.1 for each of the three grids. The resulting response estimates for both the forced heave and pitch simulations are presented in figure 6.9 through 6.12.

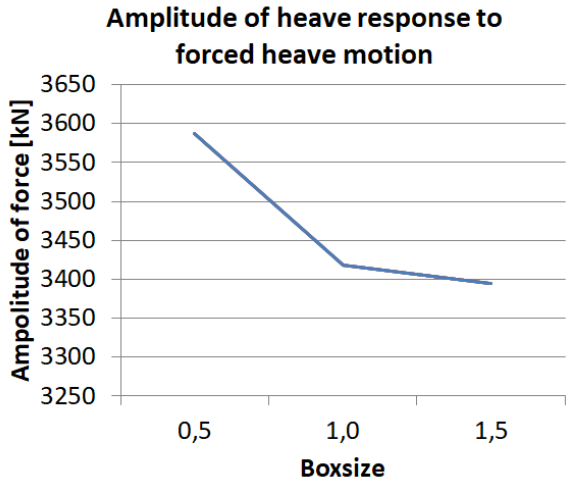

Figure 6.9: Amplitude of the heave response due to the induced heave motion for all three refinement boxsizes

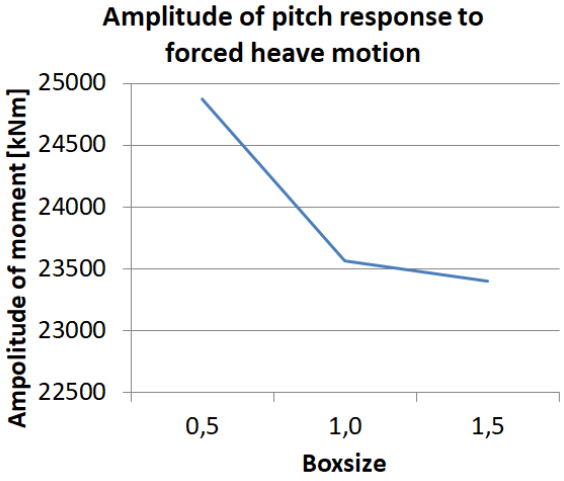

Figure 6.10: Amplitude of the pitch response due to the induced heave motion for all three refinement boxsizes

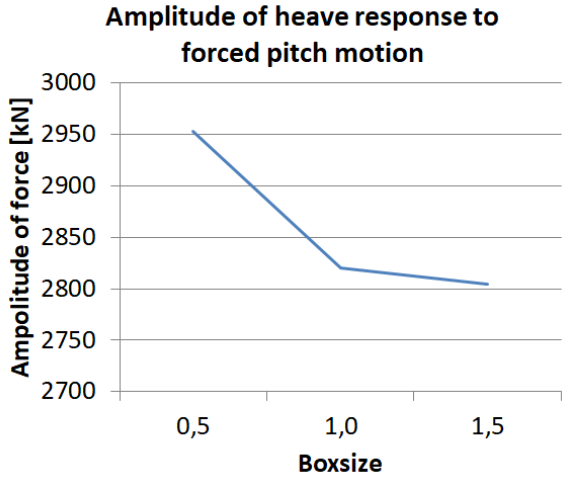

Figure 6.11: Amplitude of the heave response due to the induced pitch motion for all three refinement boxsizes

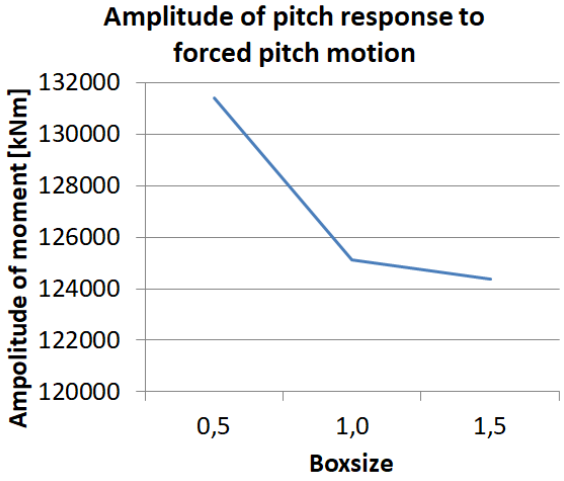

Figure 6.12: Amplitude of the pitch response due to the induced pitch motion for all three refinement boxsizes

The following conclusions can be drawn from these test results:

- It can be seen that the added resistance due to radiating waves converges for increased box sizes
- For the forced heave simulations, the vessel's response estimates for the force in heave direction and moment in pitch direction decrease by 169 kN and 1317 kNm respectively when the grid refinement boxes are increased from small to medium size. This corresponds to a relative decrease of 4.70 % and 5.29% respectively.
- For the forced heave simulations, the vessel's response estimates for the force in heave direction and moment in pitch direction decrease by 23 kN and 162 kNm respectively when the grid refinement boxes are increased from small to medium size. This corresponds to a relative decrease of 0.68 % and 0.69% respectively.

- For the forced pitch simulations, the vessel's response estimates for the force in heave direction and moment in pitch direction decrease by 133 kN and 6309 kNm respectively when the grid refinement boxes are increased from small to medium size. This corresponds to a relative decrease of 4.50 % and 4.81% respectively.
- For the forced pitch simulations, the vessel's response estimates for the force in heave direction and moment in pitch direction decrease by 16 kN and 751 kNm respectively when the grid refinement boxes are increased from small to medium size. This corresponds to a relative decrease of 0.56 % and 0.60 % respectively.
- The increase in computation costs from the medium to the large set is about 21 % as the total number of cells in the grid is increased by this amount

Based on the small changes, both absolute and relative, in the vessel's response estimates for the medium refinement boxes compared to the large sized boxes, the responses determined using the medium dimensioned grid are considered converged enough. The use of the large set will result in an improvement of the accuracy of the solution of about 0.6 %, but this comes at the cost of an increase in computation time and cost of about 21 %. Therefore the medium sized refinement box set is selected as the optimum.

6.5. Grid refinement study

To determine an optimum grid refinement level for the accurate simulation of the vessel's response to motions in heave and pitch direction, a grid refinement study is performed. Optimum as always refers to the best compromise between simulation cost and the accuracy of the vessel's response.

The grid refinements that are implemented to capture the interaction between the hull and the fluid and wave propagation at the free surface are considered optimised already. The same goes for the refinements implemented for the motion of the vessel. Both in terms of their dimensions as well as their refinement level. For the radiation refinement boxes the optimum dimensions were determined in the previous paragraph. The remaining task is to determine an optimum grid refinement level for these boxes.

In this study the number of cells per radiated shortest wave length $C_{\lambda_{rmin}}$ and longest wave length $C_{\lambda_{rmax}}$ are varied in the radiation refinement boxes whilst all other grid refinements are kept constant. This method ensures that it is possible to evaluate the effect that just these refinements have on the response estimates.

For this study, a total of four systematically increased grid refinement are tested, ranging from 12 up to 96 cells per radiated wave length $C_{\lambda_{rmin}}$ and $C_{\lambda_{rmax}}$. In table 6.5 an overview of the refinements used in the radiation boxes for the four grids are shown.

Radiation refinement box	Refinement level			
	Very coarse grid	Coarse grid	Medium grid	Fine grid
λ_{rmin} upper	12 cells / λ_{rmin}	24cells / λ_{rmin}	48 cells / λ_{rmin}	96 cells / λ_{rmin}
λ_{rmin} lower	6 cells / λ_{rmin}	12 cells / λ_{rmin}	24 cells / λ_{rmin}	48 cells / λ_{rmin}
λ_{rmax} upper	12 cells / λ_{rmax}	24 cells / λ_{rmax}	48 cells / λ_{rmax}	96 cells / λ_{rmax}
λ_{rmax} lower	6 cells / λ_{rmax}	12 cells / λ_{rmax}	24 cells / λ_{rmax}	48 cells / λ_{rmax}

Table 6.5: Overview of the radiation box refinement levels

Furthermore, table 6.6 presents the refinement levels of the refinements that were kept the same over all the grids. The dimensions of the grid refinement boxes are consistent with the specifications given in paragraph 6.3.

In figure 6.13 cross sections of the grids are shown. From these figures, the effect of the refinement level can be seen on the grid.

For each of the grids, the vessel's responses are determined by performing the 'forced motion' simulation procedure as described in chapter 6.1. This results in a total of 12 simulations as both the calm water as well as the forced heave and pitch simulations are performed for each of the grids.

Refinement group	Refinement box/ surface	Refinement
Hull - fluid interaction	Near vessel box	35 cells / B
	Surface midship	35 cells / B
	Surface bow & stern	70 cells / B
	Surface transom	140 cells / B
Grid deformation	Near vessel free surface box	5 cells / ζ_a
Free surface refinement	Free surface refinement box	5 cells / ζ_a

Table 6.6: Overview of the refinements used in all grids

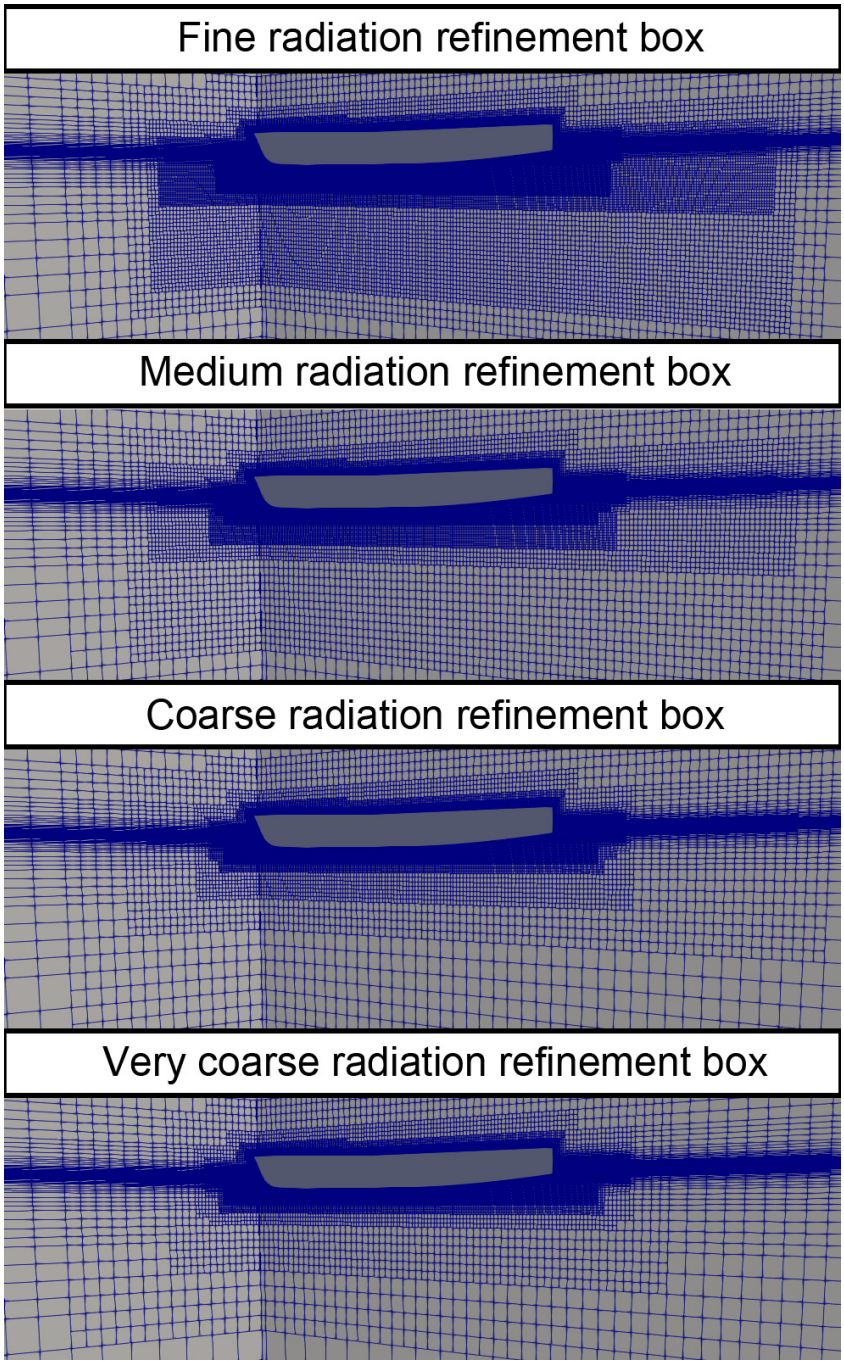

Figure 6.13: Cross sections of the grid for the various refinement levels

6.6. Results of the grid refinement study

In this paragraph the results from the grid refinement study wil be discussed. First a visual impression of the test will be presented. Next the residuals in the simulations will be analysed. After that, the effect of the grid refinement on the wave elevation near the vessel and on the wave pattern is checked. Then the convergence with grid refinement of the vessels responses due to the induced motions are checked. Finally, to check if the responses are correct, they are converted to the vessel's added resistance and damping and compared to the values from PRECAL, which are known to be accurate.

6.6.1. Visual impression

In this section images of the radiating wave simulations are presented. The idea is to give the reader a visual impression of what happens in the simulation. This is done through a series of photos that will present the different steps through which the simulation runs. See figure 6.14

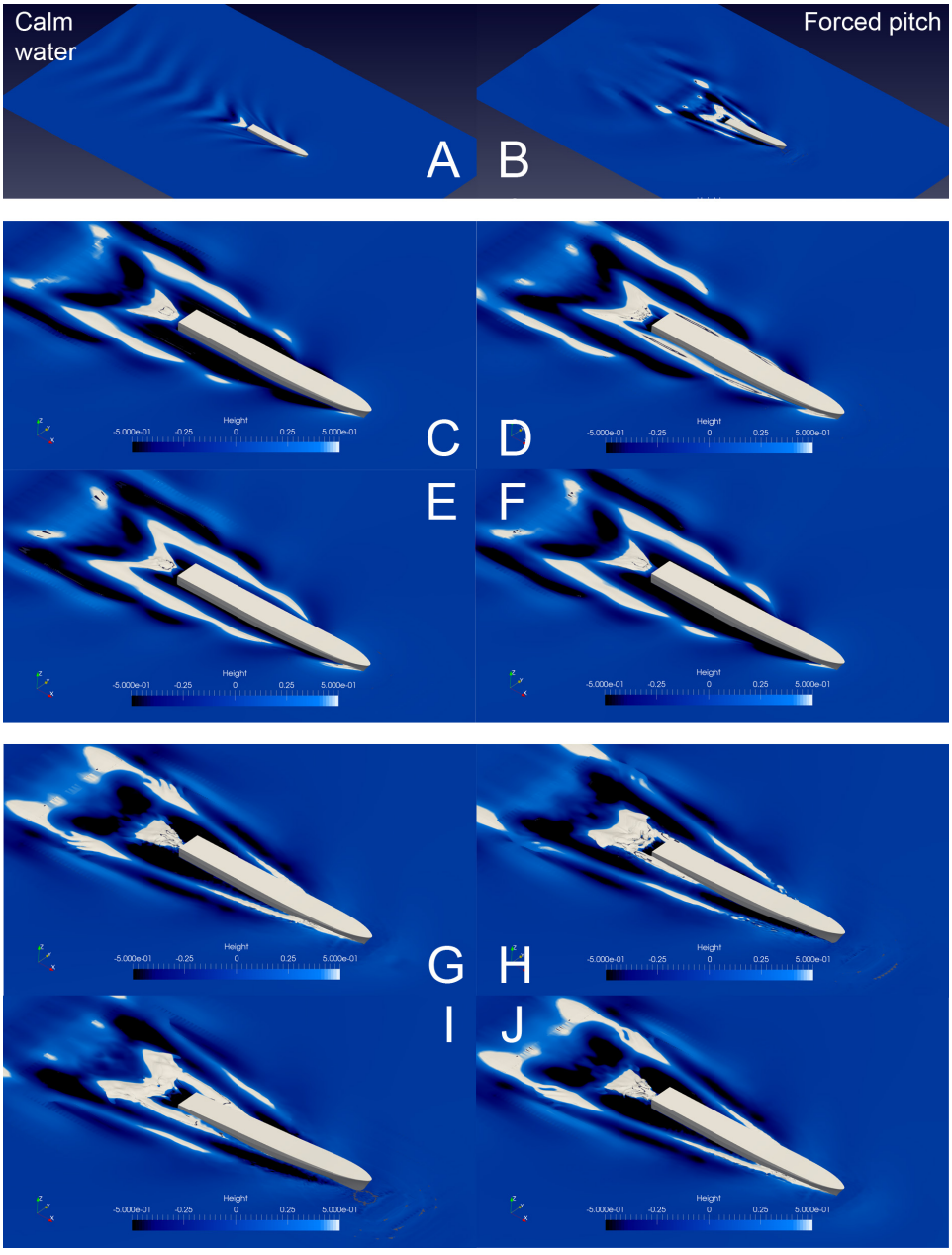

Figure 6.14: Visual impression of the simulation, A-B = steps of the simulation, C- F = one forced heave oscillation, G-J = one pitch oscillation

The simulation starts off in calm water, where the vessel is instantaneously accelerated to full speed. After the initial start it continues to sail until the flow and imposed forces and moments on the vessel have stabilised to an approved level. Then the simulation is stopped. Step A shows the vessel sailing in calm water. Next, the forced motion, being either heave or pitch is started. Step B shows the vessel while it is pitching.

After the motion has been initiated it will continue for 15 oscillations. In step C through F one oscillation of the forced heave motion is shown step by step. The same is done in step G through J for the pitch motion. From the last 10 oscillations the vessel's responses to the induced motions are determined.

6.6.2. Residuals

In order to determine if the convergence error is considered small enough to be neglected, the residuals r were analysed. For details regarding the convergence error and residuals, the user is referred to chapter 2.4.1.

From the analysis of the residuals, similar effects were noticed as were seen in the diffracting wave simulations. The $L2$ norm converged to an acceptable value of about 1E-5 or better for the largest residuals. For the L_∞ norm however, values in the region of 1E-1 or better were seen. As before, it must be considered that this norm evaluates the largest residual within the whole domain. Therefore the domain is inspected visually. Similar to the visual analysis of the residuals in the diffracting waves simulations, a threshold is set which will ensure that only the residuals larger than it will be visualised.

In figure 6.15 the residuals for the pressure parameter are visualised for the very coarse grid using three different threshold. This pressure parameter was selected for this visualisation as it was subjected to the largest residuals.

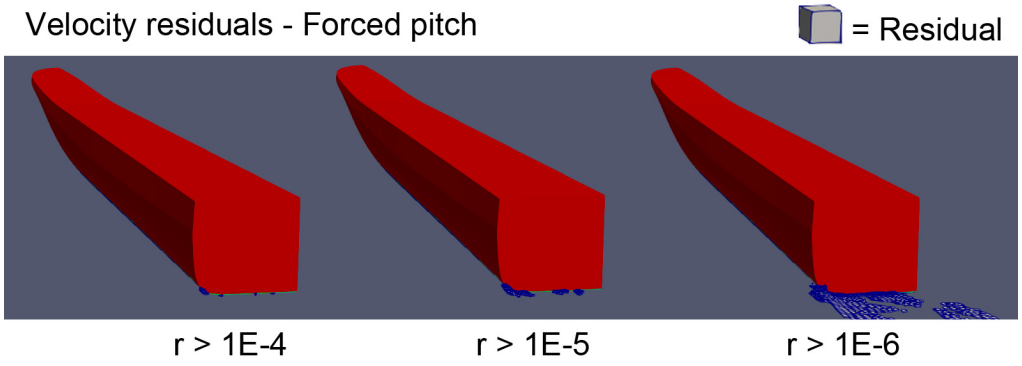

Figure 6.15: Visualisation of the residuals of the pressure parameter

A similar effect is observed here as was noticed in analysis of the diffracting wave simulation residuals. The larger residuals only occur in small numbers in local areas, in particular at the transom. Since the residuals larger than 1E-4 only occur in small quantities and only very local they are considered acceptable.

6.6.3. Wave elevation and pattern

Next, the wave elevation and pattern are checked to analyse the effect of the grid refinement on them. First, a wave cut close to the vessel is made. For both the heave and pitch, two interesting moments in time are selected for this plot. For the heave motion, wave cuts are made for the moments when the vessel is heaved all the way up and down. For the pitch motion, the cuts are made when the bow is pitched all the way up and down. In figures 6.16 through 6.19 plots of these wave cuts can be seen for the four grid refinement levels.

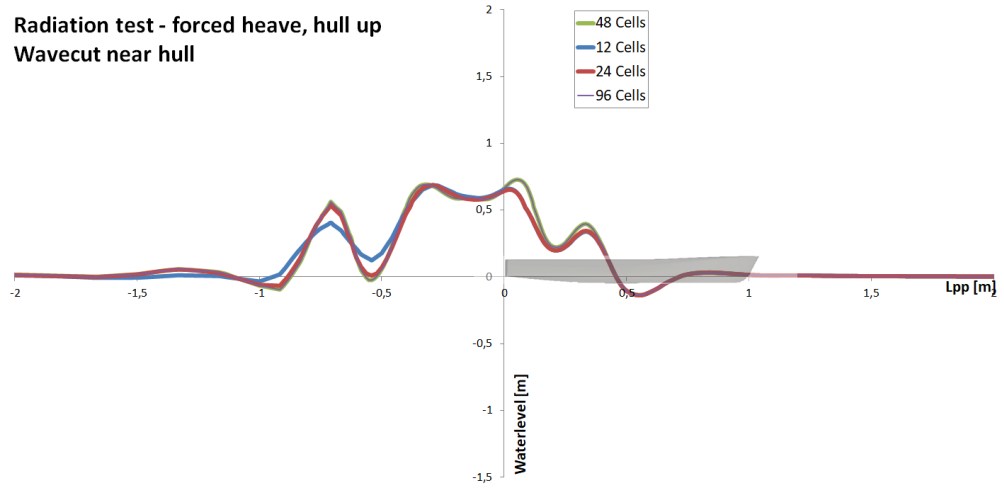

Figure 6.16: Wave cut forced heave simulation, heave up

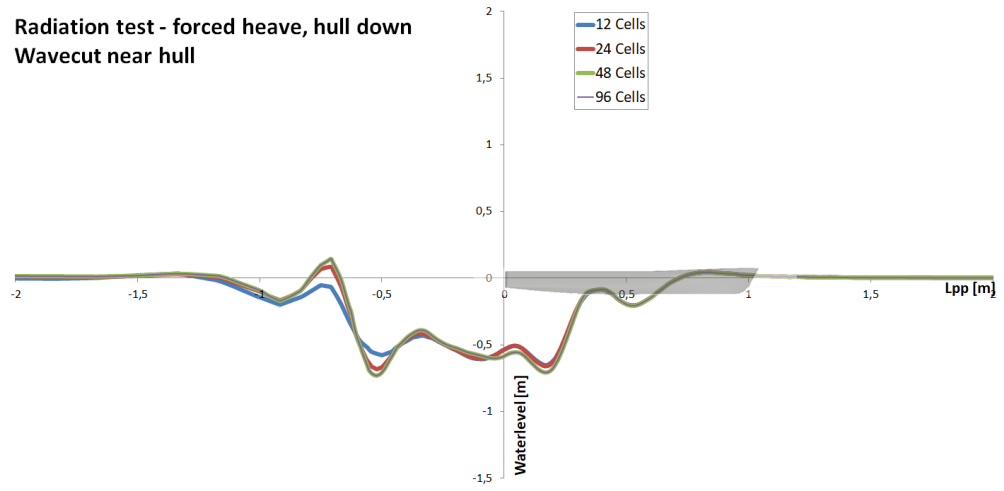

Figure 6.17: Wave cut forced heave simulation, heave down

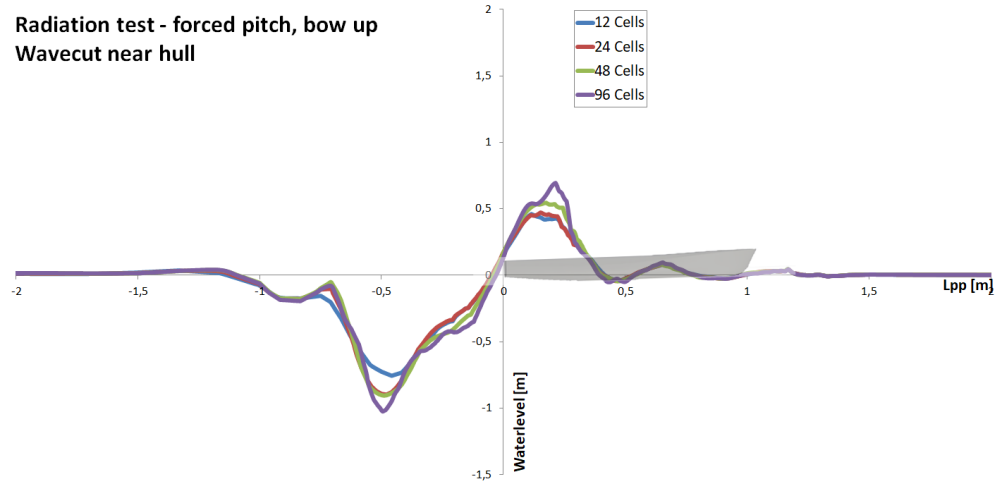

Figure 6.18: Wave cut forced pitch simulation, bow up

From these plots, it can be seen that the grid refinement level has a visible influenced on the wave elevation near the vessel. It appears that an increase in the grid refinement will lead to higher peaks

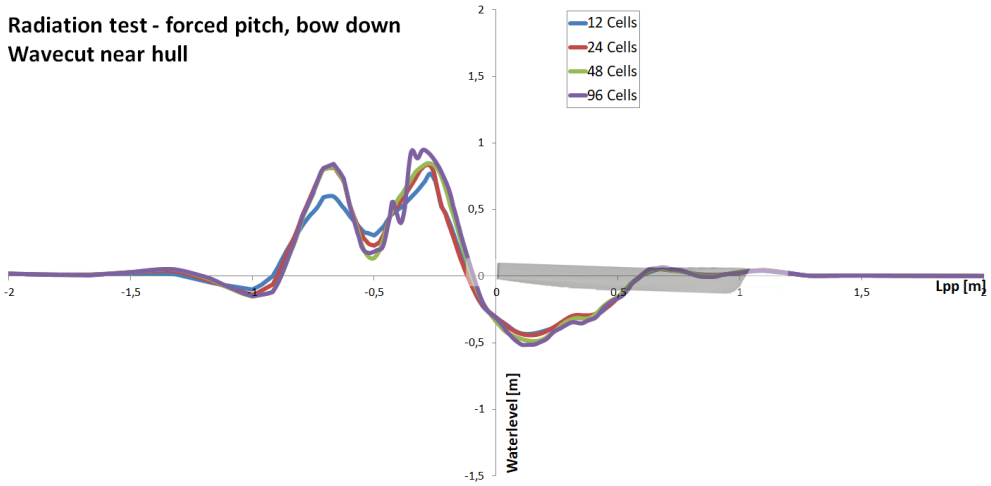

Figure 6.19: Wave cut forced pitch simulation, bow down

and lower troughs in the wave elevation.

Next, top down views of the free surface elevation are analysed. In figure 6.20 two examples of wave patterns from the forced heave simulation are shown for increased grid refinement. For the same moment in time the image on the left shows the low grid refinement simulation and the image on the right shows the high grid refinement free simulation.

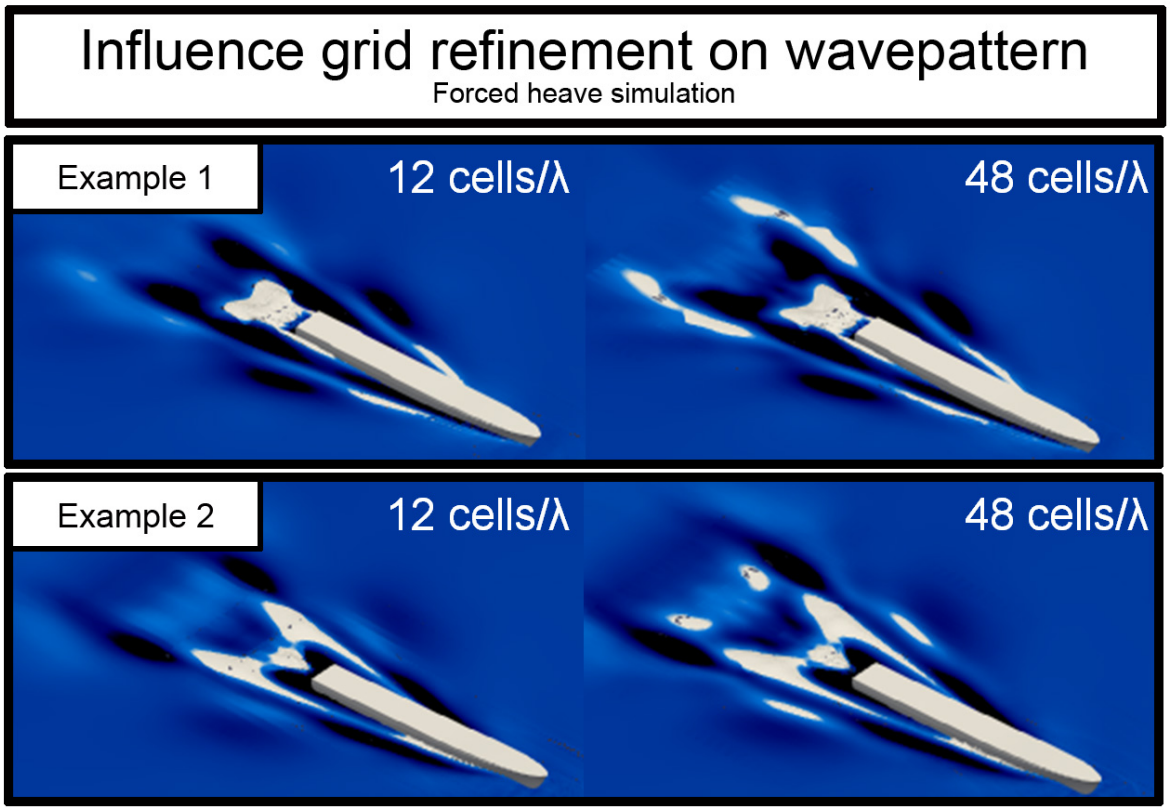

Figure 6.20: Two examples of wave patterns for increased grid refinement

Here a similar effect can be observed as was seen in the analysis of the wavecuts. The higher grid refinement appears to result in a more pronounced wave pattern. Some details in the wave pattern that were captured with the higher refinement level are not visible in the wave pattern calculated with

the lower refinement grid.

From the wave elevation and pattern analysis, it can be concluded that the grid refinements have a significant influence on the wave pattern. With increasing grid refinement, the peaks and troughs of the waves become larger and more detail becomes visible in the wave pattern.

6.6.4. Resistance convergence

Now, the convergence of the vessel's responses to the motions for increased grid refinement is analysed. First plots of the time traces of the force in heave direction and moment in pitch direction for both the forced heave and pitch simulations are compared for increased grid refinement. After that, the convergence of the amplitude and pitch of the vessel's responses is checked.

In figure 6.23 and 6.24 time traces for the vessel's responses are shown for both the forced heave and pitch simulations.

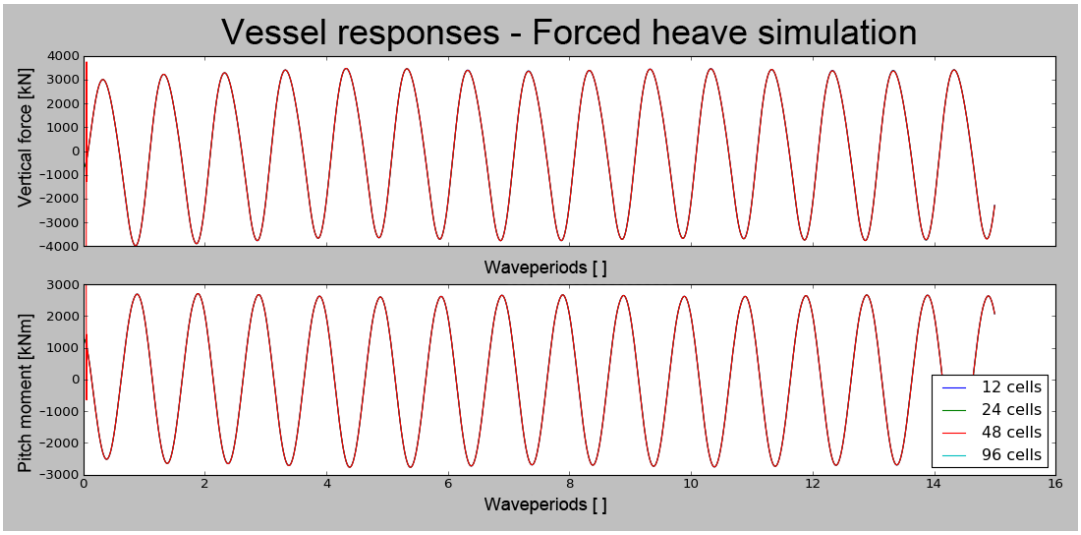

Figure 6.21: Time-trace of the vertical force and pitch moment - forced heave simulation

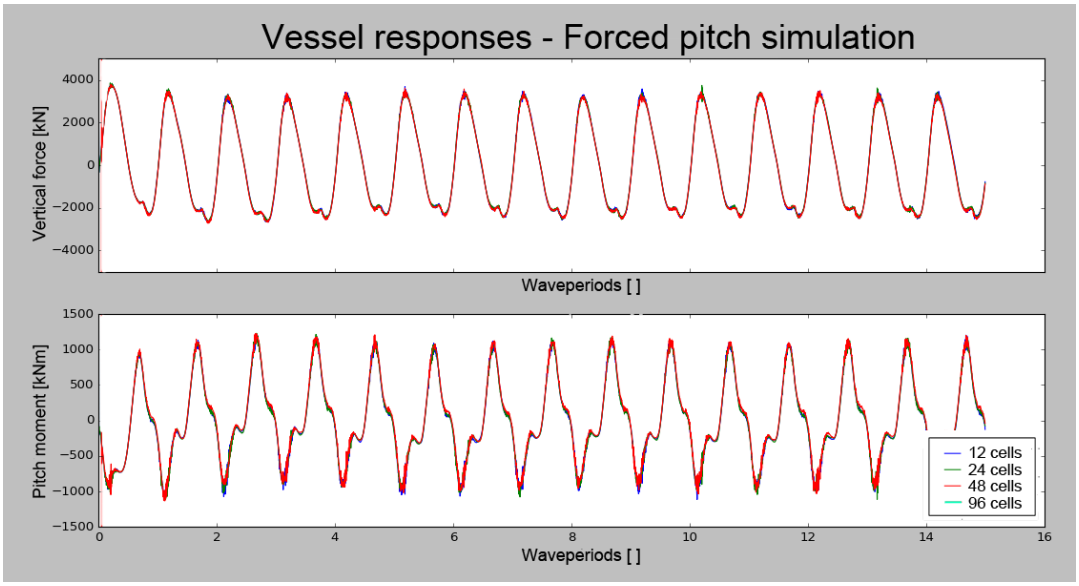

Figure 6.22: Time-trace of the vertical force and pitch moment - forced pitch simulation

From these two figures, it is seen that the vessel's responses appear insensitive to the increase in grid refinement.

Now the convergence of the vessel's response estimates is checked. In figures 6.23 and 6.24 charts are shown that plot the amplitude of the vessel's reponses for both the forced heave and pitch simulations for increased grid refinement.

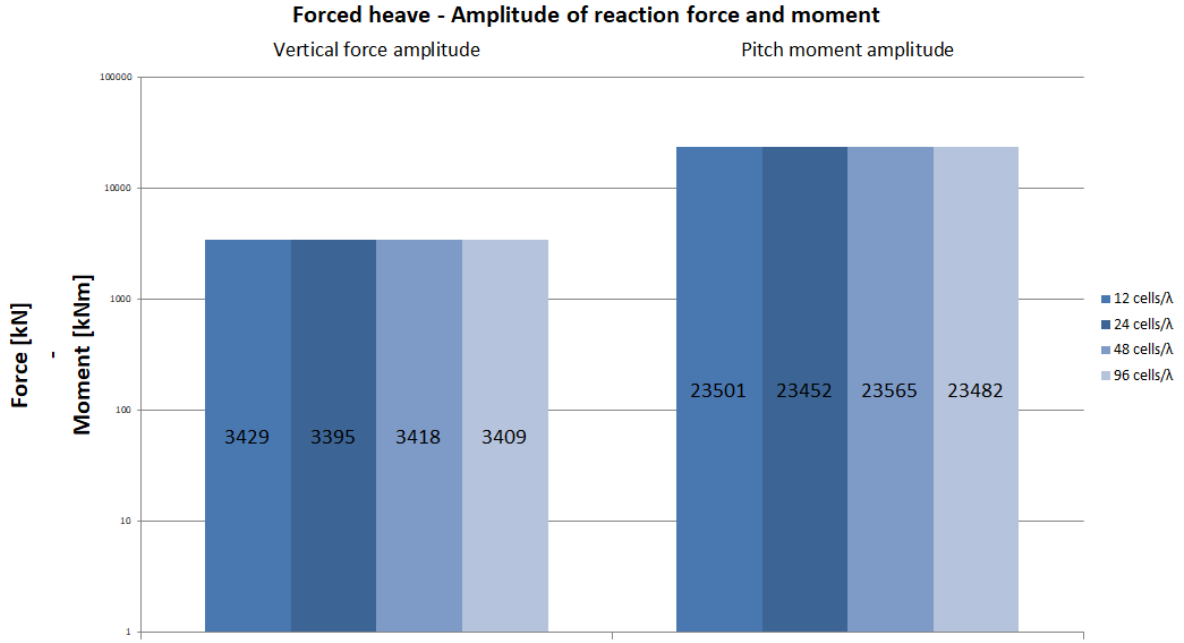

Figure 6.23: Resistance estimates - forced heave simulation

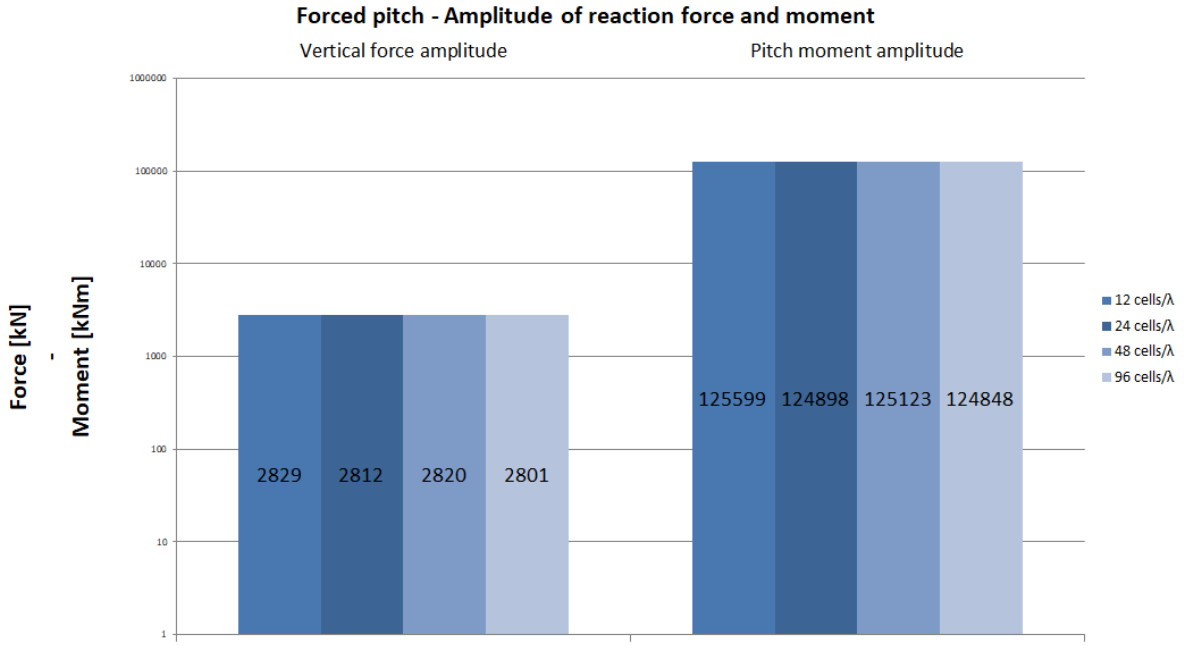

Figure 6.24: Resistance estimates - forced pitch simulation

These plots confirm the conclusion from the time-trace analysis. An increase in the grid refinement appears to have a small effect on the vessel's responses. For the forced heave simulations the amplitude of the vertical force and pitch moment varied no more than 20 kN and 113 kNm respectively which is less than 0.5 % of the amplitude. For the forced pitch simulations the amplitude of the vertical force

and pitch moment varied no more than 28 kN and 751 kNm respectively which is also less than 0.5 % of the amplitude.

6.6.5. PRECAL added mass and damping comparison

Finally, in order to check if the vessel's responses are correct, they are compared to the responses determined using the potential flow based solver PRECAL. From a verification study by D.L.Chow and K.A.McTaggart [13] it is known that PRECAL is able to provide an accurate estimate of the vessel's responses to motions. However, PRECAL outputs these responses in the form of the vessel's added mass and damping.

Therefore, they must first be calculated from the vessel's responses to the waves as was determined using CFD. In chapter 6 and 7 of the TU Delft reader 'Offshore Hydromechanics' [21], the method is described that is used to make an estimate of the vessel's frequency dependent added mass and damping from the forced pitch and heave tests based on the vessel's linear equations of motion. A description of this method is given here.

During the forced motion simulations the induced motion of the vessel equals:

$$\begin{aligned} Heave\ oscillations: \ z(t) &= z_a(t)sin(\omega t) \\ Pitch\ oscillations: \ \Theta(t) &= \Theta_a(t)sin(\omega t) \end{aligned} \tag{6.7}$$

For both simulation types, the resulting heave and pitch moment can be described as:

$$\begin{aligned} Heave\ force: \ F_z(t) &= F_a sin(\omega t + \varepsilon_{Fz}) \\ Pitch\ moment: \ M_\Theta(t) &= M_a sin(\omega t + \varepsilon_{M\Theta}) \end{aligned} \tag{6.8}$$

Heave oscillations

For the forced heave simulations, the linear equations of motion are given by:

$$\begin{aligned} (m + a_{zz})\ddot{z} + b_{zz}\dot{z} + c_z &= F_a sin(\omega t + \varepsilon_{Fz}) \\ (a_{\Theta z})\ddot{z} + b_{\Theta z}\dot{z} + c_\Theta &= M_a sin(\omega t + \varepsilon_{Mz}) \end{aligned} \tag{6.9}$$

In which a represent the vessels added inertia, b the damping and c the vessels restoring coefficients.

The components of the force and moment, which are in-phase with the heave motion are asociated with the inertia and stiffness coefficients, while the out-of-phase components are associated with damping. By inserting the heave motion, velocity and acceleration into the equations of motion:

$$z = z_a sin(\omega t) \qquad \dot{z} = z_a \omega cos(\omega t) \qquad \ddot{z} = -z_a \omega^2 sin(\omega t) \tag{6.10}$$

we obtain:

$$\begin{aligned} z_a(-a_{zz}\omega^2 + c_{zz})sin(\omega t) + z_a b_{zz}\omega cos(\omega t) &= F_a cos(\varepsilon_{Fz} sin(\omega t) + F_a sin(\varepsilon_{Fz})cos(\omega t) \\ z_a(-a_{\Theta z}\omega^2 + c_{\Theta z})sin(\omega t) + z_a b_{\Theta z}\omega cos(\omega t) &= M_a cos(\varepsilon_{M\Theta} sin(\omega t) + M_a sin(\varepsilon_{M\Theta})cos(\omega t) \end{aligned} \tag{6.11}$$

By setting ωt to 0 and $\frac{\pi}{2}$ we obtain:

$$
\begin{aligned}
a_{zz} &= \frac{c - \frac{F_a}{z_a} cos(\varepsilon_{Fz})}{\omega^2} - m \\
a_{\Theta z} &= \frac{f - \frac{M_a}{z_a} cos(\varepsilon_{Mz})}{\omega^2} \\
b_{zz} &= \frac{\frac{F_a}{z_a} sin(\varepsilon_{Fz})}{\omega} \\
b_{\Theta z} &= \frac{\frac{M_a}{z_a} sin(\varepsilon_{Mz})}{\omega}
\end{aligned}
\tag{6.12}
$$

To obtain an accurate estimate of the vessel's restoring coefficients c_{zz} and $c_{\Theta z}$, they were determined using PRECAL.

Pitch oscillations

For the forced pitch simulations, the linear equations of motion are given by:

$$
\begin{aligned}
(a_{z\Theta})\ddot{\Theta} + b_{z\Theta}\dot{\Theta} + c_{z\Theta}\Theta &= F_a sin(\omega t + \varepsilon_{F\Theta}) \\
(I_{yy} + a_{\Theta\Theta})\ddot{\Theta} + b_{\Theta\Theta}\dot{\Theta} + c_{\Theta\Theta}\Theta &= M_a sin(\omega t + \varepsilon_{M\Theta})
\end{aligned}
\tag{6.13}
$$

In which a represent the vessels added inertia, b the damping and c the vessels restoring coefficients.

The components of the force and moment, which are in-phase with the pitch motion are asociated with the inertia and stiffness coefficients, while the out-of-phase components are associated with damping. By inserting the pitch motion, velocity and acceleration into the equations of motion:

$$
\Theta = \Theta_a sin(\omega t) \qquad \dot{\Theta} = \Theta_a \omega cos(\omega t) \qquad \ddot{\Theta} = -\Theta_a \omega^2 sin(\omega t)
\tag{6.14}
$$

we obtain:

$$
\begin{aligned}
\Theta_a(-a_{z\Theta}\omega^2 + c_{z\Theta})sin(\omega t) + \Theta_a b_{z\Theta}\omega cos(\omega t) &= F_a cos(\varepsilon_{Fz} sin(\omega t) + F_a sin(\varepsilon_{Fz}) cos(\omega t) \\
\Theta_a(-d\omega^2 + c_{\Theta\Theta})sin(\omega t) + \Theta_a b_{\Theta\Theta}\omega cos(\omega t) &= M_a cos(\varepsilon_{M\Theta} sin(\omega t) + M_a sin(\varepsilon_{M\Theta}) cos(\omega t)
\end{aligned}
\tag{6.15}
$$

By setting ωt to 0 and $\frac{\pi}{2}$ we obtain:

$$
\begin{aligned}
a_{z\Theta} &= \frac{c_{z\Theta} - \frac{F_a}{\Theta_a} cos(\varepsilon_{F\Theta})}{\omega^2} \\
a_{\Theta\Theta} &= \frac{c_{\Theta\Theta} - \frac{M_a}{\Theta_a} cos(\varepsilon_{M\Theta})}{\omega^2} - I_{yy} \\
b_{z\Theta} &= \frac{\frac{F_a}{\Theta_a} sin(\varepsilon_{F\Theta})}{\omega} \\
b_{\Theta\Theta} &= \frac{\frac{M_a}{\Theta_a} sin(\varepsilon_{M\Theta})}{\omega}
\end{aligned}
\tag{6.16}
$$

To obtain the vessel's restoring coefficients $c_{z\Theta}$ and $c_{\Theta\Theta}$, they were determined using PRECAL.

The in-phase and out-of-phase parts of the force and moment time-trace are determined by integrating them over the last 10 wave periods T, multiplied by $cos(\omega t)$ and $sin(\omega t)$ respectively. This is known as a first order Fourier analysis. This results in the following equations for the heave oscillations:

$$
\begin{aligned}
F_a sin(\varepsilon_{Fz}) &= \frac{2}{10T}\int_0^{10T} F_z(t) * cos(\omega t)dt \\
F_a cos(\varepsilon_{Fz}) &= \frac{2}{10T}\int_0^{10T} F_z(t) * sin(\omega t)dt \\
M_a sin(\varepsilon_{Mz}) &= \frac{2}{10T}\int_0^{10T} M_\Theta(t) * cos(\omega t)dt \\
M_a cos(\varepsilon_{Mz}) &= \frac{2}{10T}\int_0^{10T} M_\Theta(t) * sin(\omega t)dt
\end{aligned}
\tag{6.17}
$$

In a similar fashion the equations the pitch oscillations can be found. The resulting added mass and damping are shown in table 6.7 and 6.8

Forced heave								
	$a_{zz}[Ns^2/m]$	error	$a_{\Theta z}[Ns^2]$	error	$b_{zz}[Ns/m]$	error	$b_{\Theta z}[Ns]$	error
PRECAL	0.301E+07		0.167E+08		0.402E+07		-0.138E+08	
CFD 12 cells	0.300E+07	-0.4 %	0.165E+08	-0.7 %	0.403E+07	0.3%	-0.137E+08	-0.6%
CFD 24 cells	0.303E+07	0.3 %	0.168E+08	0.4%	0.404E+07	0.5%	-0.139E+08	0.6 %
CFD 48 cells	0.301E+07	-0.3 %	0.166E+08	-0.5%	0.403E+07	0.3%	-0.137E+08	-0.4%
CFD 96 cells	0.303E+07	0.5%	0.168E+08	0.3%	0.404E+07	0.4%	-0.139E+08	0.5%

Table 6.7: Comparison of the vessel's added mass and damping as determined with CFD to PRECAL for the forced heave simulations

Forced pitch								
	$a_{z\Theta}[Ns^2]$	error	$a_{\Theta\Theta}[Nms^2]$	error	$b_{z\Theta}[Ns]$	error	$b_{\Theta\Theta}[Nms]$	error
PRECAL	-0.137E+08	0	0.157E+10		0.392E+08		0.233E+10	
CFD 12 cells	-0.136E+08	-0.5 %	0.158E+10	0.3 %	0.390E+08	-0.4%	0.232E+10	-0.3%
CFD 24 cells	-0.138E+08	0.4 %	0.156E+10	-0.6%	0.393E+08	0.3%	0.234E+10	0.3 %
CFD 48 cells	-0.136E+08	-0.4 %	0.158E+10	0.4%	0.394E+08	0.5%	0.234E+10	0.4%
CFD 96 cells	-0.138E+08	0.5%	0.156E+10	-0.4%	0.390E+08	-0.3%	0.232E+10	-0.4%

Table 6.8: Comparison of the vessel's added mass and damping as determined with CFD to PRECAL for the forced pitch simulations

6.7. Discussion and conclusion

On this radiating waves study the following conclusions can be drawn:

- The increase in grid refinement appears to have an influence on the wave elevation surrounding the vessel. With increased refinement, the peaks and troughs of the waves appear to become larger and the wave pattern becomes more detailed
- For the forced heave simulations the amplitude of the vertical force and pitch moment varied no more than 20 kN and 113 kNm respectively, which is less than 0.5 % of the amplitude.
- For the forced pitch simulations the amplitude of the vertical force and pitch moment varied no more than 28 kN and 751 kNm respectively, which is also less than 0.5 % of the wave amplitude.
- These variances in the amplitude of the vertical force and pitch moment when comparing the results for the four grid refinement levels, indicate that the vessel's responses to the induced heave and pitch motion appear to be insensitive to the increased grid refinement introduced by the radiation refinement boxes.
- The vessel's added mass and damping that were estimated from the CFD simulations, appear to be insensitive to increased grid refinements as the added mass a_{zz} and added damping b_{zz} varied no more than 30 tonne and 20 tonne/s respectively for the forced heave test. This is less than 1 % of the total added mass and damping.
- For the forced pitch tests, the vessel's estimated added mass and damping also appear to be insensitive to increased grid refinements as the added mass $a_{\Theta\Theta}$ and added damping $b_{\Theta\Theta}$ varied no more than 20 tonne and 20 tonne/s respectively for the forced heave test. This is less than 1 % of the total added mass and damping.
- From the comparison between CFD and PRECAL of the vessel's added mass and damping it is seen that the error is smaller than 0.7 % of the total added mass and damping for all grid refinements.
- As the increased grid refinements implemented to capture the radiating waves accurately, appear to have a negligible effect on the vessels responses to the motions, as well as the accuracy of the vessel's added mass and damping coefficients, the very coarse grid, with the lowest grid refinement is selected as the optimum for the set of radiating wave refinement boxes.
- Compared to the most refined grid in this simulation, this simulation costs about 2.7 times less and delivers similar vessel responses to the motions. This estimate is based on the number of cells in the respective grids.

7

Simulating a vessel with 2 DoFs in calm water and regular head waves

The purpose of this chapter is to determine the optimum grid refinement for the estimation of the added resistance in regular head waves. As it was the case in this entire thesis, optimum refers the best compromise between the cost of the simulation and the accuracy of the resistance estimate.

The grid topology and simulation settings used in this chapter are all based on the optimum settings that were determined in the previous chapters. These optimised settings were designed to ensure consistently propagating waves as well as accurate vessel responses to the waves as well as the induced motions. The hypothesis is that by ensuring that these three aspects of the simulation are simulated accurately, the added resistance in regular waves can be captured accurately as well. For information regarding the theoretical foundation of this concept, the reader is referred to chapter 1.4.

The chapter concludes with the verification and validation of the results. The discretisation error of the added resistance estimate is calculated by performing a grid refinement study according to the method by L.Eça and M.Hoekstra [25]. Finally, the results from this research are compared to a potential flow (PRECAL) solution as well as to the results from the CRS model tests.

7.1. Test procedure

The test procedure is similar to that of the 'diffracted waves' test. The differences in this procedure are related to the fact that the vessel now has two DoFs compared to the static vessel in the diffraction simulations. The test procedure consists of four steps, being the 'start up', 'vessel with zero DoF in calm water', 'vessel with two DoFs in calm water' and 'vessel with two DoFs in regular waves' simulations. These steps are explained in the remainder of this chapter.

7.1.1. Start up simulation

The first step in the procedure is the 'start up' of the simulation. This step is identical to the 'start up simulation' used in the wave diffraction simulations as can be seen in chapter 5.1.1. In this step the vessel starts off with zero DoF in calm water and is instantaneously accelerated up to the desired speed. This simulation runs for only a few time-steps.

7.1.2. Vessel with zero DoF in calm water

In the second step the vessel will continue to sail with 0 DoFs in calm water. This step is similar to the 'calm water simulation' used in the diffraction simulations. The difference being that the simulation will run for a shorter time. The purpose here is to let the forces on the vessel stabilise enough to not cause issues in the next step of the process, rather than to provide an accurate calm water resistance estimate.

In figure 7.1 a time-trace of the resistance during this part of the simulation is shown.

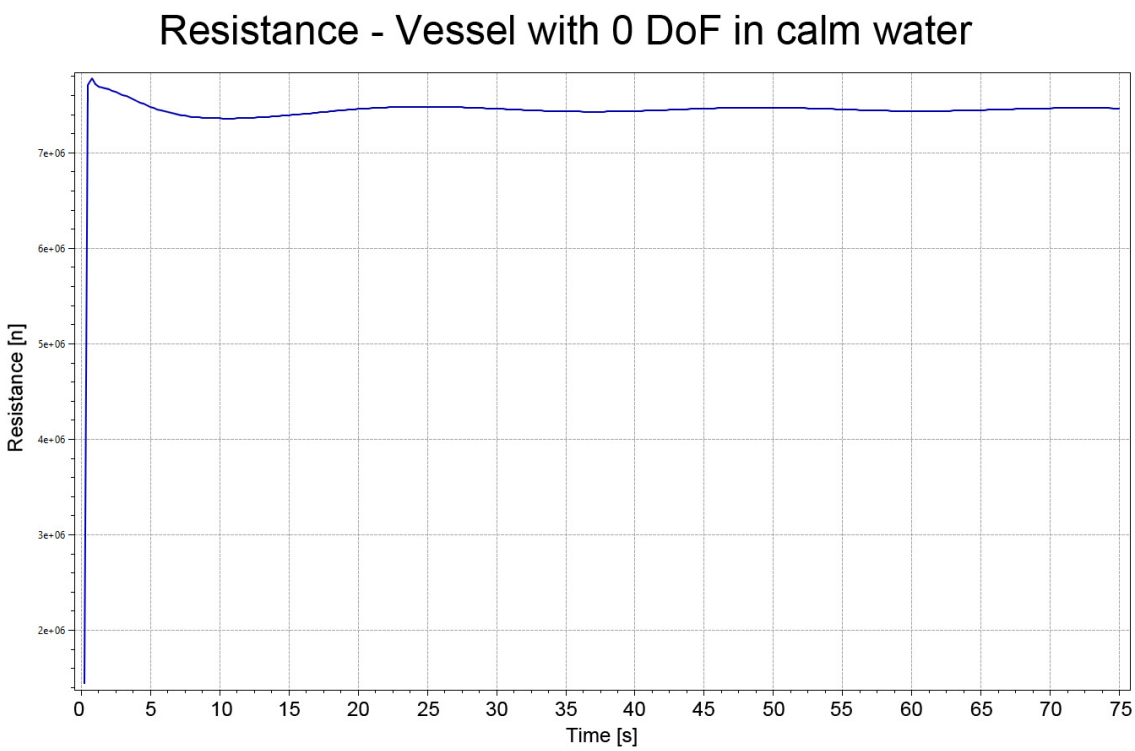

Figure 7.1: Vessel with zero DoF - Calm water resistance

From this plot it can be seen that after the initial start up of the simulation, the vessel's oscillating calm water resistance is converging over time. The simulation is stopped at the moment that the amplitude of these oscillations has reduced to less than 1 % of the mean value. In the simulation seen in the figure, that moment occurs around 40 [s]. In the simulations used in this research, all simulations were run for 70 [s]. This is longer than strictly necessary, resulting in an even more converged resistance.

7.1.3. Vessel with two DoFs in calm water

During the third step, the vessel is given the freedom to heave and pitch while sailing in calm water. From this simulation, the vessel's calm water resistance is determined.

Due to the wave pattern created by the vessel, the pressure distribution on the vessel is affected compared to when it was stationary. This change in the pressure distribution changes the force distribution on the vessel. As a result the vessel will change it's trim and sink until it is in equilibrium. This change in trim and sinkage occurs during this simulation step.

The simulation starts off from the last time step of the 'start-up' simulation. This simulation is then continued until the vessel's trim and sinkage have stabilised and the calm water resistance has converged sufficiently. In order to establish if the vessels motions have stabilised, two criteria were designed.

For the heave motion the maximum amplitude of the oscillations compared to the running mean of the signal was set at 0.001 [m]. For the pitch motion this limit was set at 0.001 [rad] which equals 0.057 [deg]. For the convergence of the vessel's calm water resistance the same criterion from the calm water part of the 'diffracted wave' simulations is used. This states that the calm water resistance is considered converged enough when the amplitude of the oscillations of the resistance signal have reduced to less than 0.1 % of the mean value. Once that criterion has been passed the simulation will stop.

In figure 7.2 time-traces of the resistance, heave and pitch are shown.

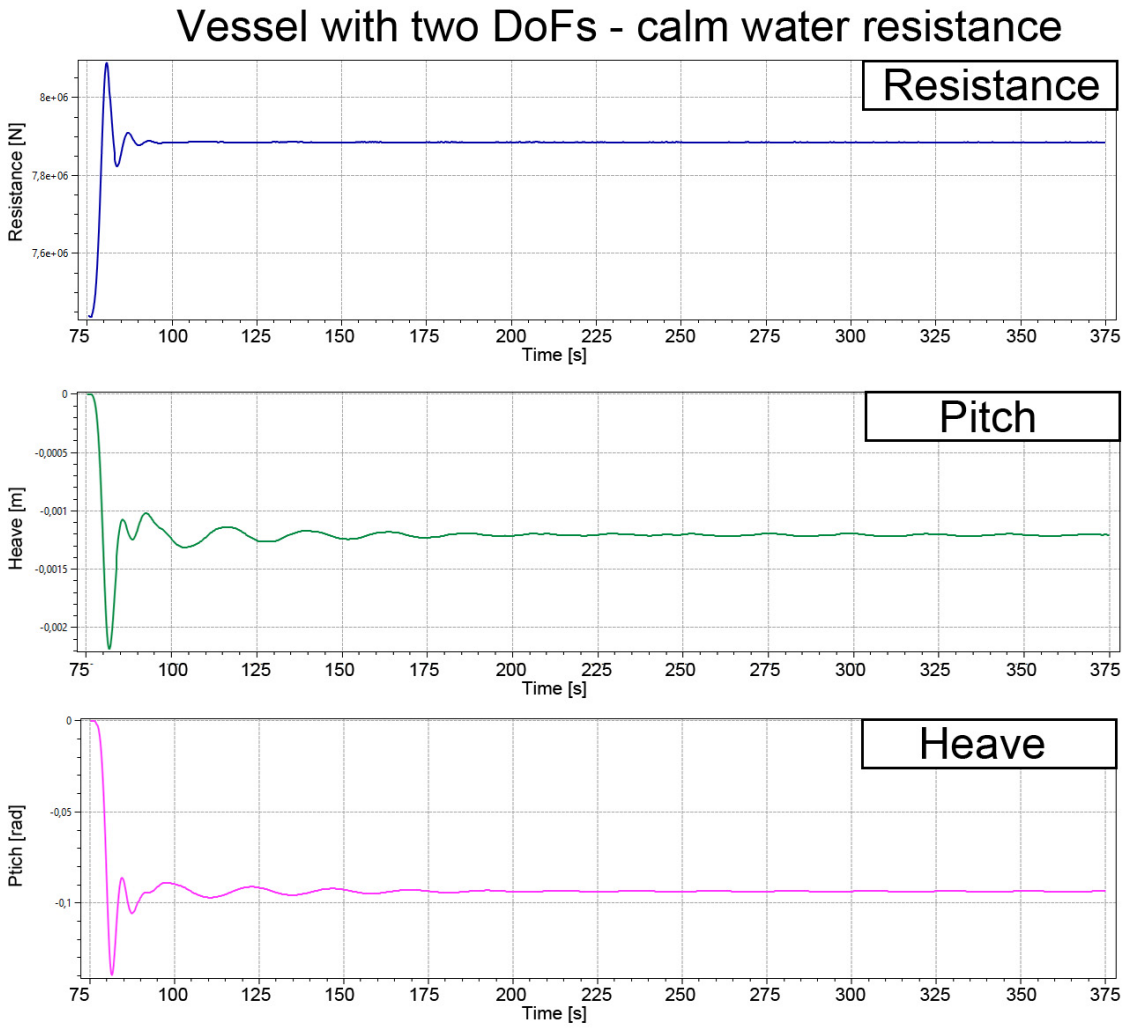

Figure 7.2: Vessel with two DoF - Calm water resistance, heave and pitch

From the heave and pitch time-traces it can be seen that the vessel's trim and sinkage adjust significantly at the beginning of the simulation and then converge over time. The simulations in this research ran longer than strictly necessary, resulting in a more converged value for the calm water resistance resistance. In these simulations, the maximum variation of the resistance signal at the end of the simulation was less than 0.01 %.

7.1.4. Vessel with two DoFs in regular head waves

In the last step the vessel is simulated with two DoFs in regular head waves. The approach taken here is very very similar to the simulation of the vessel in diffraction waves with the only exception being that the vessel now has two DoFs.

The simulation is restarted from the last time step of the 'vessel with 2 DoFs in calm water' simulation. This way, it will start of with the correct trim, sinkage and a converged calm water resistance acting on it. At the start of this simulation, the regular waves are generated at the inlet. The simulation continues until these waves have propagated to the outlet of the domain. After that, the simulation is continued for 10 more wave encounters. The average total resistance in waves is then determined by time-averaging the resistance felt by the vessel over these last 10 wave encounters. This approach is designed to ensure sufficient statistical certainty and is recommended by the ITTC [1].

7.2. Simulation parameters

The parameters for the 'vessel with two DoFs in regular head waves' simulations are now explained in this paragraph.

7.2.1. Domain, Boundary conditions, waves and vessel speed

The domain, boundary conditions, and the speed of the vessel used in these simulations as well as the waves that are generated are described in chapter 3.3. A summary of these parameters is given in table 7.1.

Domain specifications			
Length [m]	Width [m]	Height [m]	Wave absorption [m]
6 Lpp	2 Lpp	4 Lpp	1 Lpp perimeter

Boundary	Boundary Condtion
Inlet	BC wave
Outlet	BC wave
Left	BC wave
Right	BC symmetry
Upper	BC pressure
Lower	BC slipwall
Vessel	BC slipwall

Vessel speed	17.31 [Kts]

wave type	regular waves
wave frequency ω	0.85 [rad/s]
wave amplitude ζ_a	1.00 [m]

Table 7.1: Summary of the domain, boundary conditions, waves and speed specifications used in the 'Vessel with two DoFs in regular head waves' simulations

7.2.2. time-step

The time steps used for the four steps of the simulation are the same as those used in the diffracting wave simulations. For information regarding these time steps the reader is referred to chapter 5.2.4. In table 7.2 a summary of these time steps is given.

Simulation:	Start up simulation	0 DoF in calm water	2 DoF in calm water	2 DoF in waves
Δt [s]:	$\frac{1}{10}\frac{Lpp}{v}$	$\frac{Lpp}{v}$	$\frac{Lpp}{v}$	$\frac{T_e}{200}$

Table 7.2: Time steps used in the vessel with two DoFs simulations

7.2.3. Simulation time

The simulation will start with the simulation of the vessel with zero DoF in calm water. This simulation is continued until the maximum variance of the resistance signal converges below 1% of the running mean. Then, the simulation of the vessel with two DoFs is started. This simulation runs until the maximum variance of the resistance signal converges below 0.1 % of the running mean. The calm water resistance is determined from this simulation. Finally, the simulation of the vessel with two DoFs in regular head waves is started. This simulation runs for 14 wave encountered wave periods to fill the domain with waves. A further 10 wave encounters are then simulated in order to determine the time-averaged total resistance in waves with sufficient statistical accuracy. The total of 24 encountered waves take 100 [s] as the encountered wave period is known to be 4.17 [s].

7.3. Spatial discretisation

The grid topology used to discretise the domain for these simulations consists of several grid refinements that were designed and optimised in the previous chapters. First of all, the grid refinements designed to capture the incoming regular waves accurately are implemented. Furthermore, the grid refinements designed to capture the hull - fluid interaction are present. The grid refinements that are designed to capture the diffracted and radiated waves also used. And finally the grid deformation refinements, which are designed to maintain the accuracy of the solution are implemented.

All the implemented grid refinement boxes and surface refinements are summarised in table 7.3 on the next page.

The resulting grid consists of 3.45 million cells. In figure 7.3 an impression of this grid is given. The picture shows an overview of the grid, a more zoomed in section and a detailed view of the bow.

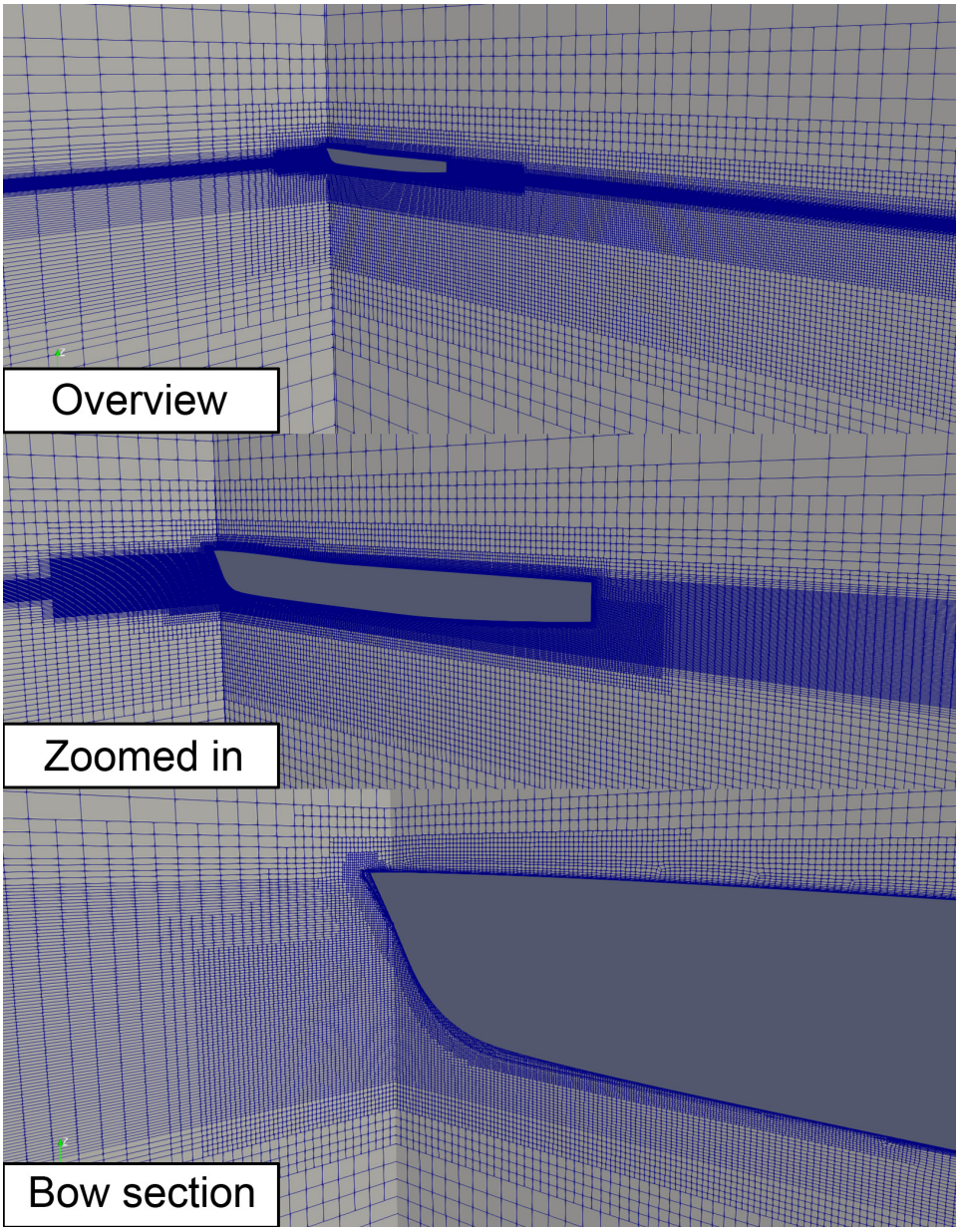

Figure 7.3: Grid for the 'Vessel with two DoFs in regular waves' simulations. From top to bottom an overview, zoomed in section and detailed view of the bow are shown

Refinement group	Refinement box/ surface	Refinement	Coordinates [m]					
			x+	x-	y+	y-	z+	z-
Incoming waves	Free surface	5 cells / ζ_a	300	-300	+200	0	+1.1 ζ_a	-1.1 ζ_a
	Upper	48 cells / λ	300	-300	+200	0	+1.1 ζ_a	-0.2 λ
	Lower	24 cells / λ	300	-300	+200	0	+1.1 ζ_a	-0.6 λ
Hull - fluid interaction	Near vessel box	35 cells / B	Lpp + 0.1 Lpp	-0.1Lpp	B/2 + 0.25B	0	+1.1 ζ_a	-1.1 ζ_a
	Surface midship	35 cells / B	-	-	-	-	-	-
	Surface bow & stern	70 cells / B	-	-	-	-	-	-
	Surface transom	140 cells / B	-	-	-	-	-	-
Diffracted waves	Upper	12 cells / λ_d	Lpp + 0.1 λ_d	-0.5 λ_d	B/2 + 0.50 λ_d	0	1.1 ζ_a	-0.2 λ_d
	Lower	6 cells / λ_d	Lpp + 0.1 λ_d	-0.5 λ_d	B/2+0.50 λ_d	0	1.1 ζ_a	-0.6 λ_d
Radiated waves	λ_{rmin} upper	12 cells / λ_{rmin}	Lpp + 0.1 Lpp	$\lambda_{rmin} cos(\theta_{min})$	$B/2 + \lambda_{rmin} sin(\theta_{min})$	0	1.1 ζ_a	-0.2 λ_{rmin}
	λ_{rmin} lower	6 cells / λ_{rmin}	Lpp + 0.1 Lpp	$\lambda_{rmin} cos(\theta_{min})$	$B/2 + \lambda_{rmin} sin(\theta_{min})$	0	1.1 ζ_a	-0.6 λ_{rmin}
	λ_{rmax} upper	12 cells / λ_{rmax}	Lpp + 0.1 Lpp	$-\lambda_{rmax}$	B/2 + λ_{rmax}	0	1.1 ζ_a	-0.2 λ_{rmax}
	λ_{rmax} lower	6 cells / λ_{rmax}	Lpp + 0.1 Lpp	$-\lambda_{rmax}$	B/2 + λ_{rmax}	0	1.1 ζ_a	-0.6 λ_{rmax}
Grid deformation	Near vessel box	5 cells / ζ_a	Lpp + $\frac{\lambda_{rmax}}{3}$	$-\frac{\lambda_{rmax}}{3}$	B/2 + $\frac{\lambda_{rmax}}{3}$	0	$\zeta_{fmax} + \zeta_a$	$-\zeta_{fmax} - \zeta_a$

Table 7.3: Specifications of the refinements implemented in the grid for the simulation of the vessel with two DoFs in regular head waves

7.4. Verification: Grid refinement study

In order to determine the discretisation uncertainty of the added resistance estimate, a grid refinement study according to the method by L.Eça and M.Hoekstra [25] is performed. For details regarding this method, including the generation of geometrically similar grids, the reader is referred to chapter 2.4.2.

This study was performed using four systematically refined, geometrically similar grids. These are named the very coarse, coarse, medium and fine grid. The grid as shown in the previous chapter was used as the medium grid. Two coarser and one finer geometrically similar grid were generated from it according to the method described in chapter 2.4.2. The refinement levels of those grids range from 0.5 up to 1.25 times the refinement level of the original grid. The specifications of these grids are shown in table 7.4.

Parameter	Grid			
	Very coarse	Coarse	Medium	Fine
n [-]	1.0	1.5	2.0	2.5
Nx [-]	18	27	36	45
Ny [-]	6	9	12	15
Nz [-]	12	18	24	30
d [-]	1	2	3	4
S_0 [m]	0.0242	0.0147	0.0105	0.0082
r [-]	1.69	1.42	1.30	1.23
Total number of cells [-]	0.49 M	1.35M	3.45M	6.64M

Table 7.4: Parameters of the four geometrically similar grids

Where n is the refinement level, Nx, Ny and Nz the initial number of cells in the grid in x, y and z direction and d the diffusion. S_0 is the initial cell size of the boundary layer and r is the stretching ratio.

In figure 7.4 an image of the four resulting grids are shown. From this image it can be seen that the geometrical similarity is maintained over the four grids with varying refinement levels.

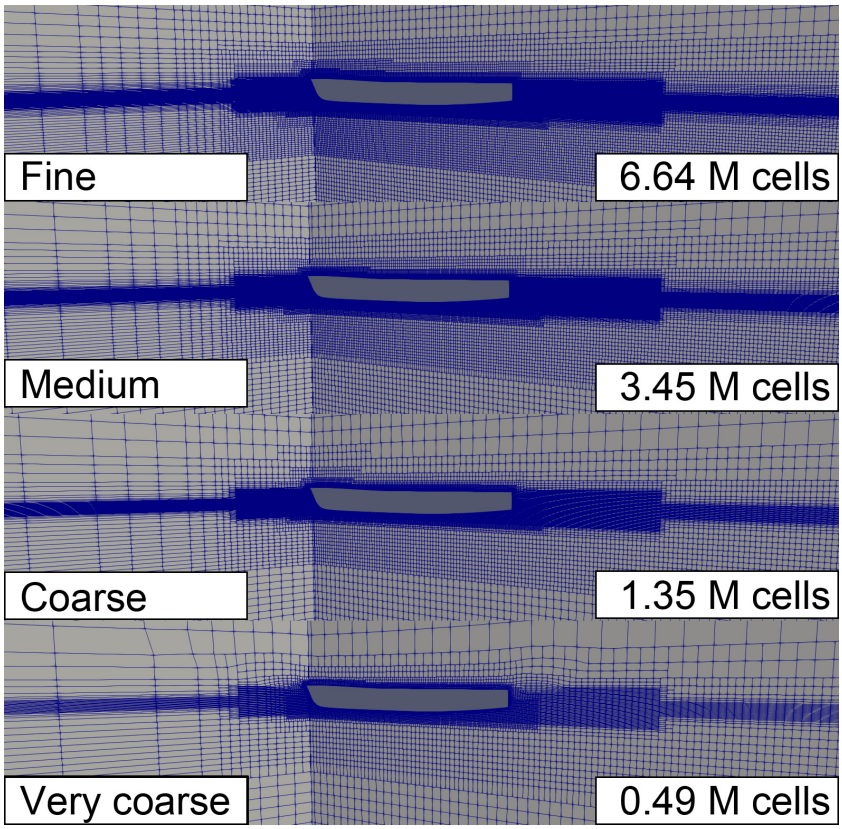

Figure 7.4: Four systematically refined, geometrically similar grids as used in the grid refinement study

7.5. Results of the grid refinement study

In this paragraph the results of the grid refinement study will be discussed. First, a visual impression will be presented. Second, the iterative error is analysed by checking the residuals. This step is followed by a convergence check of the forces and moments in the simulation. The convergence of the solution is checked to ensure that the forces and moments in the simulation are sufficiently converged within each time-step. Finally, the discretisation uncertainty is determined using the method by L.Eça and M.Hoekstra.

7.5.1. Visual impression

In this section images of the 'vessel with two DoFs in regular head waves' simulations are presented to give the reader a visual impression of the simulation. In figure 7.5 a picture of medium grid simulation is shown. Here, the breaking bow wave can clearly be seen.

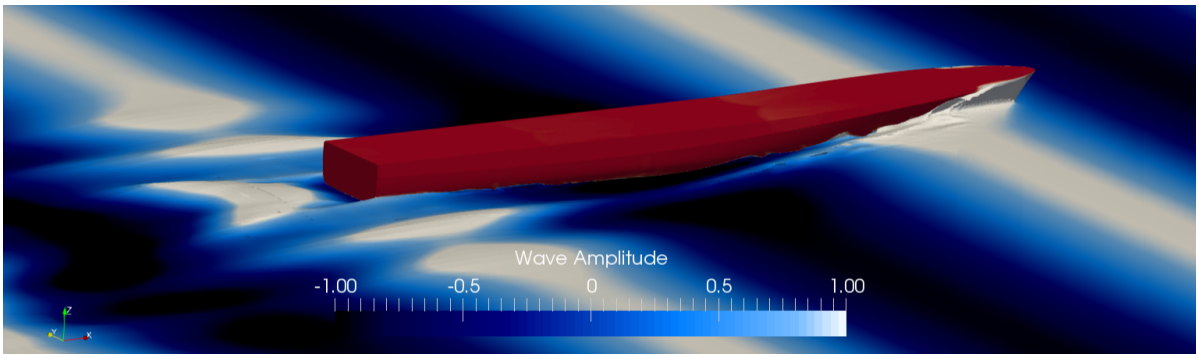

Figure 7.5: Visual impression of the vessel with two DoFs in regular head waves simulation

Unfortunately, no test footage of the CRS mode sailing in regular waves with the same height and frequency as was simulated was available at this time. However, there was a photo available of the vessel while it was tested in a slightly higher regular wave with a slightly lower wave frequency. This wave had an amplitude of 1.25 [m] compared to 1.00 [m] and a frequency of 0.75 [rad/s] compared to 0.85 [rad/s] for the CFD simulation.

In figure 7.6 a side by side comparison is shown of the CRS footage next to a visualisation of the CFD simulation. These images indeed show similar behaviour, with the bow coming out of the water and a similar wave elevation on the hull.

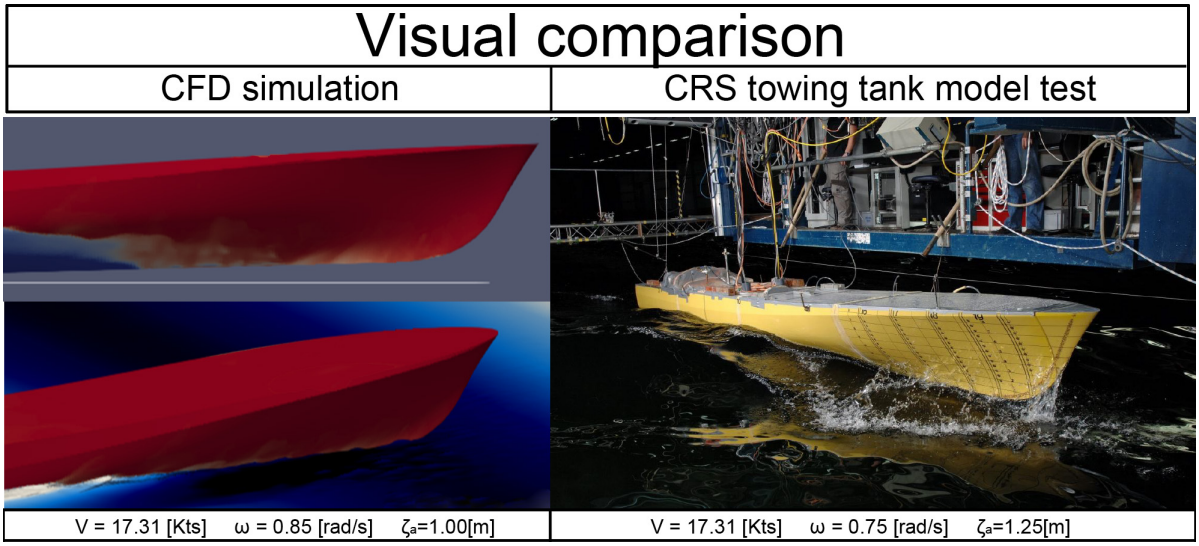

Figure 7.6: Side by side comparison of the CFD simulation and the CRS model test photo as shown in the CRS test report [11]

To illustrate what happens during one wave encounter, a series of photos is shown in figure 7.7. Here one wave encounter is shown in 10 steps.

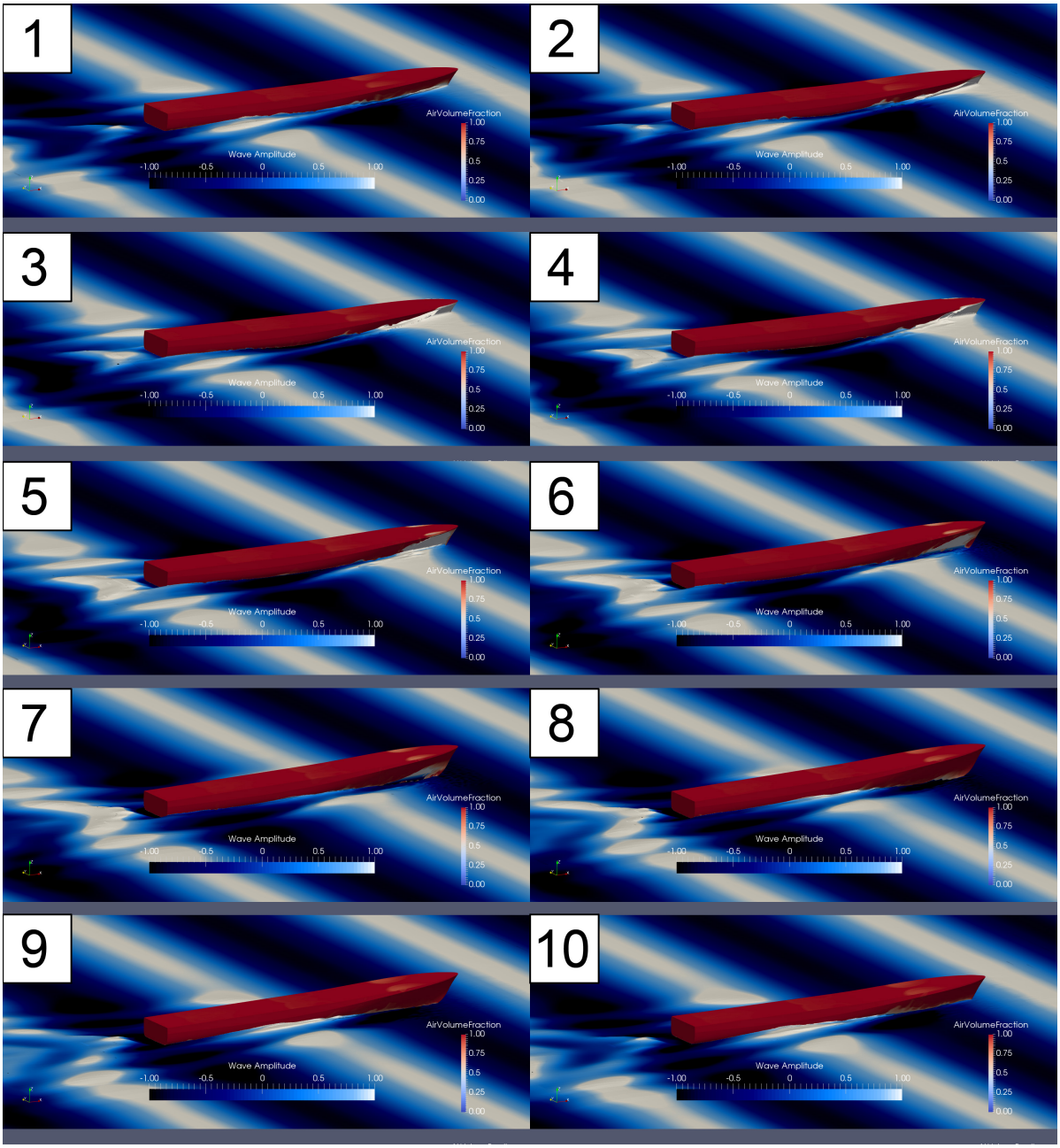

Figure 7.7: Step by step view of one wave encounter - medium grid

7.5.2. Residuals

In this section the iterative error of the solution is checked. This is done by checking the convergence of the L_2 and L_∞ norms of the residuals. For the very coarse grid, the residuals are shown in figure 7.8.

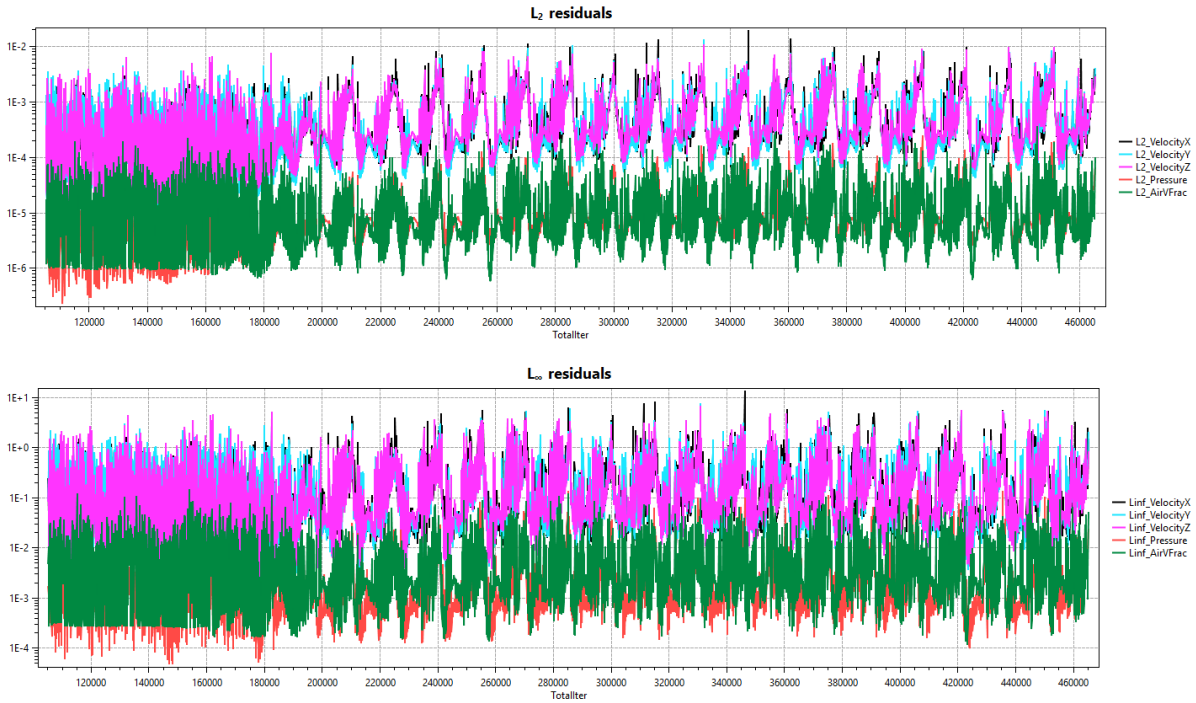

Figure 7.8: Residuals of the 'vessel with two DoFs in regular head waves' simulation for the very coarse grid

As can be seen, the residuals converge to values of about 1E-4 and 1E+0 for the L_2 and L_∞ norm respectively. This was also the case for the coarse, medium and fine grid. The order of the L_2 norm is considered acceptable as it is at least two orders of magnitude lower than the discretisation error. The order of the L_∞ norm however, is considered on the high side. This can indicate that there is a hard to converge area present. Further research confirmed that this is indeed the case.

In figure 7.9 the residuals larger than 1E-2 are visualised for velocity in longitudal direction parameter. This parameter was subjected to the largest residuals present in the simulation.

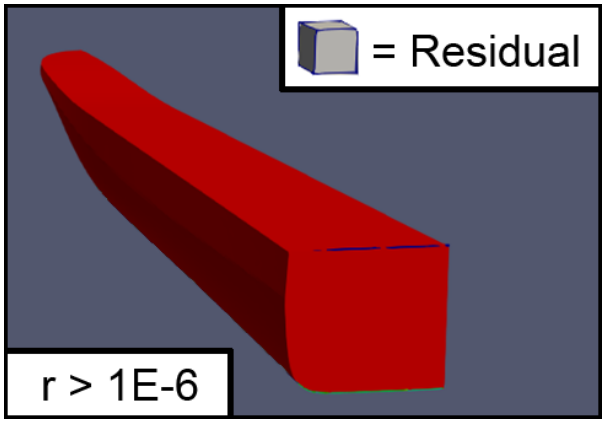

Figure 7.9: Visualisation of residuals larger than 1E-2 for the velocity in longitudal direction parameter

From figure 7.9 it is clear that these large residuals appear only at the top edge of the stern where the airflow separates from the hull. As only air is flowing here, the influence on the wave added resistance is considered small. Therefore these larger residuals are considered acceptable.

7.5.3. Convergence of the forces and moment

At each time step ReFRESCO runs a number of outer loops in which it iteratively converges the solution, after which it continues to the next time step. It is possible that the specified number of iterations is not large enough for the solution to converge well at each time step. This is checked by looking at the unsteady forces and moments. The unsteady forces and moments not only show their respective value at each time step but also at each outer loop. See figure 7.10 and 7.11 for plots of the unsteady total resistance in regular head waves for the coarse grid.

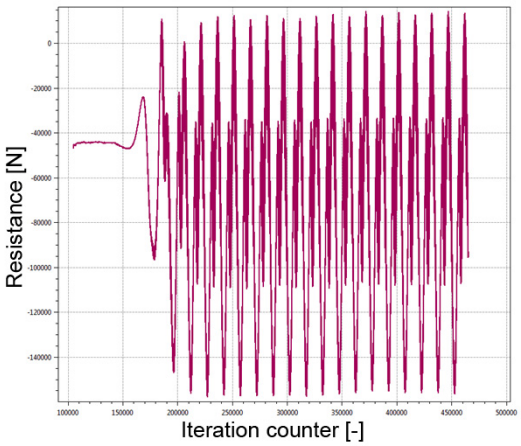

Figure 7.10: Unsteady total resistance in waves - coarse grid

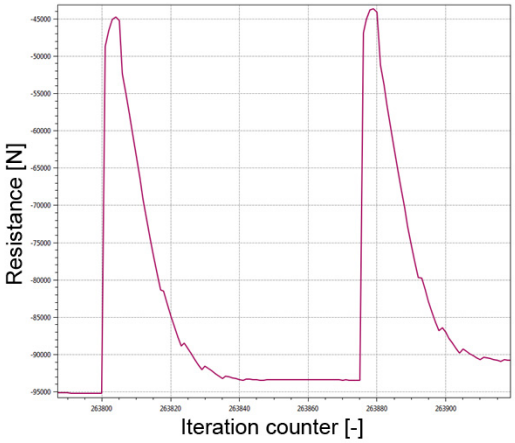

Figure 7.11: Zoomed in total resistance in waves - coarse grid

From the zoomed in plot in 7.11 it can be seen that the total wave resistance spikes up at the beginning of a new time step. It then converges for 75 outer loops until it reaches its final value after which a new time step is started. In this case the force is converged well after about 50 iterations which confirms that the force is converged well within a time step. However, this only proves the convergence for this one time step. Rather than checking the convergence by hand, a more convenient method is used. This method is based on the relative change of the force between the outer loops. The relative change for a parameter x is calculated according to equation 7.1.

$$Relative\ change(x_i, x_{i-1}) = \frac{\Delta x}{x_i} = \frac{x_i - x_{i-1}}{x_i} \tag{7.1}$$

With i the iteration. Within each time step the relative change between two outer loops will be relatively large at the first few iterations and become smaller as more iterations pass. By plotting the relative change of the unsteady resistance, it is possible to quickly see up the order of magnitude of the convergence. A plot of this relative change for the total wave resistance for the coarse grid can be seen in figure 7.12 and 7.13.

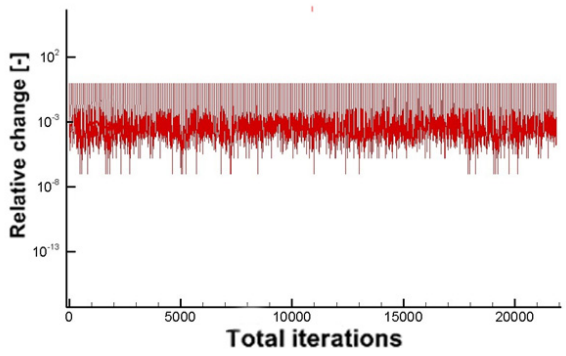

Figure 7.12: Relative change of the total wave resistance - coarse grid

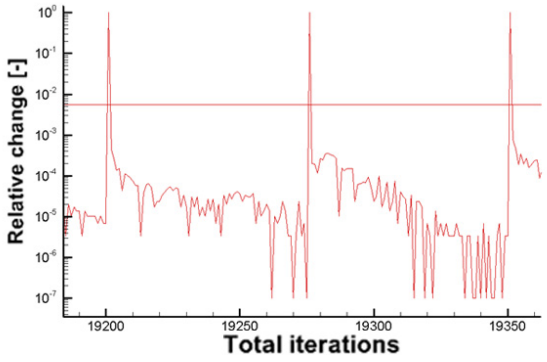

Figure 7.13: Zoomed in relative change of the total wave resistance - coarse grid

From the zoomed in plot in figure 7.13 it can be seen that the relative change starts with a value of about one and quickly decreases down to an order of magnitude of between 10^{-3} and 10^{-5}. This means that the resistance is only changing about 0.1 % - 0.001% in between the last steps in the outer loops. This indicates that the solution has converged well.

The same check was performed for the resistance, vertical force and pitch moment for all grids. The results can be seen in table 7.5.

	Order of magnitude of the relative change [-]		
	Resistance (Force in x-direction)	Force in z-direction	Pitch moment
Very coarse grid	10^{-3}	10^{-5}	10^{-2}
Coarse grid	10^{-3}	10^{-5}	10^{-2}
Medium grid	10^{-3}	10^{-5}	10^{-2}
Fine grid	10^{-3}	10^{-5}	10^{-2}

Table 7.5: Order of magnitude of the relative change of the resistance, force in z-direction and pitch moment for all four grids

The pitch moment needed the most steps to converge which resulted in an order of magnitude of its relative change of about 10^{-2}. Furthermore, all grid refinement levels have shown a similar order of magnitude of the relative change for the forces and moments. All checks confirmed that the solution was converged enough in between time steps.

7.5.4. Verification of the solution

The discretisation uncertainty of the resistance estimates is determined with a grid refinement study as proposed by Eça and Hoekstra. This is done for both the averaged total resistance in regular head waves and the averaged calm water resistance. As the added resistance in regular head waves is determined from these two resistances it is subjected to the discretisation uncertainties of both their resistances. Therefore the discretisation uncertainty of the added resistance itself is not calculated.

The determined calm water and total resistances for all four grids are shown in table 7.6.

Grid	Averaged calm water resistance [kN]	Averaged total resistance in waves [kN]
Very coarse	112.3	188.1
Coarse	89.2	178.0
Medium	79.8	177.2
Fine	76.2	176.9

Table 7.6: Calm water and total resistances for each of the four refined grids

For each of these resistances their corresponding uncertainties was calculated. The results of these calculations are plotted on uncertainty graphs which are analysed. These graphs plot the relative step size of the grid refinement on the horizontal axis and the resistance on the vertical axis. The calculated resistance estimates for the four grids are shown as data points on the plot. A power function is fitted through them, which is displayed as the line connecting the data points. The point where the line crosses the vertical axis indicates the estimated resistance for an infinitely refined grid. Finally, for each of the data points on the grid, their corresponding diffraction uncertainty is indicated with the vertical bar. This bar indicates the resistance range that falls within the uncertainty of the resistance.

For the calm water resistance, the uncertainty graph is shown in figure 7.14. From this graph it can be seen that the discretisation uncertainty is relatively high, with a minimum uncertainty of 15.1 % for the finest grid. This is also indicated in the top right corner. The computed resistances do appear to converge towards one value with increased grid refinement.

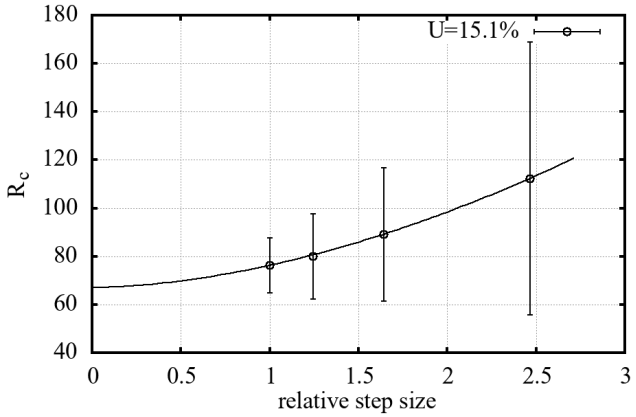

Figure 7.14: Uncertainty graph of the calm water resistance for four systematically refined, geometrically similar grids

For the total resistance in regular head waves, the uncertainty graph is shown in figure 7.15. In this figure it can be seen that the discretisation uncertainty is relatively low with an uncertainty of 4.4% for the fine grid. However, the data point from the very coarse grid, which is the one on the right, doesn't appear to follow the trend of the other three points. This can cause an overestimation of the uncertainty.

A recalculation of the uncertainty without this very coarse grid data point has proven that that was indeed the case. In figure 7.16 the recalculated uncertainty plot is shown. The recalculation of the discretisation uncertainty resulted in a very low value of 0.5 % for the fine grid.

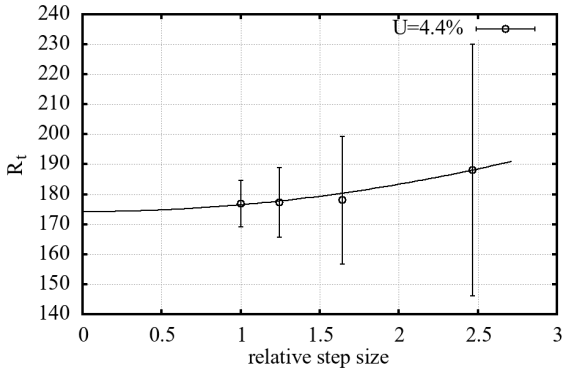

Figure 7.15: Uncertainty graph of the total resistance for four systematically refined, geometrically similar grids

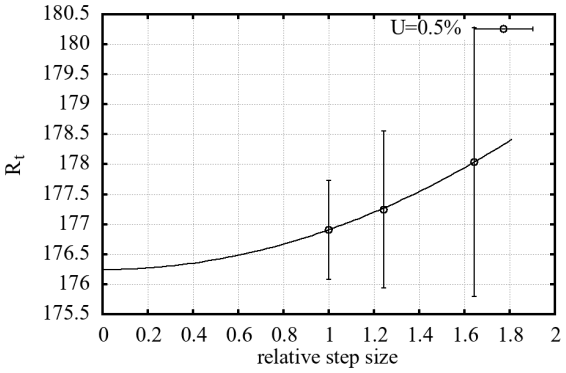

Figure 7.16: Uncertainty graph of the total resistance for the coarse, medium and fine grids

In table 7.7 the discretisation uncertainties for both the calm water and the total resistance in regular head waves are shown for all three grid refinements.

Grid	Discretisation uncertainty [%]	
	Calm water resistance	Total resistance in waves
Fine	15.1	0.5
Medium	23.2	0.7
Coarse	36.2	1.3
Very coarse	74.1	23.7

Table 7.7: Discretisation uncertainty for the calm water and total resistance estimates of the four grids

7.5.5. Calm water discretisation uncertainty

From the grid refinement study it is seen that the time-averaged total resistance in regular head waves has converged very well. This is expected as the results from the radiation and diffraction simulations have shown similar results. This results in a very low discretisation uncertainty for the time-averaged total resistance in regular head waves of 0.5 % for the fine grid.

The time-averaged calm water resistance however, is not sufficiently converged, which results in a large discretisation uncertainty. As the time-averaged resistance estimate is a derived property of the calm water resistance, it is also subjected to this large discretisation uncertainty. Therefore it is considered usefull to research this effect.

Further research has shown that this effect can be explained by the relative size of the motions and waves. In a calm water simulation the motions of the vessel and the height of the waves generated by the vessel are much smaller than those present in the diffraction and radiation simulations. In order to capture such small motions and waves a much finer grid is required. This is confirmed by performing a comparison of the grids used in this research to a typical grid used for a calm water simulation according to the specifications in use at DSNS.

According to experienced DSNS CFD user A.Mikelic, a calm water grid would typically require a much higher grid refinement of 80 cells per wavelength compared to the 48 used in this research. Furthermore, she also stated that the grid refinement area in a calm water resistance simulation would typically be significantly larger compared to the refinement areas used in the regular wave simulations.

7.6. Comparison: FDS towing tank data

For the validation of the result, the results from the CFD simulations are compared to the results from the CRS model tank experiments. Both the motions as well as the forces are compared.

7.6.1. Motions

The motions of the vessel in the ReFRESCO simulations are first compared to those from the model test. Amplitude as well as phasing relative to the wave elevation at the CoG are checked. First, a analysis was performed on the time-traces of the heave and pitch motion as well as on the wave elevation to determine their peak frequency. A plot of this analysis for the medium grid can be seen in figure 7.17. As was expected, all signals had a frequency that matched the encounter frequency of 1.505 [rad/s].

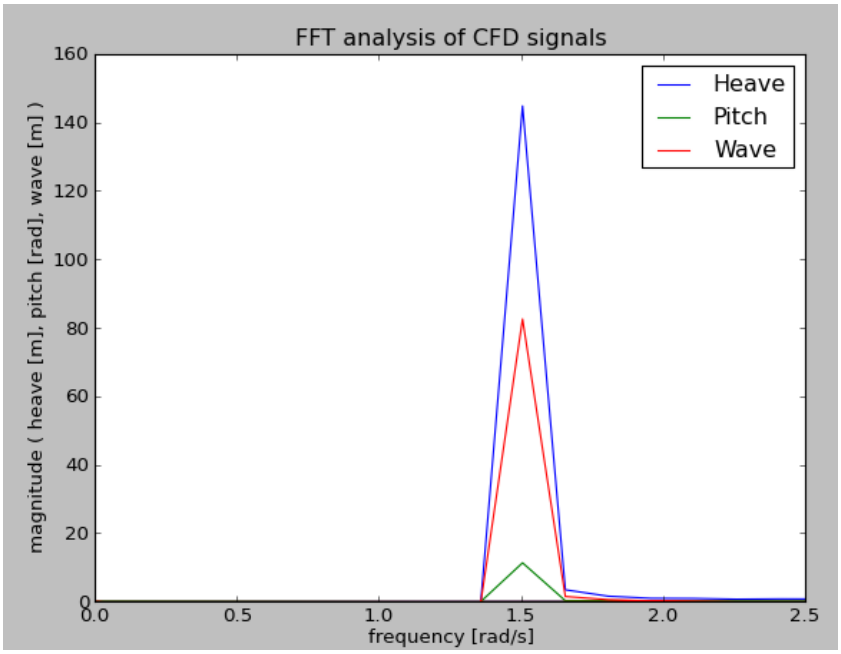

Figure 7.17: FFT plot of the vessel's motions and the wave elevation - medium grid

Next, the phase and amplitude of the motions measured in the FDS towing tank experiments are used to create time traces. These traces are overlaid with the corresponding time traces from the CFD simulations to visually compare them. See figure 7.18 and 7.19. From the zoomed in plot it is clear that the phasing of the CFD signals is very similar to that of the towing tank. What can also be seen is that the amplitude of the signals is slightly overestimated.

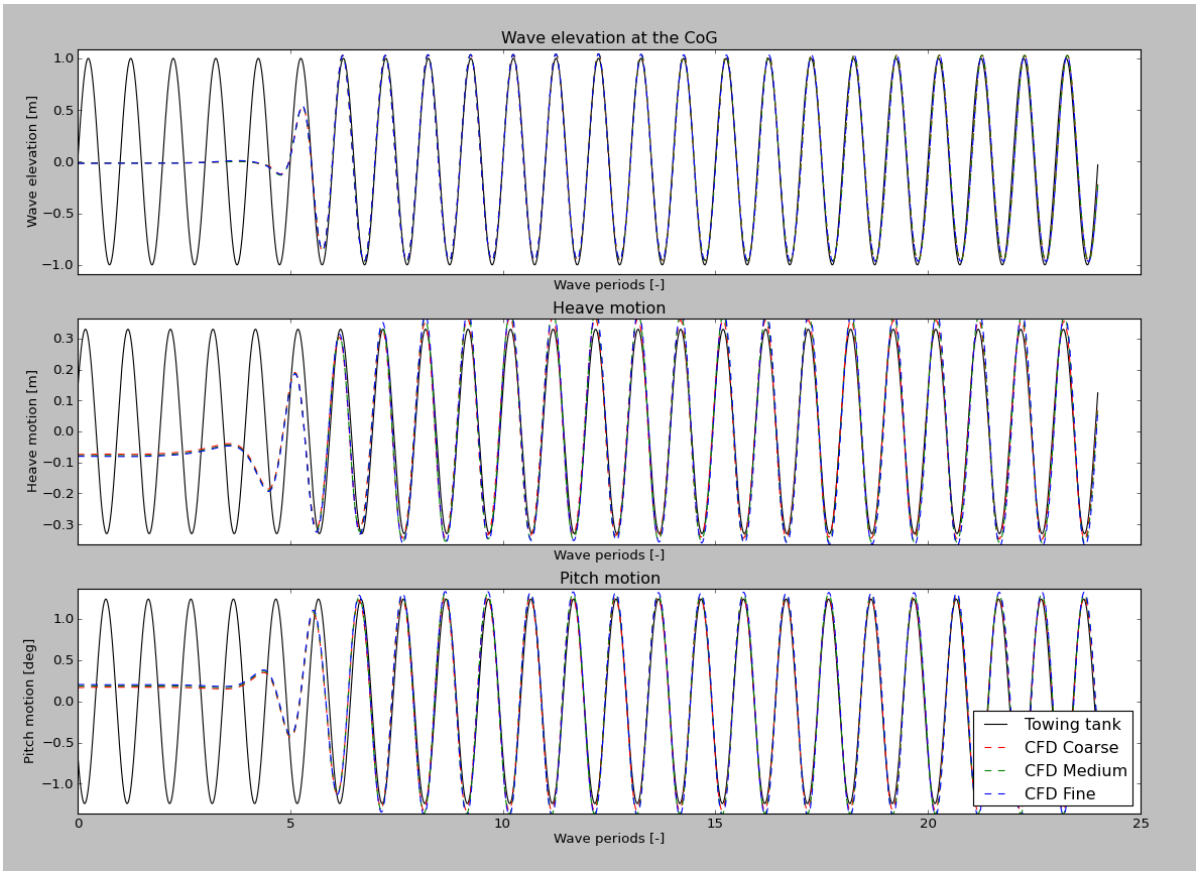

Figure 7.18: Comparison of the motions from the CRS model test to the CFD simulation

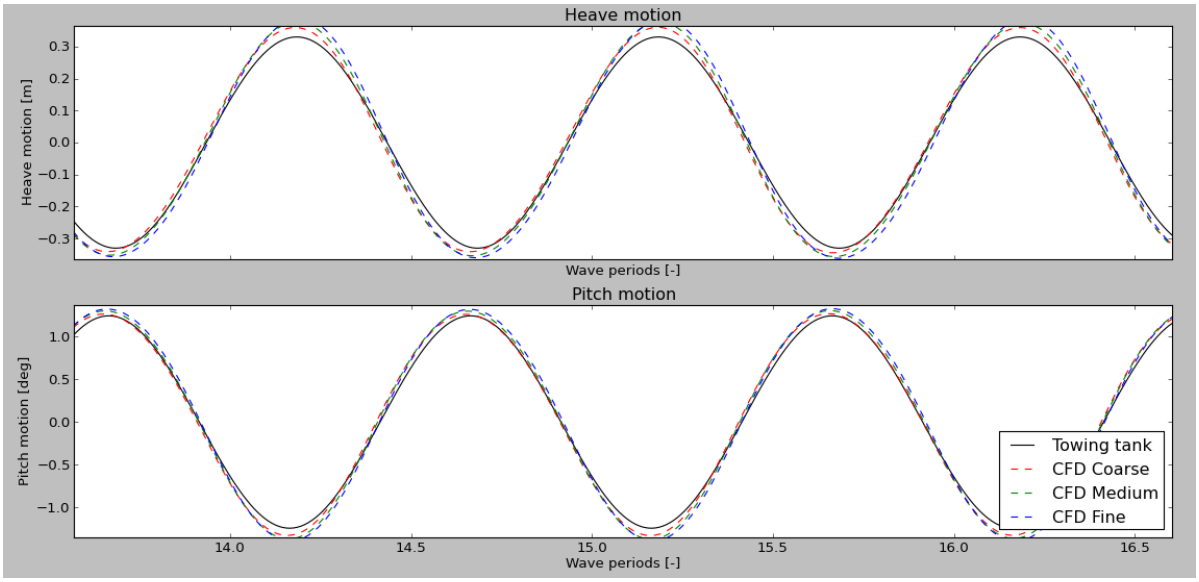

Figure 7.19: Zoomed in comparison of the motions from the CRS model test to the CFD simulation

Finally, the vessel's motions over the last ten wave encounters were analysed for their amplitude and phase and compared to the results from the towing tank. The result is shown in table 7.8.

Test	Heave				Pitch			
	Amp. [m]	Difference [m]	Phase [deg]	Difference [deg]	Amp. [deg]	Difference [deg]	Phase [deg]	Difference [deg]
Model test	0.33	-	42.0	-	1.24	-	229	-
Very coarse	0.35	0.02	42.1	0.10	1.29	0.05	234	5.00
Coarse	0.35	0.02	43.8	1.80	1.29	0.05	233	4.00
Medium	0.36	0.03	42.0	0.00	1.33	0.09	232	3.00
Fine	0.37	0.04	38.4	3.60	1.35	0.11	230	1.00

Table 7.8: Comparison of the vessel's motions calculated with CFD to the CRS model test results

Both the amplitude and phase match the results from the towing tank very well. The amplitudes are slightly overestimated by about 0.03 [m] for the heave and 0.09 [deg] for the pitch. The phase of both motions matches the phase from the model test very well as the difference ranged between 1 and 5 [deg].

7.6.2. Forces

In this section the time-averaged added resistance estimate determined using CFD is compared to the time-averaged added resistance estimate from the FDS model tests. First, the time-averaged wave added resistance is calculated for all the grids by subtracting the time-averaged calm water resistance from the time-averaged total resistance. The result is shown in table 7.9

Grid	Time-averaged calm water resistance [kN]	Time-averaged total resistance in waves [kN]	Time-averaged wave added resistance [kN]
Very Coarse	122.3	188.0	75.8
Coarse	89.2	178.0	88.8
Medium	79.8	177.2	97.4
Fine	76.2	176.9	100.7

Table 7.9: Calculation of the wave added resistance for the four simulated grids

It is possible that the actual wave amplitude at the vessel's CoG was not the same over all simulations. This variation in the wave amplitude would affect the resistance felt by the vessel. In order to compensate for any variations in the wave amplitude, the time-averaged wave added resistance is first converted to a QTF. The comparison is then made between the QTFs of the CRS model test and the CFD simulations.

The QTF is calculated by dividing the wave added resistance by the square root of the actual wave amplitude that was present at the vessel's CoG during the model test or CFD simulation respectively. The calculation of the QTFs and their comparison are shown in table

Grid	Time averaged Wave added resistance [kN]	Wave amplitude at CoG [m]	QTF [kN/m^2]	Error [%]
Towing tank	105.0	1.011	102.7	-
Very Coarse	75.8	0.997	76.3	25.7
Coarse	88.8	0.997	89.3	13.0
Medium	97.4	0.997	98.0	4.6
Fine	100.7	0.997	101.3	1.4

Table 7.10: Calculation and comparison of the QTF of the time-averaged wave added resistance

These results show that the wave added resistance converges well for increased grid refinement. This comparsion study proves that it is possible to estimate the QTF of the time-averaged wave added resistance with an error of 1.4 % compared to the model test result.

It must be noted that not only CFD simulations are subjected to uncertainties in their solutions. Model test experiments are also subjected to uncertainties in the solution. According to G.K.Kapsenberg [18]

the calm water and total resistance in regular head waves estimates measured in the towing tank are subjected to an uncertainty of about 2%.

The added resistance is determined by subtracting the measured calm water resistance from the total resistance in regular head waves and is therefore also subjected to these uncertainties. Due to the fact that the added resistance is a relatively small part of the total resistance, the relatively large uncertainties are magnified in the added resistance. It can be said that the smaller the added resistance is in relation to the total resistance in regular head waves, the larger the uncertainty margin becomes in the the added resistance. Table 7.11 gives three examples that show this effect.

Wave added resistance / Total resistance in waves [%]	Uncertainty in towing tank Wave added resistance estimate [%]
10	20
20	10
40	2.5

Table 7.11: Uncertainty in the wave added resistance estimate as a function of the relative size of the wave added resistance

In the case of the FDS, which is sailing at 17.3 [kts], the added resistance accounts for about 30% of the total resistance in regular head waves. This would result in an uncertainty of 7%. This would put the results achieved with the fine grid well within the uncertainty range of the model tests.

7.6.3. Conclusions

Simulations of the FDS with 2 DoFs in head waves have been performed using 3 similar grids with increased refinement. Verification was performed using a grid refinement study as specified by Eça and Hoekstra, after which the results were compared with results from model tests performed at MARIN in 2015. From this research, the following conclusions can be drawn.

- For the proposed procedure, verification has proven that the time-averaged total resistance in regular head waves is relatively insensitive to grid refinement. This insensitivity has resulted in very low discretisation uncertainties in the range of 0.5 to 1.3 % on relatively coarse grids. This is very beneficial as it means that it is possible to determine the time-averaged total resistance in regular head waves accurately using a grid with a relatively low number of cells.
- Furthermore, the comparison with the model data has shown that it is possible to estimate the QTF of the time-averaged wave added resistance with an error of 1.4% which is smaller than the estimated 7% uncertainty margin of the model test result.
- The time-averaged calm water resistance however, didn't converge to an acceptable level on the tested grids. This resulted in minimum discretisation uncertainty of 15.1%. The estimate of the time-averaged wave added resistance is dependent on the estimate of the calm water resistance. As a result, the estimate of the QTF of the time-averaged wave added resistance is also subjected to this large discretisation uncertainty.

Therefore it must be concluded that the proposed method for the estimation of the time-averaged wave added resistance using CFD is not yet applicable in its proposed form.

It must be noted that it is possible to estimate the time-averaged total resistance in regular head waves accurately and efficiently on a relatively coarse grid using this method. However, due to the large uncertainty present in the calm water resistance, a large uncertainty is present in the prediction of the time-averaged added resistance in regular head waves.

Further research on the proposed method is required to improve the large uncertainty present in the calm water resistance estimate. As CFD is already used in the maritime industry to estimate a vessel's calm water resistance accurately, it is known that this can be done.

8

Conclusions

With the increase in available computational power in the recent years it has become possible to estimate a vessels added resistance in regular head waves using CFD. CFD promises cheaper and faster predictions than model testing but the result comes without the comforting 'truth' of the towing tank. In this study the applicability of CFD for the estimation of the time-averaged added resistance in regular head waves is researched by assessing the error and uncertainty of the solution.

In this research, simulations were performed with the FDS sailing at 17.31 [Kts] in regular head waves with a frequency of 0.85[rad/s] and a height of 1.0 [m] for the diffraction simulation and 2.0 [m] for the 2 DoF simulation. From this research, the following conclusions can be drawn:

For the 2D-wave simulations:

- The proposed procedure is capable of simulating accurately propagating incoming regular waves with a low wave dissipation between 0 and 0.18% and a low dispersion between 0.19 and 1.5 % for wave lengths ranging between 0.5 and 2.0 Lpp. These low values ensure that the propagating waves have a consistent wave length and height over the entire domain.
- The relaxation zone implemented in the proposed procedure is considered very effective as it is capable of keeping reflections at the domain boundaries below 1 %

For the diffracted wave simulations:

- The amplitude of vessel's responses to the incoming waves vary less than 0.4 kN and 70 kNm for the vertical force and pitch moment respectively over all four grid refinements. This is less than 0.4 and 0.2 % of the total amplitude respectively.
- The phase shift of the vessel's responses in relation to the phase of the incoming wave varied no more than 3 degrees over all the grid refinements for both the vertical force as well as the pitch moment.
- From the relatively similar results for both the response amplitude as well as the phase of the vessels responses over the four grid refinements that were tested, it is seen that the vessel's responses appear insensitive to the grid refinement implemented to capture the diffracting waves.
- A comparison with potential flow solver PRECAL indicates that both the amplitude and phase of the vessel's responses, as determined using CFD, have the right order of magnitude.
- The grid refinements implemented to capture the propagating diffracted waves appear to have a negligible effect on the accuracy of the vessel's responses. Therefore the lowest grid refinement of 12 cells per diffracted wavelength C_{λ_d} is selected as the optimum for the set of diffracting wave refinement boxes.
- Compared to the most refined grid this simulation costs about 5 times less and delivers a similar resistance estimate. This estimation is based on the number of cells in each respective grid.

For the radiated wave simulations:

- The increase in grid refinement appears to have an influence on the wave elevation surrounding the vessel. With increased refinement, the peaks and troughs of the waves appear to become larger and the wave pattern becomes more detailed
- For the forced heave simulations the amplitude of the vertical force and pitch moment varied no more than 20 kN and 113 kNm respectively, which is less than 0.5 % of the amplitude.
- For the forced pitch simulations the amplitude of the vertical force and pitch moment varied no more than 28 kN and 751 kNm respectively, which is also less than 0.5 % of the wave amplitude.
- These variances in the amplitude of the vertical force and pitch moment when comparing the results for the four grid refinement levels, indicate that the vessel's responses to the induced heave and pitch motion appear to be insensitive to the increased grid refinement introduced by the radiation refinement boxes.
- The vessel's added mass and damping that were estimated from the CFD simulations, appear to be insensitive to increased grid refinements as the added mass a_{zz} and added damping b_{zz} varied no more than 30 tonne and 20 tonne/s respectively for the forced heave test. This is less than 1 % of the total added mass and damping.
- For the forced pitch tests, the vessel's estimated added mass and damping also appear to be insensitive to increased grid refinements as the added mass $a_{\Theta\Theta}$ and added damping $b_{\Theta\Theta}$ varied no more than 20 tonne and 20 tonne/s respectively for the forced heave test. This is less than 1 % of the total added mass and damping.
- From the comparison between CFD and PRECAL of the vessel's added mass and damping it is seen that the error is smaller than 0.7 % of the total added mass and damping for all grid refinements.
- As the increased grid refinements implemented to capture the radiating waves accurately, appear to have a negligible effect on the vessels responses to the motions, as well as the accuracy of the vessel's added mass and damping coefficients, the very coarse grid, with the lowest grid refinement is selected as the optimum for the set of radiating wave refinement boxes.
- Compared to the most refined grid in this simulation, this simulation costs about 2.7 times less and delivers similar vessel responses to the motions. This estimate is based on the number of cells in the respective grids.

For the vessel with two DoFs in regular head waves simulations:

- For the proposed procedure, verification has proven that the time-averaged total resistance in regular head waves is relatively insensitive to grid refinement. This insensitivity has resulted in very low discretisation uncertainties in the range of 0.5 to 1.3 % on relatively coarse grids. This is very beneficial as it means that it is possible to determine the time-averaged total resistance in regular head waves accurately using a grid with a relatively low number of cells.
- Furthermore, the comparison with the model data has shown that it is possible to estimate the QTF of the time-averaged wave added resistance with an error of 1.4% which is smaller than the estimated 7% uncertainty margin of the model test result.
- The time-averaged calm water resistance however, didn't converge to an acceptable level on the tested grids. This resulted in minimum discretisation uncertainty of 15.1%. The estimate of the time-averaged wave added resistance is dependent on the estimate of the calm water resistance. As a result, the estimate of the QTF of the time-averaged wave added resistance is also subjected to this large discretisation uncertainty.

Therefore it must be concluded that the proposed method for the estimation of the time-averaged wave added resistance using CFD is not yet applicable in its proposed form.

It must be noted that it is possible to estimate the time-averaged total resistance in regular head waves accurately and efficiently on a relatively coarse grid using this method. However, due to the large

uncertainty present in the calm water resistance, a large uncertainty is present in the prediction of the time-averaged added resistance in regular head waves.

Further research on the proposed method is required to improve the large uncertainty present in the calm water resistance estimate. As CFD is already used in the maritime industry to estimate a vessel's calm water resistance accurately, it is known that this can be done.

9

Recommendations

In this chapter recommendations for further research are given.

1. A large part of the calm water resistance originates from the viscous friction. This friction could be captured by adding a boundary layer and non-slip walls to the hull. An interesting research topic would be to investigate if capturing this large extra factor would result in the convergence of the calm water resistance.
2. From practice it is known that a more refined grid is required to simulate the calm water resistance compared to the resistance in regular head waves. A further research topic would be to investigate whether combining the current grid with a grid suitable for calm water resistance simulations would result in the convergence for both the calm water as well as the total wave resistance.
3. In practice only 20% of the total simulation time in this study is used to simulate the vessel in calm water. Therefore the current approach of using the same, highly refined grid for both the calm water as well as the wave simulation may not the most economical solution. An interesting research topic would be to research the validity, accuracy and efficiency of the use of a second grid for the calm water simulation.
4. The grid used in the 2D-wave simulations was designed for a range of wave frequencies. A recommendation would be to extent this approach to the grid for the simulation of the vessel with 2DoFs in waves.
5. Another interesting research topic would be to optimise the domain dimensions further to improve the efficiency and accuracy of the simulation.

Bibliography

[1] Ittc - recommended procedures and guidelines 7.5-02-07-02.8 calculation of the weather factor f_w for decrease of ship speed in waves. 2017.

[2] Ittc - prediction of power increase in irregular waves from model test. 2017.

[3] Refresco theory manual. 2017.

[4] Refresco theory manual v2.4.0. page 14, 10 2017.

[5] CRS ships home, 2018. URL `www.crships.org`.

[6] Seoul national university towing tank (snutt), 2018. URL `snutt.snu.ac.kr`.

[7] Jan Jacobus Blok. The resiantce increase of a ship in waves. 1993.

[8] J. Bougis. Asymptotic study of the wave field generated by a steadily moving pulsating source.

[9] John Chawner. Quality and Control, two reasons why structured grids aren't going away, 2013. URL `www.pointwise.com`.

[10] R. Courant, K. Friedrichs, and H. Lewy. Über die partiellen Differenzengleichungen der mathematischen Physik. *Mathematische Annalen*, 100:32–74, 1928. doi: 10.1007/BF01448839.

[11] Ir. R.P. Dallinga. Crs raw+ naval hull experiments - test results. page 5, 2015.

[12] Vincent Denisart. Generation and absorption of numerical waves with refresco. 02 2018.

[13] K.A.McTaggart D.L.Chow. Validation of shipmo7 and precal with a warship model. 1996.

[14] Karthik Duraisamy, James Baeder, and Jian-guo Liu. Concepts and application of time-limiters to high resolution schemes. 19:139–162, 12 2003.

[15] L. Eça, G. Vaz, and M.Hoekstra. A contribution for the assesment of discretization error estimators based on grid refinement studies. *Journal of verification, validation and Uncertainty Quantification*, 3, 2018.

[16] H. Bandringa et al. Validation of cfd for run-up and wave impact on a semi submersible. 2016.

[17] Joel H. Ferziger and Milovan Perić. *Computational Methods for Fluid Dynamics*. Springer, 2002. ISBN 9783540420743.

[18] G.K.Kapsenberg. The marin systematic series fast displacement hulls. *22nd Int. HISWA Symposium on Yacht Design and Yacht Construction, Amsterdam*, 2012.

[19] M. Hoekstra G.Vaz, F. Jaouen. Free surface viscous flow computations, validation of urans code fresco.

[20] J.H.Ferziger and M.Perić. *Computational methods for fluid dynamics*. 2002.

[21] J.M.J. Journée and W.W. Massie. *Offshore Hydromechanics*. TU Delft, 2008.

[22] J.W.Slater. Uncertainty and error in cfd simulations, 2008. URL `https://www.grc.nasa.gov/WWW/wind/valid/tutorials/errors.html`.

[23] Christiaan Klaij, Guilherme Vaz, and Martin Hoekstra. Design, analysis and verification of a volume-of-fluid model with interface-capturing scheme. 170, 07 2018.

[24] Dimitri Kuzmin. Introduction to CFD, 2010. URL www.methematik.uni-dortmund.de/~kuzmin/cfdintro/cfd.html.

[25] L.Eça and M.Hoekstra. A procedure for the estimation of the numerical uncertainty of cfd calculations based on grid refinement studies. *Journal of computational physics*, 262:104–130, 2014. URL www.elsevier.com/locate/jcp.

[26] F. Moukalled, L. Mangani, and M. Darwish. *The Finite Volume Method in Computational Fluid Dynamics: An Advanced Introduction with OpenFOAM and Matlab*. Springer Publishing Company, Incorporated, 1st edition, 2015. ISBN 3319168738, 9783319168739.

[27] P.Crepier. Ship resistance prediction: Verification and validation exercise on unstructured grids. *VII International Conference on Computational Methods in Marine Engineering*, 2017.

[28] Stephane Rapuc, Pierre Crepier, Frédérick Jaouen, Tim Bunnik, and Pauline Regnier. Towards guidelines for consistent wave propagation in cfd simulations. 2018.

[29] S.Rapuc. Ships seakeeping - cfd guidelines for near ship refinement. 2018.

[30] J. Strom-Tejsen, H.Y.H. Yeh, D.D. Moran, Society of Naval Architects, and Marine Engineers (U.S.). Meeting. *Added Resistance in Waves*. Paper (Society of Naval Architects and Marine Engineers). Society of Naval Architects and Marine Engineers, 1973. URL https://books.google.nl/books?id=5GNouAAACAAJ.

[31] H. K. Versteeg and Malalasekera W. *An introduction to computational fluid dynamics*. 1995. ISBN 0-470-23515-2.

[32] G. Vossers W.A. Swaan. The effect of forebody section shape on ship behaviour in waves, 1961.

[33] Jiao Xiangmin and Heath Michael T. Common-refinement-based data transfer between non-matching meshes in multiphysics simulations. *International Journal for Numerical Methods in Engineering*, 61(14):2402–2427. doi: 10.1002/nme.1147. URL https://onlinelibrary.wiley.com/doi/abs/10.1002/nme.1147.

A

HEXPRESS input

In this section the HEXPRESS input for the generation of the grid for the vessel with 2DoF in regualr head waves is given.

```
import os
import numpy as np
import shutil
import sys
import ConfigParser
import math

#script by S.A.Hulsbergen on 22/10/2018
#This script is used to set up a 3D domain for the simulation of the FDS with 2 DoF (Heave &
                                                    Pitch) in regular head waves
#The grid contains refinement specified to capture:

# -Incoming waves,                  Which propagate with constant amplitude and length
                                                    throughout the domain
# -Diffracting waves,                 Waves that diffract off of the hull
# -Radiating waves,                   Waves generated by the vessel due to its motions
# -MARIN recommended grid refinement,         In place to capture the interaction between the
                                                     vessel and the hull


def safe_run_function(func,iggFileName):                #Check if Hexpress is connected to
                                                    the license server
    '''
    The funciton runs func and check in the that in the last 10lines of the log file that
                                                          there are no
    "WARNING:Connection to license server lost or license check failed"

    This prevents Hexpress to stop in the middle of the mesh process due to missing license.

    func should a be  function
    iggFileName is the fileName used to open the log file and check if the calcualtions
                                                          worked
    '''
    _logPath = os.path.splitext(iggFileName)[0]+".log"
    print(_logPath)
    while True:
        func() # run function

        try:
            with open(_logPath) as fLog:
                _endLog  = " ".join(fLog.readlines()[-10:])

                if "WARNING:Connection to license server lost or license check failed" in
                                                                    _endLog:
                    print "Waiting for license - try again in 30s"
                    time.sleep(30)
```

```
                else:
                    return
        except:
            return

def addBox(xMin, xMax, boxWidth, zMin, zMax, enable, volumic, sx, sy, sz, refinement, shearX=
                                                0, transX=0, shearY=0, transY=0, waterDepth =
                                                -10000.0):       #Create a refinement box in
                                                Hexpress
    i = HXP.get_number_of_refinement_boxes()
    if zMin < -waterDepth:
        zMin = -waterDepth
    HXP.create_refinement_cube(xMin, -0.5*boxWidth, zMin,
                               xMax, 0.5*boxWidth, zMax)
    HXP.refinement_box(i).set_adaptation_flags(enable, volumic)
    HXP.refinement_box(i).set_target_size(sx, sy, sz)
    if not isinstance(refinement, int):
        raise Exception("Refinement should be interger! : %0.2f"%refinement)
    HXP.refinement_box(i).set_refinement_level(refinement)
    HXP.refinement_box(i).set_transformation([[1.0, shearX, 0.0, transX], [shearY, 1.0, 0.0,
                                                transY], [0.0, 0.0, 1.0, 0.0]])

#Input parameters
Wavefreq = 0.85        #[rad/s]    wave frequency
Waveamplitude = 1      #[m]      wave amplitude
Velocitykts = 17.30      #[kts]      velocity of the vessel
Cells_top = 48         #[]       number of cells \ wavelenght in top wave ref. box
Cells_free = 5         #[]       number of cells \ waveamplitude in the free surface box
Cells_dif_top = 12       #[]       number of cells \ encountered wavelength in the top
                                                diffraction box
Cells_rad_top = 12
Lpp = 100          #[m]      Length of vessel between perpendiculars
Breadth = 12.5         #[m]      Breadth of vessel
Draught = 3.125        #[m]      Draught of vessel
Cell_init = Lpp/ float(6) #[m]      Initial cell size
Domain_x = 6*Lpp       #[m]      Domain dimension in x
Domain_y = 2*Lpp       #[m]      Domain dimension in x
Domain_z = 4*Lpp       #[m]      Domain dimension in x
theta_steps = 3600          #[-]            Number of radiated wave directions calculated
g = 9.81
baseFilePath = "/data/home/DSNS/SimulationBasH/2DoF/Grid_coarse" # Save location

#Calculate required parameters
Velocityms = Velocitykts * 0.5144                          #[m/s] velocity of vessel in m/s
Encounterfreq = Wavefreq + ((Wavefreq * Wavefreq) / 9.81) * Velocityms        #[rad/s]
                                                encounter frequency (deep water assumption)
lambdaw = (9.81 * 2 * math.pi) / (Wavefreq * Wavefreq)                #[m] wavelength
lambdae = (9.81 * 2 * math.pi) / (Encounterfreq * Encounterfreq)          #[m] encounter
                                                wavelength

###################################
#Set up boxes for the incoming wave##############
###################################

#Calculate the free surface refinement box
free_ref = math.ceil(math.log10(Waveamplitude/(Cell_init*Cells_free))/math.log10(0.5))    #[]
                                                 required refinement level for the diffraction
                                                 refinement box
free_x1 = Domain_x/2
free_y1 = 0
free_z1 = (1.1 * Waveamplitude) + Draught
free_x2 = -Domain_x/2
free_y2 = Domain_y
free_z2 = (-1.1 * Waveamplitude) + Draught

#Calculate the upper refinement box
Up_ref = math.ceil(math.log10(lambdaw/(Cell_init*Cells_top))/math.log10(0.5))   #[] required
                                                refinement level for the diffraction
                                                refinement box
Up_x1 = Domain_x/2
Up_y1 = 0
```

```
Up_z1 = (1.1 * Waveamplitude) + Draught
Up_x2 = -Domain_x/2
Up_y2 = Domain_y
Up_z2 = (-0.2 * lambdaw) + Draught

#Calculate the lower refinement box
Low_ref = math.ceil(math.log10(lambdaw/(Cell_init*(Cells_top/2)))/math.log10(0.5))     #[]
                                                    required refinement level for the diffraction
                                                    refinement box
Low_x1 = Domain_x/2
Low_y1 = 0
Low_z1 = (1.1 * Waveamplitude) + Draught
Low_x2 = -Domain_x/2
Low_y2 = Domain_y
Low_z2 = (-0.6 * lambdaw) + Draught

#####################################
#Set up boxes for the diffracting waves###############
#####################################

#Calculate the diffraction upper refinement box
Diff_Up_ref = math.ceil(math.log10(lambdae/(Cell_init*Cells_dif_top))/math.log10(0.5))     #[]
                                                     required refinement level for the diffraction
                                                     refinement box
Diff_Up_x1 = Lpp + 0.1*lambdae
Diff_Up_y1 = 0
Diff_Up_z1 = (1.1 * Waveamplitude) + Draught
Diff_Up_x2 = -0.5 * lambdae
Diff_Up_y2 = Breadth/2 + 0.5*lambdae
Diff_Up_z2 = (-0.2 * lambdae) + Draught

#Calculate the diffraction lower refinement box
Diff_Low_ref = math.ceil(math.log10(lambdae/(Cell_init*(Cells_dif_top/2)))/math.log10(0.5))
                                                      #[] required refinement level for the
                                                    diffraction refinement box
Diff_Low_x1 = Lpp + 0.1*lambdae
Diff_Low_y1 = 0
Diff_Low_z1 = (1.1 * Waveamplitude) + Draught
Diff_Low_x2 = -0.5 * lambdae
Diff_Low_y2 = Breadth/2 + 0.5*lambdae
Diff_Low_z2 = (-0.6 * lambdae) + Draught

################################
#Set up boxes fo the radiating waves##########
################################

#Calculate required parameters and vectors#####
################################

#Create vector with radiation angles
Theta = np.linspace(0,2*np.pi,theta_steps)           #set up linear spaced radiation angles

#Tau (Dimensionless parameter, ratio of vessel speed to wave propagation speed)
Tau = Velocityms * Encounterfreq / g

###Calculate wave celerity, Earth fixex, as a function of the propagation angle
Phi1 = (g / 2*Encounterfreq) * (1 + np.sqrt(1 - 4*Tau*np.cos(Theta)))

###Calcluate wave lenght from celerity
lambda1 = ((np.pi * g)/(Encounterfreq**2)) * (1 + np.sqrt(1 - 4*Tau*np.cos(Theta)))

###Calculate wave propagation angle in the ship reference frame
Phi1_SFx = Phi1 * 0.5 * np.cos(Theta) - Velocityms
Phi1_SFy = Phi1 * 0.5 * np.sin(Theta)
Theta_c1 = np.arctan2(Phi1_SFy, Phi1_SFx)

#Minimum radiated wave length
lambda_min = np.nanmin(lambda1)

#Corresponding minimum propagation angle
Theta_cmin = Theta_c1[np.nanargmin(lambda1)]
```

```
#Maximum radiated wave length
lambda_max = np.nanmax(lambda1)

#Maximum wavelength perpendicular to the vessel
lambda_ymax = np.nanmax(lambda1*np.sin(Theta_c1))

#Calculate the x_plus box dimension
if np.max(lambda1*np.cos(Theta_c1)) > 0.1*Lpp:
  X_plus = np.max(lambda1*np.cos(Theta_c1))
else:
  X_plus = 0.1*Lpp

#Set up required boxes ####################
###################################


#Ref.boxes for the shortest wave length:
X_short_min = lambda_min * np.cos(Theta_cmin)
X_short_max = Lpp + X_pluslong_ref_upper = math.ceil(math.log10(lambda_max/(Cell_init*
                                                Cells_rad_top))/math.log10(0.5))
Y_short_min = 0
Y_short_max = 0.5*Breadth + (lambda_min * np.sin(Theta_cmin))
Z_short_upper_min = -0.2*lambda_min + Draught
Z_short_lower_min = -0.6*lambda_min + Draught
Z_short_max = 1.1* Waveamplitude + Draught
short_ref_upper = math.ceil(math.log10(lambda_min/(Cell_init*Cells_rad_top))/math.log10(0.5))
short_ref_lower = short_ref_upper-1

#Ref.boxes for the longest wave length:
X_long_min = -lambda_max
X_long_max = Lpp + X_plus
Y_long_min = 0
Y_long_max = 0.5*Breadth + lambda_ymax
Z_long_upper_min = -0.2*lambda_max + Draught
Z_long_lower_min = -0.6*lambda_max + Draught
Z_long_max = 1.1* Waveamplitude + Draught

long_ref_lower = long_ref_upper-1

#Ref.box for extra refinement in z-direction with a boxheight as high as the amplitude of the
                                                 vessels motions and dimensions 1/3 of the
                                                largest
#X_extra_min = X_long_min * 0.33
#X_extra_max = (X_long_max - Lpp) * 0.33 + Lpp
#Y_extra_min = Y_long_min * 0.33
#Y_extra_max = (Y_long_max - 0.5*Breadth) * 0.33 + 0.5*Breadth
X_extra_min = X_long_min
X_extra_max = X_long_max
Y_extra_min = Y_long_min
Y_extra_max = Y_long_max
Max_amp_motion = (np.tan(Waveamplitude * ((2*np.pi)/lambdaw)) * (Lpp/2)) + Waveamplitude
                                                    #maximum vessel motion is basis for the
                                                height of this box. The pitch will be defining
                                                , maximum pitch angle can be calculated from
                                                the wave, for now -1 refinement is used to
                                                test if everything works
Z_extra_min = -Max_amp_motion + Draught                          #The max. slope angle is
                                                calculated from the incoming wave with
                                                slope_max = wave_amp * K.  This angle is used
                                                to calculate the maximum amplitude of the bow
                                                / stern moving up and down
Z_extra_max = Max_amp_motion + Draught

#Calculate ref.box for extra refinement in z-direction with a boxheight as high as 1/3
                                                amplitude of the vessels motions and
                                                dimensions of the largest box
X_extra2_min = X_long_min
X_extra2_max = X_long_max
Y_extra2_min = Y_long_min
Y_extra2_max = Y_long_max                                  #maximum vessel motion is basis for
```

```
                                                the height of this box. The pitch will be
                                               defining, maximum pitch angle can be
                                               calculated from the wave
Z_extra2_min = -Max_amp_motion * 1/3 + Draught                      #The max. slope angle is
                                               calculated from the incoming wave with
                                               slope_max = wave_amp * K.  This angle is used
                                               to calculate the maximum amplitude of the bow
                                               / stern moving up and down
Z_extra2_max = Max_amp_motion * 1/3 + Draught


################################################
#Mesh the grid##########################################
################################################

#Load geometry from Rhino
HXP.delete_stl_triangulation ()
HXP.delete_bodies(HXP.get_all_bodies())
HXP.close_project()
HXP.open_project("/home/bhulsbergen/3D_vessel_in_waves/ForBas/FDS.igg",1,0,"",0,0,0)
HXP.import_domain("/home/bhulsbergen/3D_vessel_in_waves/ForBas/FDS.dom")
#Initialize grid
HXP.set_active_domain("FDS")
HXP.set_mesh_generation_mode("3D")
HXP.set_global_number_of_refinements(12)
HXP.init_cartesian_mesh(27,9,18)
HXP.generate_initial_mesh()
HXP.set_advanced_global_parameters(2,0,1E+20,2,7)
HXP.delete_all_refinement_boxes()
#Standard MARIN refinement box
HXP.create_refinement_cube(-10.3914,-3.33572,-2.27986,114.305,10.0072,3.937)
HXP.refinement_box(0).set_adaptation_flags(1,1)
HXP.refinement_box(0).set_refinement_level(6)
#Incoming waves refinement boxes
HXP.create_refinement_cube(free_x1,free_y1,free_z1,free_x2,free_y2,free_z2)
HXP.refinement_box(1).set_adaptation_flags(1,1)
HXP.refinement_box(1).set_target_size(1000,1000,0)
HXP.refinement_box(1).set_refinement_level(int(free_ref))
HXP.create_refinement_cube(Up_x1,Up_y1,Up_z1,Up_x2,Up_y2,Up_z2)
HXP.refinement_box(2).set_adaptation_flags(1,1)
HXP.refinement_box(2).set_target_size(0,1000,0)
HXP.refinement_box(2).set_refinement_level(int(Up_ref))
HXP.create_refinement_cube(Low_x1,Low_y1,Low_z1,Low_x2,Low_y2,Low_z2)
HXP.refinement_box(3).set_adaptation_flags(1,1)
HXP.refinement_box(3).set_target_size(0,1000,0)
HXP.refinement_box(3).set_refinement_level(int(Low_ref))
#Diffracting waves refinement boxes
HXP.create_refinement_cube(Diff_Up_x1,Diff_Up_y1,Diff_Up_z1,Diff_Up_x2,Diff_Up_y2,Diff_Up_z2)
HXP.refinement_box(4).set_adaptation_flags(1,1)
HXP.refinement_box(4).set_target_size(0,0,0)
HXP.refinement_box(4).set_refinement_level(int(Diff_Up_ref))
HXP.create_refinement_cube(Diff_Low_x1,Diff_Low_y1,Diff_Low_z1,Diff_Low_x2,Diff_Low_y2,
                                               Diff_Low_z2)
HXP.refinement_box(5).set_adaptation_flags(1,1)
HXP.refinement_box(5).set_target_size(0,0,0)
HXP.refinement_box(5).set_refinement_level(int(Diff_Low_ref))
#Radiating waves refinement boxes
#Short radiating waves
HXP.create_refinement_cube(X_short_min,Y_short_min,Z_short_upper_min,X_short_max,Y_short_max,
                                               Z_short_max)
HXP.refinement_box(6).set_adaptation_flags(1,1)
HXP.refinement_box(6).set_target_size(0,0,0)
HXP.refinement_box(6).set_refinement_level(int(short_ref_upper))
HXP.create_refinement_cube(X_short_min,Y_short_min,Z_short_lower_min,X_short_max,Y_short_max,
                                               Z_short_max)
HXP.refinement_box(7).set_adaptation_flags(1,1)
HXP.refinement_box(7).set_target_size(0,0,0)
HXP.refinement_box(7).set_refinement_level(int(short_ref_lower))
#Long radiating waves
HXP.create_refinement_cube(X_long_min,Y_long_min,Z_long_upper_min,X_long_max,Y_long_max,
                                               Z_long_max)
```

```
HXP.refinement_box(8).set_adaptation_flags(1,1)
HXP.refinement_box(8).set_target_size(0,0,0)
HXP.refinement_box(8).set_refinement_level(int(long_ref_upper))
HXP.create_refinement_cube(X_long_min,Y_long_min,Z_long_lower_min,X_long_max,Y_long_max,
                                                    Z_long_max)
HXP.refinement_box(9).set_adaptation_flags(1,1)
HXP.refinement_box(9).set_target_size(0,0,0)
HXP.refinement_box(9).set_refinement_level(int(long_ref_lower))
#Extra radiating wave boxes to capture deformed free surface z-refinement
HXP.create_refinement_cube(X_extra_min,Y_extra_min,Z_extra_min,114.305,Y_extra_max,
                                                    Z_extra_max)
HXP.refinement_box(10).set_adaptation_flags(1,1)
HXP.refinement_box(10).set_target_size(1000,1000,0)
HXP.refinement_box(10).set_refinement_level(int(free_ref))

#Create mesh
HXP.adapt_mesh()
HXP.snap_mesh()
HXP.regularize_mesh()
HXP.set_optimization_params(1,4,100,7,3,3,30)
HXP.domain_face(6).set_viscous_layer_params(5,1.4188,0.01472,5,1.2)
HXP.domain_face(7).set_viscous_layer_params(5,1.4188,0.01472,5,1.2)
HXP.domain_face(8).set_viscous_layer_params(9,1.4188,0.01472,5,1.2)
HXP.domain_face(9).set_viscous_layer_params(9,1.4188,0.01472,5,1.2)
HXP.domain_face(10).set_viscous_layer_params(6,1.4188,0.01472,5,1.2)
HXP.domain_face(11).set_viscous_layer_params(9,1.4188,0.01472,5,1.2)
HXP.domain_face(12).set_viscous_layer_params(6,1.4188,0.01472,5,1.2)
HXP.set_viscous_layers_global_params(1,0,0,19,2,1)
HXP.insert_viscous_layers()

#export cgns file
HXP.export_cgns(baseFilePath + ".cgns")
HXP.save_project(baseFilePath + ".igg")
```

B

ReFRESCO input

In this section the ReFRESCO input for the simulation of the vessel with 2 DoF simulations in regualar head waves is given.

```
<?xml version="1.0"?>
<controls>
  <general>
    <codeVersion>2.5</codeVersion>
    <name>FDS</name>
    <description>FDS – 2DoF_Fine</description>
    <caseid>42_2DoF_W</caseid>
    <material>SALTWATER</material>
    <referenceLength>100.0000</referenceLength>
    <referenceVelocity>8.9050</referenceVelocity>
    <referenceMaterial>SALTWATER</referenceMaterial>
    <referencePressure>0.0</referencePressure>
    <outFileName>out</outFileName>
    <outFilePath>Data</outFilePath>
    <nsave>10</nsave>
    <suppressOutput>false</suppressOutput>
  </general>
  <userCode/>

  <grids>
    <grid>
      <gridFilePath>../Test_40_2DoF_Fine_Grid_Calmwater_startup/Grid
          </gridFilePath>
      <gridFileName>grid1</gridFileName>
      <subGrids>
        <subGrid name="Interior">
          <moveGridApply>false</moveGridApply>
          <calcEqsOfMotion>true</calcEqsOfMotion>
        </subGrid>
      </subGrids>
    </grid>
  </grids>
  <deformGrid>
    <deformGridSetup name="general">
      <general>
        <deformGridApply>true</deformGridApply>
```

```
        <deformGridUserDefined>false </deformGridUserDefined>
        <exactWallDistanceFrequencyInTimeLoop>10
                </exactWallDistanceFrequencyInTimeLoop>
        <updateFrequency>-1</updateFrequency>
      </general>
    </deformGridSetup>
    <deformGridSetup name="method">
      <deformMethod_RBF>
        <supportRadius>67.2850</supportRadius>
        <maxiter>500</maxiter>
        <convergenceTolerance>1.0E-04</convergenceTolerance>
        <greedyApply>true </greedyApply>
        <greedyTolerance>1.0E-02</greedyTolerance>
        <updateStep>1</updateStep>
        <solver>GMRES</solver>
        <preconditioner>SUPERLU</preconditioner>
        <exactNearWallCorrFrequencyInTimeLoop>10
                </exactNearWallCorrFrequencyInTimeLoop>
      </deformMethod_RBF>
    </deformGridSetup>
  </deformGrid>
  <freeMotion>
    <ifreeMotion name="FreeHeavePitch">
      <apply>true </apply>
      <bodyFamilies>Ship_1 Ship_2 Ship_3 Ship_4 Ship_5
          Ship_Deck Ship_Transom</bodyFamilies>
      <structPropertiesFileName>structProperties </structPropertiesFileName>
      <motionFileName>motion </motionFileName>
      <saveConvergence>true </saveConvergence>
      <subGridName>Interior </subGridName>
      <rotationOrigin>44.709  0.0  6.049</rotationOrigin>
      <centerOfGravity>44.709  0.0  6.049</centerOfGravity>
      <nDOFs>2</nDOFs>
      <translationDOFs>0 0 1</translationDOFs>
      <rotationDOFs>0 1 0</rotationDOFs>
      <startAtTimestep>1495</startAtTimestep>
      <initialRelaxation>
        <relax_min>0.1</relax_min>
        <relax_max>1.0</relax_max>
        <relax_fac>20</relax_fac>
      </initialRelaxation>
      <method>
        <IMPLICIT_PC_TYPE4/>
      </method>
      <correctorConvergenceTolerance>0.100000E-04
          </correctorConvergenceTolerance>
      <correctorMaxIteration>10</correctorMaxIteration>
      <correctorStartAtOuterLoop>2</correctorStartAtOuterLoop>
      <correctorOuterLoopStep>6</correctorOuterLoopStep>
      <correctorOuterLoopConvergenceTolerance>1E-6
          </correctorOuterLoopConvergenceTolerance>
      <correctorRelaxation>0.5</correctorRelaxation>
      <pseudoAddedMassCorrection>0</pseudoAddedMassCorrection>
      <usexmf>false </usexmf>
    </ifreeMotion>
  </freeMotion>
```

```
<adaptiveGrid/>
<imposedMotion/>
<adaptLoop/>
<fsi/>
<restart>
  <restart>true</restart>
  <resetCounter>false</resetCounter>
  <restartFileName>out-00001500</restartFileName>
  <restartFilePath>../Test_41_2DoF_Fine_Grid_Calmwater_free/Data
      </restartFilePath>
</restart>
<timeLoop>
  <unsteady>true</unsteady>
  <solutionScheme>IMPLICIT_THREE_TIME_LEVEL</solutionScheme>
  <maxTimesteps>6300</maxTimesteps>
  <timeDelta>0.0208626</timeDelta> <!-- Te / 200 -->
</timeLoop>
<outerLoop>
  <maxIteration>75</maxIteration>
  <convergenceTolerance>1e-6</convergenceTolerance>
  <residualNorm>TWO</residualNorm>
  <divergenceTolerance>1e+20</divergenceTolerance>
</outerLoop>
<accelerationOfGravity>
  <apply>true</apply>
  <gravityVector>0.0 0.0 -9.81</gravityVector>
</accelerationOfGravity>
<bodyForces>
  <apply>true</apply>
  <userDefined>true</userDefined>
  <toSave>true</toSave>
  <bodyforceTreatment>EXPLICIT_SOURCE</bodyforceTreatment>
  <bodyForce>0.0 0.0 0.0</bodyForce>
</bodyForces>
<boundaries>
  <!-- OUTER BOUNDARY CONDITIONS -->
  <family name="Inlet">
    <BCWave>
      <waveGeneration>true</waveGeneration>
      <waveAbsorption>false</waveAbsorption>
      <velocity userCode="false">-8.9050 0.0 0.0</velocity>
      <absorptionType>NONE</absorptionType>
      <velocityBCAir>DIRICHLET</velocityBCAir>
      <referenceSystem>EARTH_FIXED</referenceSystem>
      <turbulence>
        <turbIntensity_eddyVisc>
          <turbIntensity userCode="false">1.e-2</turbIntensity>
          <eddyVisc userCode="false">10.0000</eddyVisc>
        </turbIntensity_eddyVisc>
      </turbulence>
      <extrapolationOrder>0</extrapolationOrder>
    </BCWave>
  </family>
  <family name="Outlet">
    <BCWave>
      <waveGeneration>true</waveGeneration>
```

```
      <waveAbsorption>false</waveAbsorption>
      <velocity userCode="false">-8.9050 0.0 0.0</velocity>
      <absorptionType>NONE</absorptionType>
      <velocityBCAir>DIRICHLET</velocityBCAir>
      <referenceSystem>EARTH_FIXED</referenceSystem>
      <turbulence>
        <turbIntensity_eddyVisc>
          <turbIntensity userCode="false">1.e-2</turbIntensity>
          <eddyVisc userCode="false">10.0000</eddyVisc>
        </turbIntensity_eddyVisc>
      </turbulence>
      <extrapolationOrder>0</extrapolationOrder>
    </BCWave>
  </family>
  <family name="Outer_Left">
    <BCWave>
      <waveGeneration>true</waveGeneration>
      <waveAbsorption>false</waveAbsorption>
      <velocity userCode="false">-8.9050 0.0 0.0</velocity>
      <absorptionType>NONE</absorptionType>
      <velocityBCAir>DIRICHLET</velocityBCAir>
      <referenceSystem>EARTH_FIXED</referenceSystem>
      <turbulence>
        <turbIntensity_eddyVisc>
          <turbIntensity userCode="false">1.e-2</turbIntensity>
          <eddyVisc userCode="false">10.0000</eddyVisc>
        </turbIntensity_eddyVisc>
      </turbulence>
      <extrapolationOrder>0</extrapolationOrder>
    </BCWave>

  </family>
  <family name="Symmetry">
    <BCSymmetryPlane>
      <extrapolationOrder>0</extrapolationOrder>
    </BCSymmetryPlane>
  </family>
  <family name="Outer_Bottom">
    <BCSlipWall/>
  </family>
  <family name="Outer_Top">
    <BCPressure>
      <pressure userCode="false">0e0</pressure>
      <extrapolationOrder>0</extrapolationOrder>
    </BCPressure>
  </family>
  <!-- SHIP BOUNDARY CONDITIONS -->
  <family name="Ship_1">
    <BCSlipWall>
      <extrapolationOrder>0</extrapolationOrder>
    </BCSlipWall>
  </family>
  <family name="Ship_2">
    <BCSlipWall>
      <extrapolationOrder>0</extrapolationOrder>
    </BCSlipWall>
```

```
    </family>
    <family name="Ship_3">
      <BCSlipWall>
        <extrapolationOrder>0</extrapolationOrder>
      </BCSlipWall>
    </family>
    <family name="Ship_4">
      <BCSlipWall>
        <extrapolationOrder>0</extrapolationOrder>
      </BCSlipWall>
    </family>
    <family name="Ship_5">
      <BCSlipWall>
        <extrapolationOrder>0</extrapolationOrder>
      </BCSlipWall>
    </family>
    <family name="Ship_Deck">
      <BCSlipWall>
        <extrapolationOrder>0</extrapolationOrder>
      </BCSlipWall>
    </family>
    <family name="Ship_Transom">
      <BCSlipWall>
        <extrapolationOrder>0</extrapolationOrder>
      </BCSlipWall>
    </family>
  </boundaries>
  <massMomentumSolver>
    <solverType name="SEGREGATED">
      <segregated>
        <solver>FRESCO</solver>
      </segregated>
    </solverType>
  </massMomentumSolver>
  <equations>
    <equation name="Momentum Equation">
      <EQMomentum>
        <solve_x>true</solve_x>
        <solve_y>true</solve_y>
        <solve_z>true</solve_z>
        <solver>
          <PETSC>
            <solver>GMRES</solver>
            <preconditioner>BJACOBI</preconditioner>
          </PETSC>
        </solver>
        <convergenceTolerance>0.001</convergenceTolerance>
        <maxIteration>400</maxIteration>
        <relaxationProcedure>
          <IMPLICIT_EXPLICIT>
            <imp_relax_min>0.95</imp_relax_min>
            <imp_relax_max>0.95</imp_relax_max>
            <imp_relax_fac>25</imp_relax_fac>
            <exp_relax>0.250000</exp_relax>
          </IMPLICIT_EXPLICIT>
        </relaxationProcedure>
```

```
      <convectiveFluxDiscretisation>
        <TVD_SCHEME>
          <schemeName>HARMONIC</schemeName>
        </TVD_SCHEME>
      </convectiveFluxDiscretisation>
      <gradientCalculation>
        <GAUSS/>
      </gradientCalculation>
      <applyEccentricityCorrection>true</applyEccentricityCorrection>
      <saveResidual>true</saveResidual>
      <saveCourantNo>true</saveCourantNo>
      <initialization>
        <USER_DEFINED>
          <initialVelocity>-8.9050 0.0 0.0</initialVelocity>
        </USER_DEFINED>
      </initialization>
    </EQMomentum>
  </equation>
  <equation name="Pressure Equation">
    <EQPressure>
      <solver>
        <PETSC>
          <solver>CG</solver>
          <preconditioner>BJACOBI</preconditioner>
        </PETSC>
      </solver>
      <convergenceTolerance>0.005</convergenceTolerance>
      <maxIteration>500</maxIteration>
      <relaxationProcedure>
        <EXPLICIT>
          <exp_relax>0.150000</exp_relax>
        </EXPLICIT>
      </relaxationProcedure>
      <gradientCalculation>
        <GAUSS/>
      </gradientCalculation>
      <applyEccentricityCorrection>true</applyEccentricityCorrection>
      <saveResidual>true</saveResidual>
      <initialPressure>0.0</initialPressure>
    </EQPressure>
  </equation>
  <equation name="Free Surface Equation">
    <EQFreeSurface>
      <solver>
        <PETSC>
          <solver>GMRES</solver>
          <preconditioner>BJACOBI</preconditioner>
        </PETSC>
      </solver>
      <convergenceTolerance>0.01</convergenceTolerance>
      <maxIteration>200</maxIteration>
      <relaxationProcedure>
        <IMPLICIT_EXPLICIT>
          <imp_relax_min>0.9</imp_relax_min>
          <imp_relax_max>0.9</imp_relax_max>
          <imp_relax_fac>25</imp_relax_fac>
```

```
            <exp_relax>0.3</exp_relax>
          </IMPLICIT_EXPLICIT>
        </relaxationProcedure>
        <convectiveFluxDiscretisation>
          <REFRICS/>
        </convectiveFluxDiscretisation>
        <material>AIR</material>
        <gradientCalculation>
          <GAUSS/>
        </gradientCalculation>
        <applyEccentricityCorrection>false </applyEccentricityCorrection>
        <saveResidual>true </saveResidual>
        <initialWaterLevel>3.1250</initialWaterLevel>
        <contactLineCorrection>
          <apply>false </apply>
          <distance>5.0000e-03</distance>
        </contactLineCorrection>
        <waveDefinition>
          <incomingWaveType>STOKES5</incomingWaveType>
          <waterDepth>200.000</waterDepth>
          <waveHeight>2.0</waveHeight>
          <wavePeriod>7.392</wavePeriod>
          <waveDirectionVector>-1.0  0.0  0.0</waveDirectionVector>
          <rampupTime>7.392</rampupTime>
          <silentTime>3.588120E+002</silentTime>

          <applyMomentumAbsorption>true </applyMomentumAbsorption>
          <applyFreeSurfaceAbsorption>false </applyFreeSurfaceAbsorption>
          <absorptionZoneOrigin>0.0  0.0  0.0</absorptionZoneOrigin>
          <absorptionZoneInnerRadius>200  100  99999</absorptionZoneInnerRadius>
          <absorptionZoneOuterRadius>300  200  999999</absorptionZoneOuterRadius>
          <maxAbsorption>50</maxAbsorption>
          <absorptionReferencePeriod>7.392</absorptionReferencePeriod>
          <absorptionZonePolynomialOrder>50</absorptionZonePolynomialOrder>
          <absorptionType>BODYFORCE</absorptionType>
          <absorptionFunction>EXPONENTIAL</absorptionFunction>
        </waveDefinition>
      </EQFreeSurface>
    </equation>
  </equations>
  <materials>
    <material name="FRESHWATER">
      <fluid>
        <viscosityMolecular>1.138e-3</viscosityMolecular>
        <density>0.9991e3</density>
      </fluid>
    </material>
    <material name="SALTWATER">
      <fluid>
        <viscosityMolecular>1.2201e-3</viscosityMolecular>
        <density>1026.0</density>
      </fluid>
    </material>
    <material name="AIR">
      <fluid>
        <viscosityMolecular>1.8020e-5</viscosityMolecular>
```

```
        <density>1.2250e0</density>
      </fluid>
    </material>
  </materials>
  <extraQuantities/>
  <monitors>
    <monitor name="MO_Total_Force">
      <MO_Force>
        <fileName>total_forces </fileName>
        <saveFrequency>1</saveFrequency>
        <label/>
        <families>Ship_1 Ship_2 Ship_3 Ship_4 Ship_5 Ship_Deck
                Ship_Transom</families>
        <forTecplot>true </forTecplot>
      </MO_Force>
    </monitor>
    <monitor name="MO_Total_Moment">
      <MO_Moment>
        <fileName>total_moment</fileName>
        <referencePoint>44.709  0.0  5.95436822</referencePoint>
                <!--  (6.049 - 0.09463178)  Update this -->
        <referenceSystem>BODY_FIXED</referenceSystem>
        <bodyFixedReferenceFamily>Ship_1</bodyFixedReferenceFamily>
        <saveFrequency>1</saveFrequency>
        <label/>
        <families>Ship_1 Ship_2 Ship_3 Ship_4 Ship_5
                Ship_Deck Ship_Transom</families>
        <forTecplot>true </forTecplot>
      </MO_Moment>
    </monitor>
    <monitor name="MO_Total_Force_no_transom">
      <MO_Force>
        <fileName>total_forces_no_transom </fileName>
        <saveFrequency>1</saveFrequency>
        <label/>
        <families>Ship_1 Ship_2 Ship_3 Ship_4 Ship_5 Ship_Deck</families>
        <forTecplot>true </forTecplot>
      </MO_Force>
    </monitor>
    <monitor name="MO_Total_Moment_no_transom">
      <MO_Moment>
        <fileName>total_moment_no_transom </fileName>
        <referencePoint>44.709  0.0  5.95436822</referencePoint>
                <!--  (6.049 - 0.09463178)  Update this -->
        <referenceSystem>BODY_FIXED</referenceSystem>
        <bodyFixedReferenceFamily>Ship_1</bodyFixedReferenceFamily>
        <saveFrequency>1</saveFrequency>
        <label/>
        <families>Ship_1 Ship_2 Ship_3 Ship_4 Ship_5 Ship_Deck</families>
        <forTecplot>true </forTecplot>
      </MO_Moment>
    </monitor>
    <monitor name="Courant">
      <MO_Scalar>
        <fileName>courant </fileName>
        <saveFrequency>1</saveFrequency>
```

```
      <label/>
      <fields>CourantNo</fields>
      <forTecplot>true</forTecplot>
    </MO_Scalar>
  </monitor>
  <monitor name="MO_Force_Ship_1">
    <MO_Force>
      <fileName>forces_Ship_1</fileName>
      <saveFrequency>1</saveFrequency>
      <label/>
      <families>Ship_1</families>
      <forTecplot>true</forTecplot>
    </MO_Force>
  </monitor>
  <monitor name="MO_Force_Ship_2">
    <MO_Force>
      <fileName>forces_Ship_2</fileName>
      <saveFrequency>1</saveFrequency>
      <label/>
      <families>Ship_2</families>
      <forTecplot>true</forTecplot>
    </MO_Force>
  </monitor>
  <monitor name="MO_Force_Ship_3">
    <MO_Force>
      <fileName>forces_Ship_3</fileName>
      <saveFrequency>1</saveFrequency>
      <label/>
      <families>Ship_3</families>
      <forTecplot>true</forTecplot>
    </MO_Force>
  </monitor>
  <monitor name="MO_Force_Ship_4">
    <MO_Force>
      <fileName>forces_Ship_4</fileName>
      <saveFrequency>1</saveFrequency>
      <label/>
      <families>Ship_4</families>
      <forTecplot>true</forTecplot>
    </MO_Force>
  </monitor>
  <monitor name="MO_Force_Ship_5">
    <MO_Force>
      <fileName>forces_Ship_5</fileName>
      <saveFrequency>1</saveFrequency>
      <label/>
      <families>Ship_5</families>
      <forTecplot>true</forTecplot>
    </MO_Force>
  </monitor>
  <monitor name="MO_Force_Ship_Deck">
    <MO_Force>
      <fileName>forces_Ship_Deck</fileName>
      <saveFrequency>1</saveFrequency>
      <label/>
      <families>Ship_Deck</families>
```

```
      <forTecplot>true</forTecplot>
    </MO_Force>
  </monitor>
  <monitor name="MO_Force_Ship_Transom">
    <MO_Force>
      <fileName>forces_Ship_Transom</fileName>
      <saveFrequency>1</saveFrequency>
      <label/>
      <families>Ship_Transom</families>
      <forTecplot>true</forTecplot>
    </MO_Force>
  </monitor>
  <monitor name="WaveProbe_1">
    <MO_WaveProbePoint>
      <fileName>Waveprobe_1</fileName>
      <saveFrequency>1</saveFrequency>
      <label/>
      <interfaceAirVolumeFraction>0.5</interfaceAirVolumeFraction>
      <fields/>
      <probeDirection>0. 0. 1.</probeDirection>
      <coordinates>200 150 0</coordinates>
      <forTecplot>true</forTecplot>
      <interpolation>
        <LEAST_SQUARES>
          <order>2</order>
        </LEAST_SQUARES>
      </interpolation>
    </MO_WaveProbePoint>
  </monitor>
  <monitor name="WaveProbe_2">
    <MO_WaveProbePoint>
      <fileName>Waveprobe_2</fileName>
      <saveFrequency>1</saveFrequency>
      <label/>
      <interfaceAirVolumeFraction>0.5</interfaceAirVolumeFraction>
      <fields/>
      <probeDirection>0. 0. 1.</probeDirection>
      <coordinates>100 150 0</coordinates>
      <forTecplot>true</forTecplot>
      <interpolation>
        <LEAST_SQUARES>
          <order>2</order>
        </LEAST_SQUARES>
      </interpolation>
    </MO_WaveProbePoint>
  </monitor>
  <monitor name="WaveProbe_3">
    <MO_WaveProbePoint>
      <fileName>Waveprobe_3</fileName>
      <saveFrequency>1</saveFrequency>
      <label/>
      <interfaceAirVolumeFraction>0.5</interfaceAirVolumeFraction>
      <fields/>
      <probeDirection>0. 0. 1.</probeDirection>
      <coordinates>44.709 150 0</coordinates>
      <forTecplot>true</forTecplot>
```

```
      <interpolation>
        <LEAST_SQUARES>
          <order>2</order>
        </LEAST_SQUARES>
      </interpolation>
    </MO_WaveProbePoint>
  </monitor>
  <monitor name="WaveProbe_4">
    <MO_WaveProbePoint>
      <fileName>Waveprobe_4</fileName>
      <saveFrequency>1</saveFrequency>
      <label/>
      <interfaceAirVolumeFraction>0.5</interfaceAirVolumeFraction>
      <fields/>
      <probeDirection>0. 0. 1.</probeDirection>
      <coordinates>0 150 0</coordinates>
      <forTecplot>true</forTecplot>
      <interpolation>
        <LEAST_SQUARES>
          <order>2</order>
        </LEAST_SQUARES>
      </interpolation>
    </MO_WaveProbePoint>
  </monitor>
  <monitor name="WaveProbe_5">
    <MO_WaveProbePoint>
      <fileName>Waveprobe_5</fileName>
      <saveFrequency>1</saveFrequency>
      <label/>
      <interfaceAirVolumeFraction>0.5</interfaceAirVolumeFraction>
      <fields/>
      <probeDirection>0. 0. 1.</probeDirection>
      <coordinates>-100 150 0</coordinates>
      <forTecplot>true</forTecplot>
      <interpolation>
        <LEAST_SQUARES>
          <order>2</order>
        </LEAST_SQUARES>
      </interpolation>
    </MO_WaveProbePoint>
  </monitor>
  <monitor name="WaveCut_1">
    <MO_WaveProbeLine>
      <fileName>WaveCut_1</fileName>
      <saveFrequency>1</saveFrequency>
      <label/>
      <interfaceAirVolumeFraction>0.5</interfaceAirVolumeFraction>
      <fields/>
      <lineStart>-100.0000 6.8750 0.0</lineStart>
      <lineEnd>200.0000 6.8750 0.0</lineEnd>
      <numberPoints>301</numberPoints>
      <includeBoundaryData>false</includeBoundaryData>
      <forTecplot>true</forTecplot>
      <interpolation>
        <LEAST_SQUARES>
          <order>2</order>
```

```
          </LEAST_SQUARES>
        </interpolation>
        <smoothingSteps>0</smoothingSteps>
      </MO_WaveProbeLine>
    </monitor>
    <monitor name="WaveCut_2">
      <MO_WaveProbeLine>
        <fileName>WaveCut_2</fileName>
        <saveFrequency>1</saveFrequency>
        <label/>
        <interfaceAirVolumeFraction>0.5</interfaceAirVolumeFraction>
        <fields/>
        <lineStart>-100.0000 12.5000 0.0</lineStart>
        <lineEnd>200.0000 12.5000 0.0</lineEnd>
        <numberPoints>301</numberPoints>
        <includeBoundaryData>false</includeBoundaryData>
        <forTecplot>true</forTecplot>
        <interpolation>
          <LEAST_SQUARES>
            <order>2</order>
          </LEAST_SQUARES>
        </interpolation>
        <smoothingSteps>0</smoothingSteps>
      </MO_WaveProbeLine>
    </monitor>
    <monitor name="WaveCut_3">
      <MO_WaveProbeLine>
        <fileName>WaveCut_3</fileName>
        <saveFrequency>1</saveFrequency>
        <label/>
        <interfaceAirVolumeFraction>0.5</interfaceAirVolumeFraction>
        <fields/>
        <lineStart>-100.0000 30.0000 0.0</lineStart>
        <lineEnd>200.0000 30.0000 0.0</lineEnd>
        <numberPoints>301</numberPoints>
        <includeBoundaryData>false</includeBoundaryData>
        <forTecplot>true</forTecplot>
        <interpolation>
          <LEAST_SQUARES>
            <order>2</order>
          </LEAST_SQUARES>
        </interpolation>
        <smoothingSteps>0</smoothingSteps>
      </MO_WaveProbeLine>
    </monitor>
  </monitors>
  <dynamic>
    <dynamicMode>INTERACTIVE_MODE</dynamicMode>
    <interactive>
      <startCounter>1</startCounter>
    </interactive>
    <scenario>
    </scenario>
  </dynamic>
  <developer>
    <faceInterpolation_scheme>FACEPOINT</faceInterpolation_scheme>
```

```
    <cellCenter_scheme>AreaAvCenter2 </cellCenter_scheme>
    <turbulence_applyOmegaLimiter>true </turbulence_applyOmegaLimiter>
    <linSolver_outputInfo >true </linSolver_outputInfo >
    <pwi_approxInvMomMatnoDt>false </pwi_approxInvMomMatnoDt>
    <gradients_limiter >BARTH_JESPERSEN</gradients_limiter >
  </developer>
</controls >
```